A consistent debris flow model with intergranular friction and dynamic pore-fluid pressure

Vom Fachbereich Maschinenbau
an der Technischen Universität Darmstadt
zur Erlangung des akademischen Grades
eines Doktor-Ingenieurs (Dr.-Ing.)
genehmigte

D i s s e r t a t i o n

von

Julian Heß, M. Sc.
aus Würzburg

Berichterstatter:	apl. Prof. Dr.-Ing. Yongqi Wang
1. Mitberichterstatter:	Prof. Dr.-Ing. Martin Oberlack
2. Mitberichterstatter:	apl. Prof. Dr. rer. nat. Amsini Sadiki
Tag der Einreichung:	02.04.2019
Tag der mündlichen Prüfung:	03.07.2019

Darmstadt, 2019
D17

Abstract

This work presents the thermodynamically consistent development of a scaled, depth-integrated model for granular-fluid flows. Considering a general topography, the model is used for the numerical simulation of debris flows in different scenarios. With regard to important physical mechanisms in such flows and the underlying dynamics, additional fields are included, an extra pore-fluid pressure and hypoplastic, intergranular friction. The combined recourse to these two fields takes place in the context of a derivation with the entropy principle, beginning with general laws of thermodynamics, and ends with the application to real, large-scale debris flow events.

As a starting point, within the framework of mixture theory and the entropy principle, a continuum model for a general granular-fluid mixture is derived. Amending the basic fields of mass, momentum and energy, as well as a balance equation for the volume fraction, an additional field for the intergranular contact forces is considered, together with, newly introduced in the context of thermodynamic consistent modeling, a dynamic partial pressure. Assuming a shallow, saturated flow, the derived model is then non-dimensionalized and depth-integrated. The resulting model is further transferred into general coordinates. This allows for the easy representation of debris flows on real mountainous topography.

Implemented with a shock-capturing non-oscillatory central (NOC) scheme, several numerical simulations are performed, ranging from parameter studies on a laboratory scale and the comparison with a dam break experiment to a large-scale event. The numerical parameter studies confirm the expected behavior of the additional physical fields. Since the extra pore-fluid pressure arises from the interaction of the granular skeleton and the pore-fluid, it interferes with the hydrostatic pressure and is able to push the granular particles apart, thus reducing their apparent friction and prolongating the movement of the bulk mass. It accelerates the whole mixture and prevents the mass from settling, while the intergranular friction helps the granular structure to maintain its form, hindering it from dissolving like a fluid and accounting for the non-linear, anelastic behavior of granular material.

It should be emphasized that the presented modeling establishes a transfer from investigations on granular materials in the context of the entropy principle to the more practically orientated class of depth-integrated models. With this, the additional fields can be seen as the incorporation of information on the granular skeleton, i.e. the microstructure, in its interdependency with the fluid phase – something that is usually not depicted similarly in the framework of mixture theory. A central aim here is therefore to provide a consistent debris flow model, developed with regard to these additional fields, which is applicable for numerical studies.

It is noted that this thesis is based on accepted publications (Heß, Wang & Hutter 2017, Heß & Wang 2019, Heß & Cheviakov 2019) and a submitted manuscript (Heß, Wang & Tai 2019).

Zusammenfassung

In dieser Arbeit wird die thermodynamisch konsistente Entwicklung eines skalierten, tiefen integrierten Modells für Granulat-Flüssigkeits-Strömungen vorgestellt. Unter Verwendung einer allgemeinen Topographie wird das Modell zur numerischen Simulation von Schuttströmungen in verschiedenen Kontexten eingesetzt. Im Hinblick auf die für solche Strömungen wichtigen physikalischen Mechanismen und die zugrunde liegenden Dynamiken werden zusätzliche Felder berücksichtigt, einmal ein Extra-Porendruck und weiterhin ein Feld zur Beschreibung von hypoplastischer, intergranularer Reibung. Die Verknüpfung dieser zwei Felder erfolgt im Rahmen einer Herleitung nach dem Entropieprinzip, ausgehend von den allgemeinen Gesetzen der Thermodynamik, und endet mit der Anwendung auf reale, großskalige Szenarien von Schuttströmungen.

Als Ausgangspunkt wird im Rahmen der Mischungstheorie und des Entropieprinzips ein Kontinuumsmodell für ein allgemeines Granulat-Flüssigkeits-Gemisch hergeleitet. Die Grundgrößen Masse, Impuls und Energie, sowie die Bilanzgleichung für den Volumenanteil, werden hierbei um zwei zusätzliche Felder ergänzt, von denen eines die intergranularen Kontaktkräfte berücksichtigt, und, neu eingeführt im Rahmen der thermodynamisch konsistenten Modellierung, ein dynamischer Partialdruck. Weiterhin wird ausgehend von einer flachen, gesättigten Strömung das so hergeleitete Modell entdimensioniert und tiefen integriert. Das Modell wird außerdem in allgemeine Koordinaten übertragen, welche die einfache Darstellung von Schuttströmungen auf echter Gebirgstopographie ermöglichen. Implementiert mit einem auch Schocks erfassenden non-oscillatory central (NOC)-Schema werden mehrere numerische Simulationen durchgeführt, die von Parameterstudien im Labormaßstab und dem Vergleich mit einem Dammbruch-Experiment bis hin zu einem großskaligen Ereignis reichen. Die numerischen Parameterstudien bestätigen das erwartete Verhalten der zusätzlichen physikalischen Felder. Da der Extra-Porendruck durch das Zusammenwirken von granularem Skelett und Porenflüssigkeit entsteht, überlagert er sich mit dem hydrostatischen Druck und kann die Granulatspartikel auseinander drücken, wodurch ihre Reibung reduziert und die Bewegung der Schüttgutmasse verlängert wird. Er beschleunigt somit die gesamte Mischung und verhindert das Absetzen der Masse, während die intergranulare Reibung dazu beiträgt, dass die Struktur der Körner ihre Form behält, also nicht einfach wie eine Flüssigkeit zerfließt und weiterhin auch das nichtlineare, anelastische Verhalten des körnigen Materials berücksichtigt.

Hervorzuheben ist, dass die vorgestellte Modellierung einen Transfer von Untersuchungen an granularen Materialien im Kontext des Entropieprinzips und der stärker an der Praxis orientierten Klasse von tiefen integrierten Modelle herstellt. Damit können die zusätzlichen Felder verstanden werden als die Berücksichtigung von Informationen über das granulare Skelett, d.h. die Mikrostruktur, in ihrer Wechsel-

wirkung mit der flüssigen Phase – etwas, das normalerweise nicht im Rahmen der Mischungstheorie derartig berücksichtigt wird. Ein zentrales Ziel ist es daher, ein konsistentes Modell für Schuttströmungen bereitzustellen, das unter Berücksichtigung dieser zusätzlichen Felder entwickelt wurde und für numerische Studien geeignet ist.

Es wird darauf hingewiesen, dass diese Arbeit auf angenommenen Publikationen (Heß et al. 2017, Heß & Wang 2019, Heß & Cheviakov 2019) und einem eingesandten Manuskript (Heß et al. 2019) basiert.

Acknowledgments

I would like to thank my supervisor Prof. Dr.-Ing. Yongqi Wang, not only for the opportunity to work on the research resulting in this PhD thesis, but for the support and patience during the past years. I am very happy to have gained insights into very different fields through this multifaceted task. That being said, I also would like to thank Prof. Dr.-Ing. Martin Oberlack for giving me the chance to do this work at the Chair of Fluid Dynamics and providing me the scientific environment for this research and the necessary resources, as well as being one of my second supervisors. Additionally, I am grateful to Prof. Dr. rer. nat. Amsini Sadiki for being second supervisor as well.

Moreover, I am deeply grateful for the possibility to work with researchers from abroad during the stages of this work, including Prof. Kolumban Hutter from ETH Zürich, helping me with the thermodynamically groundwork of this thesis, as well as Prof. Dr. Yih-Chin Tai, who, with his solver, provided the numerical framework and thus made the broad applicability of the model possible, but was also always open for questions and further developments. I am also very thankful to Prof. Alexei Cheviakov from the University of Saskatchewan, who offered me a fruitful collaboration, a pleasant stay in Saskatoon and many interesting discussions.

I also want to thank my colleagues at the Chair of Fluid Dynamics, both past and present ones, and in particular the long-term office mates Xiannan Meng, Martina Costa Reis and Anna-Lena Gruber, as well as our secretary Ruth Völker, for the friendly atmosphere during these almost four years, the interesting, often long-running talks and the support, whenever needed. With respect to this thesis, special thanks goes to Tim Gebler, Dominik Plümacher, Martin Smuda and Alparslan Yalcin for proof reading.

And finally, I want to appreciate the encouragement and support of my family, friends and in particular my girlfriend Pauline, who helped me to realize – not only – this work. Here as well, I want to thank my mother Carmen and my sister Iris for the proof reading.

This work was enabled financially by the support of the Deutsche Forschungsgemeinschaft (DFG) within the project number WA 2610/3-1.

Contents

List of Figures

List of Tables

Nomenclature

Symbol	Description
$\mathbf{a}$	Vector in the formulation of Liu's Lemma
a_Z^s	Intergranular parameter function
a_i^w	Wave speed
$a_1^\alpha, ..., a_7^\alpha$	Scalar coefficients in the stress tensor of α
$\boldsymbol{A}$	Inverse of the basal Jacobian
$\mathbb{A}_{\mathbb{P}}$	Drag-measure for fluid flow in granular material, for c_D^{sf}
b	Basal surface/ topography
B_{ij}^α	Left Cauchy-Green deformation tensor
$\mathfrak{B}$	Material body
$\mathbb{B}_{\mathbb{P}}$	Drag-measure for granular particle in fluid, for c_D^{sf}
c	Z-component of normal unit vector
c^α	Mass interaction rate of constituent α
$c_D^{\alpha\beta}$	General parameter for the drag between two constituents α, β
c_D^s	Solid drag coefficient
$c_i^{\alpha,w}$	Wave speed for phase α
$c_1, ..., c_4$	Scalar coefficients of hypoplastic source Φ_{ij}^s
C_e^α	Extra pressure parameter for constituent α
$C_{j,\alpha}^{\omega,\beta}$	Term in the equilibrium stress tensor
C_{max}	CFL-number
$\boldsymbol{C}_1, ..., \boldsymbol{C}_4$	Non-conservative term of system of equations
D_{ij}^α	Strain rate of constituent α
$\mathbf{e}_i$	Basis vector
$\mathcal{E}$	Mixture energy balance
Eu	Euler number
f	Superscript for fluid phase
f_b	Barotropy function

f_s	Stiffness factor in Φ^s_{ij}
f_D	Density factor in Φ^s_{ij}
$F_{x_I,i}$	Pfaffian form, vectorial
$\boldsymbol{F}_i$	Flux term of system of equations
$\mathcal{F}_S$	Function describing the surface $\mathcal{S}$
$\mathtt{F}$	Flux of a physical quantity Φ
g	Gravitational constant
g_i	Volume force
Ga_f	Galilei number
h	Mixture height
$\mathcal{H}$	Height scale
I_ϕ	Short for a balance equation of Φ
I^α_ϕ	For balance equation of Φ^α
$\mathbf{I}_\phi$	For balance equation of Φ, all terms brought to one side
J	Determinant of the Jacobian $\boldsymbol{\Omega}$
k_i	Extra-entropy flux
k_l	Navier fluid friction coefficient
k_D	Hydraulic permeability
$K_{act/pas}$	Earth-pressure coefficient
$K^{\omega,\beta}_{ij,\alpha}$	Pressure term in the momentum interaction
$\mathbb{K}$	Configuration of material elements
$\mathbb{K}^\alpha$	Configuration of particles of a phase α
$\mathcal{L}$	Length scale
$\mathbf{L}$	Linear part of Φ^s_{ij}
m^α	Mass of constituent α
m^α_i	Momentum interaction rate of α
$\mathcal{M}^\alpha_i$	Partial momentum balance
n^α	Production rate of volume fractions of α
n_i	Normal vector
$\mathbf{N}$	Non-linear part of Φ^s_{ij}
N_γ	Dilatancy number

N_R	Non-dimensional viscous number
N_Z	Non-dimensional number of intergranular stress
$\mathcal{N}^\alpha$	Mixture entropy balance
p^α	Pressure-like quantity of α
P_{x_I}	Pfaffian form, scalar
$\mathtt{P}$	Production of a physical quantity Φ
q_i	Heat flux of the mixture
r_R	External energy supply
$\boldsymbol{r}_b$	Reference vector to a point on the surface $\mathcal{S}$
Re_P	Particle Reynolds number
$\mathcal{R}$	Typical radius of curvature
$\mathcal{R}^\alpha$	Partial balance of mass
$\mathbb{R}^3$	Three-dimensional space
s	Superscript for solid phase
$\mathbf{s}$	Vector describing the horizontal plane
$\boldsymbol{S}$	Source term of system of equations
$\mathfrak{s}$	Free flow surface
$\mathcal{S}$	Topographical surface
t	Time
T_{ij}^α	Cauchy-stress tensor of constituent α
$T_{ij}^{\alpha,e}$	Deviatoric extra stress tensor of α
T_{ij}	Mixture stress tensor
u_i^α	Diffusion velocity of α, related to v_i
$\boldsymbol{U}$	Vector of unknowns for system of equations
$\mathcal{U}_T$	Terminal falling velocity
v_i^α	Partial velocity of constituent α
v_i	(Mixture) velocity
V	Total volume of a body $\mathfrak{B}$
∂V	Boundary of a volume V
V^α	Partial volume of α
$\mathcal{V}^\alpha$	Balance of the volume fraction

W_{ij}^{α}	Spin tensor of constituent α
$\mathcal{W}^{\alpha}$	Partial pressure balance
x_i	Position vector in $\mathbb{R}^3$
x_0	Initial position of the particles of $\mathfrak{B}$
x_f	Flow front
x_L	Flow length
$\mathfrak{X}$	Material element of $\mathfrak{B}$
$\mathbb{X}$	Change in position of the particles of $\mathfrak{B}$
Y_d	Cross-slope distance to center
z_b	Additional elevation on slope
Z_{ij}^{α}	Intergranular stress tensorial variable of α
Z	Supply of a physical quantity Φ
$\mathcal{Z}_{ij}^{\alpha}$	Evolution equation for the inner stress
(x, y, z)	Set of curvilinear coordinates
(X, Y, Z)	Set of Cartesian coordinates
α	Arbitrary constituent of a mixture
α_D	Permeability function
α_ρ	Ratio of fluid to solid density
α_b^f	Non-dimensional fluid friction coefficient
β	Scalar in the formulation of Liu's Lemma
β_ψ^f	Extra pressure weighting function
γ_ϕ^α	Interaction production density rate of α
γ_f^ϖ	Extra pressure source term
$\dot{\gamma}$	Shear rate
δ_{ij}	Kronecker-Delta
δ_b	Bed friction angle
δ_P	Particle diameter
δ^Z	Plastic stress parameter
$\Delta_i^{\alpha,\varpi}$	Pressure flux quantity related to κ_ϖ^α
ϵ	Ratio of mixture height scale to length scale
ε	Specific internal energy of the mixture

ε_D	Diffusive part of the internal energy
ε_I	Non-diffusive part of the internal energy
ε_{ijk}	Permutation symbol
η^s	Specific entropy of the mixture
θ	Absolute temperature of the mixture
ϑ_s	Slope angle
κ	Curvature
$\kappa_{\varpi 1}, \kappa_{\varpi 2}$	Dilatancy coefficients
κ_{ϖ}^{α}	Pressure flux parameter of α
λ	Characteristic curvature
λ_{ϕ}	Lagrange-multiplier of the balance of ϕ
μ^{α}	Viscosity function of α
μ_b^s	Solid bed friction
ν^{α}	Volume fraction of α
ν_C^s	Critical solid volume fraction
ν_{eq}^s	Equilibrium solid volume fraction
ν_{∞}^s	Maximum packing volume fraction
$\pi^{\rho\eta}$	Mixture entropy production
π_{ϕ}	Density of production P to Φ
Π	Material variables
ϖ^{α}	Partial pressure quantity of phase α
ϖ_h^{α}	Hydrostatic pressure of phase α
ϖ_e^{α}	Dynamic extra pressure of phase α
ϖ_{ν}^{α}	Configuration pressure of phase α
ϖ_Z^{α}	Spherical intergranular friction of α
ρ^{α}	True density of α
$\widetilde{\rho}^{\alpha}$	Partial density of α
ρ	Mixture density
σ	Total stress state
σ_e	Extra stress
σ_{ϕ}	Density of supply Z to the quantity Φ

$\sigma^{\rho\eta}$	Entropy supply of the mixture
$\boldsymbol{\tau}_\delta$	Basis tangent on horizontal surface
τ_κ	Centrifugal forces
τ_R^s	Solid bed friction term
ϕ	Density of a physical quantity Φ
ϕ^α	Density of a partial physical quantity Φ^α
ϕ_{int}	Internal friction angle
$\boldsymbol{\phi}_C$	Variables of the defined material class
$\boldsymbol{\phi}_G$	Non-equilibrium variables
$\boldsymbol{\phi}_L$	Vector of highest derivatives
Φ	Physical quantity of a body $\mathfrak{B}$
Φ^α	Partial physical quantity of a mixture body
Φ_{ij}^α	Source term of the intergranular stress of α
ψ	Dilatancy angle
ψ_i^ϕ	Flux density related to flux $\mathtt{F}$ of Φ
$\psi_i^{\rho\eta}$	Flux density of mixture entropy
Ψ	Scaling abbreviation term
Ψ^G	Free Helmholtz energy-like quantity
Ψ_I^G	Internal part of the Free Helmholtz energy-like quantity
Ψ_I^G	Diffusive part of the Free Helmholtz energy-like quantity
$\boldsymbol{\Omega}$	Jacobian matrix
(ξ, η, ζ)	Set of terrain-following coordinates

Abbreviations

CFL Courant-Friedrichs-Lewy

DEM digital elevation model

DG Discontinous Galerkin

DOF degrees of freedom

GIS geographic information system

ML Müller-Liu

MW Meng-Wang

NOC non-oscillatory central

NT Nessyahu-Tadmor

ODE ordinary differential equation

PDE partial differential equation

RHS right-hand side

RK Runge-Kutta

SH Savage-Hutter

TVD total variation diminishing

1 Introduction

While granular materials can be described as collections of solid particles, *debris flows* are moving mixtures of fluids and granular materials, often including rocks of different sizes as well as soil. As a result of heavy rainfall or snow-melt, leading to a destabilization of soil and the mobilization of water-saturated granular material, debris flows occur particularly in mountainous regions. Driven by gravity, these flows can be devastating due to their mass and speed, travel long distances while spreading into several paths and cause vigorous damages in infrastructures and sometimes even severe casualties.

In terms of classification, debris flows can be regarded as a particular case of granular-fluid flows. Distinction can be made between granular-fluid flows and so-called dry granular flows, like rock avalanches, in which the interstitial fluid – mostly gas – is of no importance and the dry granular is hindered in its dynamics by the relatively large frictional forces. In the class of granular-fluid flows, debris flows can be distinguished from streams like mud-flows and flash floods, being primarily of a fluid-like behavior. In contrast, debris flows are conditioned by the concurrence of a fluid phase, both driving and lubricating, and a ponderous solid phase. This leads to these kinds of flows being shaped by an ambivalent fluid-like and solid-like behavior, since not only the interstitial fluid is of significant relevance but also the granular particles play an essential role. The present work tries to gain insight into these dynamics and the underlying physical mechanisms.

Since debris flows occur frequently in nature, they represent an important case of granular-fluid flows. An adequate description of the physical mechanisms and the complex flow dynamics, arising from the interaction of multiple phases, is necessary for the understanding, prediction and prevention of damages in these cases – and various models seek to face this task. Modeling needs to depict complex interactions by fairly simple equations and to disregard insignificant mechanisms. Nonetheless, simplistic models can fail to grasp the core of what they seek to describe.

1.1 Modeling debris flow

In the original Savage-Hutter (SH) model, following the Coulomb theory for dry granular material, a rather simple earth-pressure correlation was adopted, coupling the driving, lateral pressure to the vertical stress via an earth pressure coefficient, see Savage & Hutter (1989). Taking up the work of Savage and Hutter and later Iverson (Iverson 1997), Jackson (Jackson 2000) or Pitman and Le (Pitman & Le 2005), the existing models differ in their emphasis on different aspects, selectively segregation

of small and big particles in Gray & Tai (1998), momentum exchange in Pudasaini (2012) as well as the generalization for a more complex terrain (Savage & Hutter 1991, Pudasaini & Hutter 2003). With the introduction of an additional fluid phase, momentum interaction effects were proposed, as well as viscous fluid behavior and sufficient boundary conditions (Pitman & Le 2005, Pudasaini 2012, Meng & Wang 2016).

These different approaches illuminate both the intricacy of the observable behavior and the uncertainties in its description, already for dry granular flows, and all the more for debris flows. Thus, the complexity of a saturated granular structure, arising from the interdependency of different effects, is not fully grasped in many previous works and essential physical mechanisms are not considered. The considerable momentum of the pore-fluid during onset and movement, resulting from pressure peaks, reduces the internal friction: Following an increased load on the granular structure, a rising pore pressure may, in return, press the granular material apart and therefore destabilize the structure itself, increasing its mobility. With this, a stress supporting structure of granular grains may transition into a granular-fluid mass flow and already moving mass may accelerate further – and as the examples mentioned above point out, often heavy rainfall, saturating the pore space and inducing higher pore pressure, has been an apparent triggering mechanism. But even without the presence of an interstitial fluid, the dynamic of granular material exhibits substantial effects not regarded in the aforementioned approaches. The irregular shape of particles and their frictional contact lead to a deformational behavior that is both anelastic and non-linear. On account of this, in the model developed and presented in this work, two additional variables, an *intergranular frictional stress* and an *extra pore-fluid pressure*, are considered. The incorporation of these fields goes back to well established findings in experiments and resulting attempts to model the behavior of granular materials and debris flows. With the presence of the two additional and interacting fields, the questions of their integration in the material behavior needs to be considered, since it is generally not clear, how such new variables enter, e.g., the stress tensor.

An instrument providing guidance in this situation of apparent arbitrariness in conception and modeling is the *thermodynamically consistent* derivation with the Müller-Liu entropy principle. Based on the field of continuum mechanics and the works of Truesdell (Truesdell 1957, Truesdell 1962), it provides a general method for the determination of constitutive relations. The approach contains the derivation of equations for a certain system, providing restriction of the material laws. It helps with the identification of parts that have to be considered whilst modeling the material behavior, especially for the stress tensor, so with this approach, the fields of extra pressure and intergranular stress are incorporated in the model in a thermodynamically consistent manner.

Many models deal with granular materials in the context of continuum mechanics and the entropy principle (Goodman & Cowin 1972, Passman 1977, Ahmadi 1982), using the entropy inequality either in the version of Clausius-Duhem or in that of Müller. The disadvantage is, however, the fact that potential results are quite often very unlikely to be applicable for simulations and calculations without questionable further closure assumptions. An example here is the explicit representation of the Helmholtz free energy, see Fang (2004), or the assumption of pressure equilibrium;

for discussion of the latter, see Schneider & Hutter (2009, p. 183). This makes the thermodynamically consistent modeling a rather academic tool, while most modeling attempts and simulations referring to practical applications are based on other approaches. In this work, the results of the exploitation with the entropy principle are brought to application in a shallow flow model. So in order to proceed with the derivation of an applicable model for debris flow simulations, the system's equations are scaled and depth-integrated due to the flow shallowness, as it was suggested in Savage & Hutter (1989) and afterwards established as the Savage-Hutter-type model class.

With this, we can now explain a first aim and feature of this work: The introduction of a thermodynamically consistent model for debris flows, accounting for the physical mechanisms of pore pressure and hypoplasticity, given as a scaled and depth-integrated system of constitutive and balance equations. With regard to the exploitation of the entropy principle, the main idea and novelty is the inclusion of an equation for the evolution of the dynamic pore pressure in the system of equations as well as in the exploitation of the second law. This enables not only to describe the significant influence of the pore pressure but also to close the unknown parts of the deduced model. Furthermore, it is, to the best of the author's knowledge, a novelty, that such a thermodynamically consistent model for granular flows or debris flows is transferred into the context of a scaled and depth-integrated shallow-flow model.

As the scaling allows for the identification of physically relevant terms, giving a measurement of their impact on the flow dynamics and the significance in relation to each other via the introduced non-dimensional numbers, the depth-integration reduces the computational efforts remarkably, and thus the complexity of the system of equations. The main assumption is that changes of all quantities in the normal depth direction can be neglected, so that the originally 3D system reduces to two dimensions, basically with a projection of all quantities on the basal plane. In return, the considered surface becomes more influential and the choice of coordinates thus challenging. While for a continuous plane, Cartesian coordinates are sufficient, see Savage & Hutter (1989), one needs to introduce a slightly more sophisticated coordinate ansatz in order to describe flows on certain reference surfaces, that resemble, for example, simple laboratory experimental setups. With the introduction of curvilinear coordinates, centrifugal terms enter the equations, accounting for the curvature of the basal surface.

Nonetheless, there are some short-comings of curvilinear-coordinates when it comes to depicting the topography of real mountainous areas, since in such cases, there is not only one clearly distinguishable flow direction in place, but a multitude of rutted channels. Here, so-called general coordinates are capable of both describing the rugged topography by maintaining Cartesian coordinates, and, at the same time, a depth-integrated flow in conjunction with terrain-following coordinates. This method, applied in Tai & Lin (2008), Tai & Kuo (2012) and Tai, Heß & Wang (2018), is possible due to the combination of unified coordinates, developed in Hui, Li & Li (1999), Hui (2004), and the approach of Bouchut & Westdickenberg (2004). It unites both the advantage of reduced equations with respect to the degrees of freedom, keeping computational costs low, but allows for the easy implementation of complex topogra-

phy data, for example from geographic information systems (GISs) and their digital elevation models.

This allows for the introduction of the second major aim of this work: The transfer of the derived equations into terrain-following coordinates and the implementation into a robust numerical framework, utilizable both for laboratory-scale simulations and studies on large scale events. Employing a non-oscillatory central (NOC) scheme, numerical studies are conducted, covering parameter studies for the newly introduced fields, comparison with the results of an experimental dam break study, and a simulation of the Hsiaolin case. With the parameter studies, the influence of the additionally introduced fields is evaluated and first investigations show the potential of the comprehensive consideration of these specific physical mechanisms. The combined influences of hypoplasticity and pore-fluid pressure determine both the shape of the bulk and its dynamics. In particular, it is shown that the consideration of a dynamic pore-fluid pressure allows the bulk mass to prolong its advancement, since the internal friction is lowered and the material is kept from settling. Additional tests illustrate the role of the extra pore-fluid pressure in the onset and acceleration of debris flows. And in contrast, the hypoplastic intergranular friction helps to keep the granular material in shape, preventing it from fluid-like dissolving. This behavior is further clarified with the investigation of a dam break scenario and the comparison of the simulation results with experimental data, showing that due to the new fields, a qualitatively more realistic behavior can be depicted. Further studies on the Hsiaolin case are conducted to illustrate the capacity of the new physical model, as well as of the considered general coordinates in the framework of the utilized computational scheme, enabling to describe events on a large scale. In the course of the landslide that occurred in the mountains of southern Taiwan in August 2009, the village of Hsiaolin was erased after heavy rainfall during typhoon Morakot (Dong, Li, Kuo, Sung, Li, Lee, Chen & Lee 2011, Tai et al. 2018). The presented results show that it is possible to reproduce the course of events of this landslide.

1.2 State of research and progress

The systematization by Liu gave the entropy principle of Müller a wide application. Following the approach of Müller and Liu, the behavior of a material system can be described by a set of balance equations, specified for a certain constitutive class, that is itself derived – or at least restricted – due to a series of steps in the exploitation of the second law of thermodynamics. It has since then been of particular importance for the investigation of mixtures with additional fields and internal variables (Svendsen & Hutter 1995), as well as for the application to granular material and granular-fluid flows (Wang & Hutter 1999c, Wang & Hutter 1999d, Kirchner 2002, Kirchner & Teufel 2002, Schneider & Hutter 2009). For granular materials, the incorporation of an additional equation has been established, describing the development of the inner stress state. With this, the theories of plasticity, and in particular hypoplastic material behavior, have been incorporated in the derivation, thus establishing a thermodynamically

consistent material model with respect to intergranular friction in Svendsen, Hutter & Laloui (1999) and Teufel (2001), taken up later in Schneider & Hutter (2009) and Hutter & Schneider (2010a), Hutter & Schneider (2010b). The concept of *hypoplasticity* seeks to model states of low energy and high grain density, in which, different from momentary quasi-elastic grain-interactions, some sort of frictional contact-forces are dominant (Kolymbas 1991, Wu, Bauer & Kolymbas 1996). In classical hypoplastic approaches, an extra evolution law for the Cauchy stress tensor is applied, leading to some draw-backs. This is avoided by the employment of a new stress-like quantity, represented by a symmetric second order tensor.

A further field of research in this area is the discussion of possible closings for the pressure, as the derivation with the entropy principle leaves behind in part complicated and unclosed terms for which the application of a suitable pressure relation is necessary. While the description of the pore-pressure is well-established in soil mechanics, as well as in certain models for debris flows, like those of Iverson (Iverson & George 2014, Bouchut, Fernández-Nieto, Mangeney & Narbona-Reina 2016), it rarely has found its way into thermodynamically consistent modeling in a rather phenomenological context, to the best of the author's knowledge, see simply the works of Liu (Liu 1980, Liu 2010, Liu 2014), as well as in de Boer & Ehlers (1990). Yet, these models, linking the concept of pore pressure to the inferences of the Müller-Liu entropy principle, are far from being applicable to, or offering a dynamic specification of, the pore pressure. It is worth noting that so far, no evolution equation for an *extra pore-fluid pressure* has been considered in derivations of this context.

We follow Iverson's concept of a dynamic pore-fluid pressure, developed in Iverson & George (2014). This pressure is linked to dilatancy and the development of the extra stress, stating that the changes in the microstructural distribution of the solid can lead to increase and decrease of the pressure. These and other assumptions are merged together; they form an evolution equation for the extra pore-fluid pressure that is adopted here. This dynamic pore pressure allows for the modeling of processes of destabilization, called liquefaction. They are, therefore, responsible for the onset of flows and avalanches, as well as the solidification and settling, when the debris flow comes to rest again.

In terms of the entropy principle of Müller and Liu, a more general diffusion equation is embedded for the pressure, whose source term is later specified according to the pressure equation of Iverson & George (2014). New, and probably not intuitively comprehensible, is the closing assumption of this part, linking some unknown terms and results of the Müller-Liu procedure to the pore-fluid pressure and the configuration pressure, thus closing the system and embedding physical mechanisms in conjunction with the pore pressure. The idea goes back to the aim of including an adequate description of the pore-fluid pressure in this thermodynamic context; a first explicit suggestion can be found in Hutter & Schneider (2010a). Its authors refer to the possibility of incorporating a new evolution equation of the pressure in order to avoid dubious modeling assumptions or simplifications, like the pressure equilibrium, and criticize the lack of a mathematically consistent connection to the mixture equations in existing pore pressure models. This work can be seen as a further contribution to the works

of Schneider and Hutter (Schneider & Hutter 2009, Hutter & Schneider 2010a, Hutter & Schneider 2010b), as well as of de Boer & Ehlers (1990) and Liu (Liu 2014). It seeks to establish ties between the phenomenological foundation of continuum thermodynamics with respect to the entropy principle of Müller and Liu and the applicability of current debris flow models.

Another, largely independent line of development in the theory of granular media does not refer to the entropy principle (and usually also less explicitly to the mixture theory), but deals with the movement of granules, i.e. granular flows. The research interest here was primarily based on the investigation of avalanches, and a first important model was that of Voellmy, a mass-point model that could not yet take into account the deformation of the avalanche mass during motion, see Voellmy (1955)[1] and, for an overview, Hutter & Wang (2016). This changed with the introduction of a new model by Savage and Hutter (Savage & Hutter 1989), which not only found widespread use in the following years, but also brought with it numerous further developments and improvements, so that a model class of its own developed – referred to as the Savage-Hutter (SH) modeling in the following. The SH model is characterized by the use of shallow water-like equations in combination with a closure approach, applying so-called earth-pressure coefficients to link the normal stress, which can be derived with respect to an internal friction angle through scaling and depth-integration, to the lateral stresses, governing the motion of the mass flow. The rheological description is complemented with a Mohr-Coulomb criterion, applied as a boundary condition for the bed friction.

An important field of research was the extensions to granular-fluid mixtures consisting of two phases. It was initiated by Iverson with a model that combines both phases in one equation, see Iverson (1997), and brought further in a two-phase model in which both phases include their own development equations by Pitman and Le (Pitman & Le 2005). Following the two-phase model of Pitman & Le (2005), the interaction between fluid and solid was be taken into account in further works, see Pudasaini (2012) and Meng & Wang (2016), also concerned with an adequate description of the fluid behavior.

Also challenging were developments focusing on models with multiple layers (Hutter & Luca 2012, Luca, Kuo, Hutter & Tai 2012) with further developments in Meng, Wang, Wang & Fischer (2017), as well as in the approach of Bouchut et al. (2016), which considers not only a saturated granular-fluid layer, but also an additional one-phase layer. Other developments investigated the interaction of several granular phases to capture phenomena such as segregation (Gray & Tai 1998, Gray & Thornton 2005, Gray & Chugunov 2006).

Another line of development can be found in the description with so-called quasi-single-phase models, analogously to the one of Iverson (1997) introduced above, and further stimulated in particular by Jackson's work, see Jackson (2000). This was taken up in the work of Pailha & Pouliquen (2009), and Kowalski & McElwaine (2013), the

[1] As noted in Hutter & Wang (2016), a previous avalanche model, usually not referred to, was developed already in 1922 by the french forest engineer Paul Mougin.

latter with an evolution law for the vertical mass center. As for the modeling of the behavior of the granular material, an empirical friction law, also called $\mu(I)$-rheology, has been proposed in a series of works (Jop, Forterre & Pouliquen 2005, Jop, Forterre & Pouliquen 2006), linking the bed friction to an internal friction number that is itself employed for a viscosity law. This rheology has been combined with a depth-averaged approach by Gray & Edwards (2014).

As outlined above, in the general framework of the SH-model, there is a simple relation between stress and shear and between normal and horizontal stresses, dependent on the internal friction angle and the bed friction angle. Thought of as a material behavior, this can roughly capture the behavior of dynamic granular flows, but disregards important aspects of the mechanical behavior of especially debris flows, see Iverson (1997). The pressure is regarded as hydrostatic and well known phenomena like liquefaction are ignored. Furthermore, the deformational paths of soil and variations in stiffness and strength due to the stress levels and density are disregarded (Arnold & Herle 2006). Although rheology is thought to describe the observable macroscopic behavior in rather simple terms, we seek to overcome the apparent lack of descriptiveness by accounting for both the role of a dynamic pore pressure, elaborated first of all in the works of Iverson et al. (Iverson 1997, Savage & Iverson 2003, George & Iverson 2011, Iverson & George 2014), and a hypoplastic relation between stress and strain, following Kolymbas (Kolymbas 1977, Kolymbas 1985, Kolymbas 1991).

Not only the phases discussed and their material models were subject to continuous development, but also the applied coordinate systems and the corresponding topography developed further. This already started in Savage & Hutter (1991) with the introduction of curvilinear coordinates, was continued with the addition of a transverse direction for complex terrain (Gray, Wieland & Hutter 1999, Wieland, Gray & Hutter 1999), and brought further in Tai, Gray, Hutter & Noelle (2001), Pudasaini & Hutter (2003).

Advancement for the treatment of general topography has been achieved with the introduction of general coordinates. Their implementation is a response to the difficulties of complex, rugged topography being treated in the framework of a depth-integrated model and originates in the connection of the so-called unified coordinate method of Hui (Hui et al. 1999, Hui 2004), to the system of terrain-following coordinates of Bouchut & Westdickenberg (2004). They have since then been applied in the work of Tai and coworkers (Tai & Lin 2008, Luca et al. 2012, Tai & Kuo 2012, Tai et al. 2018). For a detailed overview, covering the transfer of model equations to topography-following coordinates, see Luca, Tai & Kuo (2016). With the transformation of the applied system of equations into these respective general coordinates, this line of development is also taken up and extended. A necessary preliminary work was the embedding of the two-phase model of Meng & Wang (2016) in general coordinates, see Tai et al. (2018).

The work starts with a brief summary of the fundamentals of continuum mechanics and mixture theory follows in Chapter 2, together with an introduction to the concept of entropy, the physics of debris flows, as well as some remarks on the notation. In Chapter 3, after a recapitulation on entropy principles, the given system and chosen assumptions are presented, followed by the derivation, the discussion of the results

and a first application to a simple shear flow. With this, the derivation of a scaled and depth-integrated model follows in Chapter 4, accompanied by a discussion of the applied coordinates and the coordinate transformation. The Chapter 5 on numerical simulation follows, covering parameter studies, comparison with experimental results and a case study of the Hsiaolin event, before closing with a conclusion in Chapter 6.

2 Fundamentals and physics

In this chapter, the fundamental concepts providing the frame of this work are presented. Starting with a brief introduction to continuum mechanics and mixture theory in Sections 2.1 and 2.2, some key mechanisms of debris flows are discussed (Section 2.3). Furthermore, the concept of entropy is recapitulated in Section 2.4, followed by remarks on the notation (Section 2.5).

2.1 Continuum mechanics

The foundation of this work is continuum mechanics. It governs the basic principles by which the configuration and continuous motion of an arbitrary three-dimensional body $\mathfrak{B}$ can be described. For a detailed description we refer e.g. to Hutter & Jöhnk (2004) or any other book treating the subject.

The material body $\mathbb{B}$ is assumed to continuously occupy an open region in the three-dimensional space $\mathbb{R}^3$. Any open subset of such a body is again a body, and its elements $\mathfrak{X}$ are allocated to a certain point in $\mathbb{R}^3$. These elements $\mathfrak{X}$, called material particles, are thought to be equipped with densities of physical properties: mass, momentum, energy and possibly more. Figure 2.1 depicts the relation between different configurations and the abstract, material body. All functions are regarded to be referred to the spatial coordinates, i.e., x_i with $i = 1, 2, 3$ and to time t, so $\phi = \phi(x_i, t)$. Specifically, the current configuration $\mathbb{K}$ is defined as the vectorial mapping x_i at time t over the body manifold $\mathbb{B}$:

$$\mathbb{K} : \mathfrak{B} \to \mathbb{R}^3, \quad \mathfrak{X} \to x_i = x_i(\mathfrak{X}, t). \tag{2.1}$$

The motion, also see Fig. 2.1, can be described as a change of configuration over a certain time interval, i.e. the re-allocation $\mathbb{X}$ of the material elements of the body, described by their current mappings. It therefore converts a reference mapping into the current configuration. Thus, the relation between these different configurations is given by

$$\mathbb{X} : \mathbb{R}^3 \to \mathbb{R}^3, \quad \mathbf{x}_0 \to x_i = x_i(\mathbf{x}_0, t). \tag{2.2}$$

The velocity v_i, related to this motion, is then given by the derivative of a re-allocation with respect to time,

$$v_i = \frac{\partial \mathbb{X}}{\partial t} = \frac{\mathrm{d}x_i}{\mathrm{d}t}. \tag{2.3}$$

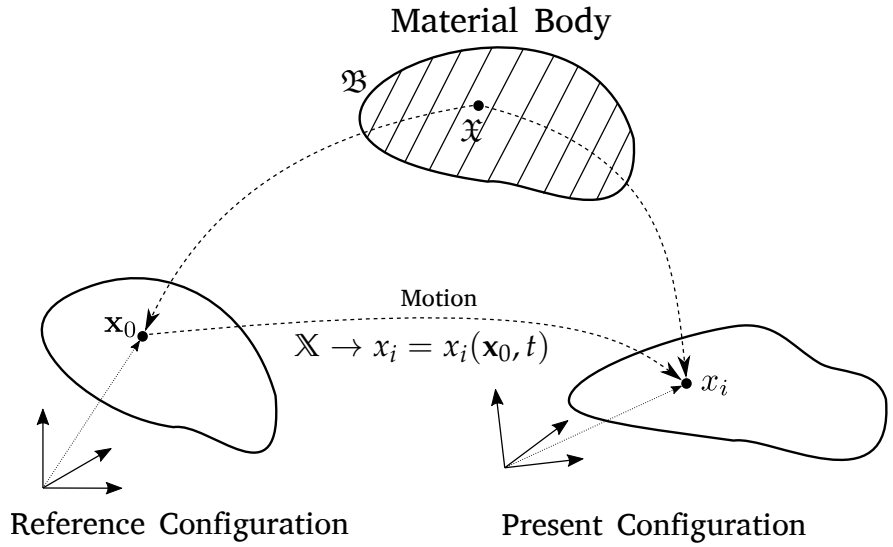

Figure 2.1: The relation between an abstract, material body $\mathbb{B}$ with its elements $\mathfrak{X}$, the initial, reference configuration $\mathbf{x}_0$ and the present one $x_i (i = 1, 2, 3)$ is depicted, after a process of motion $\mathbb{X}$. This figure reproduces a figure of Hutter & Jöhnk (2004).

Furthermore, for the description of certain processes, physical quantities Φ are assigned to the material body as mentioned above. These quantities depend on the position at a certain instant in time and account for a particular property, for example the temperature. For fluids, one usually is referring all functional relations to the position x_i and not the particle $\mathfrak{X}$, so the Eulerian representation is employed. In the following, such a physical quantity or field is accounted for in a material volume V of the Body $\mathfrak{B}$ with its borders ∂V. Hence, a quantity Φ is related to its density ϕ via

$$\Phi = \int_V \phi dV. \tag{2.4}$$

The changes in space and time of such a field are described with the aid of a balance equation. The change of the field Φ over space and time is equal to changes caused by the flux $\mathtt{F} = -\int_{\partial V} \psi_i^\phi n_i ds$ over the boundaries ∂V with a normal vector n_i, the production $\mathtt{P} = \int_V \pi_\phi dV$ in the body itself and the supply $\mathtt{Z} = \int_V \sigma_\phi dV$. Here, we introduced the density ψ_i^ϕ related to the flux of Φ through the boundary ∂V, furthermore, the production density π_ϕ and the supply rate density σ_ϕ, as a source of production outside the body itself. Now, the changes of a quantity Φ indicated by the material derivative in time $d_t\Phi = d\Phi/dt$ can be balanced, viz.,

$$I_\phi : \frac{\mathrm{d}\Phi}{\mathrm{d}t} = \mathtt{F} + \mathtt{P} + \mathtt{Z}. \tag{2.5}$$

With this representation, a balance equation I_ϕ, we can account for the changes of physical quantities in a certain volume and over time, i.e. the development of fields depicting the state of a material body. Since this body is not homogeneous in its

composition, it is further important to describe the concurrence of distinct material phases.

2.2 Mixture theory

Since mixtures and not single constituent bodies are the focus of this work, one must account for a body composed of a set of different continua. Each of these continua is the sum of specific material particles and will be referred to as a constituent $\mathbb{K}^\alpha$. The Greek superscript index indicates that a range of n different constituents, i.e. $\alpha = 1, ..., n$, forms the body. Different approaches exist to cope with this; among these a well known one is the *mixture theory*. Within mixture theory, it is assumed that a multiphase system consists of a number ($\alpha = 1, \dots, n$) of constituents, phases or components that are interpenetrating each other, i.e. equally present at every point in space. This means that such a mixture can be thought of as a superposition of different, continuous phases, each one following own balances of motion and density and further fields, but coupled via interaction terms.

Specifically, a mixture body consists of particles or elements of the *same* number of phases. A material region consisting of $m \geq 2$ subregions with different numbers of subregions is thus composed of m mixture bodies. In the ensuing analysis, it is assumed that all constituents together fill the entire space of the observed volume. A mixture of this quality is called to be *structured*. In contrast, the principle of phase separation only allows one constituent at a certain location, thus splitting the body up into different separated continua, bounded by phase boundaries. Dealing with debris-flows in which granular particles build a skeleton, containing a network of pores, the concept of mixtures is used here, since the small scaled volumes that are occupied by the phases would not allow for a meaningful description of the internal pore surfaces in the material, but calls for a representation that, alike averaging procedures, blurs the small scale distinction between the phases.

The consequences emerging from such metaphysical axioms were expressed by Clifford Truesdell, describing the transfer from continuum mechanics to those of a mixture in his so-called three metaphysical principles, see Truesdell (1984).

In the following, all quantities tagged with a Greek index like Φ^α, belong to a separate phase, whilst those without are mixture quantities Φ. For the balance equation of an arbitrary constituent α this yields

$$I_\phi^\alpha : \frac{\mathrm{d}\Phi^\alpha}{\mathrm{d}t} = \mathtt{F}^\alpha + \mathtt{P}^\alpha + \mathtt{Z}^\alpha. \tag{2.6}$$

For these quantities, an integral representation is employed, as listed in Eq. (2.4) and the subsequent text, while also imposing the continuity and differentiability of the

density fields. Applying the Reynolds and Gauss theorems, see e.g. Hutter & Jöhnk (2004), this leads to the local statement

$$I_\phi^\alpha : \frac{\partial \phi^\alpha}{\partial t} + \frac{\partial v_i^\alpha \phi^\alpha}{\partial x_i} = -\frac{\partial \psi_i^{\phi,\alpha}}{\partial x_i} + \pi_\phi^\alpha + \sigma_\phi^\alpha + \gamma_\phi^\alpha. \tag{2.7}$$

Here, an additional production density appears, since we distinguish now between the self production rate π_ϕ^α of a constituent $\mathbb{K}^\alpha$ and the density γ_ϕ^α accounting for the production rate due to other constituents. So with this, a term describing the interchange of the different phases is supplemented.

To model certain physical behavior, a set of balance equations is assigned to the observed volume. Their choice defines the given system and thus provides the possibility of mathematically describing the aforesaid physical behavior. The equations governing a multiphase system must be similar to those of a homogeneous body, with respect to the occurring interferences. So, with the balance equation I_ϕ for a variable ϕ of the mixture or a homogeneous body, and the corresponding balance equations for the constituents I_ϕ^α, one of Truesdell's principles postulates the equivalence of the sum of the latter ones with I_ϕ,

$$I_\phi = \sum_{\alpha=1}^{n} I_\phi^\alpha. \tag{2.8}$$

This means that all effects of the interaction of different constituents vanish when summed, $\sum_\alpha \gamma_\phi^\alpha = 0$, so that the particular balance equations for a homogeneous body can be applied to the mixture as a whole. Besides, a range of mixture-specific quantities have to be explained; because of the possibility of referring the density either to the volume of the whole body or to the volume of the particular constituent, there are two kinds of densities. With the mass of a constituent m^α and its volume V^α, one has to distinguish between the partial density $\widetilde{\rho}^\alpha = dm^\alpha/dV$ and the true density $\rho^\alpha = dm^\alpha/dV^\alpha$. They are connected via the volume fraction $n^\alpha = \widetilde{\rho}^\alpha/\rho^\alpha$. The density of the mixture is equal to the sum of the partial densities, i.e. $\rho = \sum_\alpha n^\alpha \rho^\alpha$. Whenever the volume fraction is included in a quantity, one can abbreviate this by $\widetilde{\phi}^\alpha = n^\alpha \phi^\alpha$. The diffusion velocity is introduced as $u_i^\alpha = v_i^\alpha - v_i$, with the mixture velocity $v_i = \rho^{-1} \sum_\alpha n^\alpha \rho^\alpha v_i^\alpha$, as the sum of all partial velocities v_i^α and the respective densities, divided by the mixture density. The mixture stress tensor is assembled with $T_{ij} = \sum_\alpha T_{ij}^\alpha - \sum_\alpha \rho^\alpha n^\alpha u_i^\alpha u_j^\alpha$.

Well known statements are the balance equations of mass, $\phi^\alpha \to \widetilde{\rho}^\alpha$, and momentum, $\phi^\alpha \to \widetilde{\rho}^\alpha v_i^\alpha$, which we do not need to derive here; note that, for the sake of brevity, only important results are presented in the following chapters, while most of the calculation is omitted. To gain deeper insight in the fundamental equations and the steps of derivation for comparable systems, see Schneider & Hutter (2009) or Heß (2014). Starting with the mass balance relation for the partial density $\widetilde{\rho}^\alpha$, we derive a similar equation for the volume fraction with a volume production rate $\pi_\phi^\alpha \to n^\alpha$, see e.g. Svendsen & Hutter (1995). With the help of this equation, we can recast the mass

balance to an equation for the true density. Likewise, the balance equations for energy and entropy need no further explanation at this point. We only refer to the latter ones as mixture quantities since it is assumed that the temperature of all constituents is equal, and the assumption of a non-negative entropy production rate should only be valid for the mixture as a whole.

These fields, i.e. density, velocity, temperature and entropy, together with their balance equations of mass, momentum, energy and entropy, denote our *basic system of equations*. They are complemented by a balance equation for the volume fraction, for which different formulations have been proposed, ranging from the very simple mentioned above, which is structured analogously to the balance of mass, to the so-called balance of equilibrated forces. The latter was introduced in Goodman & Cowin (1972) for the evolution of the volume fraction, describing the microstructure of a granular material in its development.

These basic and generally accepted fields, to which the volume fraction is numbered along in the following, are not the focus of further discussion. Of greater interest are fields that supplement and extend the basic quantities, which will be called *additional fields* below. Their introduction and formulation is accompanied by some remarks on the physics of granular-fluid mixtures, especially debris flows.

2.3 The physics of debris flows

There is an extensive literary field about the various physical mechanisms in the context of granular material, granular-fluid mixtures and debris flows. Two key properties are discussed and, with that, accounted for in the following by the additional fields.

2.3.1 Dynamic pore-fluid pressure

Soil can be described as a granular-fluid mixture in a resting state, a network of pores, built by a granular material and filled – completely or in parts – with fluids, such as air and (more or less muddy) water. The contact between granular particles is of frictional nature and can be altered by the pore-fluid. This can be described in terms of the effective stress principle, marking a transition from load on the granular structure into increased pore-fluid pressure, which in return destabilizes the granular structure, as visualized in Fig. 2.2. The granular particles are themselves subject to the pressure of the pore-fluid, which may surround the single particles, as depicted in 2.2b. At the same time, these particles act collectively as a structure that induces pressure upon the pore-fluid, increasing the pressure level of the fluid or even, if possible, squeezing it out of the material, see Fig. 2.2a. Such mechanisms are discussed in soil mechanics since the early works of Fillunger and von Terzaghi on porous media (Terzaghi 1923, Fillunger 1936, Terzaghi 1936), see, for an overview, de Boer & Ehlers

(1990).[1]
With this, it is concluded that the pore-fluid pressure is not hydrostatic and should be modeled accordingly, since it is not only important for the mobilization of debris flows but also affecting the dynamic behavior, preventing the material, once in motion, from resting and, with this, prolonging the runout length. Therefore, the impact of the dynamic pore pressure evolution on the velocity of the granular mass and on their material distribution is apparent.

An approach of Iverson and various coworkers seeks to describe this behavior, developed in a series of publications from early attempts (Iverson & Denlinger 2001, Savage & Iverson 2003), to George & Iverson (2011) and a final formulation (Iverson & George 2014, George & Iverson 2014). We take up the modeling work of Iverson & George (2014), where a diffusion equation for the extra pore-fluid pressure is formulated in conjunction with a depth-integrated model for a granular-fluid mass flow, describing the evolution of the pore-fluid pressure in response to the stress state and the deformational behavior of the granular material. In particular, this is done via the incorporation of dilatancy effects in a source term $\gamma_{\phi}^{\alpha} \rightarrow \gamma_{\varpi}^{f}$, stating

$$\gamma_{\varpi}^{f} = \frac{\mathrm{d}\left(\sigma - \varpi_{h}^{f}\right)}{\mathrm{d}t} - \frac{\dot{\gamma}}{\alpha_{D}} \tan(\psi), \tag{2.9}$$

where the first term induces changes in the stress state, described as the temporal change of the difference between stress state σ and (hydrostatic) fluid pressure ϖ_{h}^{f}, and the second term accounts for changes in the pore space due to shearing, i.e. dilatancy, with the shear rate $\dot{\gamma}$ and the tangent of the dilatancy angle ψ. Denoting a possible volume change due to shearing in granular material, the latter gives a relation between vertical stress to shear stress, i.e. also of the ratio of vertical height difference to shear length. The tangent of the dilatancy angle can be modeled as the difference of the solid volume fraction and its equilibrium value, $\tan(\psi) = \kappa_{\varpi 1}(\nu^{s} - \kappa_{\varpi 2}\nu_{eq}^{s})$, with two coefficients $\kappa_{\varpi 1}$ and $\kappa_{\varpi 2}$. A positive value of the extra pore pressure depicts a state in which the excess pressure unburdens the granular structure and reduces intergranular friction, as the fluid is pushed in between the granular particles. In contrast, a negative extra pore-fluid pressure means that the pore space is absorbing the fluid. So it is apparent, that the pore pressure evolution is connected to the pore space, which is resembled by the fluid volume fraction, respectively also the solid volume fraction in this saturated mixture. This is also captured in the formulation for the tangent of the dilatancy angle: If the actual value of the solid volume fraction is smaller than the equilibrium volume fraction ν_{eq}^{s}, the dilatancy term, $-\tan(\psi) \geq 0$, becomes positive (with $\dot{\gamma} > 0$, $\alpha_{D} > 0$). From this relation, it follows that large values of ν_{eq}^{s} correspond to an increasing extra pore-fluid pressure, since the granular structure allows for a more dense packing until the effects of dilatancy induce a shift to negative values of

[1] In de Boer & Ehlers (1990), a historical outline retraces the origin of the concept of effective stresses in Fillunger's works, which have often been disregarded by the following developments in soil mechanics. The tragic conflict between these two researching pioneers in soil mechanics, Fillunger and von Terzaghi, is highlighted in de Boer (2005).

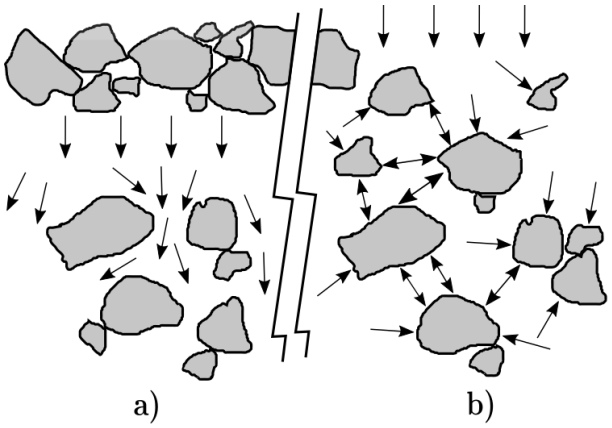

Figure 2.2: Pore-fluid pressure mechanism during loading cycle. Panel **a)** on the left-hand side illustrates how the granular skeleton transfers external forces into extra fluid pressure and, on the right-hand side in panel **b)**, this pore-fluid pressure subsequently presses apart the granular material.

this part of the source term, linked to decreasing extra pore pressure. For the modeling of $\nu^s_{eq} = \hat{\nu}^s_{eq}(\nu^s_C, \dot{\gamma}, \mu^f, \delta_P)$, including values for the average particle size δ_P, the fluid viscosity μ^f and the critical volume fraction ν^s_C, we refer to the detailed derivation in Iverson & George (2014). This approach has been adopted and included in the modeling process of this work. Also note that different dynamic pressure models are presented in various works (Goren, Aharonov, Sparks & Toussaint 2010, Kowalski & McElwaine 2013, Bouchut et al. 2016), but will not be subject to further discussion.

2.3.2 Intergranular friction

Besides this interdependency of pore-fluid pressure and granular material, the behavior of (also just dry) granular material can be tackled with hypoplasticity. This concept reflects the dependence of the stress on the deformational history of the granular material, i.e that the material exhibits different paths of deformation during loading and unloading. Going back to Kolymbas (Kolymbas 1977, Kolymbas 1991), hypoplasticity enhanced previous approaches of elasto-plasticity and has been adopted in various works, see, e.g., Bauer (1996), Wu et al. (1996) or Arnold & Herle (2006), and, for a comparison to elasto-plasticity, Niemunis (1993).

Hypoplasticity establishes a model for the development of stress and contact forces in simple granular skeletons, see Fig 2.3 and also Fig. 3 in Herle & Gudehus (1999), together with the companying explanation for more details. The idea is that the temporal evolution of a stress tensor, described with an objective, corotational time-derivative, as introduced by Jaumann, can be balanced by a source term Φ^s_{ij} that comprises both a linear and a nonlinear part, **L** and **N**, respectively. While the first part, linear with respect to D^s_{ij}, couples the temporal development of the stress to a product of the stress state itself and the strain rate, the nonlinear term introduces a

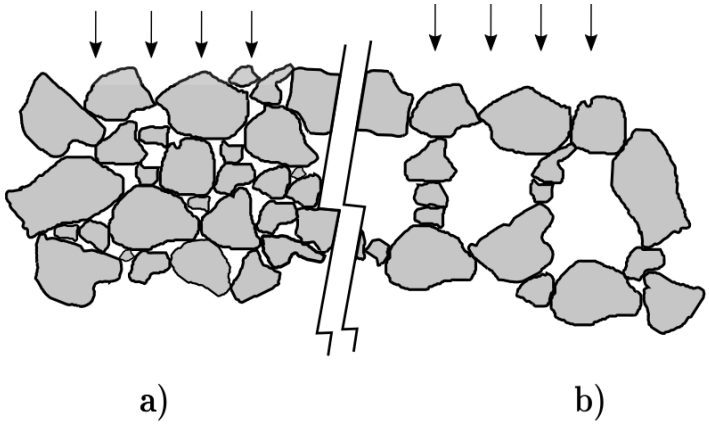

Figure 2.3: Intergranular transmission of load with respect to different microstructures: Panel **a)** on the left-hand side shows a dense granular skeleton that will redirect forces in a different way than the skeleton depicted on the right-hand side in **b)**, which will likely reduce the pore space. Even more, since the structure in panel **b)** will change under load, e.g. to a structure alike the one depicted in panel **a)**, it will react in different way if the load is changing or reversed.

rate-dependent behavior. Following the formulation in Teufel (2001) and Fang, Wang & Hutter (2006), the source term is employed as

$$\begin{aligned}\Phi_{ij}^s =& \mathbf{L}(Z_{ij}^s, D_{ij}^s) + \mathbf{N}(Z_{ij}^s)|D_{ij}^s| \\ =& f_S \left(a_Z^s D_{ij}^s + \frac{Z_{ij}^s Z_{kl}^s D_{kl}^s}{(Z_{mm}^s)^2} + f_D a_Z^s |D_{ij}^s| \left(\frac{Z_{ij}^s}{Z_{mm}^s} + \frac{\mathrm{dev}(Z_{ij}^s)}{Z_{mm}^s} \right) \right),\end{aligned} \tag{2.10}$$

where, the absolute value of the strain tensor, equivalent here to the strain rate, is $|D_{ij}^s| = \sqrt{D_{ik}^s D_{ki}^s}$ and the deviatoric part of the evolution of the intergranular stress tensor Z_{ij}^s is given as $\mathrm{dev}(Z_{ij}^s) = Z_{ij}^s - \frac{1}{3} Z_{kk}^s \delta_{ij}$. Further material parameters, such as the stiffness factor f_s and the density factor f_D, as well as a_Z^s, will be introduced later, see Section 4.5. At this point it is worth noting that their formulation will be related to several limiting values of the solid volume fraction, referring to the microstructure of the granular material in its development and thus the relation between pore-fluid and the pore space.

2.3.3 Material behavior and additional fields

As pointed out above in Section 2.2, the general system of equations, used to describe a general flow, consists of the basic balance equations for mass, momentum and energy, supplemented by the corresponding material laws, for example for the stress tensor and the momentum interactive terms. Furthermore, the incorporation of additional equations is needed, describing the development of certain material properties, the so-called inner or *internal variables*, which are, with the exception of the volume fraction, equivalent to the previously introduced additional fields. So in our case, these

quantities further describing the internal behavior include the volume fraction, an internal stress and the extra pore-fluid pressure. And while the volume fraction depicts the inner material distribution and some sort of internal structure, sometimes also specified by the balance of equilibrated forces, the internal stress – not to be confused with the stress in the material itself – embeds hypoplastic material behavior. Moreover, the interdependency of the fluid pressure and the solid component is depicted via a pressure-diffusion equation.

An important presupposition is the possibility of the representation of certain physical mechanisms by corresponding evolution equations for the development of "abstract" quantities, provided that source and flux terms are equally correctly given. The introduced evolution equations for additional degrees of freedom and the corresponding inner variables can be connected via physical argumentation to other parts of the system. Here, this means especially to the remaining unknown quantities, to close the system. Svendsen (Svendsen 1999) points out that the volume fraction is an additional degree of freedom due to the microstructure of the material that is not completely determined by the other quantities of the field; therefore, a supplementary equation, describing this field, is needed. The same can be said of a dynamic pore pressure. It can easily be thought as some kind of intermediary quantity for the transmission of forces as well, while, for example, a hydrostatic pressure is fully determined by other quantities. For a description in terms of internal variables, see Papenfuss & Forest (2006).

With that, we generalize the concepts presented above to a mixture of α constituents and introduce a quantity ϖ^α, referring to partial pressure, with a balance law $\phi^\alpha \to \varpi^\alpha$ accounting for its evolution due to flux $\psi_i^{\varpi,\alpha} = -\kappa_\varpi^\alpha \partial_i \varpi^\alpha$, where κ_ϖ^α is a pressure flux parameter, and production $\gamma_\phi^\alpha \to \gamma_\varpi^\alpha$,

$$\frac{\partial \varpi^\alpha}{\partial t} + v_i^\alpha \frac{\partial \varpi^\alpha}{\partial x_i} = \frac{\partial}{\partial x_i}\left(\kappa_\varpi^\alpha \frac{\partial \varpi^\alpha}{\partial x_i}\right) + \gamma_\varpi^\alpha. \tag{2.11}$$

Furthermore, taking up the theory of hypoplasticity, another balance law for the mechanism of inner contact stress in the granular material is deployed with $\phi^\alpha \to Z_{ij}^\alpha$, consisting of the co-rotational time derivative on the left-hand and a production rate $\pi_\phi^\alpha \to \pi_{ij,Z}^\alpha = \Phi_{ij}^\alpha$, see Eq. (2.10), on the right-hand side,

$$\begin{aligned} \overset{\triangle}{Z}{}_{ij}^\alpha &= \Phi_Z^\alpha : \\ \overset{\triangle}{Z}{}_{ij}^\alpha = \frac{\partial Z_{ij}^\alpha}{\partial t} + v_k^\alpha \frac{\partial Z_{ij}^\alpha}{\partial x_k} + Z_{ik}^\alpha W_{kj}^\alpha - W_{ik}^\alpha Z_{kj}^\alpha &= \nu^\alpha \sum_{\beta=1}^{n} \frac{\left(\rho^\alpha - \rho^\beta\right)}{\rho} \frac{\partial v_k^\alpha}{\partial x_k} Z_{ij}^\alpha + \Phi_{ij}^\alpha. \end{aligned} \tag{2.12}$$

For details see Schneider & Hutter (2009). The material time derivative $\mathrm{d}_t Z_{ij}^\alpha$ is supplemented with a rotational term, usually described with Lie brackets as $[W_{ij}^\alpha, Z_{ij}^\alpha]$ and employing the spin tensor $W_{ij}^\alpha = \frac{1}{2}(\partial_j v_i^\alpha - \partial_i v_j^\alpha)$. The resulting co-rotated time derivative, also Jaumann stress rate, is a special form of the Lie derivative, appropriate for stress changes under rotation. For a discussion of different stress rate in the context

of hypoplasticity, see Kolymbas & Herle (2003). The constitutive term Φ_{ij}^{α} is enhanced with a further term $\rho^{-1}\nu^{\alpha}\sum_{\beta}\left(\rho^{\alpha}-\rho^{\beta}\right)\left(\partial_k v_k^{\alpha}\right)Z_{ij}^{\alpha}$, which is explained below, together constituting the influence due to self production. Also note that Eqs. (2.11) and (2.12) apply $v_i\partial_i(\phi)$ instead of the conservative form $\partial_i(v_i\phi)$ since this form applied for the derivation with the entropy principle. The occurring differences are affecting only the isotropic part of the equilibrium stress tensor and are rather little, but will not be discussed here.

Now that various additional fields have been introduced in a general, the question arises as to how these fields affect material behavior. Here, the entropy principle offers an assistance, which is why the idea behind, namely the concept of entropy, will be presented first.

2.4 The concept of entropy

The term entropy was introduced by Rudolf Clausius in 1865 to describe certain observations in connection with heat transport and conversion, see Clausius (1865). His descriptions adopted some earlier discoveries, among others by Nicolas Leonard Sadi Carnot and Antoine Laurent de Lavosier, regarding the nature of heat and following debates around the portability of energy. The driving insight was that processes of energy transformation seem to have a clear preferential direction in time. This was in particular a constraint to the enthusiastic perceptions of the energy principle, the first law of thermodynamics, that promised the prospect of unlimited energy sources and convertibility. In other words, while the convertibility of energy contained a *promise*, regarding the transfer of human labor into material wealth, the ideas of fatigue or entropy rather implied a drawback in terms of potential progress.[2]

The discussions around the term entropy followed a speculative reasoning about a substance analogously to heat, which itself could be governed by similar balance laws. Thus, rather than resulting solely from precise and quantitative physical measurements, the term entropy also denotes qualitative observations and insights, and determined the establishment of a second law of thermodynamics. This second law or *entropy principle* basically states that not every form of energy is convertible equally in other forms of energy, so while, for example, mechanical work can be transformed into heat completely, this is not possible in reverse. While there were first statistical formulations for these circumstances by Ludwig Boltzmann and Josiah Willard Gibbs, a formulation in the framework of continuum mechanics was established by Pierre Maurice Marie Duhem with regard to the work and less general formulations of Clausius, thus named the Clausius-Duhem inequality. In this inequality, the entropy is in particular linked to the development of the internal energy (Gurtin & Williams 1966).

[2] Authors like Rabinbach (1992) argue that the formulation of the concept of entropy reflects the historical upheavals of early modernity, drawing a parallel from the articulation of critique (regarding maldevelopment and contradictions of the new system of factories, social shifts and rapidly growing slums) to a, maybe subliminal, awareness in science and scientific findings for the limitation both of newly developed technical possibilities and natural resources.

In the theoretical discussions that accompanied the development of thermodynamics, in the years following Clausius and Duhem, a distinction was drawn between thermodynamics and thermostatics, particularly with recourse to the work of Gibbs. Differing from thermostatics and their treatment of equilibrium states (or those close to equilibrium), Carl Eckart and Josef Meixner established a theory for the thermodynamics of irreversible processes in the 1940s (Eckart 1940a, Eckart 1940b, Eckart 1940c, Meixner 1943, Eckart 1948). Taking up their work, Clifford Truesdell (Truesdell 1957, Truesdell 1962), extended these thoughts and their implications, establishing a school of thought called *rational thermodynamics*, especially interested in the mathematical consequences, as well as in the formulation of a continuum mechanical mixture theory. The mixture theory suggested by Truesdell was able to present a systematic approach for multicomponent fluid systems, incorporating previous ad hoc approaches, e.g. of Fick and Jaumann, see Hutter & Wang (2003) and Wilmański (2005).

In the framework of rational thermodynamics, a range of works was concerned with the further investigation of mixtures, see Noll (1958) and Truesdell (1962). Bernhard Coleman and Walter Noll extended the consequences of the second law for continuum mechanics and Truesdell's mixture theory, so their work pioneered the attempts of thermodynamically consistent derivation, employing the Clausius-Duhem inequality (Coleman & Noll 1963). Many works in the field of mixtures of fluids and plasticity followed their approach, which became known as the *Coleman-Noll entropy principle* (Coleman & Gurtin 1967, Nunziato & Walsh 1980, Passman, Nunziato & Walsh 1984), also including research on internal state variables and chemical reactions. Of further interest here is in particular the investigation of how thermodynamic restrictions can be applied to a theory of plasticity, see Green & Naghdi (1965), and the prominent work of Goodman & Cowin (1972), establishing a continuum theory for granular media with recourse to the entropy principle. It is also here, in Goodman & Cowin (1972), that the volume fraction is introduced as an additional field including an own balance equation; a concept that was soon picked up in different works.

This approach utilizing the entropy principle, i.e. the entropy inequality, to systematically derive constraints on constitutive functions was further enhanced by Ingo Müller, switching from the Clausius-Duhem inequality to a more general formulation of the second law, see Müller (1968) as well as Müller (1971a), Müller (1971b). The new approach was then formalized by I-Shih Liu (Liu 1972a), arriving at the algorithmic form which is called the *Müller-Liu entropy principle*. An overview can be found in Müller & Liu (1984), and, for a comparison between the approaches of Coleman-Noll and Müller-Liu, see Wang & Hutter (1999a) and Triani, Papenfuss, Cimmelli & Muschik (2008).

Since it is generally accepted that the entropy principle must hold, the entropy principle plays a special role in the field of physical modeling. Rather than a constraint on processes, this can be seen as a restriction of the material models, so one can derive constraints in terms of the material behavior; what this means will be unfurled in the next chapter. For more details on the topic of entropy and entropy principles, Hutter & Wang (2003) and Wang & Hutter (2018) are recommended, as well as Ingo Müller's

book (Müller 2007), for an extensive overview both on the history of thermodynamics and the entropy principle, as well as on the arousing philosophical debates.

2.5 On the notation

Before coming to the specific constraints following from the entropy principle and their mathematical derivation, some remarks on applied notation are necessary, to simplify the further understanding of the work:

- In general, index notation is applied for coordinates and vectors, unless it serves the purpose of clarity, to deviate from it, e.g.: $\phi_i, i = 1, 2, 3$.
- The (unspecified) phases of the mixture are denoted with superscript Greek letters, later specified to (s) and (f) for solid and fluid, respectively, e.g.: $\phi^\alpha, \alpha = s, f$.
- A small index b denotes that the value is given at the basal plane: ϕ_b.
- A superscript 0 can denote the constant of a parameter function, e.g. as $\phi = \phi^0 \cdot f(x_i, t)$, and, with a vertical bar, the initial values of a field: $\phi|^0 = \phi(x_i, t = 0)$.
- A tilde over a quantity denotes a partial quantity, i.e. derived with respect to the partial volume: $\widetilde{\phi}^\alpha = \nu^\alpha \phi^\alpha$.
- A superscript asterisk denotes a non-dimensional value: ϕ^*.
- An overbar is used to denote depth-integrated values: $\overline{\phi}$.
- If convenient, partial and material derivatives are written in a short-form, e.g.: $\partial_i \phi = \frac{\partial \phi}{\partial x_i}$.

A short introduction to continuum mechanics and mixture theory has been given in this chapter, together with some remarks on the underlying physical mechanisms and the concept of entropy. In the next chapter, the employed material and its constitutive functions are constrained with regard to the exploitation of the entropy principle.

3 Entropy principle and thermodynamically consistent derivation

As described above, in the context of continuum mechanics, Truesdell (Truesdell 1957, Truesdell 1962) proposed a set of heuristic postulates on the interdependence and mathematical specification of the distinct phases within a mixture, known as *mixture theory*. In particular, it is assumed that every point in space is simultaneously occupied by every phase, and that each phase is governed by the same balance laws as the mixture, amended by additional terms that account for interchanges between the phases. Müller (1968), generalizing the previous work of Coleman and Noll (Coleman & Noll 1963), complemented these postulates by suggesting that for every process, i.e. the solutions of the balance laws, the constitutive functions of such a mixture (and its constituents) are restricted by the need to obey the second law of thermodynamics. The latter was posed in terms of an *entropy inequality*, introduced in Müller (1967), expressing the fact that the entropy production in the system is non-negative. This entropy principle was brought into an algorithmic form, known as the Müller-Liu (ML) entropy principle, by Liu, see Liu (1972a).

In the following chapter, the general method of evaluation, based on the entropy principle of Müller and Liu, is presented (Section 3.1), before the used system as well as limitations and assumptions are discussed in Section 3.2. This is followed by the exploitation of the entropy principle and the presentation of the results (in Sections 3.3 and 3.4), which are finally applied to the case of a simple shear flow in Section 3.5.

3.1 Entropy principles: an outline

Following the summary in Cheviakov & Heß (2018), we first outline the main points of Müller (1968), both to present his approach and to compare it with the more general, systematic Müller-Liu algorithm that will follow. We conclude this section with a few thoughts on the computational treatment of such modeling approaches and refer to a new, solution set-based approach.

3.1.1 Müller's original approach

1. A mixture of substances involving several constituents is considered.
2. The classical partial differential equations (PDEs) describing the dynamics of the mixture in Eulerian coordinates (balance of mass, momentum, and internal

energy) are written for each phase, and for the mixture as a whole. The momentum equations involve an additional source term, responsible for inter-species interactions. The energy supply term of the energy equation includes a radiation part, ρr_R.

3. An entropy production inequality is formulated, accounting for the entropy advection, spatial fluxes, and external supply. With this, it is stated that physically relevant thermodynamic processes satisfy the entropy inequality.

4. The external entropy supply term is assumed to equal the external radiative energy supply divided by the temperature:

$$\sigma^{\rho\eta} = r_R/\theta. \tag{3.1}$$

It should be noted that the condition holds for perfect gases, but is not generally true for other substances.

5. The constitutive functions of the model, to be determined, include the densities of energy and entropy (in terms of the specific free energy function) and energy and entropy fluxes (accounted for as flux vectors). Additionally, the stress tensor of the medium, the entropy and energy fluxes, and constituent mass production terms, are also treated as unknown constitutive functions.

6. In the entropy production inequality, the external entropy supply term $\sigma^{\rho\eta}$ is replaced by terms of the energy balance equation, using (3.1). In the energy balance equation, in turn, the inter-species interaction term is substituted through a similar term in the momentum balance equation. As a result, the entropy inequality becomes a linear combination involving essential parts of the energy and momentum equations. This form may be referred to as *the extended form of the entropy inequality*.

7. A form of the constitutive functions, involving dependent variables of the problem and their specific partial derivatives, is assumed, and simplified according to Noll's principle of material objectivity.

8. Several additional simplifying assumptions on the form of constitutive functions are made, including linear dependence on certain higher derivatives of the dependent variables.

9. The constitutive functions are substituted in the entropy inequality in its extended form. In the result, which is linear in certain highest derivatives of the field variables, the corresponding terms are collected.

10. Since the extended entropy production inequality is required to hold for *all* solutions of the dynamic balance equations, the independent partial derivatives can assume any value. This allows one to set the corresponding coefficients to zero.

11. One consequently obtains an underdetermined set of partial differential equations for the unknown constitutive functions, providing restrictions on the previously posed forms of these constitutive functions.

The original form of Müller's approach, as outlined above, is mathematically and physically sound, yet applicable only to models described by PDEs with source terms of rather special structure, which makes it, in general, not applicable to a broad range of modeling problems.

3.1.2 Liu's Lemma and the Müller-Liu approach

The procedure outlined above has been extended first in Müller (1971b), and then by Liu (Liu 1972a), through the consideration of a constrained entropy inequality and the use of Lagrange multipliers, resulting in what is generally known as the entropy principle of Müller and Liu. In their approach, all external supply terms are neglected, since they are said to not affect the material behavior. Instead of a sequence of substitutions that yields a linear combination of source-free energy and momentum equations within the entropy inequality, as in Müller's original work, the Müller-Liu procedure gives a similar, extended entropy inequality by the addition of the dynamic equations of the model, forming a linear combination. The application of Liu's lemma to this extended entropy inequality leads to constraints on the constitutive functions, referred to as Liu identities. Even though it was formulated for algebraic equations, the Lemma is generally used to analyze entropy-type inequalities, provided that the model of interest is linear in some parametric derivatives. Since an important subsequent work of Müller, see Müller (1971b), is written in German, for further information the reader may refer to Hutter (1977), which contains both a general overview of the method and a comparison with other methods.

Liu's generalized approach (Liu 1972a, Liu 1972b, Müller & Liu 1984) is based on the following lemma, stated for linear algebraic equations.

Lemma 1 (Liu) *Let $\varphi \in \mathbb{R}^p$ and let M be a $p \times n$ real matrix. Consider a linear system $M\boldsymbol{\phi} + \varphi = 0$ of p equations on the components of the unknown vector $\boldsymbol{\phi} \in \mathbb{R}^n$, with a non-empty solution set S. Let also $\mathbf{a} \in \mathbb{R}^n$, $\mathbf{a} \neq 0$, and $\beta \in \mathbb{R}$ be given. Then the following statements are equivalent to each other:*

1. $\forall \boldsymbol{\phi} \in S$, $\mathbf{a}^T\boldsymbol{\phi} + \beta \geq 0$;
2. $\exists \lambda \in \mathbb{R}^p$ *such that* $\forall \boldsymbol{\phi} \in \mathbb{R}^n$, $\mathbf{a}^T\boldsymbol{\phi} + \beta - \lambda^T(M\boldsymbol{\phi} + \varphi) \geq 0$;
3. $\exists \lambda \in \mathbb{R}^p$ *such that* $\mathbf{a} = M^T\lambda$, *and* $\beta \geq \lambda^T\varphi$.

In contrast to Müller's procedure (Müller 1968), in Liu's approach, all external source terms are neglected, and the coupling of the set of balance equations is achieved through the introduction of so-called Lagrange multipliers. Instead of a sequence of substitutions, every equation I_ϕ of the given system is regarded as a constraint on the entropy inequality, with a respective Lagrange multiplier $\lambda \to \lambda_\phi$. The inequality for the mixture entropy density η^s is introduced as

$$\mathbf{I}_\eta : \frac{\partial \rho\eta^s}{\partial t} + \frac{\partial \rho\eta^s v_i}{\partial x_i} + \frac{\partial \psi_i^{\rho\eta}}{\partial x_i} - \sigma^{\rho\eta} = \pi^{\rho\eta} \geq 0, \tag{3.2}$$

with the entropy flux density $\psi_i^{\rho\eta}$, the entropy supply $\sigma^{\rho\eta}$ and the central assumption that the entropy production density is non-negative, $\pi^{\rho\eta} \geq 0$. Furthermore, with the system's balance equations being brought into a form in which their right-hand sides (RHSs) are equal to zero, so that $I_\phi \to \mathbf{I}_\phi$, with $\mathbf{I}_\phi = 0$ being a reformulation of the balance equation I_ϕ, a linear combination

$$\mathfrak{I}_\eta : \ \mathbf{I}_\eta - \sum_\phi \lambda_\phi \mathbf{I}_\phi \geq 0 \tag{3.3}$$

is called the *extended entropy inequality*. Again, the constitutive functions with their postulated dependencies ϕ_C are substituted into Eq. (3.3), and the coefficients of the highest derivatives are set to zero, in accordance with Lemma 1. This yields constraint equations, called the *Liu identities*, and a residual entropy inequality, as constraints on the constitutive functions. The entropy principle in its formulation by Müller and Liu has been used in numerous works to the present, including both articles (Liu 2014, Reis & Wang 2016, Heß et al. 2017) as well as extensive books (Müller & Ruggeri 1998, Liu 2002, Hutter & Jöhnk 2004, Schneider & Hutter 2009).
According to equation (3.3), the Müller-Liu approach is based on the linear superposition of the entropy inequality and the governing equations. It is appropriate only in the special case of linearly occurring highest derivatives, and there is no relationship between such derivatives. With this, the linear algebra-based Lemma 1 holds for the differential equations, and the Liu identities yield meaningful restrictions on constitutive functions. Also note that Liu's algorithm can be utilized for models that do not necessarily have the entropy defined. Instead, one generally considers an inequality formulated for a scalar, additive and objective thermodynamic constitutive quantity η^s, which we still refer to as "entropy" below, see Hauser & Kirchner (2002).

3.1.3 A solution set-based approach

As a result of Heß & Cheviakov (2019), a re-formulation of the entropy principle in a physically and mathematically sound form has been presented, proposed in the spirit of the approach suggested by Müller in his later works (Müller 1970, Müller 1971a, Müller 1971b). The proposed algorithm, called *solution set-based approach*, offers the technical flexibility of Liu's algorithm, i.e. the splitting of the problem by setting to zero the coefficients at "free" higher-order derivatives, but provides a necessary and sufficient condition for the entropy inequality to hold, through the consideration of the entropy inequality on the solution manifold of the given model. The latter is achieved through the use of substitutions of a set of *leading derivatives* of the model PDEs and their differential consequences. In other words, the proposed algorithm is a mathematically justified nonlinear generalization of the classical Müller-Liu procedure, related to Müller's revised approach in his mostly neglected work (Müller 1970), providing a more precise, and usually less restrictive set of constraints on the constitutive

functions of interest. It should be noted that the solution set approach does not require the use of the Lagrange multipliers in any form, thus the number of unknown functions compared to the Müller-Liu algorithm is significantly reduced. Moreover, the simplification of constraint equations following from the solution set approach allows for *classification* (case splitting) that leads to separate families of admissible constitutive dependencies.
Similar to the original Müller-Liu algorithm and its implementation in Cheviakov & Heß (2018) the newly proposed solution set-based approach is fully algorithmic, and is implemented using the existing `GeM` package for `Maple` computer algebra system. The `GeM` package, originally created for symbolic calculations of Lie-type symmetries and conservation laws of differential equations, represents a PDE system in a symbolic form, which allows for efficient collection of coefficients in (differential) polynomial expressions, and thus the automated generation of constraint equations on the constitutive functions (Cheviakov 2007, Cheviakov 2010a, Cheviakov 2010b). The constraint equations can be consequently simplified using the efficient `rifsimp` routine, and possibly solved explicitly using the built-in `Maple` PDE solver. Nonetheless, the derivation below has been achieved with the classical ML entropy principle. In the following, we introduce the system of equations and respective assumptions, before proceeding with the exploitation of the entropy principle.

3.2 The governing system and limiting assumptions

We now seek to describe the fields trough a combined set of equations, determining the thermodynamic process within the considered continuum. This system consists of the following set of equations, describing the thermodynamic process as their solution with certain boundary conditions:

$$
\left.\begin{aligned}
&\text{Balance of mass}\\
&\mathcal{R}^\alpha = \nu^\alpha \frac{\partial \rho^\alpha}{\partial t} + \nu^\alpha v_i^\alpha \frac{\partial \rho^\alpha}{\partial x_i} - \nu^\alpha \rho^\alpha c^\alpha + \rho^\alpha n^\alpha = 0;\\
&\text{Balance of momentum}\\
&\mathcal{M}_i^\alpha = \nu^\alpha \frac{\partial \rho^\alpha v_i^\alpha}{\partial t} + \nu^\alpha v_j^\alpha \frac{\partial \rho^\alpha v_i^\alpha}{\partial x_j} - \frac{\partial T_{ij}^\alpha}{\partial x_j} - \rho^\alpha \nu^\alpha g_i - m_i^\alpha + \rho^\alpha v_i^\alpha n^\alpha = 0;\\
&\text{Balance of energy}\\
&\mathcal{E} = \frac{\partial \rho\varepsilon}{\partial t} + \frac{\partial \rho\varepsilon v_i}{\partial x_i} + \frac{\partial q_i}{\partial x_i} - T_{ij}\frac{\partial v_i}{\partial x_j} - \rho r_R = 0;\\
&\text{Evolution equation for the volume fraction}\\
&\mathcal{V}^\alpha = \frac{\partial \nu^\alpha}{\partial t} + \frac{\partial \nu^\alpha v_i^\alpha}{\partial x_i} - n^\alpha = 0;\\
&\text{Evolution equation for the inner stress}\\
&\mathcal{Z}_{ij}^\alpha = \frac{\partial Z_{ij}^\alpha}{\partial t} + v_k^\alpha \frac{\partial Z_{ij}^\alpha}{\partial x_k} + Z_{ik}^\alpha W_{kj}^\alpha - W_{ik}^\alpha Z_{kj}^\alpha - \nu^\alpha \sum_{\beta=1}^{n} \frac{\left(\rho^\alpha - \rho^\beta\right)}{\rho} \frac{\partial v_k^\alpha}{\partial x_k} Z_{ij}^\alpha - \Phi_{ij}^\alpha = 0;\\
&\text{Evolution equation for a partial pressure}\\
&\mathcal{W}^\alpha = \frac{\partial \varpi^\alpha}{\partial t} + \frac{\partial \varpi^\alpha}{\partial x_i}\left(v_i^\alpha - \Delta_i^{\alpha,\varpi}\right) - \kappa_\varpi^\alpha \frac{\partial^2 \varpi^\alpha}{\partial x_i \partial x_i} - \gamma_\varpi^\alpha = 0;\\
&\text{Entropy Balance}\\
&\mathcal{N} = \frac{\partial \rho\eta^s}{\partial t} + \frac{\partial \rho\eta^s v_i}{\partial x_i} + \frac{\partial \psi_i^{\rho\eta}}{\partial x_i} - \sigma^{\rho\eta} = \pi^{\rho\eta} \geq 0.
\end{aligned}\right\} \tag{3.4}
$$

These equations describe the development of certain fields, including the constituent true density ρ^α and volume fraction ν^α, the velocity v_i^α, the inner stress Z_{ij}^α and the partial pressure ϖ^α. Furthermore, the internal energy ε or empirical temperature θ of the mixture, as well as its entropy η^s are incorporated in the system and depicted through an equation. We are referring to the thermal temperature, describing the fluctuation energy of atoms and molecules, not the granular one. Besides, there is a range of quantities, describing in particular the material behavior: the constituent stress tensor T_{ij}^α and that of the mixture T_{ij}, the momentum interaction term m_i^α, the heat flux vector of the mixture q_i and the pressure flux coefficient κ_ϖ^α, with a further pressure flux quantity $\Delta_i^{\alpha,\varpi}$. A range of production terms and external influences affect the fields, beginning with the corresponding production rates c^α for mass and n^α for the volume fraction, as well as the source terms Φ_{ij}^α for Z_{ij}^α and γ_ϖ^α for ϖ^α, and finally, as external influences, the radiation r_R and the gravity g_i. The entropy balance is composed of an entropy flux $\psi_i^{\rho\eta}$, a supply rate $\sigma^{\rho\eta}$ and a production rate density $\pi^{\rho\eta}$. Also note that modifications in comparison with the usual or expected form of some of the equations have been applied, like the incorporation of an additional term in $\mathcal{Z}_{ij}^\alpha$, the introduction of a more general variable $\Delta_i^{\alpha,\varpi}$ instead of $\partial_i \kappa_\varpi^\alpha$, as well as the balance equations of mass $\mathcal{R}^\alpha$ and momentum $\mathcal{M}_i^\alpha$, which are employed for the true, not the partial density. To get Eq. $(3.4)_1$, one may start from

$$\frac{\partial \nu^\alpha \rho^\alpha}{\partial t} + \frac{\partial \nu^\alpha v_i^\alpha \rho^\alpha}{\partial x_i} = \nu^\alpha \rho^\alpha c^\alpha,$$

perform the product differentiations and substitute the evolution equation for the volume fraction $(3.4)_4$; the result is $(3.4)_1$. Equation $(3.4)_2$ can be derived in a similar way from the balance of momentum with the partial density. While the balance equations of mass, momentum and internal energy are well-known and need no further justification, for the evolution equation $(3.4)_4$ we mention that it is postulational and not based on a solid physical law. As already pointed out, the literature also knows different versions. Among these are Goodman-Cowin's (Goodman & Cowin 1972), Wilmański's (Wilmański 1996), Bluhm's (Bluhm, de Boer & Wilmański 1995) and Fang's versions (Fang 2016a, Fang 2016b), which are all distinct from one another. And as introduced in Section 2.3.3, in Eq. $(3.4)_5$, the first four terms on the RHS combine together to an objective time derivative (Lie derivative) of Z_{ij}^α.

At this point we highlight a difference in the apparent variables. There is one class of quantities which describes the properties of the state of the observed thermodynamical field clearly and, therefore, it is our aim to determine these so-called *field variables* ϕ. Besides them, there are further quantities, also appearing as unknowns in the governing equations. In order to determine the field variables that can be deduced on the basis of the balance equations for the fields, one must express these *material quantities* Π with the help of constitutive relations, i.e. describe them as functions of the independent field variables ϕ and further dependent derivatives of the field variables $\partial_t \phi = \partial \phi / \partial t$ and $\partial_i \phi = \partial \phi / \partial x_i$. These formulations for the last unknowns beside the field variables themselves are called closure conditions and require a cut in generality, since so far, in the balance equations, only basic physical principles have

been formulated. So, the lack of determination in these balance equations indicates the need for further restrictions, given by the material and its physical properties.

The definition of these kinds of dependencies is made with the *material class* and the associated *constitutive equations* $\Pi = \widehat{\Pi}(\phi_C)$. A set of constitutive variables ϕ_C – composed of the field variables and their derivatives in time and space – is defined, thus stating that any of the unknown dependent – or material – quantities is constituted of this set of variables. Having determined the constitutive variables ϕ_C of which the material quantities Π are composed, one then needs to specify these relations and give the constitutive equations for each of the material quantities an explicit form. For the latter one, the Müller-Liu entropy principle is consulted, giving restrictions on the material quantities at hand. The final goal is to determine the remaining unknowns in order to close the system of equations. The postulation of dependencies of material quantities is a first step towards the identification and also specification of a certain material behavior. The choice of the constitutive variables is made among density quantities, thermal quantities and those of the motion. As thermodynamic fields, velocity, temperature and density are essential quantities for the material behavior; furthermore, also their derivatives can be employed to determine constitutive relations for a more specified physical behavior. For example, the gradient of the mass density, $\partial_i \rho^\alpha$, being included in the material behavior, can be important for the momentum balance since it describes the material distribution. On the other hand, a larger number of constitutive variables not only means greater universality of the modeled processes, but sometimes also the necessity of extra restrictions, which might not be well justified.

In this model, the temperature of the mixture θ and its derivative in time and space are employed for the material behavior. The consideration of the temperature indicates the material as thermal, the gradient of the temperature introduces as heat-conducting. Incorporation of the time derivative of the temperature $\partial_t \theta$ as an independent constitutive variable achieves the generalization of the absolute temperature to the universal coldness function for processes of thermodynamic non-equilibrium and partially finite wave speed of thermal signals, as originally demonstrated by Müller (Müller 1971a). Quantities describing the density and the material distribution are the true mass densities ρ^α, the partial mass densities $\widetilde{\rho}^\alpha$ and the volume fractions ν^α and their derivatives. So with their inclusion, a compressible material behavior that is also dependent on the material distribution is considered. Moreover, mechanical quantities such as the velocity v_i^α and the strain tensor $D_{ij}^\alpha = \frac{1}{2}(\partial_j v_i^\alpha + \partial_i v_j^\alpha)$ are employed, expressing viscous material behavior, as well as the spin tensor W_{ij}^α, which accounts for grain rotation (Huang, Nübel & Bauer 2002). The deformation gradients for elastic material behavior in the form of the left Cauchy-Green deformation tensors B_{ij}^α are also accounted for. Furthermore, the stress-like tensor Z_{ij}^α incorporates plastic material behavior and the pressure-quantities, ϖ^α and $\partial_i \varpi^\alpha$, account for an influence of the partial pressure. With this, the constitutive class, dealing with elasto-visco-plastic material behavior, reads

$$\Pi = \widehat{\Pi}(\boldsymbol{\phi}_C) = \widehat{\Pi}\left(\theta, \frac{\partial\theta}{\partial t}, \frac{\partial\theta}{\partial x_i}, \rho^\alpha, \frac{\partial\rho^\alpha}{\partial x_i}, \nu^\alpha, \frac{\partial\nu^\alpha}{\partial x_i}, v_i^\alpha,\ D_{ij}^\alpha,\ W_{ij}^\alpha,\ B_{ij}^\alpha,\ Z_{ij}^\alpha,\ \varpi^\alpha, \frac{\partial\varpi^\alpha}{\partial x_i}\right), \quad (3.5)$$

for the material variables

$$\Pi \in \left\{ \eta^s,\ \varepsilon,\ q_i,\ \psi_i^{\rho\eta}, T_{ij}^{\alpha},\ m_i^{\alpha}, \Phi_{ij}^{\alpha},\ \gamma_{\omega}^{\alpha},\ n^{\alpha},\ c^{\alpha},\ \Delta_i^{\alpha,\omega}, \kappa_{\omega}^{\alpha} \right\}.$$

Important in this formulation is the principle of *material objectivity*, see, for example, Hutter & Jöhnk (2004) and Schneider & Hutter (2009). It states that the characteristics of the system is invariant under a change of observer. This is especially relevant for the incorporated velocities and velocity gradients; for the sake of reduced complexity in calculations, this principle is applied later on, see Schneider & Hutter (2009, p. 73). This means that, at this point, we keep the non-objective velocity v_i (and its gradient), but it is later replaced. Furthermore, since the material is considered to be isotropic, no rotational changes should affect the material behavior.

3.3 Derivation: Exploiting the entropy principle

Following Truesdell's principle of equipresence, we now assume all constitutive quantities to be expressed as functions of the form (3.5). These dependencies are substituted into the evolution equations (3.4). This leads to a system of partial differential equations, which, when complemented by appropriate initial and boundary conditions, is thought to be uniquely integrable. These differential equations are called the *field equations*, and any solution for the field variables is called a *thermodynamic process*. However, not all these processes are physically realizable. Only those processes are physically realizable, which are also in conformity with the second law. It is clear therefore that the entropy inequality must condition the constitutive relations and, due to that, the thermodynamic processes, in such a way that the entropy imbalance is never violated for any of these processes. For this reason, these processes are denoted as *thermodynamically admissible*. Two in principle different procedures for the derivation of restrictions on the constitutive relations, coming from the entropy inequality constrained by the field equations, are the respective exploitations for *open* and *closed thermodynamic systems*. The former has been introduced by Coleman & Noll (1963), the latter by Liu (1972a).

The incorporation of the field equations in the process of exploitation of the entropy inequality is done by applying the method of *Lagrange multipliers*, which will be conducted below. In a second step, the extended inequality is transformed by incorporating the material class and its corresponding dependencies. This leads to the explicit form of the entropy inequality, to which Liu's Lemma is applied, thus, providing the opportunity to derive formulations for the unknown material quantities after some further processing. Proceeding in this way, the constitutive equations are deduced from the entropy inequality, satisfying the second law of thermodynamics.

The other, earlier approach of exploitation of the entropy inequality, due to Coleman & Noll (1963), employs the Clausius-Duhem inequality for *open systems*. In this approach, some of the field equations with external supply terms are not considered as constraint conditions in the exploitation of the entropy imbalance. The justification to do so is

the supposition that the supply terms can have any arbitrarily assigned values, so that any neighborhood in our universe (i.e. in the physical space) can be found, at which the value will 'equilibrate' its field equations. Moreover, the existence of the absolute (Kelvin) temperature whose existence is only ascertained for thermostatic processes, is accepted without questioning, as are expressions for the constituent supply and entropy flux. The approach of Müller and Liu thus is less restrictive, a fact which affects for example the treatment of e.g. polar or structured continua, see for example Hutter, Jöhnk & Svendsen (1994) and Wang & Hutter (1999a).

To gain an extended entropy inequality $\mathfrak{I}_\eta$, the balance laws $\mathbf{I}_\phi$, see Eq. (3.4), multiplied by the referring Lagrangian multiplier λ_ϕ, are added up as a linear combination and incorporated in the entropy inequality $I_\eta = \mathcal{N}$. This introduction is part of the ML approach and the resulting extended entropy inequality $\mathfrak{I}_\eta = \mathcal{N} - \sum_\phi \lambda_\phi \mathbf{I}_\phi \geq 0$ is of the form

$$\mathcal{N} - \sum_{\alpha=1}^{n} \lambda_\rho^\alpha \mathcal{R}^\alpha - \sum_{\alpha=1}^{n} \lambda_\nu^\alpha \mathcal{V}^\alpha - \sum_{\alpha=1}^{n} \lambda_i^{v,\alpha} \mathcal{M}_i^\alpha - \lambda^\varepsilon \mathcal{E} - \sum_{\alpha=1}^{n} \lambda_{ij}^{Z,\alpha} \mathcal{Z}_{ij}^\alpha - \sum_{\alpha=1}^{n} \lambda_\varpi^\alpha \mathcal{W}^\alpha \geq 0. \quad (3.6)$$

It is emphasized here that inequality (3.6) is no longer subject to the constraints of the field equations. As a compensation for this increased flexibility, however, the Lagrange parameters must be determined. Note also that the saturation restriction $\nu^n = 1 - \sum_{\alpha=1}^{n-1} \nu^\alpha$ needs to be incorporated. With this, we get

$$\begin{aligned}
&\frac{\partial \rho\eta^s}{\partial t} + \frac{\partial \rho\eta^s v_i}{\partial x_i} - \frac{\partial \psi_i^{\rho\eta}}{\partial x_i} - \sigma^{\rho\eta} \\
&- \sum_{\alpha=1}^{n} \lambda_\rho^\alpha \left\{ \nu^\alpha \frac{\partial \rho^\alpha}{\partial t} + \nu^\alpha v_i^\alpha \frac{\partial \rho^\alpha}{\partial x_i} - \nu^\alpha \rho^\alpha c^\alpha + \rho^\alpha n^\alpha \right\} \\
&\quad - \sum_{\alpha=1}^{n-1} \left\{ (\lambda_\nu^\alpha - \lambda_\nu^n) \frac{\partial \nu^\alpha}{\partial t} + (\lambda_\nu^\alpha v_i^\alpha - \lambda_\nu^n v_i^n) \frac{\partial \nu^\alpha}{\partial x_i} \right. \\
&\qquad \left. + \nu^\alpha \left(\lambda_\nu^\alpha \frac{\partial v_i^\alpha}{\partial x_i} - \lambda_\nu^n \frac{\partial v_i^n}{\partial x_i} \right) - \lambda_\nu^\alpha n^\alpha \right\} - \lambda_\nu^n \frac{\partial v_i^n}{\partial x_i} + \lambda_\nu^n n^n \\
&- \sum_{\alpha=1}^{n} \lambda_i^{v,\alpha} \left\{ \nu^\alpha \frac{\partial \rho^\alpha v_i^\alpha}{\partial t} + \nu^\alpha v_j^\alpha \frac{\partial \rho^\alpha v_i^\alpha}{\partial x_j} - \frac{\partial T_{ij}^\alpha}{\partial x_j} - \rho^\alpha \nu^\alpha g_i - m_i^\alpha + \rho^\alpha v_i^\alpha n^\alpha \right\} \\
&\quad - \lambda^\varepsilon \left\{ \frac{\partial \rho\varepsilon}{\partial t} + \frac{\partial \rho\varepsilon v_i}{\partial x_i} + \frac{\partial q_i}{\partial x_i} - T_{ij} \frac{\partial v_i}{\partial x_j} - \rho r_R \right\} \\
&- \sum_{\alpha=1}^{n} \lambda_{ij}^{Z,\alpha} \left\{ \frac{\partial Z_{ij}^\alpha}{\partial t} + v_k^\alpha \frac{\partial Z_{ij}^\alpha}{\partial x_k} + Z_{ik}^\alpha W_{kj}^\alpha - W_{ik}^\alpha Z_{kj}^\alpha - \Phi_{ij}^\alpha \right\} \\
&- \sum_{\alpha=1}^{n} \lambda_\varpi^\alpha \left\{ \frac{\partial \varpi^\alpha}{\partial t} + \frac{\partial \varpi^\alpha}{\partial x_i} \left(v_i^\alpha - \Delta_i^{\alpha,\varpi} \right) - \kappa_\varpi^\alpha \frac{\partial^2 \varpi^\alpha}{\partial x_i \partial x_i} - \gamma_\varpi^\alpha \right\} \geq 0.
\end{aligned} \quad (3.7)$$

Furthermore, the constitutive properties do not depend on external sources, as it is expected that the material behavior is independent of these specific external influences. Consequently,

$$\sum_{\alpha=1}^{n} \lambda_i^{v,\alpha} \rho^\alpha v^\alpha g_i + \lambda^\varepsilon \rho r_R - \sigma^{\rho\eta} \equiv 0. \tag{3.8}$$

In the deployed entropy inequality (3.7), the derivatives of unknown material quantities with respect to time and space are next replaced in a next step by respective linear combinations of the derivatives of the field variables contained in these material quantities. This explicates the incorporated dependencies of the material quantities on the field variables, thus leading to the explicit form of the entropy inequality. For an arbitrary material variable $\Pi(\boldsymbol{\phi}_C)$, the derivatives are executed according to the chain rule of differentiation, for instance,

$$\frac{\partial \Pi}{\partial t} = \sum_{\phi_C} \frac{\partial \Pi}{\partial \boldsymbol{\phi}_C} \frac{\partial \boldsymbol{\phi}_C}{\partial t}, \quad \frac{\partial \Pi}{\partial x_i} = \sum_{\phi_C} \frac{\partial \Pi}{\partial \boldsymbol{\phi}_C} \frac{\partial \boldsymbol{\phi}_C}{\partial x_i}. \tag{3.9}$$

Next, the arising series are grouped with respect to the occurring derivatives of the field variables. In this way, the extended and explicit entropy inequality is derived. This process of transformation of the entropy inequality is lengthy, complex and cumbersome, but essentially straightforward. This is a main reason for the development of a corresponding `Maple` algorithm that automates exactly this type of mathematical operation, see Cheviakov & Heß (2018) and Heß & Cheviakov (2019). The structure of this resulting inequality is

$$\mathbf{a} \cdot \boldsymbol{\phi}_L + \beta \geq 0, \tag{3.10}$$

where $\boldsymbol{a}$ and β are functions of the constitutive class ϕ_C, specified in (3.5), and depend on time and space derivatives of these quantities. Hence, inequality (3.10) is linear in $\boldsymbol{\phi}_L$, and since these variables can take any value, following from Liu's Lemma, it would be able to violate it unless

$$\boldsymbol{a} = \mathbf{0} \quad \text{and} \quad \beta \geq 0. \tag{3.11}$$

In the next section, the inferences deducible from this lengthy imbalance will be discussed. Equations $(3.11)_1$ are referred to as *Liu identities*, and imbalance $(3.11)_2$ is called the *reduced entropy inequality*.

3.3.1 Liu identities and integrability

The explicit entropy inequality is arranged more clearly by introducing abbreviations for the incorporated differentials. These are

$$\begin{aligned} P_{\phi_C} &= \frac{\partial \rho\eta^s}{\partial \boldsymbol{\phi}_C} - \lambda^\varepsilon \frac{\partial \rho\varepsilon}{\partial \boldsymbol{\phi}_C}, \\ F_{\phi_C,i} &= \frac{\partial \psi_i^{\rho\eta}}{\partial \boldsymbol{\phi}_C} - \lambda^\varepsilon \frac{\partial q_i}{\partial \boldsymbol{\phi}_C} + \sum_{\alpha=1}^{n} \lambda_j^{v,\alpha} \frac{\partial T_{ij}^\alpha}{\partial \boldsymbol{\phi}_C}. \end{aligned} \tag{3.12}$$

These terms appear in the Liu identities. They have the form of the coefficients of *Pfaffian forms*, constructs of a certain mathematical significance, which will be explicated later on. The vector $\boldsymbol{\phi}_L$ contains as components all (higher order) derivatives of the independent constitutive variables, stated in (3.5) and is composed of

$$\begin{aligned} \boldsymbol{\phi}_L = \Big(&\frac{\partial^2\theta}{\partial t^2}, \frac{\partial^2\theta}{\partial t \partial x_i}, \frac{\partial \rho^\alpha}{\partial t}, \frac{\partial^2 \rho^\alpha}{\partial t \partial x_i}, \frac{\partial \nu^\alpha}{\partial t}, \frac{\partial^2 \nu^\alpha}{\partial t \partial x_i}, \frac{\partial^2 \rho^\alpha}{\partial x_i \partial x_j}, \frac{\partial^2 \nu^\alpha}{\partial x_i \partial x_j}, \frac{\partial^2 \theta}{\partial x_i \partial x_j}, \\ &\frac{\partial v_i^\alpha}{\partial t}, \frac{\partial D_{ij}^\alpha}{\partial t}, \frac{\partial D_{ij}^\alpha}{\partial x_k}, \frac{\partial W_{ij}^\alpha}{\partial t}, \frac{\partial W_{ij}^\alpha}{\partial x_k}, \frac{\partial Z_{ij}^\alpha}{\partial t}, \frac{\partial Z_{ij}^\alpha}{\partial x_k}, \frac{\partial \varpi^\alpha}{\partial t}, \frac{\partial^2 \varpi^\alpha}{\partial x_i \partial x_j}, \frac{\partial^2 \varpi^\alpha}{\partial x_i \partial t} \Big). \end{aligned} \tag{3.13}$$

The Liu identities are a first result of the application of Lemma 1 on the explicit entropy inequality and compose a set of restrictions. These help to further transform the residual inequality and to deduce representations for the Lagrange multipliers, since these make up a new set of additional internal variables. Specifically the Liu identities are $\mathbf{a} = \mathbf{0}$ or

$$\begin{aligned} &P_{\left(\frac{\partial \rho^\alpha}{\partial x_i}\right)} = 0; \quad P_{\nu^\alpha} = \lambda_\nu^\alpha - \lambda_\nu^n; \quad P_{\left(\frac{\partial \nu^\alpha}{\partial x_i}\right)} = 0; \quad P_{v_i^\alpha} = \lambda_i^{v,\alpha} \rho^\alpha \nu^\alpha; \quad P_{\left(\frac{\partial \theta}{\partial t}\right)} = 0; \\ &P_{\left(\frac{\partial \theta}{\partial x_i}\right)} + F_{\left(\frac{\partial \theta}{\partial t}\right),i} = 0; \quad P_{\rho^\alpha} = \lambda_\rho^\alpha \nu^\alpha + \lambda_i^{v,\alpha} \nu^\alpha v_i^\alpha; \quad P_{D_{ij}^\alpha} = 0; \quad P_{B_{ij}^\alpha} = 0; \\ &P_{W_{ij}^\alpha} = 0; \quad P_{Z_{ij}^\alpha} = \lambda_{ij}^{Z,\alpha}; \quad F_{\left(\frac{\partial \nu^\alpha}{\partial x_j}\right),i} = 0; \quad F_{\left(\frac{\partial \rho^\alpha}{\partial x_j}\right),i} = 0; \quad F_{D_{ij}^\alpha,k} = 0; \\ &F_{\left(\frac{\partial \theta}{\partial x_j}\right),i} + v_i P_{\left(\frac{\partial \theta}{\partial x_j}\right)} = 0; \quad F_{B_{ij}^\alpha,k} = 0; \quad F_{W_{ij}^\alpha,k} = 0; \quad F_{Z_{ij}^\alpha,k} = \lambda_{ij}^{Z,\alpha} u_k^\alpha; \\ &P_{\varpi^\alpha} = \lambda_\varpi^\alpha; \quad P_{\left(\frac{\partial \varpi^\alpha}{\partial x_i}\right)} = 0; \quad F_{\left(\frac{\partial \varpi^\alpha}{\partial x_i}\right),j} = -\lambda_\varpi^\alpha \kappa_\varpi^\alpha \delta_{ij}. \end{aligned} \tag{3.14}$$

Particularly remarkable are the last three of these identities, since they are newly emerging due to the incorporation of the partial pressure equation. Stating these results, the residual inequality is further scrutinized. The Lagrange multipliers will be determined by exploiting the Liu identities and the mathematical inferences of the fact that

$$P = \mathrm{d}(\rho\eta^s) - \lambda^\varepsilon \mathrm{d}(\rho\varepsilon) = \sum_{\phi_C} P_{\phi_C} \mathrm{d}\boldsymbol{\phi}_C, \tag{3.15}$$

is a Pfaffian differential form, also called a one-form. Such expressions per se do not automatically represent a total differential and thus are not always integrable. For P

(and incidentally also F_i) to be an integrable form, the coefficients P_{ϕ_C} (and also $F_{\phi_C,i}$) must satisfy certain conditions, which are expressed by **(i)** the Poincaré theorem and **(ii)** the Frobenius conditions, for details see Svendsen & Hutter (1995), Bauer (1997) or Hutter & Jöhnk (2004). Poincaré's theorem states that the Pfaffian form is total, if and only if

$$P_{\phi_1,\phi_2} = P_{\phi_2,\phi_1} \qquad \phi_1, \phi_2 \in \boldsymbol{\phi}_C. \tag{3.16}$$

And the Frobenius condition states that, if (3.15) does not automatically satisfy the condition (3.16) of the Poincaré theorem, then this differential can be made complete (or total) by multiplying it with an integrating factor, if

$$\sum_{i,j,k} \varepsilon_{i,j,k} \left(P_{\phi_i,\phi_j} \right) P_{\phi_k} = 0, \tag{3.17}$$

in which $\phi_i, \phi_j, \phi_k \in \boldsymbol{\phi}_C$ are elements of the phase space and $(\cdot)_{\phi_i,\phi_j} = \partial(\cdot)_{\phi_i}/\partial\phi_j$. Condition (3.17) is sometimes expressed as a *conditional vanishing in rotation*. Further, with its coefficients P_{ϕ_C}, including the results of (3.14), the generalized Gibbs' relation can be deployed as

$$\begin{aligned} P = d(\rho\eta^s) - \lambda^\varepsilon d(\rho\varepsilon) = P_\theta d\theta + P_{\left(\frac{\partial\theta}{\partial x_i}\right)} d\left(\frac{\partial\theta}{\partial x_i}\right) + \sum_{\alpha=1}^{n} d\rho^\alpha P_{\rho^\alpha} \\ + \sum_{\alpha=1}^{n-1} d\nu^\alpha P_{\nu^\alpha} + \sum_{\alpha=1}^{n} dv_i^\alpha P_{v_i^\alpha} + \sum_{\alpha=1}^{n} P_{Z_{ij}^\alpha} dZ_{ij}^\alpha + \sum_{\alpha=1}^{n} P_{\varpi^\alpha} d\varpi^\alpha. \end{aligned} \tag{3.18}$$

We shall now alter this expression with the incorporation of $d(\rho\varepsilon) = d(\rho\varepsilon_I) + d(\rho\varepsilon_D)$ as well as the Helmholtz free energy Ψ^G. The one-form P, as in (3.15), is transformed with $\mathrm{d}(\rho\eta^s) - \lambda^\varepsilon \mathrm{d}(\rho\varepsilon) = -\lambda^\varepsilon \mathrm{d}\left(\rho\varepsilon - \frac{1}{\lambda^\varepsilon}\rho\eta^s\right) + \frac{1}{\lambda^\varepsilon}\rho\eta^s \mathrm{d}\lambda^\varepsilon$, in which $\varepsilon_I - \frac{1}{\lambda^\varepsilon}\eta^s = \Psi_I^G$ and $\mathrm{d}\lambda^\varepsilon = \frac{\partial\lambda^\varepsilon}{\partial\theta}\mathrm{d}\theta + \frac{\partial\lambda^\varepsilon}{\partial(\partial_t\theta)}\mathrm{d}(\partial_t\theta)$ is applied. Here, the internal energy is split into a constitutive and a non-constitutive part, referred to as inner and as diffusive parts, respectively, $\varepsilon = \varepsilon_I + \varepsilon_D$, with $\varepsilon_D = \frac{1}{2}\rho^{-1}\sum_\alpha \nu^\alpha \rho^\alpha u_i^\alpha u_i^\alpha$. The introduced Helmholtz free energy $\Psi^G = \varepsilon - (\lambda^\varepsilon)^{-1}\eta^s = \Psi_I^G + \Psi_D^G$ also consists of a constitutive and a non-constitutive part. We remark that for example Svendsen & Hutter (1995) and Schneider & Hutter (2009) apply this split of the internal energy though it may be uncommon. Also, for the sake of brevity, we refer to the Helmholtz free energy and not to a Helmholtz free energy-like quantity, as it is correctly done in Schneider & Hutter (2009, p. 117), since $\lambda^\varepsilon = \theta^{-1}$ has so far not been assumed. Incorporating these specifications in (3.18) yields

$$\begin{aligned} -\lambda^\varepsilon d(\rho\Psi_I^G) = \frac{1}{\lambda^\varepsilon}\rho\eta^s \left(\frac{\partial\lambda^\varepsilon}{\partial\theta}\mathrm{d}\theta + \frac{\partial\lambda^\varepsilon}{\partial(\partial_t\theta)}\mathrm{d}(\partial_t\theta) \right) + P_\theta d\theta + P_{\left(\frac{\partial\theta}{\partial x_i}\right)} d\left(\frac{\partial\theta}{\partial x_i}\right) \\ + \sum_{\alpha=1}^{n} d\rho^\alpha \left(P_{\rho^\alpha} + \frac{1}{2}\lambda^\varepsilon (u_i^\alpha)^2 \nu^\alpha \right) + \sum_{\alpha=1}^{n-1} d\nu^\alpha \left(P_{\nu^\alpha} + \frac{1}{2}\lambda^\varepsilon (u_i^\alpha)^2 \rho^\alpha - \frac{1}{2}\lambda^\varepsilon (u_i^n)^2 \rho^n \right) \\ + \sum_{\alpha=1}^{n} dv_i^\alpha \left(P_{v_i^\alpha} + \lambda^\varepsilon u_i^\alpha \rho^\alpha \nu^\alpha \right) + \sum_{\alpha=1}^{n} P_{Z_{ij}^\alpha} dZ_{ij}^\alpha + \sum_{\alpha=1}^{n} P_{\varpi^\alpha} d\varpi^\alpha, \end{aligned} \tag{3.19}$$

which can be differentiated with respect to the appearing differentials of v_i^α, ρ^α, ν^α, Z_{ij}^α, ϖ^α, θ, $\partial_t\theta$ and $\partial_i\theta$, implying a series of restrictions and providing expressions for the Lagrangian multipliers or one-forms still unknown. Moreover, the Langrange multiplier for the energy is assumed to have the reduced form

$$\lambda^\varepsilon = \hat{\lambda}^\varepsilon\left(\theta, \partial_t\theta\right). \tag{3.20}$$

With this limitation of the dependency of λ^ε, the differentiations of (3.19) imply
1) For $\partial P/\partial\rho^\alpha$:

$$\lambda_\rho^\alpha = -\frac{\lambda^\varepsilon\rho}{\nu^\alpha}\frac{\partial\Psi_I^G}{\partial\rho^\alpha} - \lambda^\varepsilon\Psi_I^G - \lambda_i^{v,\alpha}v_i^\alpha - \frac{1}{2}\lambda^\varepsilon(u_i^\alpha)^2. \tag{3.21}$$

2) For $\partial P/\partial\nu^\alpha$:

$$\lambda_\nu^\alpha = \lambda_\nu^n - \lambda^\varepsilon(\rho^\alpha - \rho^n)\Psi_I^G - \lambda^\varepsilon\rho\frac{\partial\Psi_I^G}{\partial\nu^\alpha} - \frac{\lambda^\varepsilon\rho^\alpha}{2}(u_i^\alpha)^2 + \frac{\lambda^\varepsilon\rho^n}{2}(u_i^n)^2. \tag{3.22}$$

3) For $\partial P/\partial v_i^\alpha$ and with the assumption of $\partial\Psi_I^G/\partial v_i^\alpha = 0$:

$$\lambda_i^{v,\alpha} = -\lambda^\varepsilon u_i^\alpha. \tag{3.23}$$

4) For $\partial P/\partial Z_{ij}^\alpha$:

$$\lambda_{ij}^{Z,\alpha} = -\lambda^\varepsilon\rho\frac{\partial\Psi_I^G}{\partial Z_{ij}^\alpha}. \tag{3.24}$$

5) For $\partial P/\partial\varpi^\alpha$:

$$\lambda_\varpi^\alpha = -\lambda^\varepsilon\rho\frac{\partial\Psi_I^G}{\partial\varpi^\alpha} - \lambda^\varepsilon\Psi_I^G\frac{\partial\rho}{\partial\varpi^\alpha}. \tag{3.25}$$

6) For $\partial P/\partial\theta$:

$$P_\theta = \frac{\rho\eta^s}{\lambda^\varepsilon}\frac{\partial\lambda^\varepsilon}{\partial\theta} - \lambda^\varepsilon\rho\frac{\partial\Psi_I^G}{\partial\theta}. \tag{3.26}$$

7) For $\partial P/\partial(\partial_i\theta)$:

$$P_{\left(\frac{\partial\theta}{\partial x_i}\right)} = -\lambda^\varepsilon\rho\frac{\partial\Psi_I^G}{\partial\left(\frac{\partial\theta}{\partial x_i}\right)}. \tag{3.27}$$

8) For $\partial P/\partial(\partial_t\theta)$:

$$\eta^s = \frac{(\lambda^\varepsilon)^2}{\frac{\partial\lambda^\varepsilon}{\partial\left(\frac{\partial\theta}{\partial t}\right)}}\frac{\partial\Psi_I^G}{\partial\left(\frac{\partial\theta}{\partial t}\right)}. \tag{3.28}$$

Note that, with Eqs. (3.21)-(3.28), the Liu identities are identically satisfied. Furthermore, with the help of these results, the residual inequality can be transformed, leaving only λ^η, λ^ε – as integrating factors – and the inner part of the Helmholtz free energy Ψ_I^G as unknowns.

Employing the results (3.21)-(3.28) and the Liu identities (3.14), together with some further transformations and the introduction of the extra entropy flux

$$k_i = \psi_i^{\rho\eta} - \lambda^\varepsilon \left(q_i + \sum_\alpha T_{ij}^\alpha u_j^\alpha \right), \tag{3.29}$$

the reduced entropy inequality now can further be elaborated.

3.3.2 The state of thermodynamic equilibrium

The form of the residual inequality derived so far allows deduction of first resulting forms of our constitutive functions. To this end, the state of *thermodynamic equilibrium* must be defined and the evaluation of its accompanying restrictions derived. Thermodynamic equilibrium describes a state of minimum entropy production; specifically, the entropy production reduces to the minimum zero. Such processes imply no growth in entropy and, thus, are theoretically reversible. This points at certain mathematical constraints, which are detailed below.

It is assumed that in thermodynamic equilibrium no phase changes occur, so $c^\alpha = n^\alpha = 0$, and the constitutive frictional production rates of the inner stress are set to zero, $\Phi_{ij}^\alpha = 0$. Furthermore, we will also apply $\partial k_i / \partial \rho^\alpha = \partial k_i / \partial v^\alpha = 0$.

The main assumption of thermodynamic equilibrium requires that

$$\pi^{\rho\eta}|_E = 0, \tag{3.30}$$

in which the index $(\cdot)|_E$ identifies the equilibrium. Practically, this state demands the extinction of a group of field variables referred to as non-equilibrium variables $\boldsymbol{\phi}_G$. If $\pi^{\rho\eta}$ is continuously differentiable close to thermodynamic equilibrium, its first derivatives with respect to $\boldsymbol{\phi}_G$ must equally vanish, and the Hessian matrix of $\pi^{\rho\eta^s}(\boldsymbol{\phi}_G)$ must be positive semidefinite. This must be so, since thermodynamic equilibrium is a point $\boldsymbol{\phi}_G$ where $\pi^{\rho\eta}(\boldsymbol{\phi}_G)$ is a minimum.

$$\left.\frac{\partial \pi^{\rho\eta}}{\partial \phi_G}\right|_E = 0, \quad \left.\frac{\partial^2 \pi^{\rho\eta}}{\partial \phi_G \partial \phi_G}\right|_E \geq 0, \tag{3.31}$$

where

$$\phi_G \in \left\{ \frac{\partial \theta}{\partial t}, \frac{\partial \theta}{\partial x_i}, v_i^\alpha, D_{ij}^\alpha, W_{ij}^\alpha \right\}, \quad \boldsymbol{\phi}_G \subset \boldsymbol{\phi}_C.$$

This constraint establishes a new set of equations which help to derive terms for material quantities at the state of thermodynamic equilibrium. The residual entropy inequality thus is differentiated with respect to these non-equilibrium variables and the appearing non-equilibrium quantities are set to zero, with each of these differentiations yielding a new equation.

The results of $(3.31)_1$ are:
1) First, with $\partial \pi^{\rho\eta} / \partial v_i^\alpha = 0$, the equilibrium momentum interaction term can be determined

$$\begin{aligned}
m_i^\alpha|_E = \sum_{\beta=1}^{n} \frac{\partial \varpi^\beta}{\partial x_j} \Bigg(& -\frac{1}{\lambda^\varepsilon} \frac{\partial^2 k_j}{\partial \varpi^\beta \partial v_i^\alpha} + \rho \frac{\partial \Psi_I^G}{\partial \varpi^\beta} \frac{\partial u_j^\beta}{\partial v_i^\alpha} - \rho \frac{\partial^2 \Psi_I^G}{\partial \varpi^\beta \partial v_i^\alpha} \Delta_j^{\beta,\varpi} \\
& - \rho \frac{\partial \Psi_I^G}{\partial \varpi^\beta} \frac{\partial \Delta_j^{\beta,\varpi}}{\partial v_i^\alpha} \Bigg) + \sum_{\beta=1}^{n-1} \frac{\partial \nu^\beta}{\partial x_j} \Bigg(-\frac{1}{\lambda^\varepsilon} \frac{\partial^2 k_j}{\partial \nu^\beta \partial v_i^\alpha} + \frac{\lambda_\nu^n}{\lambda^\varepsilon} \left(\delta_{n\alpha} - \delta_{\alpha\beta} \right) \delta_{ij} \\
& + \rho^n \Psi_I^G \left(\delta_{n\alpha} - \delta_{\alpha\beta} \right) \delta_{ij} + \rho \frac{\partial \Psi_I^G}{\partial \nu^\beta} \left(\delta_{\alpha\beta} - \frac{\rho^\alpha \nu^\alpha}{\rho} \right) \delta_{ij} \Bigg) \\
& - \rho \sum_{\beta=1}^{n} \frac{\partial \Psi_I^G}{\partial Z_{kj}^\beta} \frac{\partial \Phi_{kj}^\beta}{\partial v_i^\alpha} + \sum_{\beta=1}^{n} \Bigg\{ \nu^\beta \rho^\beta \frac{\partial c^\beta}{\partial v_i^\alpha} \left(-\frac{\rho}{\nu^\beta} \frac{\partial \Psi_I^G}{\partial \rho^\beta} - \Psi_I^G \right) \\
& + \frac{\partial n^\beta}{\partial v_i^\alpha} \left(\frac{\lambda_\nu^n}{\lambda^\varepsilon} + \rho^n \Psi_I^G - \rho \frac{\partial \Psi_I^G}{\partial \nu^\beta} + \frac{\rho^\beta \rho}{\nu^\beta} \frac{\partial \Psi_I^G}{\partial \rho^\beta} \right) \Bigg\} - \rho \sum_{\beta=1}^{n} \frac{\partial \Psi_I^G}{\partial \varpi^\beta} \frac{\partial \gamma_\varpi^\beta}{\partial v_i^\alpha} \\
& + \sum_{\beta=1}^{n} \frac{\partial \rho^\beta}{\partial x_j} \Bigg(-\frac{1}{\lambda^\varepsilon} \frac{\partial^2 k_j}{\partial \rho^\beta \partial v_i^\alpha} + \rho \frac{\partial \Psi_I^G}{\partial \rho^\beta} \left(\delta_{\alpha\beta} - \frac{\rho^\alpha \nu^\alpha}{\rho} \right) \delta_{ij} \Bigg).
\end{aligned} \tag{3.32}$$

2) For $\partial \pi^{\rho\eta} / \partial D_{ij}^\alpha = 0$, the equilibrium part of the stress tensor is obtained as

$$\begin{aligned}
T_{ij}^\alpha \Big|_E = & \frac{1}{\lambda^\varepsilon} \frac{\partial k_j}{\partial v_i^\alpha} + \frac{\lambda_\nu^n}{\lambda^\varepsilon} \nu^\alpha \delta_{ij} + \nu^\alpha \rho^n \Psi_I^G \delta_{ij} + \left(\rho^\alpha - \rho^n \right) \frac{\partial \Psi_I^G}{\partial Z_{kl}^\alpha} Z_{kl}^\alpha \nu^\alpha \delta_{ij} \\
& - \nu^\alpha \rho \frac{\partial \Psi_I^G}{\partial \nu^\alpha} \delta_{ij} + \sum_{\beta=1}^{n} \frac{\partial \varpi^\beta}{\partial x_k} \Bigg(-\frac{1}{\lambda^\varepsilon} \frac{\partial^2 k_k}{\partial \varpi^\beta \partial D_{ij}^\alpha} - \rho \frac{\partial^2 \Psi_I^G}{\partial \varpi^\beta \partial D_{ij}^\alpha} \Delta_k^{\beta,\varpi} - \rho \frac{\partial \Psi_I^G}{\partial \varpi^\beta} \frac{\Delta_k^{\beta,\varpi}}{\partial D_{ij}^\alpha} \Bigg) \\
& + \rho \sum_{\beta=1}^{n} \frac{\partial \Psi_I^G}{\partial \varpi^\beta} \frac{\partial \gamma_\varpi^\beta}{\partial D_{ij}^\alpha} + \rho \sum_{\beta=1}^{n} \frac{\partial \Psi_I^G}{\partial Z_{kl}^\beta} \frac{\partial \Phi_{kl}^\beta}{\partial D_{ij}^\alpha} + \sum_{\beta=1}^{n} \Bigg\{ \nu^\beta \rho^\beta \frac{\partial c^\beta}{\partial D_{ij}^\alpha} \left(\frac{\rho}{\nu^\beta} \frac{\partial \Psi_I^G}{\partial \rho^\beta} + \Psi_I^G \right) \\
& + \frac{\partial n^\beta}{\partial D_{ij}^\alpha} \left(\frac{\lambda_\nu^n}{\lambda^\varepsilon} + \rho^n \Psi_I^G - \rho \frac{\partial \Psi_I^G}{\partial \nu^\beta} + \frac{\rho^\beta \rho}{\nu^\beta} \frac{\partial \Psi_I^G}{\partial \rho^\beta} \right) \Bigg\}.
\end{aligned} \tag{3.33}$$

3) For $\partial \pi^{\rho\eta}/\partial(\partial_i\theta) = 0$, the equilibrium heat flux follows as

$$\begin{aligned} q_i|_E \left.\frac{\partial \lambda^\varepsilon}{\partial \theta}\right|_E = {} & \lambda^\varepsilon \rho \sum_{\alpha=1}^{n} \frac{\partial \Psi_I^G}{\partial Z_{kj}^\alpha} \frac{\partial \Phi_{kj}^\alpha}{\partial \left(\frac{\partial \theta}{\partial x_i}\right)} + \lambda^\varepsilon \rho \sum_{\alpha=1}^{n} \frac{\partial \Psi_I^G}{\partial \varpi^\alpha} \frac{\partial \gamma_\varpi^\alpha}{\partial \left(\frac{\partial \theta}{\partial x_i}\right)} \\ & + \sum_{\alpha=1}^{n} \left\{ \nu^\alpha \rho^\alpha \frac{\partial c^\alpha}{\partial \left(\frac{\partial \theta}{\partial x_i}\right)} \left(\frac{\lambda^\varepsilon \rho}{\nu^\alpha} \frac{\partial \Psi_I^G}{\partial \rho^\alpha} + \lambda^\varepsilon \Psi_I^G \right) \right. \\ & \left. - \frac{\partial n^\alpha}{\partial \left(\frac{\partial \theta}{\partial x_i}\right)} \left(\lambda_\nu^n + \lambda^\varepsilon \rho^n \Psi_I^G - \lambda^\varepsilon \rho \frac{\partial \Psi_I^G}{\partial \nu^\alpha} + \frac{\lambda^\varepsilon \rho^\alpha \rho}{\nu^\alpha} \frac{\partial \Psi_I^G}{\partial \rho^\alpha} \right) \right\} \\ & + \sum_{\alpha=1}^{n} \frac{\partial \varpi^\alpha}{\partial x_i} \left(\frac{\partial^2 k_i}{\partial \varpi^\alpha \partial \left(\frac{\partial \theta}{\partial x_i}\right)} + \lambda^\varepsilon \rho \frac{\partial^2 \Psi_I^G}{\partial \varpi^\alpha \partial \left(\frac{\partial \theta}{\partial x_i}\right)} \Delta_i^{\alpha,\varpi} \right). \end{aligned} \tag{3.34}$$

4) For $\partial \pi^{\rho\eta}/\partial(\partial_t\theta) = 0$ the equilibrium entropy takes the form

$$\begin{aligned} \eta^s|_E = {} & \frac{(\lambda^\varepsilon)^2}{\left(\frac{\partial \lambda^\varepsilon}{\partial \theta}\right)} \left(\frac{P_\theta}{\rho \lambda^\varepsilon} + \frac{\partial \Psi_I^G}{\partial \theta} \right) = \\ & \frac{(\lambda^\varepsilon)^2}{\left(\frac{\partial \lambda^\varepsilon}{\partial \theta}\right)} \left[\sum_{\alpha=1}^{n} \frac{\partial \Psi_I^G}{\partial \varpi^\alpha} \frac{\partial \gamma_\varpi^\alpha}{\partial \left(\frac{\partial \theta}{\partial t}\right)} + \frac{\partial \Psi_I^G}{\partial \theta} + \sum_{\alpha=1}^{n} \left\{ \nu^\alpha \rho^\alpha \frac{\partial c^\alpha}{\partial \left(\frac{\partial \theta}{\partial t}\right)} \left(\frac{\rho}{\nu^\alpha} \frac{\partial \Psi_I^G}{\partial \rho^\alpha} + \Psi_I^G \right) \right. \right. \\ & \left. \left. + \frac{\partial n^\alpha}{\partial \left(\frac{\partial \theta}{\partial t}\right)} \left(\frac{\lambda_\nu^n}{\lambda^\varepsilon} + \rho^n \Psi_I^G - \rho \frac{\partial \Psi_I^G}{\partial \nu^\alpha} + \frac{\rho^\alpha \rho}{\nu^\alpha} \frac{\partial \Psi_I^G}{\partial \rho^\alpha} \right) \right\} + \sum_{\alpha=1}^{n} \frac{\partial \Psi_I^G}{\partial Z_{ij}^\alpha} \frac{\partial \Phi_{ij}^\alpha}{\partial \left(\frac{\partial \theta}{\partial t}\right)} \\ & + \frac{1}{\rho \lambda^\varepsilon} \sum_{\alpha=1}^{n} \frac{\partial \varpi^\alpha}{\partial x_i} \left(\frac{\partial^2 k_i}{\partial \varpi^\alpha \partial \left(\frac{\partial \theta}{\partial t}\right)} + \lambda^\varepsilon \rho \frac{\partial^2 \Psi_I^G}{\partial \varpi^\alpha \partial \left(\frac{\partial \theta}{\partial t}\right)} \Delta_i^{\alpha,\varpi} \right. \\ & \left. \left. + \frac{\partial \lambda^\varepsilon}{\partial \left(\frac{\partial \theta}{\partial t}\right)} \rho \frac{\partial \Psi_I^G}{\partial \varpi^\alpha} \Delta_i^{\alpha,\varpi} \right) \right]. \end{aligned} \tag{3.35}$$

In the following, these results are further processed and brought into a closed, applicable form.

3.4 On the results of the derivation

So far, the conlusions drawn from the entropy principle of Müller and Liu have been deduced in a consistent way for a particularly chosen system of equations. Besides the material law for the constitutive system and the chosen balance laws, there has been little room for further modeling efforts. This will mainly be done in the following section, which, therefore, is both a most essential part as well as a most arguable one of the derivations in this chapter.

3.4.1 The general results for an arbitrary mixture

Given the results of the Müller and Liu exploitation of the entropy inequality in Eqs. (3.32)-(3.35), the structure of the pressure becomes clear, together with the influence of the newly added extra pressure. This allows for the identification of several (spherical) terms in connection with different partial pressures. Still left open is the postulation of the non-equilibrium parts (to complete the terms) and further closing assumptions for the remaining unknown material quantities, which will also be given below. The stress tensor can be decomposed into a spherical pressure part and an extra stress tensor,

$$T_{ij}^{\alpha} = -\nu^{\alpha} p^{\alpha} \delta_{ij} + T_{ij}^{e,\alpha}. \tag{3.36}$$

Comparison of the occurring spherical terms in Eq. (3.33) with this structure suggests the definition of the partial pressure as

$$p^{\alpha}|_E = -\underbrace{\frac{\lambda_{\nu}^{n}}{\lambda^{\varepsilon}}}_{\text{saturation pressure}} - \rho^{n}\Psi_I^G + \underbrace{\rho\frac{\partial \Psi_I^G}{\partial \nu^{\alpha}}}_{\text{configuration pressure}}. \tag{3.37}$$

It is important to notice that for the n-th component, with $p^n|_E$, the last part vanishes, leaving $p^n|_E = -(\lambda_\nu^n/\lambda^\varepsilon) - \rho^n \Psi_I^G$ and suggesting the other term to be the configuration pressure, such that $p^\alpha|_E = p^n|_E + \rho(\partial \Psi_I^G/\partial \nu^\alpha)$.

This configuration pressure $\rho(\partial \Psi_I^G/\partial \nu^\alpha)$ is a result of the material distribution and its microstructure; therefore, it arises as the derivative of the Helmholtz free energy with respect to the volume fraction. With this, the assumption of pressure equilibrium, equalizing all partial pressures, is avoided. Now, the equilibrium stress tensor (3.33) can be represented as

$$\begin{aligned} T_{ij}^{\alpha}\Big|_E &= \frac{1}{\lambda^{\varepsilon}}\frac{\partial k_j}{\partial v_i^{\alpha}} + p^{\alpha}|_E \nu^{\alpha}\delta_{ij} + (\rho^{\alpha} - \rho^{n})\frac{\partial \Psi_I^G}{\partial Z_{kl}^{\alpha}} Z_{kl}^{\alpha}\nu^{\alpha}\delta_{ij} \\ &+ \sum_{\beta=1}^{n}\left\{ \nu^{\beta}\rho^{\beta}\frac{\partial c^{\beta}}{\partial D_{ij}^{\alpha}}\left(\frac{\rho}{\nu^{\beta}}\frac{\partial \Psi_I^G}{\partial \rho^{\beta}} + \Psi_I^G\right) + \frac{\partial n^{\beta}}{\partial D_{ij}^{\alpha}}\left(-p^{\alpha}|_E + \frac{\rho^{\beta}\rho}{\nu^{\beta}}\frac{\partial \Psi_I^G}{\partial \rho^{\beta}}\right)\right\} \\ &+ \rho\sum_{\beta=1}^{n}\frac{\partial \Psi_I^G}{\partial Z_{kl}^{\beta}}\frac{\partial \Phi_{kl}^{\beta}}{\partial D_{ij}^{\alpha}} + \rho\sum_{\beta=1}^{n}\frac{\partial \Psi_I^G}{\partial \varpi^{\beta}}\frac{\partial \gamma_{\varpi}^{\beta}}{\partial D_{ij}^{\alpha}} - \sum_{\beta=1}^{n}\frac{\partial \varpi^{\beta}}{\partial x_k} C_{j,\alpha}^{\varpi,\beta}, \end{aligned} \tag{3.38}$$

in which a term $C_{j,\alpha}^{\varpi,\beta}$ has been introduced to provide a clearer view on the remaining structure of the tensor

$$C_{j,\alpha}^{\varpi,\beta} = \frac{1}{\lambda^{\varepsilon}}\frac{\partial^2 k_k}{\partial \varpi^{\beta}\partial D_{ij}^{\alpha}} + \rho\frac{\partial^2 \Psi_I^G}{\partial \varpi^{\beta}\partial D_{ij}^{\alpha}}\Delta_k^{\beta,\varpi} + \rho\frac{\partial \Psi_I^G}{\partial \varpi^{\beta}}\frac{\Delta_k^{\beta,\varpi}}{\partial D_{ij}^{\alpha}}.$$

Some further, simplifying assumptions are made by ruling out derivatives of the Helmholtz free energy in the plastic part of the stress tensor, in agreement with Teufel (2001). Therefore, it is assumed that

$$\begin{aligned} \rho \sum_{\beta=1}^{n} \frac{\partial \Psi_I^G}{\partial Z_{kl}^{\beta}} \frac{\partial \Phi_{kl}^{\beta}}{\partial D_{ij}^{\alpha}} &= \rho \delta^Z Z_{ij}^{\alpha}, \\ (\rho^{\alpha} - \rho^n) \frac{\partial \Psi_I^G}{\partial Z_{kl}^{\alpha}} Z_{kl}^{\alpha} &= \underbrace{(\rho^{\alpha} - \rho^n) \delta^Z Z_{ii}^{\alpha}}_{:=\varpi_Z^{\alpha}}. \end{aligned} \tag{3.39}$$

In the material class (3.5), the left Cauchy-Green strain tensor B_{ij}^{α} has been incorporated, yet, its influence has been ruled out during the derivation, due to the vanishing of the apparent Liu identities, see $P_{B_{ij}^{\alpha}} = 0$ in Eq. (3.14). To preserve the elastic response of the stress tensor, different approaches are conceivable, of which one is presented in Schneider & Hutter (2009, p. 88). This transformation leads to the incorporation of $\rho(\partial \Psi_I^G / \partial B_{ik}^{\alpha}) B_{jk}^{\alpha}$ in the resulting stress tensor, here Eq. (3.33), a term that can be approximated by $\mu_B^{\alpha} B_{ij}^{\alpha}$ (Schneider & Hutter 2009, p. 162). In short, this is the elastic part of the depicted material behavior, which could, with this, be amended as Neo-Hookean behavior. Another way to keep the elastic part would be to account for the gradient $\partial_k B_{ij}^{\alpha}$ in the material class; since we want to avoid further needs for the description, e.g. with an own evolution equation like that suggested in Schneider & Hutter (2009, p. 185), we omit these transformations for the elastic part.

Below, the term related to the pressure derivative is left out of consideration by setting $C_{j,\alpha}^{\varpi,\beta} = 0$; moreover, it is assumed that $\partial \gamma_{\varpi}^{\alpha} / \partial D_{ij}^{\beta} \approx 0$. It should be noted that here lies one of the possible links for an incorporation of the evolution of the extra pore-fluid pressure in the stress tensor. The reason for these assumptions is quite simple; nothing points towards a need of incorporation of these omitted terms. This is of course not astonishing, since they occur due to the enlargement of the model with respect to a pressure diffusion equation, which is new. However, this might be one point of contact for further modeling efforts. In addition, also all terms connected to phase interchanges are omitted, i.e. $n^{\alpha} = c^{\alpha} = 0$. Thus, chemical reactions and phase interchanges are not considered, which is quite justifiable especially for binary solid-fluid mixtures. Nonetheless, this is another point for which further work might have to be taken up. Note also that $\partial k_i / \partial v_j^{\alpha} = 0$ is assumed.

A next step in the modeling process has to turn towards the pressure term. It is not unusual to subsume the spherical parts in a pressure-like share of the stress tensor. The crucial point is, however, the determination of this part. For this, we follow the arguments pointing towards the existence of a dynamic pressure part of the fluid ϖ_e^f, supplementing the hydrostatic fluid pressure and, thereby, giving the fluid pressure the form $\varpi^f = \varpi_h^f + C_e^f \varpi_e^f$, as already done by Iverson & George (2014) and Kowalski & McElwaine (2013). The parameter C_e^f, introduced here together with the extra pressure, is not further discussed at this point. Now, for the pressure consisting of

its equilibrium and its non-equilibrium part, the assumed partial pressure p^α arising during the derivation is replaced by the actual pressure ϖ^α with

$$p^\alpha = p^\alpha|_E + p^\alpha|_N = \varpi^\alpha = \varpi_h^\alpha + C_e^\alpha \varpi_e^\alpha. \tag{3.40}$$

This allows us to model the pressure of the fluid, for we know the hydrostatic part $\varpi_h^f = g\rho^f \Delta h$ and we also can compute the dynamic extra pressure of the fluid ϖ_e^f with the help of a specialization of the pressure evolution equation incorporated in the model. In fact, Eq. (3.40) is first of all helpful for the estimation of the fluid pressure, which is identified with the n-th constituent and its partial pressure p^n, thus with ϖ^n. While p^α is an auxiliary quantity in the modeling process, replacing some unknowns in the results of the entropy principle, ϖ^α *is* this pressure – and they are identified with each other because of the apparent pressure-like character of p^α. This is a central closing assumption in our model. With this, we have $p^n|_E = \varpi_h^f$, therefore $p^\alpha|_E = \varpi_h^f + \varpi_v^\alpha = \varpi_h^\alpha$, see Eq. (3.37), with the configuration pressure part $\varpi_v^\alpha = \rho\left(\partial\Psi_I^G/\partial\nu^\alpha\right)$ that distinguishes the partial pressures, and further $p^n = \varpi_h^f + C_e^f \varpi_e^f$.

With this, a non-equilibrium part $T_{ij}^\alpha|_N$ for the stress tensor is postulated and added to the equilibrium part $T_{ij}^\alpha|_E$, see Eq. (3.38), yielding, together with the aforesaid restrictions and simplifications,

$$\begin{aligned} T_{ij}^\alpha = T_{ij}^\alpha|_E + T_{ij}^\alpha|_N = &-\varpi^\alpha \nu^\alpha \delta_{ij} + \left(\rho^\alpha - \rho^n\right)\delta^Z Z_{kk}^\alpha \nu^\alpha \delta_{ij} + \rho\delta^Z Z_{ij}^\alpha \\ &+ a_1^\alpha D_{kk}^\alpha \delta_{ij} + a_2^\alpha D_{ij}^\alpha + a_3^\alpha D_{ik}^\alpha D_{kj}^\alpha + a_4^\alpha \frac{\partial\nu^\alpha}{\partial x_i}\frac{\partial\nu^\alpha}{\partial x_j} + a_5^\alpha \left(\frac{\partial\nu^\alpha}{\partial x_k}\right)^2 D_{ij}^\alpha \\ &+ a_6^\alpha \left(\frac{\partial\nu^\alpha}{\partial x_k}\right)^2 D_{ik}^\alpha D_{kj}^\alpha + a_7^\alpha u_i^\alpha u_j^\alpha. \end{aligned} \tag{3.41}$$

We will further discuss the structure of the stress tensor below.

The next step is analogous, but executed for the momentum interaction term, in which an equivalent pressure-part can be detected and incorporated by introducing $p^\alpha|_E$, $p^n|_E$ and ϖ_v^α in Eq. (3.32). This yields

$$\begin{aligned} m_i^\alpha|_E = &\sum_{\beta=1}^{n} \frac{\partial\rho^\beta}{\partial x_j}\left(-\frac{1}{\lambda^\varepsilon}\frac{\partial^2 k_j}{\partial\rho^\beta\partial v_i^\alpha} + \rho\frac{\partial\Psi_I^G}{\partial\rho^\beta}\left(\delta_{\alpha\beta} - \frac{\rho^\alpha\nu^\alpha}{\rho}\right)\delta_{ij}\right) \\ &+ \sum_{\beta=1}^{n-1}\frac{\partial\nu^\beta}{\partial x_j}\left(-\frac{1}{\lambda^\varepsilon}\frac{\partial^2 k_j}{\partial\nu^\beta\partial v_i^\alpha} + p^\beta|_E\delta_{\alpha\beta}\delta_{ij} - p^n|_E\delta_{\alpha n}\delta_{ij} + \omega_v^\beta\left(\frac{\delta_{n\alpha} - \rho^\alpha\nu^\alpha}{\rho}\right)\delta_{ij}\right) \\ &- \sum_{\beta=1}^{n}\frac{\partial\varpi^\beta}{\partial x_j}K_{ij,\alpha}^{\varpi,\beta} - \rho\sum_{\beta=1}^{n}\frac{\partial\Psi_I^G}{\partial Z_{kj}^\beta}\frac{\partial\Phi_{kj}^\beta}{\partial v_i^\alpha} - \rho\sum_{\beta=1}^{n}\frac{\partial\Psi_I^G}{\partial\varpi^\beta}\frac{\partial\gamma_\varpi^\beta}{\partial v_i^\alpha} \\ &+ \sum_{\beta=1}^{n}\left\{\nu^\beta\rho^\beta\frac{\partial c^\beta}{\partial v_i^\alpha}\left(-\frac{\rho}{\nu^\beta}\frac{\partial\Psi_I^G}{\partial\rho^\beta} - \Psi_I^G\right) + \frac{\partial n^\beta}{\partial v_i^\alpha}\left(-p^\beta|_E + \frac{\rho^\beta\rho}{\nu^\beta}\frac{\partial\Psi_I^G}{\partial\rho^\beta}\right)\right\}, \end{aligned} \tag{3.42}$$

with

$$K_{ij,\alpha}^{\omega,\beta} = \frac{1}{\lambda^{\varepsilon}} \frac{\partial^2 k_j}{\partial \omega^{\beta} \partial v_i^{\alpha}} - \rho \frac{\partial \Psi_I^G}{\partial \omega^{\beta}} \frac{\partial u_j^{\beta}}{\partial v_i^{\alpha}} + \rho \frac{\partial^2 \Psi_I^G}{\partial \omega^{\beta} \partial v_i^{\alpha}} \Delta_j^{\beta,\omega} + \rho \frac{\partial \Psi_I^G}{\partial \omega^{\beta}} \frac{\partial \Delta_j^{\beta,\omega}}{\partial v_i^{\alpha}}.$$

After further simplifications, including the ad-hoc assumption $K_{ij,\alpha}^{\omega,\beta} = 0$, $\partial^2 k_j / \partial \rho^{\beta} \partial v_i^{\alpha} = \partial^2 k_j / \partial \nu^{\beta} \partial v_i^{\alpha} = 0$, the anticipation of material laws giving $\partial \gamma_{\omega}^{\beta} / \partial v_i^{\alpha} \approx 0$, $\partial \Phi_{kj}^{\beta} / \partial v_i^{\alpha} = 0$ and the restriction of $n^{\alpha} = c^{\alpha} = 0$, the non-equilibrium part $m_i^{\alpha}|_N$ is amended and obtained as:

$$\begin{aligned} m_i^{\alpha} = m_i^{\alpha}|_E + m_i^{\alpha}|_N = & \sum_{\beta=1}^{n} \frac{\partial \rho^{\beta}}{\partial x_i} \rho \frac{\partial \Psi_I^G}{\partial \rho^{\beta}} \left(\delta_{\alpha\beta} - \frac{\rho^{\alpha} \nu^{\alpha}}{\rho} \right) + \sum_{\beta=1}^{n} c_D^{\alpha\beta} \left(u_i^{\beta} - u_i^{\alpha} \right) \\ & + \sum_{\beta=1}^{n-1} \frac{\partial \nu^{\beta}}{\partial x_i} \left(\omega^{\beta} \delta_{\alpha\beta} - \omega^{n} \delta_{\alpha n} \delta_{ij} + \omega_{\nu}^{\beta} \left(\frac{\delta_{n\alpha} - \rho^{\alpha} \nu^{\alpha}}{\rho} \right) \right), \end{aligned} \tag{3.43}$$

with:

$$m_i^{\alpha}|_N = \sum_{\beta=1}^{n} c_D^{\alpha\beta} \left(u_i^{\beta} - u_i^{\alpha} \right) + \sum_{\beta=1}^{n-1} \frac{\partial \nu^{\beta}}{\partial x_i} \left(p^{\beta}|_N \delta_{\alpha\beta} - p^{n}|_N \delta_{\alpha n} \right). \tag{3.44}$$

A drag factor $c_D^{\alpha\beta}$ is introduced together with the drag term in the non-equilibrium part, denoting the constituents α and β, with $c_D^{\alpha\beta} = c_D^{\beta\alpha}$. In order to comply with the principle of objectivity, stating the requirement of the constitutive law (3.5) to be independent of the observer, we need to incorporate objective forms of v_i^{α}. Such a choice can be

$$v_i^{\alpha} \rightarrow u_i^{\alpha} = v_i^{\alpha} - v_i. \tag{3.45}$$

This is explicitly done for the non-equilibrium parts in Eqs. (3.41), (3.44). It should be noted that no further modeling is done with respect to the heat flux vector, since we are not referring to it in the subsequent analysis.

3.4.2 The results for a solid-fluid mixture

The model presented so far is still too general for the purpose of application because instead of specific constituents, only a general range of n components has been considered. Now, we seek to change this and restrict considerations to a binary flow of a solid, i.e. a granular component, and a fluid phase. In particular, this means that the stress tensors become more specific, since they now depict either the behavior of a granular solid or that of a fluid. Further simplifications are the assumption of a constant temperature $\theta = const$, and of constant true densities $\rho^{\alpha} = const$; therefore, we omit the mass balance for the true density and the energy balance. Due to the saturation condition, there remains only one unknown of the volume fractions – we

choose ν^s and drop $\nu^f = 1 - \nu^s$ as a free field variable. In this system, neither mass exchange nor phase transitions can occur, so $c^\alpha = n^\alpha = 0$.

With this, one can distinguish between a *solid* and a *fluid* stress tensor with the assigned indices s and f, respectively. As a first distinction between both, the concept of hypoplasticity 2.3.2 makes merely sense for the solid constituent and the related plastic part does not appear in the fluid stress tensor, so $Z_{ij}^f = 0$. Likewise, the elastic part would vanish for the fluid.[1] With these prerequisites, the suggested closing concept takes effect, since we can assign the n-th fluid-like pressure to the actual pressure of the fluid, i.e. $\varpi^n = \varpi^f$. The partial pressures

$$\varpi^f = \varpi_h^f + C_e^f \varpi_e^f, \quad \varpi_h^s = \varpi_h^f + \varpi_\nu^s, \tag{3.46}$$

represent two independent unknown quantities ϖ_e^f and ϖ_ν^s, for which equations have to be found. We will return to this later, in particular during the course of depth-integration. We assume the extra pressure in the solid stress term to appear as the negative fluid extra pressure, so that $\varpi^s = \varpi_h^s - C_e^f \varpi_e^f$ (or $C_e^s \varpi_e^s = -C_e^f \varpi_e^f$). Furthermore, while often, a viscous part is assumed only for the fluid stress tensor, in the first instance, we suppose viscous responses for both tensors, in their remaining postulated non-equilibrium parts. This will be changed later on, in Chapter 4.

Thus we reach a provisional end in the determination of the quantities $T_{ij}^s, T_{ij}^f, m_i^s$; starting with the stress tensor of the solid, the assumptions outlined above and inserted in Eqs. (3.41) and (3.46) imply, for $\alpha = s$,

$$\begin{aligned} T_{ij}^s = &- \left(\varpi_h^f - C_e^f \varpi_e^f + \varpi_\nu^s - \left(\rho^s - \rho^f \right) \delta^Z Z_{kk}^s \right) \nu^s \delta_{ij} + \rho \delta^Z Z_{ij}^s \\ &+ a_1^s D_{kk}^s \delta_{ij} + a_2^s D_{ij}^s + a_3^s D_{ik}^s D_{kj}^s + a_4^s \frac{\partial \nu^s}{\partial x_i} \frac{\partial \nu^s}{\partial x_j} \\ &+ a_5^s \left(\frac{\partial \nu^s}{\partial x_k} \right)^2 D_{ij}^s + a_6^s \left(\frac{\partial \nu^s}{\partial x_k} \right)^2 D_{ik}^s D_{kj}^s + a_7^s u_i^s u_j^s. \end{aligned} \tag{3.47}$$

Similarly, for the fluid stress, $\alpha = f$,

$$\begin{aligned} T_{ij}^f = &- \varpi^f \nu^f \delta_{ij} + a_1^f D_{kk}^f \delta_{ij} + a_2^f D_{ij}^f + a_3^f D_{ik}^f D_{kj}^f + a_4^f \frac{\partial \nu^f}{\partial x_i} \frac{\partial \nu^f}{\partial x_j} \\ &+ a_5^f \left(\frac{\partial \nu^f}{\partial x_k} \right)^2 D_{ij}^f + a_6^f \left(\frac{\partial \nu^f}{\partial x_k} \right)^2 D_{ik}^f D_{kj}^f + a_7^f u_i^f u_j^f. \end{aligned} \tag{3.48}$$

Here, $a_k^{s,f}\,(k = 1, 2, ..., 7)$ are scalar coefficients, which are treated as constants, but can, in principle, be functions of the invariants of $D_{ij}^{s,f}$, Z_{ij}^s, $u_i^{s,f}$, ν^s and $\rho^{s,f}$, as well as of the pressure parts, i.e. ϖ_ν^s and ϖ_e^f.

[1] This means that the fluid component is volume preserving, an assumption introduced ab initio. Note that anyway, elasticity is not considered for both phases in the following.

The solid material behavior can now be explained in greater detail, as we identify the different terms in the stress tensor. Besides the pressure, there is another spherical term in the equilibrium solid stress tensor, accounting for hypoplastic behavior, together with a further, non-spherical hypoplastic term. Coming from the postulated non-equilibrium part, there are terms in conjunction with the velocity and velocity gradients, as well as with gradients of the solid volume fraction. The latter account for development of the material distribution. Within the fluid material, while none of the elastic or plastic effects occur, the viscous and shear-rate effects are incorporated in the same manner.

The momentum interaction term, see Eq. (3.43), reduces to

$$m_i^s = c_D^{sf}\left(u_i^f - u_i^s\right) + \frac{\partial \nu^s}{\partial x_i}\left(\omega_h^s - \omega_\nu^s \frac{\rho^s \nu^s}{\rho}\right). \tag{3.49}$$

Note that only m_i^s is needed, since $m_i^f = -m_i^s$, due to a general assumption of the mixture theory, demanding $\sum_\alpha m_i^\alpha = 0$. The momentum interaction is composed of a drag term and a buoyancy term; the latter is related to the gradient of the volume fraction multiplied by a pressure.

We now specify the additional equations, giving source terms and discussing their general structure, at first for the pressure. The pressure evolution equation in its incorporated general form reads

$$\frac{\partial \omega^\alpha}{\partial t} + v_i^\alpha \frac{\partial \omega^\alpha}{\partial x_i} - \frac{\partial \kappa_\omega^\alpha}{\partial x_i}\frac{\partial \omega^\alpha}{\partial x_i} - \kappa_\omega^\alpha \frac{\partial^2 \omega^\alpha}{\partial x_i \partial x_i} = \gamma_\omega^\alpha. \tag{3.50}$$

So far in the derivation, we had replaced $\partial_i \kappa_\omega^\alpha$ by $\Delta_i^{\alpha,\omega}$, see $(3.4)_6$. Our replacement is in line with a general diffusion equation, viz.,

$$\frac{\partial \omega^\alpha}{\partial t} + v_i^\alpha \frac{\partial \omega^\alpha}{\partial x_i} = \frac{\partial}{\partial x_i}\psi_i^{\omega,\alpha} + \gamma_\omega^\alpha, \tag{3.51}$$

with a flux-term $\psi_i^{\omega,\alpha} = \kappa_\omega^\alpha\left(\partial_i \omega^\alpha\right)$, see Hutter & Schneider (2010a). Also, only one of the pressures (ω_e^f and ω_ν^s) needs to be described with its own equation. We select ω_e^f, since it is well-founded and tested. Now, specifying Eq. (3.50) for the extra pore pressure of the fluid ω_e^f, an evolution equation is derived, according to the one suggested in Iverson & George (2014). Iverson and George's (Iverson & George 2014) source term, also see Eq. (2.9), is given by

$$\begin{aligned} \gamma_\omega^f = \frac{\mathrm{d}\left(\sigma - \omega_h^f\right)}{\mathrm{d}t} - \frac{\dot{\gamma}}{\alpha_D}\tan(\psi) = \\ \frac{\mathrm{d}\left(\sigma - \omega_h^f\right)}{\mathrm{d}t} - \frac{1}{\alpha_D}\sqrt{D_{ik}^s D_{kj}^s \delta_{ij}}\kappa_{\omega 1}\left(\nu^s - \kappa_{\omega 2}\frac{\nu_C^s}{1+\sqrt{\mathrm{N}_\gamma}}\right). \end{aligned} \tag{3.52}$$

Here, two additional coefficients $\kappa_{\varpi 1}, \kappa_{\varpi 2}$ are implemented in the second term, which will be discussed later. This term generally describes dilatancy as the difference of the solid volume fraction with the equilibrium value, $\nu^s - \nu^s_{eq}$. The equilibrium volume fraction is estimated with the rate of the critical volume fraction ν^s_C by a dimensionless parameter N_γ. As already described in Section 2.3, the dilatancy term accounts for the development in the microstructure of the granular skeleton, where the values of ν^s_{eq} and ν^s_C denote certain boundaries.

Also, the flux-coefficient is specified as a pore-pressure diffusivity $\kappa^f_\varpi = k_D/(\alpha_D \mu^f)$, with the rate of the hydraulic permeability k_D to the debris compressibility α_D times the viscosity of the fluid μ^f. For more details on the physical relations behind these parameters, see Iverson & George (2014).
So, ϖ^f_e evolves according to

$$\begin{aligned} &\frac{\partial \varpi^f_e}{\partial t} + v^s_i \frac{\partial \varpi^f_e}{\partial x_i} - \frac{k_D}{\alpha_D \mu^f} \frac{\partial^2 \varpi^f_e}{\partial x_i \partial x_i} - \frac{1}{\alpha_D} \frac{\partial}{\partial x_i} \left(\frac{k_D}{\mu^f} \right) \frac{\partial \varpi^f_e}{\partial x_i} = \\ &\frac{\mathrm{d}\left(\sigma - \varpi^f_h\right)}{\mathrm{d}t} - \frac{1}{\alpha_D} \sqrt{D^s_{ik} D^s_{kj} \delta_{ij}} \kappa_{\varpi 1} \left(\nu^s - \kappa_{\varpi 2} \frac{\nu^s_C}{1 + \sqrt{\mathrm{N}_\gamma}} \right). \end{aligned} \tag{3.53}$$

This pore pressure model is developed in several of Iverson's works, but applied as a special case of the introduced general pressure diffusion equation (3.50). It is motivated by consolidation theory. In Eq. (3.53), the interactions of the porous medium and the pore-fluid is described (also see Section 2.3): the coupled development of the time rate of change of the extra pressure (first term on the RHS) and the relation of the solid volume fraction to its equilibrium value (second term on the RHS) govern the development of the extra pore-fluid pressure. Accounting for the effects of dilatancy, it is assumed that, under shearing, the pore interspace either decreases or increases, an effect which causes a change in the pore pressure, which in turn may work against or for the support of the granular structure. Similarly, the pore-fluid pressure works as damper or amplifier, depending on the granular structure and its development. These considerations lead to the extra pore-fluid pressure equation (3.53) above, employed in the following for the extra pressure of the pore-fluid, regaining information on the dynamics and micro interactions.

In general, for a configuration pressure ϖ^α_ν, a structurally equivalent equation can be suggested,

$$\frac{\partial \varpi^\alpha_\nu}{\partial t} + v^\alpha_i \frac{\partial \varpi^\alpha_\nu}{\partial x_i} - \kappa^{\nu,\alpha}_\varpi \frac{\partial^2 \varpi^\alpha_\nu}{\partial x_i \partial x_i} - \frac{\partial \kappa^{\nu,\alpha}_\varpi}{\partial x_i} \frac{\partial \varpi^\alpha_\nu}{\partial x_i} = \Phi^{\nu,\alpha}_\varpi. \tag{3.54}$$

The source-term is left unspecified, $\Phi^{\nu,\alpha}_\varpi = f(\nu^\alpha, Z^\alpha_{ij})$, as is the flux-coefficient $\kappa^{\nu,\alpha}_\varpi = f(\nu^\alpha)$, since this pressure equation will not be used in the ensuing analysis. We will instead derive the configuration pressure with the aid of one of the momentum balances for the case of simple shear in this chapter, and by further deduction in the following chapters. It is worth noting that in general, for saturated mixture of n components,

one only needs to describe $n-2$ of the $n-1$ configuration pressures via an equation like the one presented in Eq. (3.54). The remaining $(n-1)$-th configurational pressure is determined by the saturation condition, and it is assumed, that there is no n-th configuration pressure.

For the inner stress-like quantity Z_{ij}^{α}, an evolution equation is employed, see Eq. (2.12),

$$\frac{\partial Z_{ij}^{\alpha}}{\partial t} + v_k^{\alpha}\frac{\partial Z_{ij}^{\alpha}}{\partial x_k} + Z_{ik}^{\alpha}W_{kj}^{\alpha} - W_{ik}^{\alpha}Z_{kj}^{\alpha} - \nu^{\alpha}\sum_{\beta=1}^{n}\frac{\left(\rho^{\alpha}-\rho^{\beta}\right)}{\rho}\frac{\partial v_k^{\alpha}}{\partial x_k}Z_{ij}^{\alpha} = \Phi_{ij}^{\alpha}, \tag{3.55}$$

with the source term Φ_{ij}^{α}, modeling hypoplasticity due to the non-linearities,

$$\Phi_{ij}^{\alpha} = f_{s,\alpha}\left(a_Z^{\alpha}D_{ij}^{\alpha} + \frac{Z_{ij}^{\alpha}Z_{kl}^{\alpha}D_{kl}^{\alpha}}{\left(\mathrm{tr}(Z_{ij}^{\alpha})\right)^2} + f_{D,\alpha}a_Z^{\alpha}|D_{ij}^{\alpha}|\left(\frac{Z_{ij}^{\alpha}}{\mathrm{tr}(Z_{ij}^{\alpha})} + \frac{\mathrm{dev}(Z_{ij}^{\alpha})}{\mathrm{tr}(Z_{ij}^{\alpha})}\right)\right). \tag{3.56}$$

Here, note that $|D_{ij}^{\alpha}| = \sqrt{D_{ik}^{\alpha}D_{ki}^{\alpha}}$, also $\mathrm{tr}(Z_{ij}^{\alpha}) = Z_{ii}^{\alpha}$ and $\mathrm{dev}(Z_{ij}^{\alpha}) = Z_{ij}^{\alpha} - \frac{1}{3}Z_{kk}^{\alpha}\delta_{ij}$ are incorporated. As introduced below (see Section 2.3), Eqs. (3.55) and (3.56) are thought to describe the behavior of granular materials under deformation. Quite important here is the fact that granular materials, as anelastic solids, behave differently under loading and unloading. To model this behavior, the concepts of elastoplasticity have been revised, giving an alternative to the depiction of this non-linear path dependent behavior, with a rate-type equation.

Besides the co-rotational stress rate $\overset{\triangle}{Z}_{ij}^{\alpha}$, accounting for objective development of the material, it is in particular the constitutive part, $\Phi_{ij}(D_{ij}, Z_{ij}, ...)$, that introduces hypoplastic material behavior due to the incorporation of non-linear terms.

An alternative form for this source term or production tensor (3.56), with a different formulation of the respective coefficients, is

$$\Phi_{ij}^{\alpha} = D_{kl}^{\alpha}\left[c_1\mathrm{tr}(Z_{ij}^{\alpha})\delta_{ijkl} + c_2\frac{Z_{ij}^{\alpha}Z_{kl}^{\alpha}}{\mathrm{tr}(Z_{ij}^{\alpha})}\right] + |D_{ij}^{\alpha}|\left[c_3\frac{(Z_{ij}^{\alpha})^2}{\mathrm{tr}(Z_{ij}^{\alpha})} + c_4\frac{\mathrm{dev}(Z_{ij}^{\alpha})^2}{\mathrm{tr}(Z_{ij}^{\alpha})}\right]. \tag{3.57}$$

For hypoplasticity, the above representation (3.57) is justified in Kolymbas (1991) and picked up by Svendsen, Hutter and Laloui (Svendsen et al. 1999).

An influence of the pore pressure is not explicitly introduced in the development of the intergranular stress, although a mutual influence between these two quantities could for instance be described via the addition of new terms to the source term Φ_{ij}^{α} or a dependence of appearing parameters, such as $f_{s,\alpha}$ and $f_{D,\alpha}$. Here, we abstain from such alteration and maintain the structure of the source terms, as it is known in literature to describe the effects of plasticity well. Future work might research on this, and introduce such an impact of the pore pressure for example via the mentioned additional terms or the coefficients.

We choose the first form of the source term, see Eq. (3.56), which is a modification of Eq. (3.57), see Bauer (1996) or Fang (2008). The last term on the left-hand side of Eq. (3.55) is a result of a transformation of the evolution equation for Z_{ij}^{α} instead of T_{ij}^{α}, with the aim to keep the original structure of a corotational objective time derivative for an inserted frictional stress $T_{ij}^{\alpha}|_{fric} = \rho\delta^{Z} Z_{ij}^{\alpha}$, following Teufel (2001, p. 45). This change to Z_{ij}^{α} adds the term $(\rho^{\alpha} - \rho^{n})\,(\partial\Psi_{I}^{G}/\partial Z_{kl}^{\alpha})Z_{kl}^{\alpha}$ to the equilibrium stress tensor, a further spherical term, see also Fang et al. (2006) and Schneider & Hutter (2009, p. 163), the first also for another proposed frictional term with quadratic expansion.

As a result of these considerations, the equation governing the development of the inner stress-like quantity Z_{ij}^{s} of the solid takes the form

$$\begin{aligned} &\frac{\partial Z_{ij}^{s}}{\partial t} + v_{k}^{s}\frac{\partial Z_{ij}^{s}}{\partial x_{k}} + Z_{ik}^{s}W_{kj}^{s} - W_{ik}^{s}Z_{kj}^{s} - \nu^{s}\frac{\left(\rho^{s} - \rho^{f}\right)}{\rho}\frac{\partial v_{k}^{s}}{\partial x_{k}}Z_{ij}^{s} = \\ f_{S}&\left(a_{Z}^{s}D_{ij}^{s} + \frac{Z_{ij}^{s}Z_{kl}^{s}D_{kl}^{s}}{\left(Z_{mm}^{s}\right)^{2}} + f_{D}a_{Z}^{s}\sqrt{D_{lh}^{s}D_{hn}^{s}\delta_{ln}}\left(\frac{Z_{ij}^{s}}{Z_{mm}^{s}} + \frac{Z_{ij}^{s} - \frac{1}{3}Z_{kk}^{s}\delta_{ij}}{Z_{mm}^{s}}\right)\right), \end{aligned} \tag{3.58}$$

where we introduce $f_S = f_{S,s}$ and $f_D = f_{D,s}$, since no further distinction from other $f_{s,\alpha}, f_{D,\alpha}$ is necessary in the following.

Note that within several of the above assumptions, the principle of equipresence has been abandoned and replaced by the principle of phase separation. This is done, following Passman et al. (1984), as a replacement of Truesdell's principle of equipresence, which is considered being too general for multiphase mixtures.

In conclusion of the modeling process, let us assemble the results achieved so far, i.e. the closed set of equations for an isothermal process of solid-fluid composites: We have a set of 15 equations $\mathcal{V}^{s}, \mathcal{V}^{f}, \mathcal{M}_{i}^{s}, \mathcal{M}_{i}^{f}, \mathcal{Z}_{ij}^{s}, \mathcal{W}^{f}$ for 15 unknown quantities $\nu^{s}, v_{i}^{s}, v_{i}^{f}, Z_{ij}^{s}, \varpi_{\nu}^{s}, \varpi_{e}^{f}$. The material behavior is described for T_{ij}^{s} and T_{ij}^{f} in Eqs. (3.47)-(3.48), m_{i}^{s} in (3.49), the constitutive part of the inner stress Φ_{ij}^{s} in (3.56) and for the extra pore-fluid pressure source term γ_{ϖ}^{f}, see Eq. (3.52). Additional coefficients and parameter functions, for example for the viscosities μ^{s}, μ^{f}, are yet to be specified or are already included in the derivation. Thus, the system is closed and can be applied to a first, specific problem, a simple shear flow.

3.5 A simple application: shear flow

Before the system of equations is undertaken to a further transformation within the modeling procedure presented in the next chapter, in this section, our principal aim is to conduct a first test of the model as well as a comparison with other approaches. We discuss two problems of simple shearing, exemplary for the applicability of the model. Firstly, being a special case of a Couette flow for this medium, a granular-fluid mixture is considered, sheared between two infinite parallel plates with constant distance, of which the top one is moving. As a second example, a free surface flow on

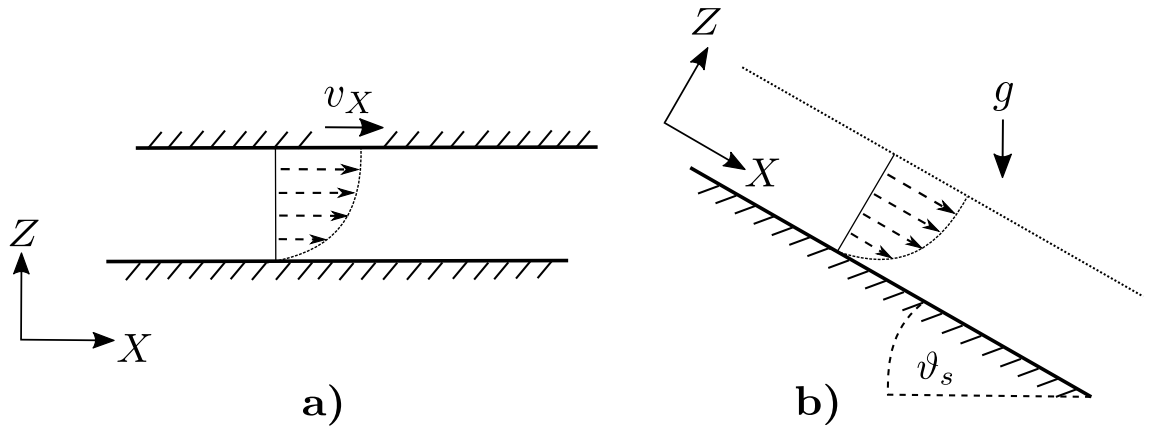

Figure 3.1: Steady shear flow, both for horizontal shearing (see Section 3.5.3.1) in panel **a)**, driven by the top plate of the velocity v_X, and, in panel **b)**, for a gravity induced free surface flow (see Section 3.5.3.2).

an inclined plane is examined. The Cartesian coordinate system O_{XZ} is fixed to the non-moving plate. Furthermore, we assume only (horizontal) velocities v_X^s and v_X^f to be different from zero, since the flow develops parallel to the plates, in the X-direction. For simple shear, it is assumed that the problem is stationary, so that the quantities only depend on the transverse coordinate Z, i.e. $\nu^s = \hat{\nu}^s(Z), v_X^s = \hat{v}_X^s(Z), v_X^f = \hat{v}_X^f(Z), \varpi_\nu^s = \hat{\varpi}_\nu^s(Z), \varpi_e^f = \hat{\varpi}_e^f(Z)$. We summarize the given restrictions as

$$\frac{\partial}{\partial t} = \frac{\partial}{\partial X} = 0, \qquad v_Z^\alpha = 0. \tag{3.59}$$

We also assume that $C_e^f = 1$. Apart from that, we specify the coefficient $a_2^\alpha = 2\mu^\alpha$ for the viscous part and will also parameterize the shear term a_4^α, see Goodman & Cowin (1972). For this first investigation of the behavior of the material under steady shear, we collected distinct possible influences and implemented them in the stress tensor, to gain a most general model, based on the extension of the Goodman-Cowin approach in the work of Savage (Savage 1979). This incorporates non-linear shear-rate effects as described by Bagnold (1954); for the application in the following chapters, we omit some of the terms again. See also Savage (1984) and Wang & Hutter (2001b) for details and a discussion.

3.5.1 The reduced system of equations for simple shearing

With the momentum balances and the applied restrictions for a simple shearing flow (3.59), four equations are obtained for $\alpha = s, f$ in the X- and Z-direction, respectively. The momentum balances of the solid and the fluid in the X-direction then state

$$m_X^s + \frac{\mathrm{d}T_{XZ}^s}{\mathrm{d}Z} = 0, \quad -m_X^s + \frac{\mathrm{d}T_{XZ}^f}{\mathrm{d}Z} = 0. \tag{3.60}$$

The remaining momentum balances of the solid and the fluid in the Z-direction take the forms

$$-\rho^s \nu^s g + m_Z^s + \frac{\mathrm{d}T_{ZZ}^s}{\mathrm{d}Z} = 0, \quad -\rho^f \left(1-\nu^s\right) g - m_Z^s + \frac{\mathrm{d}T_{ZZ}^f}{\mathrm{d}Z} = 0. \tag{3.61}$$

We further simplify the stress tensor of the general model (3.41), omitting secondary terms by assuming $a_3^\alpha = a_5^\alpha = a_6^\alpha = a_7^\alpha = 0$, i.e. introducing a linear approach. The reduced components of the solid stress tensor (3.47) then yields

$$\begin{aligned} T_{XZ}^s &= \rho\delta^Z Z_{XZ}^s + a_2^s D_{XZ}^s = \rho\delta^Z Z_{XZ}^s + \mu^s \frac{\mathrm{d}v_X^s}{\mathrm{d}Z}, \\ T_{ZZ}^s &= -\left(\varpi_h^f - \varpi_e^f + \varpi_\nu^s - \left(\rho^s - \rho^f\right)\delta^Z \left(Z_{XX}^s + Z_{YY}^s + Z_{ZZ}^s\right)\right)\nu^s \\ &\quad + \rho\delta^Z Z_{ZZ}^s + a_4^s \frac{\mathrm{d}\nu^s}{\mathrm{d}Z}\frac{\mathrm{d}\nu^s}{\mathrm{d}Z}. \end{aligned} \tag{3.62}$$

The solid stress tensor T_{XZ}^s is composed of a hypoplastic inner stress part and a viscous part in the X-direction, similarly, the pressure part T_{ZZ}^s consists of a hypoplastic stress part and a shearing component in the Z-direction. The fluid stress tensor exhibits the same structure, without the hypoplastic influence and with a reduced pressure part as deducible from Eq. (3.48), viz.,

$$T_{XZ}^f = a_2^f D_{XZ}^f = \mu^f \frac{\mathrm{d}v_X^f}{\mathrm{d}Z}, \quad T_{ZZ}^f = -\varpi^f \left(1-\nu^s\right) + a_4^f \frac{\mathrm{d}\nu^s}{\mathrm{d}Z}\frac{\mathrm{d}\nu^s}{\mathrm{d}Z}. \tag{3.63}$$

Furthermore, the momentum interaction terms in the X- and Z-directions can be deduced from (3.49) and are given by

$$m_X^s = c_D^{sf}\left(v_X^s - v_X^f\right), \quad m_Z^s = \frac{\mathrm{d}\nu^s}{\mathrm{d}Z}\left(\varpi^f + \frac{\rho^f\left(1-\nu^s\right)}{\rho}\varpi_\nu^s\right). \tag{3.64}$$

A generalized drag coefficient is chosen, referring to Pudasaini (2012), with

$$c_D^{sf} = \frac{\nu^s \nu^f \left(\rho^s - \rho^f\right) g |u_i^f - u_i^s|^{J-1}}{\left[\mathcal{U}_T\{\phi_P \mathbb{A}_\mathbb{P} + (1-\phi_P)\,\mathbb{B}_\mathbb{P}\}\right]^J}, \tag{3.65}$$

and in which $\phi_P \in [0,1]$ is a dimensionless parameter. Moreover, $\mathcal{U}_T = \sqrt{g\delta_P \rho^s/\rho^f}$ is the terminal falling velocity of a particle with density ρ^s in a fluid of density ρ^f. The formula has Toricelli-structure in a constant gravity field g and for a particle diameter δ_P. The particle Reynolds number $Re_P = \mathcal{U}_T \delta_P/\nu$ is used to define the dimensionless products

$$\mathbb{A}_\mathbb{P} = \frac{\rho^f}{\rho^s}\left(\frac{\nu^f}{\nu^s}\right)^3 \frac{Re_P}{180}, \quad \mathbb{B}_\mathbb{P} = \left(\nu^f\right)^{M(Re_P)-1}, \tag{3.66}$$

which contribute to the evaluation of c_D^{sf}. While $\mathbb{A}_{\mathbb{P}}$ is a measure for the significance of the fluid flow through a porous granular skeleton, the parameter $\mathbb{B}_{\mathbb{P}}$ measures the significance of a particle moving through a fluid. In this regime, the parameter $M(Re_P)$ describes a weak dependence on the particle Reynolds number,

$$M(Re_P) = 4.45 \cdot Re_P^{-0.1}, \mathbb{B}_{\mathbb{P}} \quad \to 0, \quad 1 < Re_P < 500,$$

see Richardson & Zaki (1954). Thus, we omit a possible contribution of $\mathbb{B}_{\mathbb{P}}$ to c_D^{sf}. This case corresponds to a debris flow with granular structure. Limit values are given as $M(0) = 4.65$ and $M(\infty) = 2.40$. Moreover, with $J = 1$ and $J = 2$, the drag coefficient accounts for smooth and linear as well as turbulent and quadratic responses, respectively.

Pudasaini (2012) introduced this generalized drag coefficient to model the drag influence on the flow. In his work, a term for the virtual mass forces, consisting of a derivative of the relative velocity with respect to time, is also incorporated in the momentum interaction term. However, such a term is not considered here, since its consideration would enlarge the class of constitutive variables and therefore call for new restrictions, something that is left for future work.

The final system of equations is derived by inserting the given stress tensors from Eqs. (3.62), (3.63) and momentum interaction terms (3.64) into the residual momentum balances (3.60), (3.61). Starting with the momentum balance in the X-direction, differential equations for the velocities of the solid and the fluid are derived. These turn out to be

$$\frac{\mathrm{d}}{\mathrm{d}Z}\left(\mu^s \frac{\mathrm{d}v_X^s}{\mathrm{d}Z}\right) + c_D^{sf} v_X^s = c_D^{sf} v_X^f - \frac{\mathrm{d}\nu^s}{\mathrm{d}Z}\left(\rho^s - \rho^f\right)\delta^Z Z_{XZ}^s, \tag{3.67}$$

$$\frac{\mathrm{d}}{\mathrm{d}Z}\left(\mu^f \frac{\mathrm{d}v_X^f}{\mathrm{d}Z}\right) + c_D^{sf} v_X^f = c_D^{sf} v_X^s. \tag{3.68}$$

For the viscosities we follow Passman, Nunziato, Bailey & Reed (1986) and Wang & Hutter (1999c),

$$\mu^s = \mu^{s,0}\left(\frac{\nu^s}{\nu_\infty^s - \nu^s}\right)^2, \quad \mu^f = \mu^{f,0}\left(1 - \nu^s\right)^2. \tag{3.69}$$

Moreover, with the particle Reynolds number $Re_P = v_X^f \delta_P \rho^f / \mu_f$, c_D^{sf}, listed in Eq. (3.65), the drag coefficient takes the form

$$c_D^{sf} = \frac{\nu^s\left(1-\nu^s\right)\left(\rho^s - \rho^f\right) g \sqrt{\left(v_X^f - v_X^s\right)^2}}{\left[\sqrt{\frac{g\delta_P\rho^f}{\rho^s}}\left(\frac{1-\nu^s}{\nu^s}\right)^3 \frac{Re_P}{180}\right]^2}. \tag{3.70}$$

The solid momentum balance in the Z-direction, (3.61), with the stress T^s_{ZZ} listed in $(3.62)_2$, reduces to

$$\begin{aligned} 2a_4^s \frac{\mathrm{d}^2 v^s}{\mathrm{d}Z^2} + \frac{\mathrm{d}a_4^s}{\mathrm{d}Z}\frac{\mathrm{d}v^s}{\mathrm{d}Z} - \varpi_\nu^s \frac{\rho^s}{\rho} v^s = \\ \frac{v^s}{\mathrm{d}_Z v^s}\left(\rho^s g - \frac{\mathrm{d}\varpi_e^f}{\mathrm{d}Z} + \frac{\mathrm{d}\varpi_\nu^s}{\mathrm{d}Z}\right) - \left(\rho^s - \rho^f\right)\delta^Z \left(Z^s_{XX} + Z^s_{YY} + 2Z^s_{ZZ}\right), \end{aligned} \tag{3.71}$$

and the fluid momentum equation, stated in (3.61), with the stress T^f_{ZZ} given in $(3.63)_2$, leads to

$$\frac{v^s - 1}{\mathrm{d}_Z v^s}\left(\rho^f g + \frac{\mathrm{d}\varpi^f}{\mathrm{d}Z}\right) - \frac{\rho^f \left(1 - v^s\right)}{\rho}\varpi_\nu^s + \frac{\mathrm{d}a_4^f}{\mathrm{d}Z}\frac{\mathrm{d}v^s}{\mathrm{d}Z} + 2a_4^f \frac{\mathrm{d}^2 v^s}{\mathrm{d}Z^2} = 0. \tag{3.72}$$

The coefficients of the shear stress components are given by

$$a_4^s = \frac{2a_4^{s,0}}{\left(v_\infty^s - v^s\right)^2}, \quad a_4^f = 2a_4^{f,0}. \tag{3.73}$$

For a_4^s, following Wang & Hutter (1999c), a formula similar to that for the solid viscosity is chosen, while a_4^f is assumed to be constant. This approach is compatible with that proposed by Goodman & Cowin (1972), giving $a_4^s = \hat{a}_4^s\left(v^s, \rho^s, \theta\right)$. Note that no explicit representation is given in these references, and the term is part of the equilibrium stress tensor.

The pore pressure evolution equation for steady simple shearing states

$$\frac{k_D}{\mu^f}\frac{\mathrm{d}^2\varpi_e^f}{\mathrm{d}Z^2} + \frac{\mathrm{d}}{\mathrm{d}Z}\left(\frac{k_D}{\mu^f}\right)\frac{\mathrm{d}\varpi_e^f}{\mathrm{d}Z} = \sqrt{2\left(D^s_{XZ}\right)^2}\left(v^s - \frac{v_C^s}{1 + \sqrt{\mathrm{N}_\gamma}}\right), \tag{3.74}$$

where the viscosity of the fluid is applied as in Eq. $(3.69)_2$, together with an empirical formula for the hydraulic permeability $k_D = k_D^0 e^{\frac{0.6 - v^s}{0.4}}$, suggested by Iverson & George (2014). Note that in simple shearing $Z^s_{XX} = Z^s_{YY} = Z^s_{ZZ}$, due to the vanishing source term $\Phi^s_{ij} = 0$, also referred to as the critical state in the context of hypoplasticity. Although we are dealing with a quasi-one-dimensional problem, the third spatial direction has to be considered, e.g. for $Z^s_{ii} = Z^s_{XX} + Z^s_{YY} + Z^s_{ZZ} = 3Z^s_{XX}$. With balance equation for the hypoplastic stress, $Z^s_{XZ} = -(3/\sqrt{2})a^s_Z Z^s_{XX}\mathrm{sgn}(\mathrm{d}_Z v^s_X)$ is derived. The quantities Z^α_{ij}, therefore, are no proper fields and become constants.

The system of equations contains now the solid and fluid momentum balances in the X-direction for the two velocities v^s_X and v^f_X, the solid momentum balance in the Z-direction for the volume fraction v^s, the fluid momentum balance in the Z-direction for the solid configuration pressure ϖ^s_ν and the pore pressure evolution equation for the fluid extra pressure ϖ^f_e, i.e. five equations for five unknown variables. There remains a number of coefficients and parameters that need to be further specified, also

see Appendix A, but the system is closed and can in principle be solved numerically. See also Wang & Hutter (1999c) for further details on the numerical steps taken.

3.5.2 Discretization and numerics

We use simple finite difference methods for the 1-D problem. This contains the discretization in space, dividing the continuum in many discrete points for which results are estimated. For this purpose, the partial differential equations are approximated by difference equations, in which the gradients are replaced by finite difference expressions. Equations (3.67) and (3.68) have the following forms

$$\frac{\mathrm{d}}{\mathrm{d}Z}\left(\alpha^{\phi}\frac{\mathrm{d}\phi}{\mathrm{d}Z}\right)+\beta^{\phi}\phi=r^{\phi}, \tag{3.75}$$

in which α^{ϕ}, β^{ϕ} and r^{ϕ} can be readily identified. Discretization with $\mathrm{d}_Z\phi \approx \Delta Z^{-1}(\phi|_{j+\frac{1}{2}} - \phi|_{j-\frac{1}{2}})$ leads to

$$\alpha^{\phi}|_j\left(\frac{\phi|_{j+1}-\phi|_j}{\Delta Z^2}\right)-\alpha^{\phi}|_{j-1}\left(\frac{\phi|_j-\phi|_{j-1}}{\Delta Z^2}\right)+\beta^{\phi}|_j\phi|_j=r^{\phi}|_j. \tag{3.76}$$

Equations (3.67) and (3.68) are thus rearranged into a tridiagonal form, $a_j^{\phi}\phi|_{j+1} + b_j^{\phi}\phi|_j + c_j^{\phi}\phi|_{j-1} = r_j^{\phi}$ and then solved with a simple algorithm. For this, the central difference quotient for first and second order derivatives are applied,

$$\frac{\mathrm{d}\phi}{\mathrm{d}Z}\approx\frac{\phi|_{j+1}-\phi|_{j-1}}{2\Delta Z},\quad \frac{\mathrm{d}^2\phi}{\mathrm{d}Z^2}\approx\frac{\phi|_{j+1}-2\phi|_j+\phi|_{j-1}}{\Delta Z^2}. \tag{3.77}$$

The system is solved using a simple Matlab-code, applying under-relaxation. For further details on the resulting equations, as well as for values and boundary conditions applied, see Appendix A.

3.5.3 Numerical results

In the following, some first numerical studies, concerning the case of a simple, steady shear flow on a horizontal plane and on an inclined plane are presented. These studies show the profile of some quantities in depth direction and can be seen as preliminary or complimentary investigations to the following simulations for depth-integrated flows, since these information about the depth direction are neglected later. The investigated case corresponds to a mixture of water and natural angular beach sand. Most of the parameters are taken from Wang & Hutter (1999b), Wang & Hutter (1999c) and Iverson & George (2014). We remark that a strong dependence on the channel width is observed, so while the flow depth is prescribed, the effects of its variation are not investigated here. See also Wang & Hutter (1999b) and Wang & Hutter (1999c) for further information on this point.

3.5.3.1 Horizontal shearing

We begin with a description of the depicted flow profile for the case of horizontal shearing, compared with analogous results of Wang & Hutter (1999b). Fang et al. (2006) examine a similar case for dry granular flows, so in order to estimate the influence of the fluid, our results can be compared with the ones presented there. For profiles of the volume fraction see Fig. 3.2, panel **a)**, for basic velocity profiles see panels **b)-c)** of Fig. 3.2. The approximately parabolic profile of the volume fraction, beginning with a region of slow decline, is followed by a steeper gradient in the lower flow region, near the bottom, denoted as a region of strong shearing. The volume fraction profile of Wang & Hutter (1999b) begins with an almost linear decrease, and always lies below our profile. The disparity can be traced to the different concepts of the pressures and their relations to the equilibrium stress tensors. The volume fraction in its development influences the velocities, mediated via changes in viscosity. This behavior also affects the pore-pressure in its evolution, see panel **d)** of Fig. 3.2. The solid and fluid velocities develop analogously, which indicates a strong coupling.

Both velocity profiles, of the solid and the fluid component, respectively, exhibit a sharp gradient at the bottom, developing towards an almost constant flow in the upper half. The related velocity profiles of Wang & Hutter (1999b) develop in a similar way, with a slightly steeper increase in the lower flow region. The differences occur because of disparities in the development of the volume fraction. It is interesting to see in the parametric studies below, that the emphasis of the hypoplasticity in our model leads to a velocity profile quite similar to theirs, but for the volume fraction, the trend proceeds in the opposite direction. Therefore, we assume that the hypoplastic part, although it seems to be one major difference in the correspondent equations for the solid velocity, is not the cause of the displayed remote differences.

Note that the possible influences on the results due to parameter choices, i.e. on the developing profiles, are further investigated in the parametric studies of Heß et al. (2017). This also indicates that the results here are not to be seen as fixed and exclusive, but rather adjustable by weighing the different effects and mechanisms.

The extra pore-fluid pressure causes an elevation of the pressure in the top region with steep gradients of the solid volume fraction and lowers the fluid pressure in the region below. This indicates an enhancement of the solid stress here, since the fluid pressure is decreased. Note that because for this quantity, there are no values to compare within the consulted works, only our results are depicted in Fig. 3.2, panel **d)**. In the work of Iverson & George (2014), the pressure profile in the vertical direction is only estimated, since these authors apply depth-integration. Nonetheless, the estimation allows for at least a comparison by trend, showing that our extra pore pressure fits qualitatively the shown graph for an estimation of the pressure with $p_b/\rho_f gh = 0$, the tension-saturated state. See also Teufel (2001) with the author's results for the solid excess pressure in simple shearing.

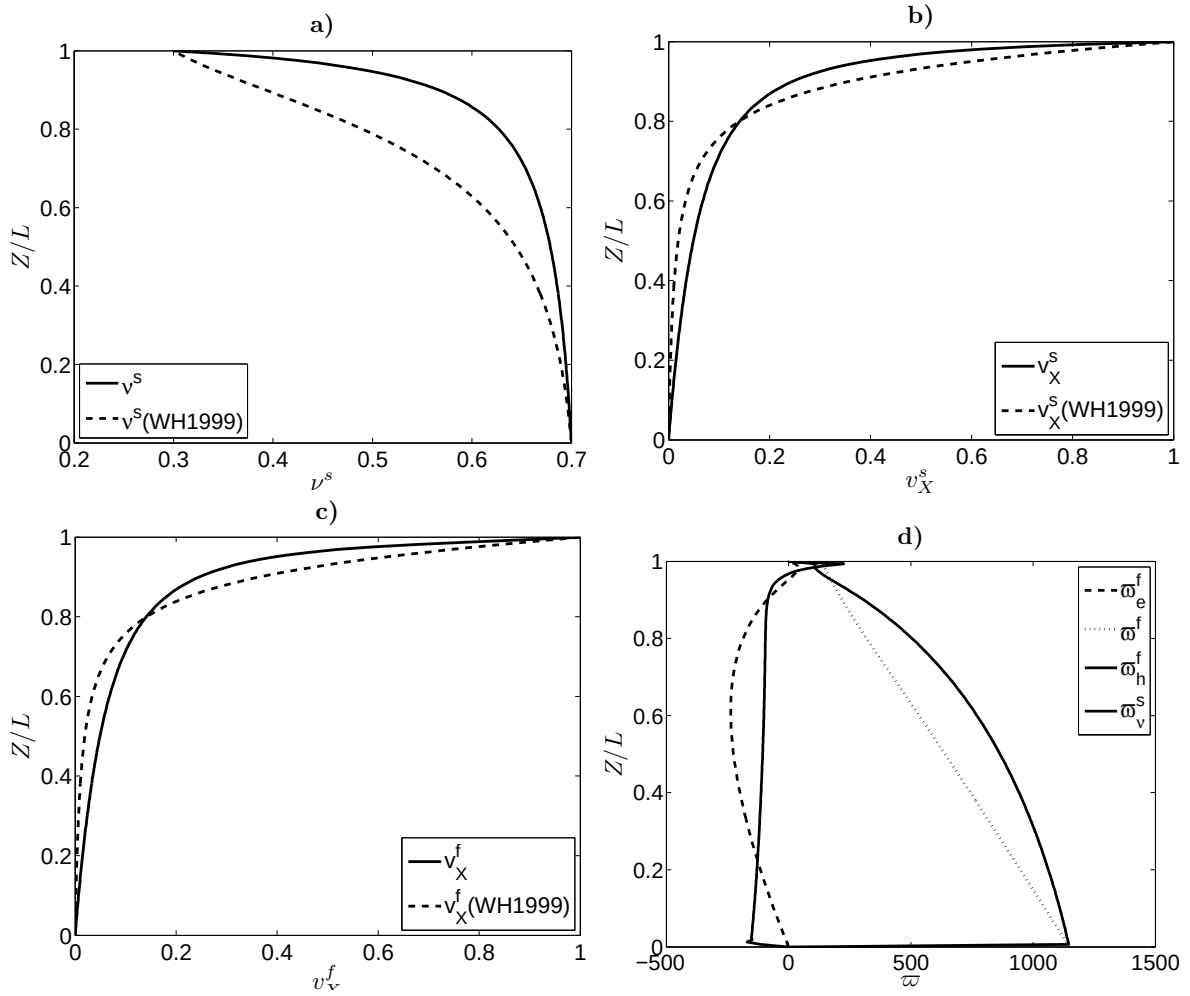

Figure 3.2: Case of horizontal shearing compared to the results of Wang & Hutter (1999b), denoted as WH1999, with adjusted parameters and boundary conditions. Profiles of the volume fraction ν^s in panel **a)**, the solid velocity v^s_X in panel **b)**, the fluid velocity v^f_X in panel **c)**, and the pressure distribution in panel **d)**

3.5.3.2 Gravity driven flow down an inclined plane

We go on with a different case, the gravitational free surface flow on an inclined plane to show the possible application to this further case. The profile of the volume fraction and the velocities of the fluid and the solid agree qualitatively with the results of Wang & Hutter (1999c), for comparison see their study; differences will be discussed below. They investigate an inclined gravity-flow problem; so our model is adjusted with respect to the gravitational term and the boundary conditions. Since this chute flow has a free surface, the flow is only caused by gravitational forces, not the moving top plate as before. Out of the range of tested cases by Wang & Hutter (1999c), we choose the case of $\mathcal{L} = 0.5$cm and an inclination angle $\vartheta_s = 20^\circ$ to compare.
Their results suggest an almost constant value in the upper region, while our results for the volume fraction seem to indicate a growing incline with depth, see Fig. 3.3**a)**. Also, the arising volume fractions at the top differ from one another. We find the

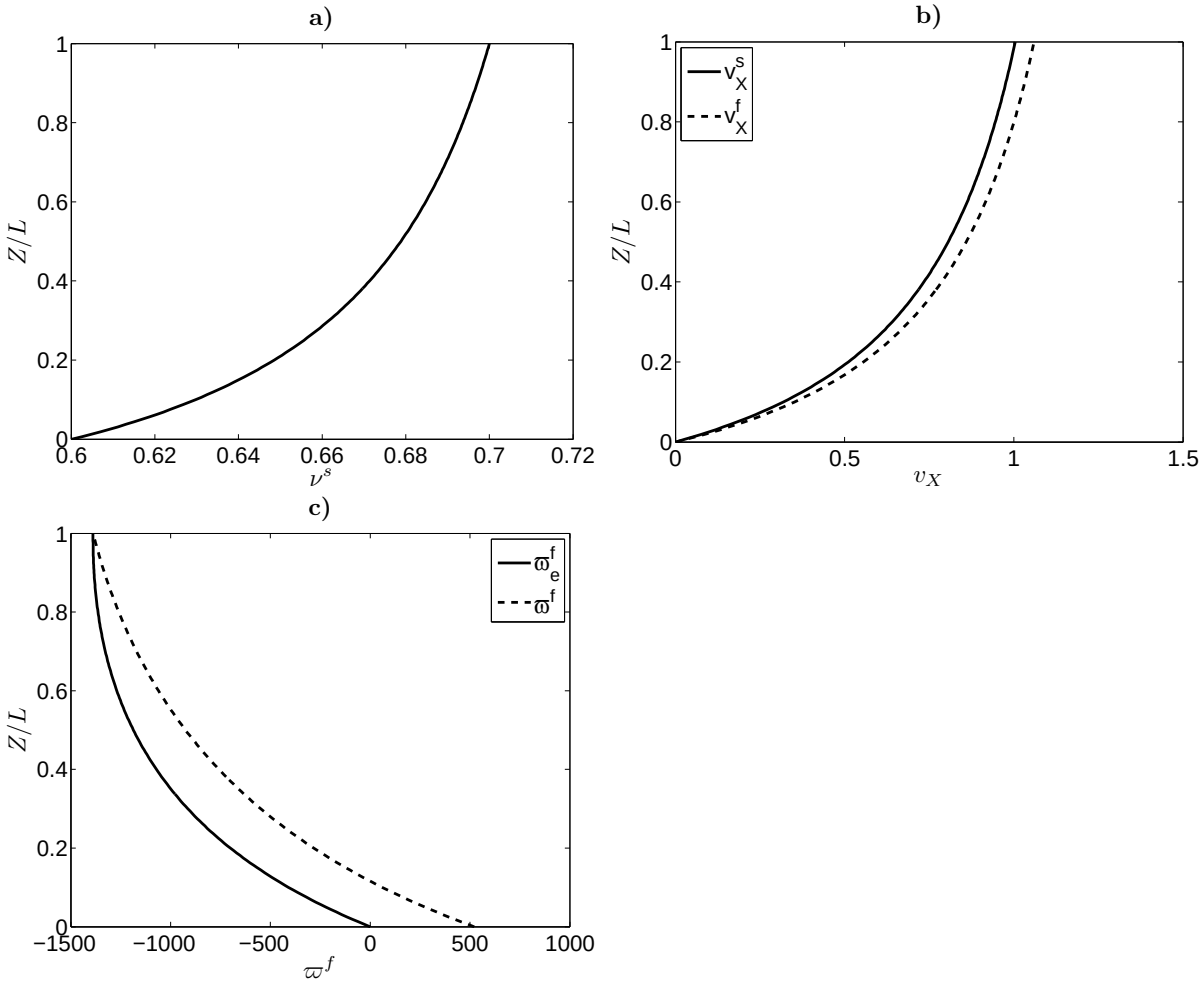

Figure 3.3: Inclined plane flow for an inclination angle $\vartheta_s = 20^\circ$. Profiles of the volume fraction ν^s in panel **a)**, the solid velocity v_X^s in panel **b)** and the fluid pressure ϖ^f in panel **c)**.

solid velocity to be slightly changed, as in panel **b)** of Fig. 3.3. The profile is now more parabolic and less exponential, i.e. in the bottom region, the gradient $\mathrm{d}_Z v_X^s$ is much smaller. The fluid now behaves differently compared to the solid component, moving faster. The changes in velocity go back to the influence of the gravitational term, which now also influences the movement in the X-direction, and the absence of a shearing top boundary. The profile of the pore-fluid pressure is changed as well, see Fig. 3.3**c)**, which can also be explained with the changed boundary conditions for the volume fraction, adjusted to the numerical experiments of Wang & Hutter (1999c), and primarily with the changes in hydrostatic pressure due to the inclined plane. The latter one causes a larger pillar of fluid to lay on top. Now that the model derived from the entropy principle in its Müller-Liu (ML) formulation has been applied for the first time, we return to the treatment of equations. In the following chapter, with regard to the approach of Savage & Hutter (1989), the model is transferred into the context of a scaled and depth-integrated formulation, which improves its applicability and raises further challenges in conjunction with the modeling.

4 Derivation of a scaled and depth-integrated model

Until now, the focus has been on the derivation of constitutive equations, and with this, a closer determination of the material behavior. To do so, the entropy principle was applied in its formulation according to Müller and Liu. In the following, the system of equations thus determined is to be non-dimensioned and depth-integrated (Sections 4.3 and 4.4). Before that, in Section 4.1, a general recapitulation of the SH approach is given, together with a discussion of the transfer and application of the results (Sections 4.2.1 and 4.2.2), derived in the previous chapter according to the ML entropy principle.

For the SH model, a process of scaling and depth-integration is applied to the given system of equations to provide closure for the otherwise unknown stress tensors. Due to the derivation in the framework of the entropy principle, the stress tensors and the momentum interaction term applied in this work already exhibit a given structure and thus are not completely unknown. Nonetheless, with the transfer to a shallow-flow model, the equations are simplified in the process of scaling, the computational efforts are reduced due to depth-integration and the hydrostatic pressure still needs an adequate form, which can be found in conjunction with depth-integration. Furthermore, the material parameters applied to close the systems are recapitulated in Section 4.5, and the system of equations will be transferred into general coordinates, allowing for the treatment of a complex, rugged topography (Section 4.6).

4.1 The Savage-Hutter model

As pointed out above, the formative work of Savage and Hutter, presented in Savage & Hutter (1989), introduced a new modeling attempt for granular(-fluid) flows. Considering a Cartesian (X, Z)-system, it describes a plane, two-dimensional granular mass flow down an inclined plane with the inclination angle ϑ_s, see Fig. 4.1, assumed to be shallow and thus independent from the depth-direction. Central assumption for this is that the ratio of height-scale $\mathcal{H}$ to length-scale $\mathcal{L}$ is small, so $\epsilon = \mathcal{H}/\mathcal{L} \ll 1$. With the assumption of shallowness, the flow can be described solely in one coordinate (and time), for which a process of scaling and depth-integration is applied. Further, with a constant mass density ρ^s, the balance of mass can be rewritten as a balance of the flow height, yielding

$$\frac{\partial h}{\partial t} + \frac{\partial \left(h v_X^s\right)}{\partial X} = 0. \tag{4.1}$$

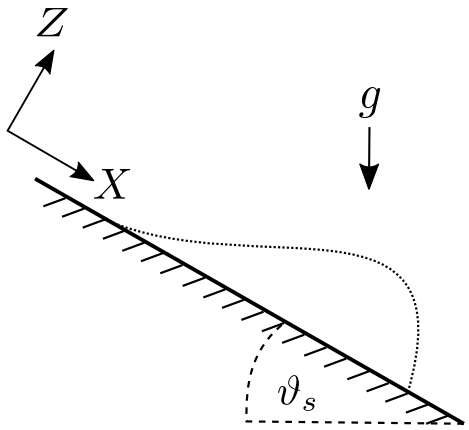

Figure 4.1: The flow configuration of the SH-model, with a Cartesian coordinate system O_{XZ} on an inclined plane (inclination angle ϑ_s) and driving gravity.

This depicts the development of the flow height $h(X,t)$ with respect to the velocity $v_X^s(X,t)$. Now to describe the velocity, the balance of momentum in the horizontal X-direction yields, after scaling and depth-integration

$$\frac{\partial\left(hv_X^s\right)}{\partial t}+\frac{\partial\left(hv_X^s v_X^s\right)}{\partial X}=h\sin\left(\vartheta_s\right)-\epsilon\cos\left(\vartheta_s\right)\frac{\partial}{\partial X}\left(T_{XX}^s h\right)-\cos\left(\vartheta_s\right)T_{XZ}^s, \tag{4.2}$$

where, for the lateral pressure, the earth pressure correlation is employed with $T_{XX}^s = K_{act/pas}T_{ZZ}^s$, and the pressure $T_{ZZ}^s = \frac{h}{2}$, $[T_{ZZ}^s]_b = h$ is derived during the depth-integration, as a result of the reduced normal momentum balance. In the term governing the basal friction, with $T_{XZ}^s = \mathrm{sgn}(v_X^s)\tan\left(\delta_b\right)[T_{ZZ}^s]_b$, a Mohr-Coulomb criterion is employed, relating the shear stress hindering the motion to a bed friction angle δ_b. In the first term of the RHS in Eq. (4.2), the driving gravitational influence is given. For a derivation of these relations in greater detail see Savage & Hutter (1989), as well as Hutter & Wang (2016), where an introduction coming from an infinitesimal column is presented, together with an ensuing discussion.

These simple equations have been amended in a lot of ways in the following years, adding more advanced, curvilinear set of coordinates (Savage & Hutter 1991), a cross-slope direction (Gray et al. 1999), and further physical aspects, concerning, e.g., phases, phase interaction, layers and the mechanics of segregation.

In the following, we refer to the model of Meng & Wang (2016) as an applicable extension of the SH equations to two phases, with respective interaction terms. With reference to this model, called Meng-Wang (MW) in the following, the influence of the additional fields will be explained and clarified, since they amend the basic system of equations for a two-phase fluid presented there.

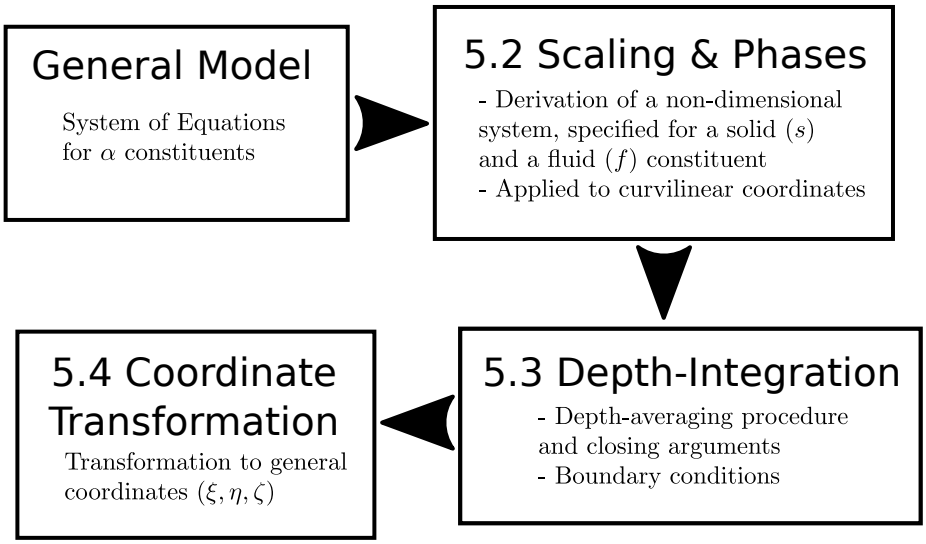

Figure 4.2: Overview of the derivational process of a scaled and depth-integrated model of the shallow-flow-type, applied to general coordinates for a rugged topography. Starting with the general model for a system with an unspecified number of constituents α, successively, the scaled and depth-integrated equations for a granular-fluid system are derived and applied to general coordinates.

4.2 On the transfer of the results

It may seem redundant, but for modeling, it is reasonable to start with a most general system of equations, comprising a wide range of quantities, even if these may later be omitted for practical application. The advantage of coming from a most general model to a simpler one by explicitly imposing restrictions is both the awareness of working with limitations, which always means abstraction from real processes, and the possibility to investigate the influence of further terms by re-taking them into account in future applications. It should be emphasized that our depth-integrated model equations are – with the help of further limitations – equivalent to well-known models in the context of debris flow modeling, see Heß & Wang (2019) and Appendix D. While the constitutive relations were the final result of the preceding chapter, for most approaches in the field of debris flow modeling, the postulation of a set of equations is the very beginning of their studies.

4.2.1 From Müller-Liu to a shallow-flow model

With the exploitation of the entropy principle in its formulation by Müller and Liu, a strict algorithm yields a set of derived constraints. These provide insights in the appearance of terms, linking general laws of thermodynamics and the balance equations of the system to their constitutive relations and as a consequence, both the apparent arbitrariness of a priori modeling as well as the neglect of fundamental basis of thermodynamics can be avoided. By these means, thermodynamically consistent constitutive equations were developed most notably for the stress tensor and the momentum

interaction term with regard to the set of equations (3.4) and the material behavior (3.5). Therefore, consistency here also means that the structure of the constitutive functions reflects the system of equations (3.4), for which the constitutive equations themselves are developed. This provides insight into the influence of the new set of internal variables on the respective rheological properties.

In a second step, these resulting equations have to be interpreted and closed by certain assumptions. In the context of debris flow modeling, this often tends to be the weak point of modeling efforts – the rather complex and theoretical manner of modeling in conjunction with the exploitation of the entropy principle often stops here. At the same time, modeling aiming at practical applicability mostly starts here, with a priori alignment of constitutive assumptions. Avoiding these two patterns, we tie in with closure suggestions made by de Boer & Ehlers (1990) and Liu (2014), linking the results of the Müller-Liu derivation to the pore-fluid pressure, see Section 3.4. With this, a closed set of equations is developed.

The further derivational process, depicted in Fig. 4.2, is outlined in the following. It should be noted that with these modeling attempts, to the best of the author's knowledge, for the first time a transfer from entropy-principle based derivations to – usually rather a priori based – shallow-flow modeling, i.e. a depth-integrated application and numerical simulation has been established in this field.

4.2.2 On the constitutive functions

As described above, the results derived with the ML entropy principle for the constitutive equations are further completed by a set of closing assumptions with the postulation of non-equilibrium parts, see Eqs. (3.41)- (3.43). After this, following the results of Section 3.4, for the general stress tensor, the following, now simplified form is given

$$\begin{aligned} T_{ij}^{\alpha} &= -\varpi^{\alpha} v^{\alpha} \delta_{ij} + T_{ij}^{e,\alpha} \\ &= -\varpi^{\alpha} v^{\alpha} \delta_{ij} + \varpi_{Z}^{\alpha} v^{\alpha} \delta_{ij} + \rho \delta^{Z} Z_{ij}^{\alpha} + a_1^{\alpha} D_{kk}^{\alpha} \delta_{ij} + a_2^{\alpha} D_{ij}^{\alpha}, \end{aligned} \tag{4.3}$$

and, for the momentum interaction term, regarding Eq. (3.43) and $\rho^{\alpha} = const$, it follows that

$$m_i^{\alpha} = \sum_{\beta=1}^{n-1} \frac{\partial v^{\beta}}{\partial x_i} \left(\varpi_h^{\alpha} \left(1 - \delta_{\alpha n}\right) - \varpi_h^{n} \delta_{\alpha n} - \varpi_v^{\beta} \frac{\rho^{\alpha} v^{\alpha}}{\rho} \right) + \sum_{\beta=1}^{n} c_D^{\alpha\beta} \left(v_i^{\beta} - v_i^{\alpha} \right).$$

The stress tensor exhibits the classical splitting with a pressure-like spherical part $\varpi^{\alpha} v^{\alpha}$ and a deviatoric extra stress $T_{ij}^{e,\alpha}$. The resulting restrictions on the form of the constitutive functions, derived previously, shape in particular the form of the pressure-related terms. $a_1^{\alpha}, a_2^{\alpha}$ are the coefficient functions of the terms entering the non-equilibrium stress tensor and $c_D^{\alpha\beta}$ is the general drag coefficient between two constituents. Also note that, since the drag term already exhibits a velocity difference,

we return to the partial velocity v_i^α instead of the objective u_i^α. The partial pressure ϖ^α can be split up into a hydrostatic part ϖ_h^α and an extra part. As mentioned before, the momentum interaction terms of all constituents sum up to zero, i.e. vanish for the mixture momentum equation. And while this interaction term also possesses classical structure, including a drag term $c_D^{\alpha\beta}(v_i^\beta - v_i^\alpha)$ and a buoyant term in conjunction with the product of pressure and volume fraction gradient, $\frac{\partial n^\beta}{\partial x_i}\varpi_h^\alpha$, it is worth noting here that in the latter, an additional term in conjunction with the configurational pressure ϖ_v^α arises. This term is a direct result from the thermodynamically consistent derivation, so far not included in postulated buoyant terms of debris flow models.

The further treatment of our system of equations follows the approach for a shallow-flow, where, similar to shallow-water equations, it can be assumed that the horizontal extent of a flow is much larger than its (normal) height, so that the changes of the fields in this direction are negligible. However, as pointed out above, unlike in most Savage-Hutter (SH)-type models, the stress tensor is given as a result of the modeling process and no closure conditions via earth-pressure correlations are required for the solid material. Instead, hypoplasticity is introduced to allow for plastic material behavior. Hypoplastic models for the description of the deformational behavior of granular materials, taking the different paths of loading and unloading into account, have been developed in a series of publications (Kolymbas 1977, Kolymbas 1985, Kolymbas 1991) and are applied in recent works e.g. by Guo, Peng, Wu & Wang (2016) and Peng, Guo, Wu & Wang (2016). Coming from soil mechanics, hypoplasticity was proposed as a rather simple model to facilitate previous, more sophisticated concepts, while retaining the core ability of accurately predicting the deformation of granular materials as both anelastic and non-linear. It gives a certain relation between the strain rate, i.e. the deformation due to shear, and an internal contact-stress, modeled as a symmetric second-order tensorial variable.

In addition to viscosity, for the fluid phase, another well-known concept from soil mechanics is referred to because of its explanatory power in terms of the increased mobility of debris flow. According to the concept of effective stress in porous media, a dynamic extra pore-fluid pressure is considered to mediate emerging load on the solid structure to the fluid. This introduces a dynamic pressure, additional to the hydrostatic fluid pressure, that influences the solid structure, the intergranular friction and therefore also the flow dynamics. This line of tradition in debris flow modeling goes mainly back to the works of Iverson (Iverson 1997, Savage & Iverson 2003, George & Iverson 2011, Iverson & George 2014). As a novelty, we are taking up both the concept of a dynamic pore-fluid pressure and hypoplasticity and merge them into a new, depth-integrated model that is able to depict some of the core features and properties of debris flows.

As already denoted in Section 3.4.2, in the following, we restrict the original system of balance laws (3.4), by neglecting changes in the true densities ($\rho^\alpha = const$) and phase transitions ($c^\alpha = n^\alpha = 0$). We also assume that changes in the mixture temperature θ are insignificant, hence the energy equation is excluded in the ensuing computations, and assume that the further influence of the left Cauchy-Green deformation tensor

B_{ij}^{α} is negligible, thus omitting elastic behavior in the following. And, as before, the saturation condition is applied, i.e. $\sum_{\alpha=1}^{n} \nu^{\alpha} = 1$ must hold, so the granular phase and the fluid occupy the entire space.

We concretize the general model with n constituents to a two-constituent solid-fluid mixture, i.e. $\alpha = s, f$. For this and as a central closing assumption, the n-th partial pressure ϖ^n is identified with the pore-fluid pressure ϖ^f, see Section 3.4.2, consisting of a hydrostatic ϖ_h^f and a dynamic extra part ϖ_e^f. Recapitulating Eqs. (3.47)-(3.48), we specify the partial pressure terms to

$$\begin{aligned} \varpi^s - \varpi_Z^s &= \varpi_h^s - C_e^f \varpi_e^f - \varpi_Z^s = \varpi_h^f + \varpi_\nu^s - C_e^f \varpi_e^f - \left(\rho^s - \rho^f\right) \delta^Z Z_{ii}^s, \\ \varpi^f &= \varpi_h^f + C_e^f \varpi_e^f, \end{aligned} \tag{4.4}$$

with a constant C_e^f, accounting for the influence of the extra pore-fluid pressure, the static solid pressure $\varpi_h^s = \varpi_h^f + \varpi_\nu^s$ and $\varpi_Z^s = \left(\rho^s - \rho^f\right) \delta^Z Z_{ii}^s$. A configurational pressure ϖ_ν^s and a term ϖ_Z^s, accounting for the spherical influence of intergranular friction, are present in the solid pressure-like term. Previous attempts to establish a link between the pore-fluid pressure and the resultant terms of the thermodynamic consistent exploitation of the entropy principle stem from the work of de Boer & Ehlers (1990) and later Liu (2014), in which the results of the exploitation of the Müller and Liu entropy principle are connected to the pore-fluid pressure of a granular-fluid mixture. Since we refrain from the assumption of pressure equilibrium, which states that $\varpi^f = \varpi^s$ and is often applied to close systems in which the configurational pressure is omitted, a configurational pressure ϖ_ν^s arises, defined as

$$\varpi_\nu^s = \left(\frac{\rho^s}{\rho^f} - 1\right) \varpi_h^f. \tag{4.5}$$

This allows the derivation of the well-known equations of momentum apparent in debris flow modeling, while the thermodynamic coherence of these equations has been proven. It is important to note that Eq. (4.4) is a direct result of the thermodynamically consistent derivation in Heß et al. (2017), but also in accordance with previous considerations on the pressure structure considered in debris flows, i.e. the fluid pressure in de Boer & Ehlers (1990) and the excess pore pressure of Iverson & George (2014), as well as on the incorporation of a spherical intergranular friction term (Teufel 2001, Schneider & Hutter 2009). The stress tensors (3.41) are applied in a reduced form, in which $a_3^\alpha = a_4^\alpha = a_5^\alpha = a_6^\alpha = a_7^\alpha = 0$, i.e. the non-linear terms are omitted, and, in the following, no solid viscous terms are considered, so $a_1^s = a_2^s = 0$. A most simple formulation for the stress tensor is chosen, leaving out the non-linear parts and the solid viscous term, since first of all, the influence of the additionally

introduced fields is to be studied in the following. From Eqs. (4.3) and (4.4), it follows that the reduced solid and fluid stress tensors are given as

$$\begin{aligned} T_{ij}^s &= -\left(\omega_h^f + \omega_v^s - C_e^f \omega_e^f - \left(\rho^s - \rho^f\right) \delta^Z Z_{kk}^s\right) \nu^s \delta_{ij} + \rho \delta^Z Z_{ij}^s, \\ T_{ij}^f &= -\left(\omega_h^f + C_e^f \omega_e^f\right) \nu^f \delta_{ij} + a_1^f D_{kk}^f \delta_{ij} + a_2^f D_{ij}^f, \end{aligned} \tag{4.6}$$

where a_1^f is a constant, see Wang & Hutter (1999a). The remaining coefficient-function in conjunction with the strain tensors is given as

$$a_2^f = 2\mu^f \left(1 - \nu^s\right)^2. \tag{4.7}$$

These relations have been proposed in Passman et al. (1986) and Wang & Hutter (1999c), accounting for viscous behavior, dependent on the microstructure and a fluid viscosity constant μ^f. A viscous, non-plastic fluid is assumed, so for the fluid stress, there is no hypoplasticity, i.e. $Z_{ij}^f = 0$. The function of the drag coefficient is applied in a simplified form, given as

$$c_D^{sf} = c_D^s \nu^s \nu^f, \tag{4.8}$$

which assures that the drag force vanishes when the fluid phase or the granular phase is absent and where c_D^s is a constant. At this point and in the following, we follow Meng & Wang (2016) and refrain from the implementation of a more complex drag term, as postulated for example by Pudasaini (2012) and applied in the example of the previous chapter, see Section 3.5, to focus on investigating the newly introduced quantities.

The applied boundary conditions do not take erosion or deposition into account and the flow surface is stress free. At the flow bottom, for the solid, Coulomb friction is applied in conjunction with a basal friction factor $\mu_b^s = \tan\left(\delta_b\right)$, connected to the bed friction angle δ_b, and, for the fluid, Navier's friction law is applied, so

$$\begin{aligned} \left[T_{ij}^s\right]_b n_j - \left[T_n^s\right]_b n_i &= \frac{v_i^s}{||\boldsymbol{v}^s||} \left[T_n^s\right]_b \mu_b^s, \\ \left[T_{ij}^f\right]_b n_j - \left[T_n^f\right]_b n_i &= k_l \nu^f \left[v_i^f\right]_b, \end{aligned} \tag{4.9}$$

where k_l is the fluid friction coefficient. Here, the normal stresses $\left[T_n^{s,f}\right]_b = \left[T_{ij}^{s,f}\right]_b n_i n_j$ are introduced, together with n_i as the normal unit vector of the basal surface.

4.3 Scaling

We now proceed towards an application for two-phase debris flow, following the shallow-flow approach, in which the system of equations (3.4) is scaled and depth-integrated due to the assumption of shallowness. For this purpose, and at this point,

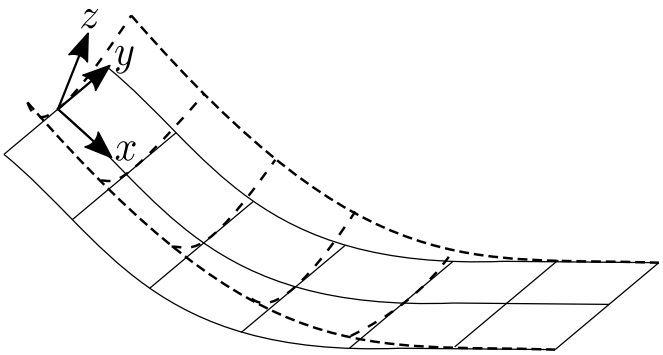

Figure 4.3: The introduced curvilinear coordinate system O_{xyz}, on an inclined slope with runout and a curved bed. Unlike with Cartesian coordinates (X, Y, Z), the curvilinear coordinates allow for the simple depiction of the transition from an inclined chute to the horizontal plane, the simplified representation of the topography of a slope from which an avalanche detaches and moves into the valley.

a simple curved slope with runout is taken into account and we introduce a three-dimensional orthogonal curvilinear coordinate system O_{xyz}, see Fig. 4.3, instead of the two-dimensional Cartesian system O_{XZ} used before (see Sections 3.5 and 4.1). The x coordinate represents the downslope direction, the talweg, while the cross-slope direction is represented with y and the z coordinate is oriented in the direction normal to the slope. The slope angle ϑ_s changes with x. The curvature of the reference surface is given as $\kappa = -\partial_x \vartheta_s$.

After the scaling analysis, a set of depth-integrated equations is derived by employing the shallow layer assumption. This vertical integration is a preliminary work to efficient numerical simulation in the following (Section 5). As it has been pointed out, the reduction is, unlike in the model of Savage & Hutter (1989) and many successive works, not strictly necessary for closure of the solid stress in the present model, since a constitutive model for the stress tensors of the solid and the fluid has been given in Eq. (4.6).

To non-dimensionalize the quantities entering the system of equations, we presume a characteristic horizontal length $\mathcal{L}$, a characteristic depth $\mathcal{H}$ and a typical radius of curvature $\mathcal{R}$. Following Savage & Hutter (1989), we then introduce a range of non-dimensional quantities, labeled by a superscript asterisk, viz.

$$x^* = \frac{x}{\mathcal{L}}; \quad y^* = \frac{y}{\mathcal{L}}; \quad z^* = \frac{z}{\mathcal{H}}; \quad t^* = \frac{t}{\sqrt{\frac{\mathcal{L}}{g}}};$$

$$v_x^{\alpha *} = \frac{v_x^\alpha}{\sqrt{\mathcal{L}g}}; \quad v_y^{\alpha *} = \frac{v_y^\alpha}{\sqrt{\mathcal{L}g}}; \quad v_z^{\alpha *} = \frac{v_z^\alpha}{\epsilon\sqrt{\mathcal{L}g}}; \quad \varpi^{\alpha *} = \frac{\varpi^\alpha}{\rho^f g \mathcal{H}};$$

$$T_{ij}^{\alpha *} = \frac{T_{ij}^\alpha}{\rho^\alpha g \mathcal{H}}; \quad Z_{ij}^{s*} = \frac{Z_{ij}^s}{Z_{kk}^0}; \quad c_D^{s*} = \frac{c_D^s}{\rho^f \sqrt{\frac{g}{\mathcal{L}}}};$$

$$\kappa^* = \frac{\kappa}{\mathcal{R}}; \quad \kappa_\varpi^{f*} = \frac{\kappa_\varpi^f}{\sqrt{g}\frac{\mathcal{H}^2}{\sqrt{\mathcal{L}}}} \quad \gamma_\varpi^{f*} = \frac{\gamma_\varpi^f}{\rho^f \mathcal{H}\sqrt{\frac{g^3}{\mathcal{L}}}}; \quad \Phi_{ij}^{s*} = \frac{\Phi_{ij}^s}{Z_{kk}^0\sqrt{\frac{g}{\mathcal{L}}}}.$$

As first non-dimensional parameters, the aspect ratio arises as $\epsilon = \mathcal{H}/\mathcal{L}$ and the characteristic curvature as $\lambda = \mathcal{L}/\mathcal{R}$. Also see Iverson & George (2014) on the non-dimensional pore-fluid pressure ϖ_e^{f*} and Teufel (2001), Fang et al. (2006) on the non-dimensionalization of Z_{ij}^s, for which a referential intergranular contact stress Z_{kk}^0 is introduced. The magnitude of the gravitational force is g.

The system of equations is specified for a solid and a fluid constituent, so $\alpha = s, f$. For the sake of brevity, and since the procedure is well known, we refrain from giving details on the derivation of the non-dimensional system of equations and just state the results. Due to the bed curvature, additional terms arise in conjunction with the spatial derivatives. Here, we introduce the abbreviation

$$\Psi = 1/\left(1 - \lambda\epsilon\kappa z\right), \tag{4.10}$$

for the term arising in conjunction with the curvilinear downslope derivatives, and also $\kappa_x^* = \partial_x \kappa^*$. Also note that at this point, source terms and stresses are not inserted and given explicitly, in order to keep the equations overseeable. For the volume fraction balance $\mathcal{V}^\alpha = 0$, it follows that

$$\begin{aligned} &\frac{\partial \nu^\alpha}{\partial t^*} + \frac{\partial \nu^\alpha v_x^{\alpha*}\Psi}{\partial x^*} + \frac{\partial \nu^\alpha v_y^{\alpha*}\Psi}{\partial y^*} + \frac{\partial \nu^\alpha v_z^{\alpha*}}{\partial z^*} \\ &-\lambda\epsilon\kappa_x^* z^* \nu^\alpha v_x^{\alpha*}\Psi^2 - \lambda\epsilon\kappa^* \nu^\alpha v_z^{\alpha*}\Psi = 0, \quad \alpha = s, f. \end{aligned} \tag{4.11}$$

The non-dimensional downslope, cross-slope and normal components of the momentum conservation equation $\mathcal{M}_i^\alpha = 0$ for the granular phase and the fluid phase are, respectively,

$$\begin{aligned} &\frac{\partial \nu^\alpha v_x^{\alpha*}}{\partial t^*} + \frac{\partial \nu^\alpha v_x^{\alpha*} v_x^{\alpha*}\Psi}{\partial x^*} + \frac{\partial \nu^\alpha v_y^{\alpha*} v_x^{\alpha*}}{\partial y^*} + \frac{\partial \nu^\alpha v_z^{\alpha*} v_x^{\alpha*}}{\partial z^*} \\ &-\lambda\epsilon\kappa_x^* z^* \nu^\alpha v_x^{\alpha*} v_x^{\alpha*}\Psi^2 - 2\lambda\epsilon\kappa^* \nu^\alpha v_x^{\alpha*} v_z^{\alpha*}\Psi \\ &= \epsilon\frac{\partial T_{xx}^{\alpha*}\Psi}{\partial x^*} + \epsilon^{1+\mu}\frac{\partial T_{xy}^{\alpha*}}{\partial y^*} + \frac{\partial T_{xz}^{\alpha*}}{\partial z^*} - \lambda\epsilon^2\kappa_x^* z^*\, T_{xx}^{\alpha*}\Psi^2 \\ &-2\lambda\epsilon^{1+\mu}\kappa^* T_{xz}^{\alpha*}\Psi + \nu^\alpha g_x^* + m_x^{\alpha*}, \quad \alpha = s, f, \end{aligned} \tag{4.12}$$

$$\begin{aligned} &\frac{\partial \nu^\alpha v_y^{\alpha*}}{\partial t^*} + \frac{\partial \nu^\alpha v_x^{\alpha*} v_y^{\alpha*}\Psi}{\partial x^*} + \frac{\partial \nu^\alpha v_y^{\alpha*} v_y^{\alpha*}}{\partial y^*} + \frac{\partial \nu^\alpha v_z^{\alpha*} v_y^{\alpha*}}{\partial z^*} \\ &-\lambda\epsilon\kappa_x^* z^* \nu^\alpha v_y^{\alpha*} v_x^{\alpha*}\Psi^2 - \lambda\epsilon\kappa^* \nu^\alpha v_y^{\alpha*} v_z^{\alpha*}\Psi \\ &= \epsilon^{1+\mu}\frac{\partial T_{xy}^{\alpha*}\Psi}{\partial x^*} + \epsilon\frac{\partial T_{yy}^{\alpha*}}{\partial y^*} + \frac{\partial T_{yz}^{\alpha*}}{\partial z^*} - \lambda\epsilon^{2+\mu}\kappa_x^* z^* T_{xy}^{\alpha*}\Psi^2 \\ &-\lambda\epsilon^{1+\mu}\kappa^* T_{yz}^{\alpha*}\Psi + \nu^\alpha g_y^* + m_y^{\alpha*}, \quad \alpha = s, f, \end{aligned} \tag{4.13}$$

$$\begin{aligned}
&\epsilon\frac{\partial \nu^\alpha v_z^{\alpha*}}{\partial t^*}+\epsilon\frac{\partial \nu^\alpha v_x^{\alpha*} v_z^{\alpha*}\Psi}{\partial x^*}+\epsilon\frac{\partial \nu^\alpha v_y^{\alpha*} v_z^{\alpha*}}{\partial y^*}+\epsilon\frac{\partial \nu^\alpha v_z^{\alpha*} v_z^{\alpha*}}{\partial z^*}\\
&-\lambda\epsilon^2\kappa_x^* z^* \nu^\alpha v_x^{\alpha*} v_z^{\alpha*}\Psi^2-\lambda\kappa^*\nu^\alpha\left(\epsilon^2\left(v_z^{\alpha*}\right)^2-\left(v_x^{\alpha*}\right)^2\right)\Psi\\
&=\epsilon^{1+\mu}\frac{\partial T_{xz}^{\alpha*}\Psi}{\partial x^*}+\epsilon^{1+\mu}\frac{\partial T_{yz}^{\alpha*}}{\partial y^*}+\frac{\partial T_{zz}^{\alpha*}}{\partial z^*}-\lambda\epsilon^{2+\mu}\kappa_x^* z^* T_{xz}^{\alpha*}\Psi^2\\
&\quad-\lambda\epsilon\kappa^*\left(T_{zz}^{\alpha*}-T_{xx}^{\alpha*}\right)\Psi+\nu^\alpha g_z^*+m_z^{\alpha*},\quad \alpha=s,f.
\end{aligned}\tag{4.14}$$

Likewise, with $\mathcal{W}^f=0$ and from Eq. (3.53), it follows for the evolution of the extra pore-fluid pressure that

$$\begin{aligned}
&\frac{\partial \omega_e^{f*}}{\partial t^*}+\frac{\partial \omega_e^{f*}\Psi}{\partial x^*}\left(v_x^{f*}-\epsilon^2\frac{\partial \kappa_\omega^{f*}\Psi}{\partial x^*}\right)-\epsilon^2\kappa_\omega^{f*}\frac{\partial^2\omega_e^{f*}\Psi^2}{\partial x^*\partial x^*}+\frac{\partial \omega_e^{f*}}{\partial y^*}\left(v_y^{f*}-\epsilon^2\frac{\partial \kappa_\omega^{f*}}{\partial y^*}\right)\\
&\quad-\epsilon^2\kappa_\omega^{f*}\frac{\partial^2\omega_e^{f*}}{\partial y^*\partial y^*}+\frac{\partial \omega_e^{f*}}{\partial z^*}\left(v_z^{f*}-\frac{\partial \kappa_\omega^{f*}}{\partial z^*}\right)-\kappa_\omega^{f*}\frac{\partial^2\omega_e^{f*}}{\partial z^*\partial z^*}=\gamma_\omega^{f*}.
\end{aligned}\tag{4.15}$$

Finally for the hypoplastic stress, Eq. (3.58) has to be specified for several components. For the sake of simplicity, hypoplasticity in this three-dimensional, but later depth-integrated shallow-flow case is restricted to the xy-plane.

Thus, the six components of the full symmetric tensorial variable are reduced to three components, $xx\rightarrow Z_{xx}^s$, $xy\rightarrow Z_{xy}^s=Z_{yx}^s$ and $yy\rightarrow Z_{yy}^s$. The respective evolution equations, $\mathcal{Z}_{xx}^s=0$, $\mathcal{Z}_{xy}^s=0$, $\mathcal{Z}_{yy}^s=0$, therefore yield

$$\begin{aligned}
&\epsilon\frac{\partial Z_{xx}^{s*}}{\partial t^*}+\epsilon\frac{\partial v_x^{s*}Z_{xx}^{s*}\Psi}{\partial x^*}+\epsilon\frac{\partial v_y^{s*}Z_{xx}^{s*}\Psi}{\partial y^*}+\epsilon\frac{\partial v_z^{s*}Z_{xx}^{s*}}{\partial z^*}-\lambda\epsilon^2\kappa_x^* z^* Z_{xx}^{s*}v_x^{\alpha*}\Psi^2\\
&-2\lambda\epsilon^2\kappa^* Z_{xx}^{s*}v_z^{\alpha*}\Psi-\epsilon\left(1+\nu^s\frac{\rho^s-\rho^f}{\rho}\right)\left(\frac{\partial v_x^{s*}\Psi}{\partial x^*}+\frac{\partial v_y^{s*}\Psi}{\partial y^*}+\frac{\partial v_z^{s*}}{\partial z^*}\right.\\
&\left.-\lambda\epsilon\kappa_x^* z^* v_x^{\alpha*}\Psi^2-\lambda\epsilon\kappa^* v_z^{\alpha*}\Psi\right)Z_{xx}^{s*}+\left(\epsilon\frac{\partial v_y^{s*}\Psi^{-1}}{\partial x^*}-\epsilon\frac{\partial v_x^{s*}}{\partial y^*}\right)Z_{xy}^{s*}\\
&-\left(\frac{\partial v_x^{s*}}{\partial z^*}-\epsilon^2\frac{\partial v_z^{s*}\Psi^{-1}}{\partial x^*}-\lambda\epsilon^2\kappa^* v_z^{\alpha*}\Psi^{-1}-\lambda\kappa^* v_x^{\alpha*}\Psi\right)Z_{xz}^{s*}=\epsilon\Phi_{xx}^{s*},
\end{aligned}\tag{4.16}$$

$$\begin{aligned}
&\epsilon\frac{\partial Z_{xy}^{s*}}{\partial t^*}+\epsilon\frac{\partial v_x^{s*}Z_{xy}^{s*}\Psi}{\partial x^*}+\epsilon\frac{\partial v_y^{s*}Z_{xy}^{s*}\Psi}{\partial y^*}+\epsilon\frac{\partial v_z^{s*}Z_{xy}^{s*}}{\partial z^*}-\lambda\epsilon^2\kappa_x^*z^*Z_{xy}^{s*}v_x^{\alpha*}\Psi^2\\
&-2\lambda\epsilon^2\kappa^*Z_{xy}^{s*}v_z^{\alpha*}\Psi+\frac{1}{2}\left(\epsilon\frac{\partial v_y^{s*}\Psi^{-1}}{\partial x^*}-\epsilon\frac{\partial v_x^{s*}}{\partial y^*}\right)\left(Z_{yy}^{s*}-Z_{xx}^{s*}\right)\\
&-\epsilon\left(1+\nu^s\frac{\rho^s-\rho^f}{\rho}\right)\left(\frac{\partial v_x^{s*}\Psi}{\partial x^*}+\frac{\partial v_y^{s*}\Psi}{\partial y^*}+\frac{\partial v_z^{s*}}{\partial z^*}\right.\\
&\left.-\lambda\epsilon\kappa_x^*z^*v_x^{\alpha*}\Psi^2-\lambda\epsilon\kappa^*v_z^{\alpha*}\Psi\right)Z_{xy}^{s*}-\frac{1}{2}\left(\frac{\partial v_y^{s*}}{\partial z^*}-\epsilon^2\frac{\partial v_z^{s*}}{\partial y^*}\right)Z_{xz}^{s*}\\
&-\frac{1}{2}\left(\frac{\partial v_x^{s*}}{\partial z^*}-\epsilon^2\frac{\partial v_z^{s*}\Psi^{-1}}{\partial x^*}-\lambda\epsilon^2\kappa^*v_z^{\alpha*}\Psi^{-1}-\lambda\kappa^*v_x^{\alpha*}\Psi\right)Z_{yz}^{s*}=\epsilon\Phi_{xy}^{s*},
\end{aligned}\tag{4.17}$$

$$\begin{aligned}
&\epsilon\frac{\partial Z_{yy}^{s*}}{\partial t^*}+\epsilon\frac{\partial v_x^{s*}Z_{yy}^{s*}\Psi}{\partial x^*}+\epsilon\frac{\partial v_y^{s*}Z_{yy}^{s*}\Psi}{\partial y^*}+\epsilon\frac{\partial v_z^{s*}Z_{yy}^{s*}}{\partial z^*}-\lambda\epsilon^2\kappa_x^*z^*Z_{yy}^{s*}v_x^{\alpha*}\Psi^2\\
&-2\lambda\epsilon^2\kappa^*Z_{yy}^{s*}v_z^{\alpha*}\Psi-\epsilon\left(1+\nu^s\frac{\rho^s-\rho^f}{\rho}\right)\left(\frac{\partial v_x^{s*}\Psi}{\partial x^*}+\frac{\partial v_y^{s*}\Psi}{\partial y^*}+\frac{\partial v_z^{s*}}{\partial z^*}\right.\\
&\left.-\lambda\epsilon\kappa_x^*z^*v_x^{\alpha*}\Psi^2-\lambda\epsilon\kappa^*v_z^{\alpha*}\Psi\right)Z_{yy}^{s*}-\left(\epsilon\frac{\partial v_y^{s*}\Psi^{-1}}{\partial x^*}-\epsilon\frac{\partial v_x^{s*}}{\partial y^*}\right)Z_{xy}^{s*}\\
&-\left(\frac{\partial v_y^{s*}}{\partial z^*}-\epsilon^2\frac{\partial v_z^{s*}\Psi^{-1}}{\partial y^*}\right)Z_{yz}^{s*}=\epsilon\Phi_{yy}^{s*}.
\end{aligned}\tag{4.18}$$

For the momentum interaction term (3.43), it follows that

$$\begin{aligned}
m_x^{s*}&=c_D^{s*}\frac{\rho^f}{\rho^s}\nu^s\nu^f\left(v_x^{f*}-v_x^{s*}\right)+\epsilon\frac{\rho^f}{\rho^s}\frac{\partial\nu^s\Psi}{\partial x^*}\left(\omega_h^{s*}-\frac{\nu^s\rho^s}{\rho}\omega_\nu^{s*}\right)=-\frac{\rho^f}{\rho^s}m_x^{f*},\\
m_y^{s*}&=c_D^{s*}\frac{\rho^f}{\rho^s}\nu^s\nu^f\left(v_y^{f*}-v_y^{s*}\right)+\epsilon\frac{\rho^f}{\rho^s}\frac{\partial\nu^s}{\partial y^*}\left(\omega_h^{s*}-\frac{\nu^s\rho^s}{\rho}\omega_\nu^{s*}\right)=-\frac{\rho^f}{\rho^s}m_y^{f*},\\
m_z^{s*}&=\sqrt{\epsilon}c_D^{s*}\frac{\rho^f}{\rho^s}\nu^s\nu^f\left(v_z^{f*}-v_z^{s*}\right)+\frac{\rho^f}{\rho^s}\left(\frac{\partial\nu^s}{\partial z^*}\omega_h^{s*}-\frac{\nu^s\rho^s}{\rho}\omega_\nu^{s*}\right)=-\frac{\rho^f}{\rho^s}m_z^{f*},
\end{aligned}$$

while for the gradients of the stress tensors (4.6) of relevant order emerging in Eqs. (4.12)-(4.14), we have for the solid

$$
\begin{aligned}
\epsilon\frac{\partial T_{xx}^{s*}}{\partial x^*} =& -\epsilon\frac{\partial}{\partial x^*}\left(\frac{\rho^f}{\rho^s}\omega_h^{f*}+\frac{\rho^f}{\rho^s}\omega_\nu^{s*}-\mathrm{Eu}\frac{\rho^f}{\rho^s}\omega_e^{f*}\right.\\
&\left.-\mathrm{N_Z}\left(1-\frac{\rho^f}{\rho^s}\right)\left(Z_{xx}^{s*}+Z_{yy}^{s*}+Z_{zz}^{s*}\right)\right)\nu^s+\frac{\epsilon}{\rho^s}\mathrm{N_Z}\frac{\partial \rho Z_{xx}^{s*}}{\partial x^*},\\
\epsilon\frac{\partial T_{yy}^{s*}}{\partial y^*} =& -\epsilon\frac{\partial}{\partial y^*}\left(\frac{\rho^f}{\rho^s}\omega_h^{f*}+\frac{\rho^f}{\rho^s}\omega_\nu^{s*}-\mathrm{Eu}\frac{\rho^f}{\rho^s}\omega_e^{f*}\right.\\
&\left.-\mathrm{N_Z}\left(1-\frac{\rho^f}{\rho^s}\right)\left(Z_{xx}^{s*}+Z_{yy}^{s*}+Z_{zz}^{s*}\right)\right)\nu^s+\frac{\epsilon}{\rho^s}\mathrm{N_Z}\frac{\partial \rho Z_{yy}^{s*}}{\partial y^*},\\
\frac{\partial T_{zz}^{s*}}{\partial z^*} =& -\frac{\partial}{\partial z^*}\left(\frac{\rho^f}{\rho^s}\omega_h^{f*}+\frac{\rho^f}{\rho^s}\omega_\nu^{s*}-\mathrm{Eu}\frac{\rho^f}{\rho^s}\omega_e^{f*}\right.\\
&\left.-\mathrm{N_Z}\left(1-\frac{\rho^f}{\rho^s}\right)\left(Z_{xx}^{s*}+Z_{yy}^{s*}+Z_{zz}^{s*}\right)\right)\nu^s+\frac{1}{\rho^s}\mathrm{N_Z}\frac{\partial \rho Z_{zz}^{s*}}{\partial z^*},
\end{aligned}
\tag{4.19}
$$

and, for the fluid

$$
\begin{aligned}
\epsilon\frac{\partial T_{xx}^{f*}}{\partial x^*} =& -\epsilon\frac{\partial}{\partial x^*}\nu^f\left(\omega_h^{f*}+\mathrm{Eu}\,\omega_e^{f*}\right)\\
&+\frac{\epsilon}{\sqrt{\mathrm{Ga}_f}}a_1^{f*}\frac{\partial}{\partial x^*}\left(D_{xx}^{f*}+D_{yy}^{f*}+D_{zz}^{f*}\right)+\frac{\epsilon}{\sqrt{\mathrm{Ga}_f}}a_2^{f*}\frac{\partial D_{xx}^{f*}}{\partial x^*},\\
\epsilon\frac{\partial T_{yy}^{f*}}{\partial y^*} =& -\epsilon\frac{\partial}{\partial y^*}\nu^f\left(\omega_h^{f*}+\mathrm{Eu}\,\omega_e^{f*}\right)\\
&+\frac{\epsilon}{\sqrt{\mathrm{Ga}_f}}a_1^{f*}\frac{\partial}{\partial y^*}\left(D_{xx}^{f*}+D_{yy}^{f*}+D_{zz}^{f*}\right)+\frac{\epsilon}{\sqrt{\mathrm{Ga}_f}}a_2^{f*}\frac{\partial D_{yy}^{f*}}{\partial y^*},\\
\frac{\partial T_{zz}^{f*}}{\partial z^*} =& -\frac{\partial}{\partial z^*}\nu^f\left(\omega_h^{f*}+\mathrm{Eu}\,\omega_e^{f*}\right)\\
&+\frac{1}{\sqrt{\mathrm{Ga}_f}}a_1^{f*}\frac{\partial}{\partial z^*}\left(D_{xx}^{f*}+D_{yy}^{f*}+D_{zz}^{f*}\right)+\frac{1}{\sqrt{\mathrm{Ga}_f}}a_2^{f*}\frac{\partial D_{zz}^{f*}}{\partial z^*}.
\end{aligned}
\tag{4.20}
$$

A range of dimensionless numbers,

$$
\mathrm{Ga}_f=\frac{(\rho^f)^2 g\mathcal{L}\mathcal{H}^2}{(\mu^f)^2}=(\mathrm{N}_R)^2,\quad \mathrm{Eu}=\frac{C_e^f\rho^f g\mathcal{H}}{\rho^f g\mathcal{H}}\sim\frac{\Delta\varpi}{\rho^f v_i^2},\quad \mathrm{N_Z}=\frac{\delta^Z\left(Z_{xx}^0+Z_{yy}^0+Z_{zz}^0\right)}{g\mathcal{H}},
$$

is introduced in the non-dimensional stress tensor, describing the influence of different terms on the stress evolution. The ratio of gravitational forces to inner, viscous friction is characterized by the Galilei number Ga_f. It appears in conjunction with the viscous terms. There is an analogous viscous number N_R, introduced in Meng & Wang (2016) and Tai et al. (2018). For the dimensionless intergranular friction, we introduce a number N_Z, referring to the hypoplastic frictional stress terms. It is assembled with the proportion of hypoplastic forces to inertial forces. Furthermore, the Euler number Eu is the non-dimensional representation of the pore pressure parameter C_e^f. It resembles the influence of a partial pressure $C_e^f \rho^f g\mathcal{H} \sim \Delta\varpi$ in relation to inertial forces $\rho^f g\mathcal{H} \sim \rho^f v_i^2$, where $\Delta\varpi$ is a pressure difference. It specifies the influence of the extra pore-fluid pressure and appears in conjunction with the non-dimensional extra pore-fluid pressure in the following. We also introduce Eu_b to denote the influence of the dynamic pore pressure on the solid bed friction, with

$$\mathrm{Eu}_b = \frac{C_{e,b}^f \rho^f g\mathcal{H}}{\rho^f g\mathcal{H}},$$

where $C_{e,b}^f$ is a constant, accounting for the influence of the basal excess pore pressure, and, as introduced in Meng & Wang (2016), for the fluid, there is the non-dimensional bed slip friction α_b^f, with

$$\alpha_b^f = \frac{k_l \mathcal{H}^2}{\mu^f}.$$

These two dimensionless values, Eu_b and α_b^f, are applied in conjunction with the boundary conditions after depth-integration, replacing $C_{e,b}^f$ and the fluid bed friction constant k_l.

4.4 Depth-integration

For further simplification, the superscript asterisk is omitted below and the shallow-flow assumption is applied, based on the small ratio of flow depth to downslope length being apparent in debris flows, i.e. $\epsilon \ll 1$. Similar to the procedure in the derivation of Savage & Hutter (1989), as well as in general in the class of SH-models, depth averaging incorporates the integration of all equations over the z-coordinate, from the bed $z = b(x, y)$ to the free surface $z = \mathfrak{s}(x, y, t)$. $b(x, y)$ represents a shallow basal topography that can be overlapped on the reference surface. It is assumed to vanish here, $b(x, y) = 0$. In the framework of depth-integration, a crucial information on the vertical dimension is maintained, the height $h(x, y, t) = \mathfrak{s} - b$, and with this, the information on the flow depth is projected on the xy-plane. For this reason, the actual

2D flow can be still mapped as quasi-3D. Depth integration of a quantity ϕ gives the corresponding depth-integrated quantity $\overline{\phi}$,

$$\int_b^{\mathfrak{s}} \phi \mathrm{d}z = h\overline{\phi},$$

and following Pitman & Le (2005) and Meng & Wang (2016), it is assumed that

$$\overline{\phi\nu^\alpha} = \frac{1}{h}\int_b^{\mathfrak{s}} \phi\nu^\alpha \mathrm{d}z \sim \frac{1}{h}\overline{\nu^\alpha}\int_b^{\mathfrak{s}} \phi \mathrm{d}z = \overline{\phi}\,\overline{\nu^\alpha},$$

where the volume fraction is assumed to be not dependent on the depth direction. As commonly done, a blunt velocity profile is assumed, so $\overline{v_i^\alpha v_i^\alpha} = \alpha_c \overline{v_i^\alpha}\,\overline{v_i^\alpha}$ with $\alpha_c = 1$. During the derivation, the Leibniz rule is applied to interchange differentiation and integration. Also following Pitman & Le (2005), a simplifying assumption for the depth-integration of the drag term is applied. Furthermore, with ordering arguments prevalent in literature (Gray et al. 1999, Meng & Wang 2016), we assume that $\lambda = \mathcal{O}(\epsilon^\iota)$ with $0 < \iota, \mu < 1$, so it follows that $\Psi = 1 + \mathcal{O}(\epsilon^\iota)$. In the following, $\chi = \min(\mu, \iota)$ is assumed.

Since the single steps of the procedure are well-known for the balance of mass, see Hutter & Wang (2016) for details, we only give the results. For the mass balance of the solid and fluid phases (4.11), it follows that

$$\begin{aligned} \frac{\partial}{\partial t}\left(h\overline{\nu^s}\right) + \frac{\partial}{\partial x}\left(h\overline{\nu^s}\,\overline{v_x^s}\right) + \frac{\partial}{\partial y}\left(h\overline{\nu^s}\,\overline{v_y^s}\right) &= 0 + \mathcal{O}(\epsilon^{1+\chi}), \\ \frac{\partial}{\partial t}\left(h\overline{\nu^f}\right) + \frac{\partial}{\partial x}\left(h\overline{\nu^f}\,\overline{v_x^f}\right) + \frac{\partial}{\partial y}\left(h\overline{\nu^f}\,\overline{v_y^f}\right) &= 0 + \mathcal{O}(\epsilon^{1+\chi}), \end{aligned} \tag{4.21}$$

giving the development of the height as

$$\frac{\partial h}{\partial t} + \frac{\partial}{\partial x}\left(h\overline{\nu^s}\,\overline{v_x^s} + h\overline{\nu^f}\,\overline{v_x^f}\right) + \frac{\partial}{\partial y}\left(h\overline{\nu^f}\overline{v_y^s} + h\overline{\nu^f}\,\overline{v_y^f}\right) = 0 + \mathcal{O}(\epsilon^{1+\chi}). \tag{4.22}$$

As for the scaling, the derivation of the depth-integrated balances of momentum is not given explicitly here and follows analogous derivations in literature. For more details on the derivation, see Appendix B, especially for the order-reduction of the balances of momentum for the normal direction and the deduced implications. For the solid bed friction terms $\left[T_{xz}^s\right]_b$ and $\left[T_{yz}^s\right]_b$, by using a Coulomb relation for the shear stress at the bed, it follows that

$$\left[T_{xz}^s\right]_b = \mathrm{sgn}\left(v_x^s\right)\mu_b^s\tau_R^s, \quad \left[T_{yz}^s\right]_b = \mathrm{sgn}\left(v_y^s\right)\mu_b^s\tau_R^s, \tag{4.23}$$

where the friction factor τ_R^s is derived during depth-integration, as a result of the normal balances of momentum, also see Appendix B. With this, the solid bed friction yields

$$\begin{aligned}\left[T_{xz}^s\right]_b &= -\mathrm{sgn}\left(v_x^s\right)\overline{\nu^s}\mu_b^s\left[\frac{\rho^f}{\rho^s}\overline{\omega_\nu^s} - \mathrm{Eu}_b\,\overline{\omega_e^f} - h\tau_\kappa\right],\\ \left[T_{yz}^s\right]_b &= -\mathrm{sgn}\left(v_y^s\right)\overline{\nu^s}\mu_b^s\left[\frac{\rho^f}{\rho^s}\overline{\omega_\nu^s} - \mathrm{Eu}_b\,\overline{\omega_e^f} - h\tau_\kappa\right],\end{aligned} \tag{4.24}$$

with the centrifugal forces factor

$$\tau_\kappa = \lambda\kappa\left(\overline{v_x^s}^2 - \frac{\rho^f}{\rho^s}\overline{v_x^f}^2\right).$$

This centrifugal term in Eq. (4.24) arises due to the curvilinear coordinate system. It was first incorporated by Savage & Hutter (1991), and while Pitman & Le (2005) as well as Pudasaini (2012) disregard this term, Meng & Wang (2016) again incorporate it as it follows from derivation in curvilinear coordinates for the solid bed friction in the vertical momentum balances.

Likewise, for the fluid resistance at the bed, a Navier slip condition is applied with

$$\begin{aligned}\left[T_{xz}^f\right]_b &= -\frac{\alpha_b^f h\overline{\nu^f}}{\epsilon \mathrm{N}_R}\overline{v_x^f},\\ \left[T_{yz}^f\right]_b &= -\frac{\alpha_b^f h\overline{\nu^f}}{\epsilon \mathrm{N}_R}\overline{v_y^f}.\end{aligned} \tag{4.25}$$

While the bed-friction μ_b^s is connected to a function of the bed friction angle δ_b by $\mu_b^s = \tan\left(\delta_b\right)$, the fluid bed-friction is governed by a coefficient α_b^f, originating from the concept of Navier slip friction.

With that, we only give the results for the downslope and cross-slope momentum balances here. The depth-integrated solid x-momentum balance follows as

$$
\begin{aligned}
&\frac{\partial}{\partial t}\left(h\overline{\nu^s}\,\overline{v_x^s}\right)+\frac{\partial}{\partial x}\left(h\overline{\nu^s}\,\overline{v_x^s}\,\overline{v_x^s}\right)+\frac{\partial}{\partial y}\left(h\overline{\nu^s}\,\overline{v_y^s}\,\overline{v_x^s}\right)\\
=&h\overline{\nu^s}g_x-\epsilon\frac{\partial}{\partial x}\left(h\overline{\nu^s}\frac{\rho^f}{\rho^s}\left(\overline{\omega_h^f}+\overline{\omega_\nu^s}\right)-\mathrm{Eu}\,h\overline{\nu^s}\frac{\rho^f}{\rho^s}\overline{\omega_e^f}\right.\\
&\left.-\mathrm{N_Z}\left(1-\frac{\rho^f}{\rho^s}\right)h\overline{\nu^s}\left(\overline{Z_{xx}^s}+\overline{Z_{yy}^s}+\overline{Z_{zz}^s}\right)\right)+\frac{\epsilon}{\rho^s}\mathrm{N_Z}\frac{\partial\overline{\rho}h\overline{Z_{xx}^s}}{\partial x}\\
&-\mathrm{sgn}\left(v_x^s\right)\overline{\nu^s}\mu_b^s\left[\frac{\rho^f}{\rho^s}\overline{\omega_\nu^s}-\mathrm{Eu}_b\,\overline{\omega_e^f}-\lambda\kappa h\left(\overline{v_x^s}^2-\frac{\rho^f}{\rho^s}\overline{v_x^f}^2\right)\right]\\
&+\frac{c_D^s h\overline{\nu^s}\overline{\nu^f}\rho^f}{\rho^s}\left(\overline{v_x^f}-\overline{v_x^s}\right)+\epsilon\frac{\rho^f}{\rho^s}\frac{\partial\overline{\nu^s}}{\partial x}\left(h\left(\overline{\omega_h^f}+\overline{\omega_\nu^s}\right)-\frac{h\overline{\nu^s}\rho^s}{\rho}\overline{\omega_\nu^s}\right)\\
&+\mathcal{O}(\epsilon^{1+\chi}),
\end{aligned}
\tag{4.26}
$$

and the y-momentum balance for the solid yields

$$
\begin{aligned}
&\frac{\partial}{\partial t}\left(h\overline{\nu^s}\,\overline{v_y^s}\right)+\frac{\partial}{\partial x}\left(h\overline{\nu^s}\,\overline{v_x^s}\,\overline{v_y^s}\right)+\frac{\partial}{\partial y}\left(h\overline{\nu^s}\,\overline{v_y^s}\,\overline{v_y^s}\right)\\
=&-\epsilon\frac{\partial}{\partial y}\left(h\overline{\nu^s}\frac{\rho^f}{\rho^s}\left(\overline{\omega_h^f}+\overline{\omega_\nu^s}\right)-\mathrm{Eu}\,h\overline{\nu^s}\frac{\rho^f}{\rho^s}\overline{\omega_e^f}\right.\\
&\left.-\mathrm{N_Z}\left(1-\frac{\rho^f}{\rho^s}\right)h\overline{\nu^s}\left(\overline{Z_{xx}^s}+\overline{Z_{yy}^s}+\overline{Z_{zz}^s}\right)\right)+\frac{\epsilon}{\rho^s}\mathrm{N_Z}\frac{\partial\overline{\rho}h\overline{Z_{yy}^s}}{\partial y}\\
&-\mathrm{sgn}\left(v_y^s\right)\overline{\nu^s}\mu_b^s\left[\frac{\rho^f}{\rho^s}\overline{\omega_\nu^s}-\mathrm{Eu}_b\,\overline{\omega_e^f}-\lambda\kappa h\left(\overline{v_x^s}^2-\frac{\rho^f}{\rho^s}\overline{v_x^f}^2\right)\right]\\
&+\frac{c_D^s h\overline{\nu^s}\overline{\nu^f}\rho^f}{\rho^s}\left(\overline{v_y^f}-\overline{v_y^s}\right)+\epsilon\frac{\rho^f}{\rho^s}\frac{\partial\overline{\nu^s}}{\partial y}\left(h\left(\overline{\omega_h^f}+\overline{\omega_\nu^s}\right)-\frac{h\overline{\nu^s}\rho^s}{\rho}\overline{\omega_\nu^s}\right)\\
&+\mathcal{O}(\epsilon^{1+\chi}),
\end{aligned}
\tag{4.27}
$$

where, in Eqs. (4.26)-(4.27) the first term on the RHS denotes the gravity (only appearing in the downslope x-balance), followed by the second, pressure term, the hypoplastic terms in the second line on the RHS-side, the solid bed friction in the third line, and finally the momentum interaction terms.

For the fluid, the x-momentum balance yields

$$\begin{aligned}
&\frac{\partial}{\partial t}\left(h\overline{\nu^f}\,\overline{v_x^f}\right)+\frac{\partial}{\partial x}\left(h\overline{\nu^f}\,\overline{v_x^f}\,\overline{v_x^f}\right)+\frac{\partial}{\partial y}\left(h\overline{\nu^f}\,\overline{v_y^f}\,\overline{v_x^f}\right)\\
=&h\overline{\nu^f}g_x-\epsilon\frac{\partial}{\partial x}\left(h\overline{\nu^f}\overline{\omega_h^f}+\mathrm{Eu}\overline{\nu^f}\,\overline{\omega_e^f}h\right)+\frac{\partial}{\partial x}\left(\epsilon\mathrm{Ga}_f^{-\frac{1}{2}}\frac{\partial\overline{v_x^f}}{\partial x}h\left(\overline{a_1^f}+\overline{a_2^f}\right)\right)\\
&-c_D^s h\overline{\nu^s}\overline{\nu^f}\left(\overline{v_x^f}-\overline{v_x^s}\right)-\epsilon\frac{\partial\overline{\nu^s}}{\partial x}\left(h\left(\overline{\omega_h^f}+\overline{\omega_\nu^s}\right)-\frac{h\overline{\nu^s}\rho^s}{\rho}\overline{\omega_\nu^s}\right)\\
&-\frac{\alpha_b^f}{\epsilon\mathrm{N}_R}h\overline{\nu^f}\overline{v_x^f}+\mathcal{O}(\epsilon^{1+\chi}).
\end{aligned}\tag{4.28}$$

The fluid momentum in the cross-slope, y-direction, is derived as

$$\begin{aligned}
&\frac{\partial}{\partial t}\left(h\overline{\nu^f}\,\overline{v_y^f}\right)+\frac{\partial}{\partial x}\left(h\overline{\nu^f}\,\overline{v_x^f}\,\overline{v_y^f}\right)+\frac{\partial}{\partial y}\left(h\overline{\nu^f}\,\overline{v_y^f}\,\overline{v_y^f}\right)\\
=&-\epsilon\frac{\partial}{\partial y}\left(h\overline{\nu^f}\overline{\omega_h^f}+\mathrm{Eu}\overline{\nu^f}\,\overline{\omega_e^f}h\right)+\frac{\partial}{\partial y}\left(\epsilon\mathrm{Ga}_f^{-\frac{1}{2}}\frac{\partial\overline{v_y^f}}{\partial y}h\left(\overline{a_1^f}+\overline{a_2^f}\right)\right)\\
&-c_D^s h\overline{\nu^s}\overline{\nu^f}\left(\overline{v_y^f}-\overline{v_y^s}\right)-\epsilon\frac{\partial\overline{\nu^s}}{\partial y}\left(h\left(\overline{\omega_h^f}+\overline{\omega_\nu^s}\right)-\frac{h\overline{\nu^s}\rho^s}{\rho}\overline{\omega_\nu^s}\right)\\
&-\frac{\alpha_b^f}{\epsilon\mathrm{N}_R}h\overline{\nu^f}\overline{v_y^f}+\mathcal{O}(\epsilon^{1+\chi}).
\end{aligned}\tag{4.29}$$

Similarly to the solid momentum equations, those for the fluid, Eqs. (4.28)-(4.29), exhibit a gravity term on the RHS, followed by the fluid pressure and a viscous term. In the second line of the RHS, the momentum interaction terms follow, and in the third, there is the basal fluid friction.

Depth-integration also needs to be performed with the evolution equation for the extra pore-fluid pressure (4.15) and the hypoplastic stress (4.16)-(4.18). For an equivalent derivation and more details on the depth-integration of such a pressure evolution equation, also see Iverson & George (2014). The assumptions with which we work are given below. The depth-integrated evolution equation for the extra pore-fluid pressure follows from Eqs. (2.9) and (4.15) as

$$\begin{aligned}
&\frac{\partial}{\partial t}\left(h\overline{\omega_e^f}\right)+\frac{\partial}{\partial x}\left(h\overline{\omega_e^f}\,\overline{v_x^f}\right)+\frac{\partial}{\partial y}\left(h\overline{\omega_e^f}\,\overline{v_y^f}\right)-\left[\kappa_\omega^f\frac{\partial\omega_e^f}{\partial z}\right]_b^{\mathfrak{s}}\\
=&h\left(\frac{\partial}{\partial t}\left(\overline{\sigma-\omega_h^f}\right)+\overline{v_x^f}\frac{\partial}{\partial x}\left(\overline{\sigma-\omega_h^f}\right)+\overline{v_y^f}\frac{\partial}{\partial y}\left(\overline{\sigma-\omega_h^f}\right)\right)\\
&+\overline{\omega_e^f}\left(\frac{\partial h}{\partial t}+\frac{\partial\overline{v_x^f}h}{\partial x}+\frac{\partial\overline{v_y^f}h}{\partial y}\right)-h\overline{\frac{\dot\gamma}{\alpha_D}\tan(\psi)}+\mathcal{O}(\epsilon^2).
\end{aligned}\tag{4.30}$$

For this, it is assumed that the diffusion coefficient κ_ω^f is not changing with depth. To close Eq. (4.30), we consider the following relations

$$\begin{aligned}
&\text{(i)}\quad \left[\kappa_\omega^f\frac{\partial\omega_e^f}{\partial z}\right]_b^{\mathfrak{s}}=2\frac{\kappa_\omega^f\beta_\psi^f}{h}\overline{\omega_e^f}=2\frac{k_D\beta_\psi^f}{h\mu^f\alpha_D}\overline{\omega_e^f},\\
&\text{(ii)}\quad \frac{\partial\left(\overline{\sigma-\omega_h^f}\right)}{\partial t}h+\frac{\partial\left(\overline{\sigma-\omega_h^f}\right)}{\partial x}h\overline{v_x^f}+\frac{\partial\left(\overline{\sigma-\omega_h^f}\right)}{\partial y}h\overline{v_y^f}\\
&\qquad=\frac{1}{2}h\left(\rho-\rho^f\right)g_z\left(\frac{\partial h\overline{\nu^s}(\overline{v_x^s}-\overline{v_x^f})}{\partial x}+h\frac{\partial\overline{v_x^f}}{\partial x}+\frac{\partial h\overline{\nu^s}(\overline{v_y^s}-\overline{v_y^f})}{\partial y}+h\frac{\partial\overline{v_y^f}}{\partial y}\right),\\
&\text{(iii)}\quad \overline{\omega_e^f}\left(\frac{\partial h}{\partial t}+\frac{\partial h\overline{v_x^f}}{\partial x}+\frac{\partial h\overline{v_y^f}}{\partial y}\right)\\
&\qquad=\overline{\omega_e^f}\frac{\partial h\overline{\nu^s}(\overline{v_x^s}-\overline{v_x^f})}{\partial x}+\overline{\omega_e^f}\frac{\partial h\overline{\nu^s}(\overline{v_y^s}-\overline{v_y^f})}{\partial y},\\
&\text{(iv)}\quad h\overline{\frac{\dot\gamma}{\alpha_D}\tan(\psi)}=\frac{1}{\alpha_D}\sqrt{(\overline{v_x^s})^2+(\overline{v_y^s})^2}\left(\kappa_{\omega1}\overline{\nu^s}-\kappa_{\omega2}\frac{\nu_C^s}{1+\sqrt{\mathrm{N}_\gamma}}\right),
\end{aligned}\tag{4.31}$$

where we have

$$\mathrm{N}_\gamma=\frac{\mu^f\dot\gamma}{\rho^s\left(\dot\gamma\delta_P\right)^2+\sigma_e},\quad \dot\gamma=\frac{2\sqrt{(\overline{v_x^s})^2+(\overline{v_y^s})^2}}{h},\quad \sigma_e=\left(\rho-\rho^f\right)g_zh.\tag{4.32}$$

The two coefficients $\kappa_{\omega1},\kappa_{\omega2}$ are introduced in conjunction with the dilatancy term, and, as before, δ_P is a medium particle size. Furthermore, a weighting function

$$\beta_\psi^f(x)=1+100\exp\left(-10\frac{x_f-x}{x_L}\right),$$

is introduced, simulating the decrease of the pore pressure at the flow front x_f due to the accumulation of larger grains there, and, therefore, the increased permeabil-

ity, where x_L is the actual length of the flow. This additional function accounts for segregational effects in a first, rudimentary way. It was proposed by Savage & Iverson (2003). (ii) and (iii) are derived with the depth-integrated extra stress $\overline{\sigma_e} = \overline{\sigma - \omega_h^f} = \frac{1}{2}\left(\rho - \rho^f\right) g_z h$ and the mass balance Eq. (4.22). (iv) is developed in Iverson & George (2014).

For the evolution equations of the hypoplastic stress, Eqs. (4.16)-(4.18), the resulting depth-integrated equations are given in the following. First, for the xx-component, it follows that

$$\begin{aligned} \epsilon\frac{\partial h\overline{Z_{xx}^s}}{\partial t} + \epsilon\frac{\partial h\overline{v_x^s}\,\overline{Z_{xx}^s}}{\partial x} + \epsilon\frac{\partial h\overline{v_y^s}\,\overline{Z_{xx}^s}}{\partial y} + \left(\epsilon\frac{\partial h\overline{v_y^s}}{\partial x} - \epsilon\frac{\partial h\overline{v_x^s}}{\partial y}\right)\overline{Z_{xy}^s} \\ -\overline{Z_{xz}^s}h\left(\left[v_x^s\right]_b^{\mathfrak{s}} - \lambda\kappa\overline{v_x^s}\right) - \epsilon\left(1 + \nu^s\frac{\rho^s - \rho^f}{\rho}\right)\overline{Z_{xx}^s}\left(\frac{\partial h}{\partial t} + \frac{\partial\overline{v_x^s}h}{\partial x} + \frac{\partial\overline{v_y^s}h}{\partial y}\right) \\ = \epsilon\overline{\Phi_{xx}^s}h + \mathcal{O}(\epsilon^2), \end{aligned} \tag{4.33}$$

for xy, see Eq. (4.17), it follows that

$$\begin{aligned} \epsilon\frac{\partial h\overline{Z_{xy}^s}}{\partial t} + \epsilon\frac{\partial h\overline{v_x^s}\,\overline{Z_{xy}^s}}{\partial x} + \epsilon\frac{\partial h\overline{v_y^s}\,\overline{Z_{xy}^s}}{\partial y} + \frac{1}{2}\left(\epsilon\frac{\partial h\overline{v_y^s}}{\partial x} - \epsilon\frac{\partial h\overline{v_x^s}}{\partial y}\right)\left(\overline{Z_{yy}^s} - \overline{Z_{xx}^s}\right) \\ -\epsilon\left(1 + \nu^s\frac{\rho^s - \rho^f}{\rho}\right)\overline{Z_{xy}^s}\left(\frac{\partial h}{\partial t} + \frac{\partial\overline{v_x^s}h}{\partial x} + \frac{\partial\overline{v_y^s}h}{\partial y}\right) \\ -\overline{Z_{xz}^s}h\left[v_y^s\right]_b^{\mathfrak{s}} - \overline{Z_{yz}^s}h\left(\left[v_x^s\right]_b^{\mathfrak{s}} - \lambda\kappa\overline{v_x^s}\right) = \epsilon\overline{\Phi_{xy}^s}h + \mathcal{O}(\epsilon^2), \end{aligned} \tag{4.34}$$

and Eq. (4.18) yields

$$\begin{aligned} \epsilon\frac{\partial h\overline{Z_{yy}^s}}{\partial t} + \epsilon\frac{\partial h\overline{v_x^s}\,\overline{Z_{yy}^s}}{\partial x} + \epsilon\frac{\partial h\overline{v_y^s}\,\overline{Z_{yy}^s}}{\partial y} - \left(\epsilon\frac{\partial h\overline{v_y^s}}{\partial x} - \epsilon\frac{\partial h\overline{v_x^s}}{\partial y}\right)\overline{Z_{xy}^s} - \overline{Z_{yz}^s}h\left[v_y^s\right]_b^{\mathfrak{s}} \\ -\epsilon\left(1 + \nu^s\frac{\rho^s - \rho^f}{\rho}\right)\overline{Z_{yy}^s}\left(\frac{\partial h}{\partial t} + \frac{\partial\overline{v_x^s}h}{\partial x} + \frac{\partial\overline{v_y^s}h}{\partial y}\right) = \epsilon\overline{\Phi_{yy}^s}h + \mathcal{O}(\epsilon^2). \end{aligned} \tag{4.35}$$

The depth-integrated, non-dimensional source terms $\overline{\Phi_{xx}^s}$, $\overline{\Phi_{xy}^s}$, and $\overline{\Phi_{yy}^s}$ of Eqs. (4.33)-(4.35) are given in Appendix C, where also a representation of the equations describing hypoplasticity in vectorial form is given.

While ϵ^2-terms will be omitted, the following assumptions are applied

$$\begin{aligned} &\text{(i)} \quad \int_b^{\mathfrak{s}} Z_{ij}^s\frac{\partial v_k}{\partial x}\mathrm{d}z = \frac{1}{h}\int_b^{\mathfrak{s}} Z_{ij}^s\mathrm{d}z\int_b^{\mathfrak{s}}\frac{\partial v_k}{\partial x}\mathrm{d}z, \\ &\text{(ii)} \quad \frac{\partial\overline{v_x^s}h}{\partial x} - \left[v_x^s\frac{\partial h}{\partial x}\right]_b^{\mathfrak{s}} \approx h\frac{\partial\overline{v_x^s}}{\partial x}. \end{aligned} \tag{4.36}$$

Moreover, we are assuming isotropic stress conditions for $Z^s_{zz} = \frac{1}{2}\left(Z^s_{xx} + Z^s_{yy}\right)$ and apply the steady-state correlation, so $Z^s_{xz} = -(3/\sqrt{2})a^s_Z Z^s_{xx}$ and $Z^s_{yz} = -(3/\sqrt{2})a^s_Z Z^s_{yy}$. The correlation is a simplification, which can be derived for a simple shearing state, in which only one stress component must be known (Teufel 2001, Fang et al. 2006).

Next, we will omit the overbar-symbol, since all quantities are regarded as depth-integrated, i.e. independent of z. For a comparison of the derived model in curvilinear coordinates to the standard two-phase model of Pitman & Le (2005) and Meng & Wang (2016), regarding the downslope momentum equations, as well as a discussion of some limiting cases, see Appendix D.

Before the now scaled and depth-integrated equations are converted into general coordinates, a brief introduction of the applied material functions and parameters is given in the next section.

4.5 Material parameters

The diffusion term in Eq. (4.30) contains a diffusivity coefficient κ^f_ϖ, also see Section 3.4.2, that is determined as

$$\kappa^f_\varpi = \frac{k_D}{\alpha_D \mu^f},$$

where, besides the fluid viscosity μ^f, the hydraulic permeability k_D and the debris compressibility α_D arise as

$$k_D = k^0_D \exp\left(\frac{\nu^s_C - \nu^s}{0.04}\right), \quad \alpha_D = \frac{\alpha^0_D}{\nu^s \sigma}.$$

Here, k^0_D and α^0_D are constants of permeability and compressibility, respectively, ν^s_C is, as before, the critical solid volume fraction, and σ denotes the stress state. While the parameter function k_D is thought to depict the permeability of the granular material with respect to the solid volume fraction (in relation to its critical value), the compressibility of the material is modeled with respect to the stress state, which can be estimated by $\sigma = \rho g_z h$. Together with Eq. (4.32), these parameter describe the behavior of granular material in its role for the evolution of the extra pore-fluid pressure.

Since the material is now fully described with respect to the pore-fluid pressure, the intergranular stress and its material parameters are further investigated. Being introduced by Kolymbas (1977), the concept of hypoplasticity generalizes elasto-plastic material behavior. The invented tensor-variable, representing an inter-granular contact stress, is determined by its corotational objective time derivative and a source term, the latter setting the behavior to be hypoelastic or hypoplastic. Hypoplastic material behavior is fundamentally determined by the hysteresis-like deformation-paths during loading and unloading phases of motion.

As material parameters, a stiffness factor f_s is introduced, together with a density factor f_D, such that

$$f_s = f_s^0 f_b \left(\frac{1 - \nu_C^s}{1 - \nu^s} \right)^{p_{e0}}, \quad f_D = f_D^0 \left(\frac{\nu_\infty^s - \nu^s}{\nu_\infty^s - \nu_C^s} \right)^{e_0},$$

see Bauer (1996), Gudehus (1996) and Herle & Gudehus (1999). Note that

$$a_Z^s = a_Z^{s,0} \frac{\sqrt{3}\,(3 - \sin(\phi_{int}))}{2\sqrt{2}\sin(\phi_{int})},$$

as in Herle & Gudehus (1999). A first material constants is chosen as $e_0 = 0.1$, fitting the range of $0.0 < e_0 < 1.0$ given in Bauer (1996) and the restriction to $0.1 < e_0 < 0.3$ in Gudehus (1996). Furthermore, the exponent p_{e0}, which is required to slightly exceed the value of 1, with Gudehus (1996) suggesting $1.0 < p_{e0} < 1.1$, so we apply $p_{e0} = 1.1$. There also is ϕ_{int} as the internal friction angle[1] and the maximum packing fraction ν_∞^s. The stiffness factor f_s includes a barotropy function f_b, given as

$$f_b = \frac{Z_{ii} \left((a_Z^s)^2 - \sqrt{3} a_Z^s \right)}{p_n},$$

which is slightly simplified compared to Bauer (1996) and where p_n, exhibiting a possible range of $0.3 < p_n < 0.5$ (Gudehus 1996), is set to $p_n = 0.3$. There is a wide literature on the formulation of these parameter functions and the possible calibration of the material constants, see for instance Herle & Gudehus (1999), Mašín (2005) and, as mentioned before, Bauer (1996), Gudehus (1996).

It is apparent, that with introduction of several limiting values for the solid volume fraction, such as ν_C^s, ν_{eq}^s and ν_∞^s, one seeks to capture the developments of the microstructure of the granular material and its influence on the pore space, thus the fluid pressure and the friction between the grains. As the formulation of the extra pore-fluid pressure, this granular material behavior is linked to Terzaghi's principle of effective stress (Herle & Gudehus 1999).

Also note that in the following, we refer to N_R instead of the classical Galilei number Ga_f, as this allows a simpler reference to the studies with MW-model, applied in Meng & Wang (2016) and Tai et al. (2018). Together with this assumption, we set $a_1^f + a_2^f = 1$, since we are not interested in a further investigation of the applied viscosity parameter functions, see also Heß & Wang (2019).

With these insights in the applied parameter functions, the developed model for curvilinear coordinates is now transformed to a system of general coordinates, before it can be applied to numerical simulations.

[1] While usually, for SH-type models, the internal friction angle ϕ_{int} appears in conjunction with the earth pressure relation, in particular to estimate the earth pressure coefficient $K_{act/pas}$, here, it arises only with a_Z^s.

4.6 Coordinate systems and coordinate transformation

For an inclined plane, the direction normal to the basal surface may not change, so that a Cartesian coordinate system O_{XYZ} is applicable, as it was the case in the originally introduced SH-model (Savage & Hutter 1989). In contrast, for a chute with transition to a runout, the (position-dependent) normal direction needs to be described by a curvilinear coordinate system O_{xyz}, as introduced for the SH-modeling approach in Savage & Hutter (1991) and extended in Gray et al. (1999). In other words, an advanced coordinate ansatz is required in order to describe flows on certain reference surfaces, that resemble, for example, simple laboratory experimental setups on a curved chute, and not only a simple plane. With the introduction of curvilinear coordinates, certain terms enter the equations, accounting for the curvature of the basal surface and the resulting centrifugal forces.

Nonetheless, there are some short-comings of curvilinear-coordinates when it comes to depicting the topography of real mountainous areas, since in such cases, there is not only one clearly distinguishable flow direction in place, but a multitude of rutted channels. Here, so-called general coordinates are capable of both describing the surface of a rugged topography by maintaining Cartesian coordinates, and, at the same time, a depth-integrated flow in conjunction with terrain-following coordinates (ξ, η, ζ). This method, applied in several works (Tai & Kuo 2008, Tai & Kuo 2012, Tai et al. 2018), is possible due to the combination of unified coordinates, developed in Hui et al. (1999) and Hui (2004), and the approach of Bouchut & Westdickenberg (2004). It unites both the advantage of reduced equations with respect to the degrees of freedom, keeping computational costs low, but allows for the easy implementation of topography data, for example from geographic information systems (GISs). For a comparison of curvilinear, Cartesian and general coordinates, see Fig. 4.4.

In such a modern GIS, land surfaces are described with cell-based digital elevation models (DEMs). Such a DEM is a raster representation of a continuous surface. This surface can be described with reference to a horizontal plane given in Cartesian coordinates, such that the X- and Y- axis lie on the horizontal plane and the Z-axis is pointing upwards against the gravity.[2] With this, the surface is described by a function $\mathcal{F}_S(X, Y, Z) = Z - Z_b(X, Y) = 0$, with a respective unit normal vector that reads

$$\boldsymbol{n} = \frac{\nabla \mathcal{F}_S}{||\nabla \mathcal{F}_S||} = n_X \mathbf{e}_X + n_Y \mathbf{e}_Y + n_Z \mathbf{e}_Z, \tag{4.37}$$

and where

$$\begin{aligned} &n_X = -c\,\partial Z_b/\partial X = -s_X\,, \quad n_Y = -c\,\partial Z_b/\partial Y = -s_Y\,, \quad n_Z = c\,, \\ &c = \left\{ (\partial Z_b/\partial X)^2 + (\partial Z_b/\partial Y)^2 + 1 \right\}^{-1/2}. \end{aligned} \tag{4.38}$$

[2] Below, we will follow the introduction of general coordinates presented in Tai et al. (2018).

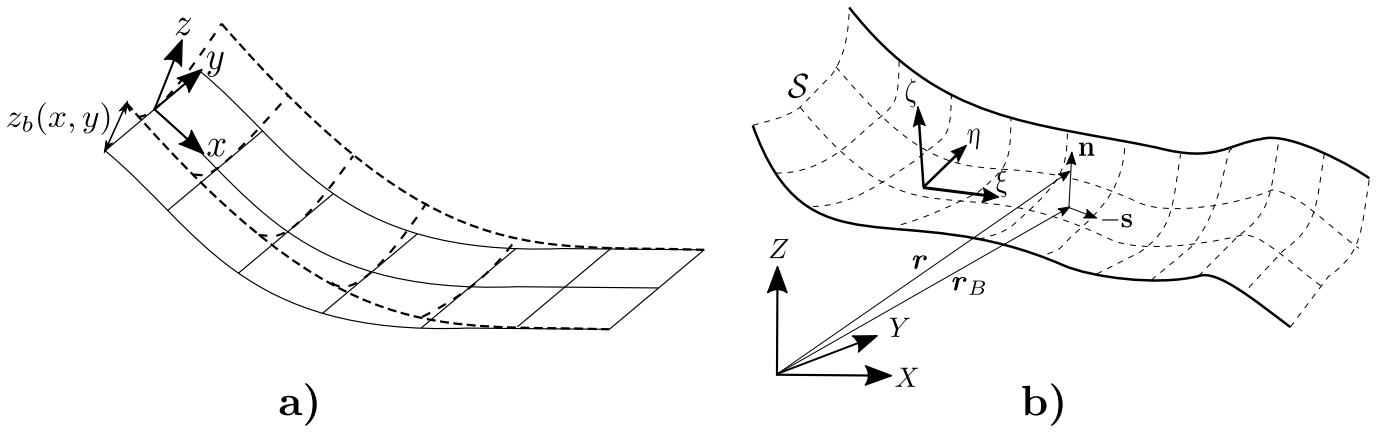

Figure 4.4: Comparison of a Cartesian coordinates (X, Y, Z), curvilinear coordinates (x, y, z) following the references plane with a shallow elevation z_b of the topography hereon on the left-hand side in panel **a)**, and terrain-following coordinates (ξ, η, ζ) on the right-hand side, see panel **b)**, depicting a general topographic surface $\mathcal{S}$. While the curvilinear coordinates are suitable for simple chutes, occurring e.g. in an experimental setup, the general coordinates allow for the depiction of large mountainous areas.

The normal unit vector $\boldsymbol{n}$ is connected to the vector $\mathbf{s} = (s_X, s_Y)^T$, which describes the horizontal development of the topographic surface, see e.g. Bouchut & Westdickenberg (2004) or Luca et al. (2016). One can define a coordinate system $O_{\xi\eta\zeta}$ on the topographic surface $\mathcal{S}$, see Fig. 4.4, panel **b)**, such that $\boldsymbol{\tau}_\xi$ and $\boldsymbol{\tau}_\eta$ are tangent to the surface with

$$\boldsymbol{\tau}_\xi = \frac{\partial \boldsymbol{r}_b}{\partial \xi}, \quad \boldsymbol{\tau}_\eta = \frac{\partial \boldsymbol{r}_b}{\partial \eta} \quad \text{and} \quad \boldsymbol{\tau}_\zeta = \frac{\boldsymbol{\tau}_\xi \times \boldsymbol{\tau}_\eta}{||\boldsymbol{\tau}_\xi \times \boldsymbol{\tau}_\eta||}, \tag{4.39}$$

for a point on the surface $\boldsymbol{r}_b = (r_{b,X}, r_{b,Y}, Z_b(r_{b,X}, r_{b,Y}))^T$ and where there is an identity $\boldsymbol{\tau}_\zeta = \boldsymbol{n}$. With this vector, referencing a point on the surface and the defined terrain-following coordinate system $O_{\xi\eta\zeta}$, now a Jacobian $\boldsymbol{\Omega}_b$, i.e. a transformation matrix, can be given as

$$\begin{aligned} \boldsymbol{\Omega}_b = \Big(\boldsymbol{\tau}_\xi,\ \boldsymbol{\tau}_\eta,\ \boldsymbol{n}\Big) &= \begin{pmatrix} \partial r_{b,X}/\partial\xi & \partial r_{b,X}/\partial\eta & n_X \\ \partial r_{b,Y}/\partial\xi & \partial r_{b,Y}/\partial\eta & n_Y \\ \partial Z_b/\partial\xi & \partial Z_b/\partial\eta & c \end{pmatrix} \\ &= \begin{pmatrix} 1 & 0 & n_X \\ 0 & 1 & n_Y \\ -n_X/c & -n_Y/c & c \end{pmatrix} \begin{pmatrix} \partial X/\partial\xi & \partial X/\partial\eta & 0 \\ \partial Y/\partial\xi & \partial Y/\partial\eta & 0 \\ 0 & 0 & 1 \end{pmatrix}. \end{aligned} \tag{4.40}$$

For the respective position vector $\boldsymbol{r}$, denoting a point at a distance ζ above this surface $\mathcal{S}$, a decomposition can be applied as $\boldsymbol{r} = \boldsymbol{r}_b + \zeta\, \boldsymbol{n}$, yielding the local natural bases, see Luca et al. (2016), as

$$\boldsymbol{g}_\xi = \boldsymbol{\tau}_\xi + \zeta \frac{\partial \boldsymbol{n}}{\partial \xi}, \quad \boldsymbol{g}_\eta = \boldsymbol{\tau}_\eta + \zeta \frac{\partial \boldsymbol{n}}{\partial \eta} \quad \text{and} \quad \boldsymbol{g}_\zeta = \frac{\boldsymbol{g}_\xi \times \boldsymbol{g}_\eta}{||\boldsymbol{g}_\xi \times \boldsymbol{g}_\eta||} = \boldsymbol{n}. \tag{4.41}$$

For this, the corresponding Jacobian matrix is given as $\boldsymbol{\Omega} = (\boldsymbol{g}_\xi, \boldsymbol{g}_\eta, \boldsymbol{n})$. Note that in Eq. (4.41), the terms $\partial \boldsymbol{n}/\partial\xi$ and $\partial \boldsymbol{n}/\partial\eta$ are related to the local curvature.

With this, we introduced a new, terrain-following set of coordinates, referenced to a topographic surface. Nonetheless, since there are two coordinate systems, vectors and tensors can both be given in the Cartesian one, O_{XYZ}, or in the terrain-following one, $O_{\xi\eta\zeta}$. The transformation between those analogous expressions, for a vector $\boldsymbol{v}$ and a tensor $\boldsymbol{T}$ is

$$\boldsymbol{v} = v_i \mathbf{e}_i = v^\gamma \boldsymbol{g}_\gamma\,, \quad \boldsymbol{T} = T_{ij}(\mathbf{e}_i \otimes \mathbf{e}_j) = T^{\gamma\delta}(\boldsymbol{g}_\gamma \otimes \boldsymbol{g}_\delta) = \tilde{T}^{i\delta}(\mathbf{e}_i \otimes \boldsymbol{g}_\delta), \tag{4.42}$$

where we now differentiate between the Cartesian indices $i, j \in \{X, Y, Z\}$ and the terrain-following ones $\gamma, \delta \in \{\xi, \eta, \zeta\}$. The last expression of Eq. (4.42) is in a mixed representation, referring both to Cartesian and terrain-following coordinates simultaneously. The components of a tensor among different coordinates are related by

$$\big(T_{ij}\big) = \boldsymbol{\Omega}\big(T^{\gamma\delta}\big)\boldsymbol{\Omega}^T \quad \Rightarrow \quad \big(\tilde{T}^{i\delta}\big) = \boldsymbol{\Omega}\big(T^{\gamma\delta}\big) = \big(T_{ij}\big)\boldsymbol{\Omega}^{-T}\,, \tag{4.43}$$

where $\boldsymbol{\Omega}^T$ denotes the transpose of $\boldsymbol{\Omega}$, and further $\boldsymbol{\Omega}^{-T}$ gives the inverse of $\boldsymbol{\Omega}^T$.

Before the transformation of our system of equations is presented, some transformation rules are recapitulated. As commonly given in many standard books on continuum mechanics, the gradient of a scalar ϕ reads

$$\operatorname{grad}\phi = \frac{\partial\phi}{\partial\xi}\boldsymbol{g}^\xi + \frac{\partial\phi}{\partial\eta}\boldsymbol{g}^\eta + \frac{\partial\phi}{\partial\zeta}\boldsymbol{g}^\zeta\,, \tag{4.44}$$

with the reciprocal basis $\{\boldsymbol{g}^\xi, \boldsymbol{g}^\eta, \boldsymbol{g}^\zeta\}$, associated to $\{\boldsymbol{g}_\xi, \boldsymbol{g}_\eta, \boldsymbol{g}_\zeta\}$. The divergence of a vector $\boldsymbol{v}$ turns into

$$\operatorname{div}\boldsymbol{v} = \frac{1}{J}\Big\{\frac{\partial}{\partial\xi}(Jv^\xi) + \frac{\partial}{\partial\eta}(Jv^\eta) + \frac{\partial}{\partial\zeta}(Jv^\zeta)\Big\}\,, \tag{4.45}$$

with the determinant of the Jacobian matrix in the aggregated form $J = \det\boldsymbol{\Omega}$. For the mixed representation of a tensorial quantity, the divergence of the tensor is given by

$$\operatorname{div}\tilde{\boldsymbol{T}} = \frac{1}{J}\Big\{\frac{\partial}{\partial\xi}(J\tilde{T}^{i\xi}) + \frac{\partial}{\partial\eta}(J\tilde{T}^{i\eta}) + \frac{\partial}{\partial\zeta}(J\tilde{T}^{i\zeta})\Big\}\mathbf{e}_i \quad \text{for} \quad i \in \{X, Y, Z\}\,. \tag{4.46}$$

For more information on the basics of these terrain-following coordinates and the respective transformations, we refer to Luca et al. (2016, p. 52ff).

Now in comparison with the simple, curved coordinate system O_{xyz} that has been applied in this section so far, the new coordinates ξ and η depict a general surface, indicating slope directions, of which the respective projections on the horizontal plane may be arranged to coincide with the X and Y directions, see panel **b)** of Fig. 4.4, and effects of the curvature are not limited to a down-slope x-direction. This allows for the application to a general topography, resembling for instance mountainous areas, while curvilinear coordinates are more likely to depict a experimental setup with a basic

slope or a rather simplified talweg. The transformed equations, embedded in general coordinates, are presented in the following. As before, we do not give explicitly the way of their derivation, since this follows from general transformation rules. Note that, although this is not denoted explicitly in the following, all quantities are both non-dimensional and depth-integrated. Also, terms of order $\mathcal{O}(\epsilon^{1+\chi})$ are omitted for the balance equations in the following. The balance of mass for both phases, Eq. (4.47), yields

$$\begin{aligned}
&\frac{\partial}{\partial t}\left(J_b h \nu^s\right) + \frac{\partial}{\partial \xi}\left(J_b h \nu^s v^s_\xi\right) + \frac{\partial}{\partial \eta}\left(J_b h \nu^s v^f_\eta\right) = 0,\\
&\frac{\partial}{\partial t}\left(J_b h \nu^f\right) + \frac{\partial}{\partial \xi}\left(J_b h \nu^f v^f_\xi\right) + \frac{\partial}{\partial \eta}\left(J_b h \nu^f v^f_\eta\right) = 0,
\end{aligned} \tag{4.47}$$

where we have the determinant of the basal Jacobian, $J_b = \det \mathbf{\Omega}_b$. For the balance of momentum of the solid phase in X-direction, following from Eq. (4.26), we have

$$\begin{aligned}
&\frac{\partial}{\partial t}\left(J_b h \nu^s v^s_X\right) + \frac{\partial}{\partial \xi}\left(J_b h \nu^s v^s_\xi v^s_X\right) + \frac{\partial}{\partial \eta}\left(J_b h \nu^s v^s_\eta v^s_X\right)\\
=&J_b h \nu^s \left(c - \epsilon^\chi \tau^s_\kappa\right) n_X - \epsilon \frac{\partial}{\partial \xi}\left[\left(1 - \frac{\rho^f}{\rho^s}\right)\nu^s \frac{J_b h^2 c}{2} A_{11} - \mathrm{Eu}\frac{J_b h \nu^s \rho^f}{\rho^s}\omega^f_e A_{11}\right]\\
&- \epsilon \frac{\partial}{\partial \eta}\left[\left(1 - \frac{\rho^f}{\rho^s}\right)\nu^s \frac{J_b h^2 c}{2} A_{21} - \mathrm{Eu}\frac{J_b h \nu^s \rho^f}{\rho^s}\omega^f_e A_{21}\right]\\
&+ \epsilon \mathrm{N_Z}\left(1 - \frac{\rho^f}{\rho^s}\right)\left(A_{11}\frac{\partial J_b h \nu^s \left(Z^s_{\xi\xi} + Z^s_{\eta\eta}\right)}{\partial \xi} + A_{21}\frac{\partial J_b h \nu^s \left(Z^s_{\xi\xi} + Z^s_{\eta\eta}\right)}{\partial \eta}\right)\\
&+ \frac{\epsilon}{\rho^s}\mathrm{N_Z}\left(\frac{\partial J_b h \rho Z^s_{X\xi}}{\partial \xi} + \frac{\partial J_b h \rho Z^s_{X\eta}}{\partial \eta}\right)\\
&- \epsilon \frac{\rho^f}{\rho^s}\frac{\nu^s}{2}\left(A_{11}\frac{\partial J_b h^2 c}{\partial \xi} + A_{21}\frac{\partial J_b h^2 c}{\partial \eta}\right) + \frac{c^s_D J_b h \nu^s \nu^f \rho^f}{\rho^s}\left(v^f_X - v^s_X\right)\\
&+ \epsilon \frac{\rho^f}{\rho^s}\frac{\nu^f\left(\rho^s - \rho^f\right)}{\rho}\frac{h^2 c J_b}{2}\left(A_{11}\frac{\partial \nu^s}{\partial \xi} + A_{21}\frac{\partial \nu^s}{\partial \eta}\right)\\
&- \mathrm{sgn}\left(v^s_X\right)\tan(\delta_b) h \nu^s \left(c\left(1 - \frac{\rho^f}{\rho^s}\right) - \mathrm{Eu}_b \omega^f_e - \tau^s_\kappa\right),
\end{aligned} \tag{4.48}$$

where, please, be reminded that

$$Z^s_{X\xi} = \Omega^{11}_b Z^s_{\xi\xi} + \epsilon^\chi \Omega^{12}_b Z^s_{\eta\xi}\,, \quad Z^s_{X\eta} = \epsilon^\chi \Omega^{11}_b Z^s_{\xi\eta} + \Omega^{12}_b Z^s_{\eta\eta}\,.$$

Furthermore, we introduced the values of the inverse of the basal Jacobian $\boldsymbol{A}$, where $\boldsymbol{A} = A_{ij} = \boldsymbol{\Omega}_b^{-1}$. For the balance of the solid Y-momentum, coming from Eq. (4.27), we get

$$
\begin{aligned}
&\frac{\partial}{\partial t}\left(J_b h \nu^s v_Y^s\right) + \frac{\partial}{\partial \xi}\left(J_b h \nu^s v_\xi^s v_Y^s\right) + \frac{\partial}{\partial \eta}\left(J_b h \nu^s v_\eta^s v_Y^s\right) \\
=&J_b h \nu^s \left(c - \epsilon^\chi \tau_\kappa^s\right) n_Y - \epsilon \frac{\partial}{\partial \xi}\left[\left(1 - \frac{\rho^f}{\rho^s}\right) \nu^s \frac{J_b h^2 c}{2} A_{12} - \mathrm{Eu} \frac{J_b h \nu^s \rho^f}{\rho^s} \omega_e^f A_{12}\right] \\
&- \epsilon \frac{\partial}{\partial \eta}\left[\left(1 - \frac{\rho^f}{\rho^s}\right) \nu^s \frac{J_b h^2 c}{2} A_{22} - \mathrm{Eu} \frac{J_b h \nu^s \rho^f}{\rho^s} \omega_e^f A_{22}\right] \\
&- \epsilon \mathrm{N_Z} \left(1 - \frac{\rho^f}{\rho^s}\right) \left(A_{12} \frac{\partial J_b h \nu^s \left(Z_{\xi\xi}^s + Z_{\eta\eta}^s\right)}{\partial \xi} + A_{22} \frac{\partial J_b h \nu^s \left(Z_{\xi\xi}^s + Z_{\eta\eta}^s\right)}{\partial \eta}\right) \\
&+ \frac{\epsilon}{\rho^s} \mathrm{N_Z} \left(\frac{\partial J_b h \rho Z_{Y\xi}^s}{\partial \xi} + \frac{\partial J_b h \rho Z_{Y\eta}^s}{\partial \eta}\right) \\
&- \epsilon \frac{\rho^f}{\rho^s} \frac{\nu^s}{2} \left(A_{12} \frac{\partial J_b h^2 c}{\partial \xi} + A_{22} \frac{\partial J_b h^2 c}{\partial \eta}\right) + \frac{c_D^s J_b h \nu^s \nu^f \rho^f}{\rho^s} \left(v_Y^f - v_Y^s\right) \\
&+ \epsilon \frac{\rho^f}{\rho^s} \frac{\nu^f \left(\rho^s - \rho^f\right)}{\rho} \frac{h^2 c J_b}{2} \left(A_{12} \frac{\partial \nu^s}{\partial \xi} + A_{22} \frac{\partial \nu^s}{\partial \eta}\right) \\
&- \operatorname{sgn}\left(v_Y^s\right) \tan(\delta_b) h \nu^s \left(c \left(1 - \frac{\rho^f}{\rho^s}\right) - \mathrm{Eu}_b \omega_e^f - \tau_\kappa^s\right),
\end{aligned}
\tag{4.49}
$$

again with the hypoplastic tensors in mixed representation,

$$
Z_{Y\xi}^s = \Omega_b^{21} Z_{\xi\xi}^s + \epsilon^\chi \Omega_b^{22} Z_{\eta\xi}^s, \quad Z_{Y\eta}^s = \epsilon^\chi \Omega_b^{21} Z_{\xi\eta}^s + \Omega_b^{22} Z_{\eta\eta}^s .
$$

Likewise, for the fluid phase, the balance of momentum yields in X-direction

$$\begin{aligned}
&\frac{\partial}{\partial t}\left(J_b h \nu^f v_X^f\right) + \frac{\partial}{\partial \xi}\left(J_b h \nu^f v_\xi^f v_X^f\right) + \frac{\partial}{\partial \eta}\left(J_b h \nu^f v_\eta^f v_X^f\right) \\
=&J_b h \nu^f \left(c - \epsilon^\chi \tau_\kappa^f\right) n_X - \epsilon J_b \frac{\partial}{\partial \xi}\left(\nu^f \frac{h^2 c}{2} A_{11} + \mathrm{Eu} h \nu^f \omega_e^f A_{11}\right) \\
&- \epsilon J_b \frac{\partial}{\partial \eta}\left(\nu^f \frac{h^2 c}{2} A_{21} + \mathrm{Eu} h \nu^f \omega_e^f A_{21}\right) - c_D^s J_b h \nu^s \nu^f \left(v_X^f - v_X^s\right) \\
&+ \frac{\epsilon}{\mathrm{N}_R} \frac{\partial}{\partial \xi}\left(h A_{11} \frac{\partial J_b v_\xi^f}{\partial \xi} + h A_{21} \frac{\partial J_b v_\xi^f}{\partial \eta}\right) \\
&+ \frac{\epsilon^{1+\chi}}{\mathrm{N}_R} a_2^f \frac{\partial}{\partial \eta}\left(h\left(A_{12} \frac{\partial J_b v_\xi^f}{\partial \xi} + A_{22} \frac{\partial J_b v_\xi^f}{\partial \eta} + A_{11} \frac{\partial J_b v_\eta^f}{\partial \xi} + h A_{21} \frac{\partial J_b v_\eta^f}{\partial \eta}\right)\right), \\
&- J_b \frac{\alpha_b^f h \nu^f}{\epsilon \mathrm{N}_R} v_X^f - \epsilon \frac{h^2 c J_b}{2}\left(A_{11} \frac{\partial \nu^s}{\partial \xi} + A_{21} \frac{\partial \nu^s}{\partial \eta}\right) \\
&- \epsilon \frac{\nu^f \left(\rho^s - \rho^f\right)}{\rho} \frac{h^2 c J_b}{2}\left(A_{11} \frac{\partial \nu^s}{\partial \xi} + A_{21} \frac{\partial \nu^s}{\partial \eta}\right),
\end{aligned} \tag{4.50}$$

and in Y-direction

$$\begin{aligned}
&\frac{\partial}{\partial t}\left(J_b h \nu^f v_Y^f\right) + \frac{\partial}{\partial \xi}\left(J_b h \nu^f v_\xi^f v_Y^f\right) + \frac{\partial}{\partial \eta}\left(J_b h \nu^f v_\eta^f v_Y^f\right) \\
=&J_b h \nu^f \left(c - \epsilon^\chi \tau_\kappa^f\right) n_Y - \epsilon J_b \frac{\partial}{\partial \xi}\left(\nu^f \frac{h^2 c}{2} A_{12} + \mathrm{Eu} h \nu^f \omega_e^f A_{12}\right) \\
&- \epsilon J_b \frac{\partial}{\partial \eta}\left(\nu^f \frac{h^2 c}{2} A_{22} + \mathrm{Eu} h \nu^f \omega_e^f A_{22}\right) - c_D^s J_b h \nu^s \nu^f \left(v_Y^f - v_Y^s\right) \\
&+ \frac{\epsilon}{\mathrm{N}_R} \frac{\partial}{\partial \eta}\left(h A_{12} \frac{\partial J_b v_\eta^f}{\partial \xi} + h A_{22} \frac{\partial J_b v_\eta^f}{\partial \eta}\right) \\
&+ \frac{\epsilon^{1+\chi}}{\mathrm{N}_R} a_2^f \frac{\partial}{\partial \xi}\left(h\left(A_{12} \frac{\partial J_b v_\xi^f}{\partial \xi} + A_{22} \frac{\partial J_b v_\xi^f}{\partial \eta} + A_{11} \frac{\partial J_b v_\eta^f}{\partial \xi} + h A_{21} \frac{\partial J_b v_\eta^f}{\partial \eta}\right)\right), \\
&- J_b \frac{\alpha_b^f h \nu^f}{\epsilon \mathrm{N}_R} v_Y^f - \epsilon \frac{h^2 c J_b}{2}\left(A_{12} \frac{\partial \nu^s}{\partial \xi} + A_{22} \frac{\partial \nu^s}{\partial \eta}\right) \\
&- \epsilon \frac{\nu^f \left(\rho^s - \rho^f\right)}{\rho} \frac{h^2 c J_b}{2}\left(A_{12} \frac{\partial \nu^s}{\partial \xi} + A_{22} \frac{\partial \nu^s}{\partial \eta}\right).
\end{aligned} \tag{4.51}$$

We note that a terms of order $\mathcal{O}(\epsilon^{1+\chi})$, related to viscosity, is emerging in Eqs. (4.50) and (4.51), respectively. This term is kept in order not to overly simplify the viscous behavior. In addition to the solid bed friction term, where for curvilinear coordinates, the centrifugal forces emerged as τ_κ, these forces now also enter the equations together with the gravity shares.

For the solid,

$$\tau_\kappa^s = v_X^s \frac{\partial n_X}{\partial \xi} v_\xi^s + v_Y^s \frac{\partial n_Y}{\partial \xi} v_\xi^s + v_Z^s \frac{\partial c}{\partial \xi} v_\xi^s + v_X^s \frac{\partial n_X}{\partial \eta} v_\eta^s + v_Y^s \frac{\partial n_Y}{\partial \eta} v_\eta^s + v_Z^s \frac{\partial c}{\partial \eta} v_\eta^s ,$$

and for the fluid, i.e. in Eqs. (4.50)-(4.51), the respective centrifugal term is given as

$$\tau_\kappa^f = v_X^f \frac{\partial n_X}{\partial \xi} v_\xi^f + v_Y^f \frac{\partial n_Y}{\partial \xi} v_\xi^f + v_Z^f \frac{\partial c}{\partial \xi} v_\xi^f + v_X^f \frac{\partial n_X}{\partial \eta} v_\eta^f + v_Y^f \frac{\partial n_Y}{\partial \eta} v_\eta^f + v_Z^f \frac{\partial c}{\partial \eta} v_\eta^f .$$

These term additionally account for the centripetal acceleration due to local curvature of the topographic surface (Tai, Kuo & Hui 2012). The velocity in the z-direction can be calculated via the relations $v_Z = \Omega_B^{31} v_\xi + \Omega_B^{32} v_\eta$ and $v_Z = -v_X A_{31}/A_{33} - v_Y A_{32}/A_{33}$, respectively. For more details, see Tai et al. (2018).

Equations (4.49)-(4.50) describe the development of the velocities, referring to the ones for Cartesian coordinates. This formulation has the advantage, that with the physical quantities being formulated in Cartesian coordinates, the calculation of Christoffel symbols and a changing coordinate orientation can be avoided (Tai & Kuo 2008).

The depth-integrated evolution equation for scalar pressure variable ϖ_e^f, Eq. (4.30), is transformed as well and yields

$$\begin{aligned}
&\frac{\partial}{\partial t}\left(J_b h \varpi_e^f\right) + \frac{\partial}{\partial \xi}\left(J_b h \varpi_e^f v_\xi^f\right) + \frac{\partial}{\partial \eta}\left(J_b h \varpi_e^f v_\eta^f\right) - 2\frac{k_D \beta_\psi^f}{h \mu^s \alpha_D} J_b \varpi_e^f \\
=&\frac{\sigma_e}{2}\left[\frac{\partial J_b h \nu^s (v_\xi^s - v_\xi^f)}{\partial \xi} + \frac{\partial J_b h \nu^s (v_\eta^s - v_\eta^f)}{\partial \eta} + h\left(\frac{\partial J_b v_\xi^f}{\partial \xi} + \frac{\partial J_b v_\eta^f}{\partial \eta}\right)\right] \\
&+ \varpi_e^f\left[\frac{\partial J_b h \nu^s (v_\xi^s - v_\xi^f)}{\partial \xi} + + \frac{\partial J_b h \nu^s (v_\eta^s - v_\eta^f)}{\partial \eta}\right] - J_b h \dot{\gamma} \tan(\psi),
\end{aligned} \tag{4.52}$$

where for the last term on the RHS-side, the dilatancy term, see Eqs. (4.31) and (4.32).

A set of depth-integrated equations for second order tensorial variable $Z_{i\delta}$, depicting the inner stress state of the material, has been derived with Eqs. (4.33)-(4.35), complemented by the source terms in Eqs. (C.6)-(C.8), see Appendix C. Here, a mixed

representation of the tensorial variable is chosen, so, in the framework of a general coordinate system, it follows that

$$\begin{aligned}
&\epsilon\frac{\partial J_b h Z^s_{X\xi}}{\partial t}+\epsilon\frac{\partial J_b h v^s_\xi Z^s_{X\xi}}{\partial \xi}+\epsilon\frac{\partial J_b h v^s_\eta Z^s_{X\xi}}{\partial \eta}\\
&+\epsilon\left(A_{11}\frac{\partial J_b h v^s_\eta}{\partial \xi}+A_{21}\frac{\partial J_b h v^s_\eta}{\partial \eta}-A_{12}\frac{\partial J_b h v^s_\xi}{\partial \xi}-A_{22}\frac{\partial J_b h v^s_\xi}{\partial \eta}\right)Z^s_{X\eta}\\
&-\epsilon\left(1+\nu^s\frac{\rho^s-\rho^f}{\rho}\right)Z^s_{X\xi}\left[A_{11}\frac{\partial J_b h \nu^s(v^s_X-v^f_X)}{\partial \xi}+A_{21}\frac{\partial J_b h \nu^s(v^s_X-v^f_X)}{\partial \eta}\right.\\
&\left.+A_{12}\frac{\partial J_b h \nu^s(v^s_Y-v^f_Y)}{\partial \xi}+A_{22}\frac{\partial J_b h \nu^s(v^s_Y-v^f_Y)}{\partial \eta}\right]\\
&-Z^s_{X\zeta}J_b h v^s_X\left(1-\lambda\kappa\right)=\epsilon\Phi^s_{X\xi}J_b h,
\end{aligned}\tag{4.53}$$

$$\begin{aligned}
&\epsilon\frac{\partial J_b h Z^s_{X\eta}}{\partial t}+\epsilon\frac{\partial J_b h v^s_\xi Z^s_{X\eta}}{\partial \xi}+\epsilon\frac{\partial J_b h v^s_\eta Z^s_{X\eta}}{\partial \eta}\\
&+\frac{1}{2}\left(A_{11}\frac{\partial J_b h v^s_\eta}{\partial \xi}+A_{21}\frac{\partial J_b h v^s_\eta}{\partial \eta}-A_{12}\frac{\partial J_b h v^s_\xi}{\partial \xi}-A_{22}\frac{\partial J_b h v^s_\xi}{\partial \eta}\right)\left(Z^s_{Y\eta}-Z^s_{X\xi}\right)\\
&-\epsilon\left(1+\nu^s\frac{\rho^s-\rho^f}{\rho}\right)Z^s_{X\eta}\left[A_{11}\frac{\partial J_b h \nu^s(v^s_X-v^f_X)}{\partial \xi}+A_{21}\frac{\partial J_b h \nu^s(v^s_X-v^f_X)}{\partial \eta}\right.\\
&\left.+A_{12}\frac{\partial J_b h \nu^s(v^s_Y-v^f_Y)}{\partial \xi}+A_{22}\frac{\partial J_b h \nu^s(v^s_Y-v^f_Y)}{\partial \eta}\right]\\
&-Z^s_{Y\zeta}J_b h v^s_X\left(1-\lambda\kappa\right)-Z^s_{X\zeta}hJ_b v^s_y=\epsilon\Phi^s_{X\eta}J_b h,
\end{aligned}\tag{4.54}$$

$$\begin{aligned}
&\epsilon\frac{\partial J_b h Z^s_{Y\eta}}{\partial t}+\epsilon\frac{\partial J_b h v^s_\xi Z^s_{Y\eta}}{\partial \xi}+\epsilon\frac{\partial J_b h v^s_\eta Z^s_{Y\eta}}{\partial \eta}\\
&-\left(A_{11}\frac{\partial J_b h v^s_\eta}{\partial \xi}+A_{21}\frac{\partial J_b h v^s_\eta}{\partial \eta}-A_{12}\frac{\partial J_b h v^s_\xi}{\partial \xi}-A_{22}\frac{\partial J_b h v^s_\xi}{\partial \eta}\right)Z^s_{X\eta}\\
&-\epsilon\left(1+\nu^s\frac{\rho^s-\rho^f}{\rho}\right)Z^s_{Y\eta}\left[A_{11}\frac{\partial J_b h \nu^s(v^s_X-v^f_X)}{\partial \xi}+A_{21}\frac{\partial J_b h \nu^s(v^s_X-v^f_X)}{\partial \eta}\right.\\
&\left.+A_{12}\frac{\partial J_b h \nu^s(v^s_Y-v^f_Y)}{\partial \xi}+A_{22}\frac{\partial J_b h \nu^s(v^s_Y-v^f_Y)}{\partial \eta}\right]\\
&-Z^s_{Y\zeta}hJ_b v^s_Y=\epsilon\Phi^s_{Y\eta}J_b h.
\end{aligned}\tag{4.55}$$

As for the source terms $\Phi^s_{X\xi}$, $\Phi^s_{X\eta}$ and $\Phi^s_{Y\eta}$, we again refer to the Appendix C, where these are given.

This provides a closed, comprehensive system of equations for the description of debris flows. The equations are non-dimensionalized, depth-integrated and transfered into general coordinates. The following chapter applies the system of equations for numerical simulations to test the behavior of the additional fields, to compare them with experimental results, and finally to apply them to a real scenario.

5 Model applications and numerical results

In this chapter, the previously derived equations are tested, that is implemented in a numerical scheme and applied to various flow problems, and the results are discussed. Therefore, in Section 5.1, the background of the numerical computations and the used scheme are introduced, before some fundamental parameter studies are presented in Section 5.2. We conclude with a comparison to experimental results (Section 5.3) and, finally, with the application of the model to the Hsiaolin event (Section 5.4), a disastrous landslide that occurred in Taiwan, demonstrating the ability to govern different flow configurations, from a laboratory scale to real events.

Since the simulations aim at a first investigation of the influence of the fields of extra pore-fluid pressure and hypoplasticity, as well as application to diverse scenarios, the chosen values and material parameters are mostly simple and not subject to a detailed investigation. Most of the parameters are either physical values and/or have been suggested in the literature, most notably in Meng & Wang (2016), and are just adopted here, so we refrain from a detailed discussion. As elaborated in Chiou, Wang & Hutter (2005), we choose $\epsilon = 1$ and $\lambda = 1$. This means that the aspect ratio of the physical debris flow is preserved.

5.1 Numerical scheme

The difficulties in the numerical treatment of a system of depth-integrated equations for granular-fluid flows are well known, arising due to steep gradients and phase coupling (Wang & Hutter 2001a, Wang, Hutter & Pudasaini 2004). A main requirement here is a robust numerical solver that can handle shocks. Therefore, a non-oscillatory central (NOC) scheme for conservative laws is employed, derived by Kurganov & Tadmor (2000), together with total variation diminishing through a minmod-limiter. The time stepping of the semi-discrete scheme is handled with a two-step Runge-Kutta scheme. As for insights into the numerical implementation for a (simpler) system of partial differential equations, its vectorial form and the discretization, we refer to Tai et al. (2018).

To solve the system, the final balance equations for mass (4.47), momentum, Eqs. (4.48)-(4.51), extra pore-fluid pressure (4.52) and the hypoplastic stress, Eqs. (4.53)-(4.55), are rewritten in vectorial form. Here, a convection-diffusion equation with source term is considered, given as

$$\partial_t \left(\mathbf{U}\right) + \partial_{\tilde{\xi}} \left(\mathbf{F}_X\right) + \partial_\eta \left(\mathbf{F}_Y\right) = \mathbf{S} + \mathbf{C}_1 \partial_{\tilde{\xi}} \left(\mathbf{C}_2\right) + \mathbf{C}_3 \partial_\eta \left(\mathbf{C}_4\right) \tag{5.1}$$

with the vectors of unknowns in terms of conservative variables

$$\mathbf{U} = \begin{pmatrix} h\nu^s \\ h\nu^f \\ h\nu^s v_X^s \\ h\nu^s v_Y^s \\ h\nu^s v_X^f \\ h\nu^s v_Y^f \\ h\omega_e^f \\ hZ_{X\xi}^s \\ hZ_{X\eta}^s \\ hZ_{Y\eta}^s \end{pmatrix}, \tag{5.2}$$

the flux terms $\mathbf{F}_X, \mathbf{F}_Y$, the source term $\mathbf{S}$ and the non-conservative terms $\mathbf{C}_k, k = 1, ..., 4$.

Equation (5.1) comprises a two-dimensional equation with diffusion, non-conservative terms and a source, and can be treated with the numerical scheme of Kurganov & Tadmor (2000). For this, a uniform spatial grid is applied as $(X_j, Y_k) = (j\triangle X, k\triangle Y)$ and the vectorial Eq. (5.1) is discretized, so

$$\begin{aligned} \frac{\mathrm{d}}{\mathrm{d}t} U_{j,k}(t) = &- \frac{F^X_{j+1/2,k} - F^X_{j-1/2,k}}{\triangle X} - \frac{F^Y_{j,k+1/2} - F^Y_{j,k-1/2}}{\triangle Y} \\ &+ \frac{P^X_{j+1/2,k} - P^X_{j-1/2,k}}{\triangle X} + \frac{P^Y_{j,k+1/2} - P^Y_{j,k-1/2}}{\triangle Y} + s_{j,k}\triangle X \triangle Y. \end{aligned} \tag{5.3}$$

This semi-discrete form exhibits numerical convection fluxes $F^X_{j\pm1/2,k}, F^Y_{j,k\pm1/2}$ which can be computed with regard to the values of $\mathbf{U}$ left and right of the midpoints, i.e. $U^+_{j\pm1/2,k}$, $U^-_{j\pm1/2,k}$, $U^+_{j,k\pm1/2}$ and $U^-_{j,k\pm1/2}$. These values next to the midpoints are themselves estimated with the help of total variation diminishing (TVD) limiters, which approximate derivatives while retaining a non-oscillatory behavior, applying – in this work – a minmod-limiter. $P^X_{j\pm1/2,k}$ and $P^Y_{j,k\pm1/2}$ refer to the non-conservative terms. This semi-discrete system, forming an ordinary differential equation (ODE), is then solved with a second-order Runge-Kutta (RK) method, see Shu & Osher (1988).

The applied NOC-scheme of Kurganov & Tadmor (2000) is a further development of the central Nessyahu-Tadmor (NT)-scheme, see Nessyahu & Tadmor (1990), a central scheme obtaining high resolution with a Riemann-solver-free approach. An advantage is the independence of the eigenstructure of the problem (Kurganov & Tadmor 2000). The TVD-limiter, due to its shock-capturing features, prevents an increasing oscillation with time. Further developments have been the central-upwind scheme of Kurganov & Miller (2014), while, for hyperbolic conservation laws in fluid dynamics, also the Discontinous Galerkin (DG)-method has grown in popularity (Hutter & Wang 2016). For an overview, regarding the numerical handling of the related SH-type modeling, see Wang & Hutter (2001a) and Hutter & Wang (2016).

The Courant-Friedrichs-Lewy (CFL) condition is set to hold during the computation, determining the time step size via estimates of the wave speeds and the grid size. The associated CFL number is set to 0.1 during the computations, so

$$C_{max} = \frac{a_X^w \triangle t}{\triangle X} + \frac{a_Y^w \triangle t}{\triangle Y} = 0.1,$$

with the grid length in X and Y directions, $\triangle X$ and $\triangle Y$, respectively, and the time-step size $\triangle t$. During the computation, the CFL condition serves to condition the time-step size according to the apparent wave speeds. Since we are not interested in issues of numerical performance at this point, a small CFL number is chosen to increase the stability of this complex system with additional fields.

The speeds of local propagation, or so-called wave speeds, describe the maximum characteristic speeds via the apparent fluxes. These wave speeds can be determined as the eigenvalues of the Jacobians of the flux-term. Here, we are not interested in deriving all eigenvalues exactly, i.e. a number of wave speeds equivalent to the number of variables (or fields), but only in the maximum wave speed. For this, estimated values are derived according to Kurganov & Miller (2014) and, closer to the equations handled here, in Meng et al. (2017). The estimated maximum wave speeds

$$a_X^w = max\left(c_X^{s,w}, c_X^{f,w}\right), \quad a_Y^w = max\left(c_Y^{s,w}, c_Y^{f,w}\right),$$

are composed of the maximum wave speeds for both phases, respectively. In order to get these, i.e. $c_X^{s,w}, c_Y^{s,w}, c_X^{f,w}, c_Y^{f,w}$, as elaborated in Kurganov & Miller (2014), not the actual eigenvalues are determined, but bounds can be found with the coefficients of the characteristic equation, so that the maximum and minimal eigenvalue can be evaluated. For these computations, the wave numbers are left as in Tai et al. (2018).

It might appeal to the reader that, although this is not the aim of the numerical investigations, the actual performance of the numerical code is quite satisfactory in terms of computational time and resources, especially in comparison to discrete particle studies. An average computation for studies of the laboratory scale with about 10^5 (here: $1.2E5$) degrees of freedom (DOF), as in Sections 5.2 and 5.3, takes about 5 minutes, a large scale study, as in section 5.4, with 10^6 DOF (here: $8.2E5$) from 5 up to 8 hours, all on a simple personal computer.[1]

5.2 Parameter studies

It is the aim of this first series of investigations to explore the impact of the additional fields of extra pore-fluid pressure and hypoplasticity, and, with this, provide a comparison to a "regular" or MW-model, as presented in Meng & Wang (2016) and transferred to general coordinates in Tai et al. (2018). While results for such a comparison for a 1D case, treated in a system of curvilinear coordinates, have been presented in Heß &

[1] Where the configuration is: Intel i5 CPU @3.10 GHz with 4 cores and 8 GB memory, Ubuntu OS.

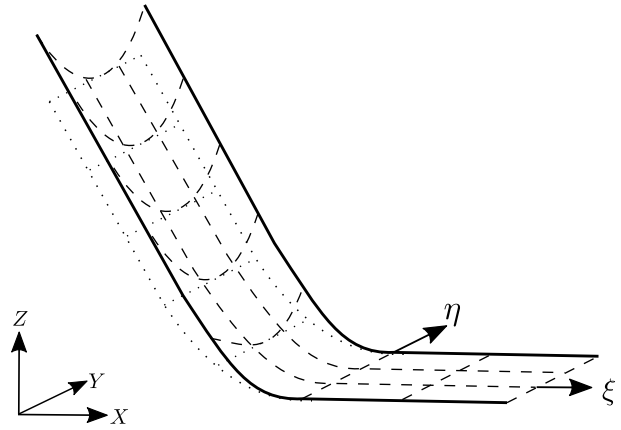

Figure 5.1: A chute with curved bed, applied for parametric studies in Section 5.2. The actual topographic surface, indicated by the dashed lines, is superposed over a simple curved plane, denoted by the dotted lines.

Wang (2019), in this study, the distribution in two dimensions is investigated. Moreover, the results presented here shall provide a first overlook, dealing with the general behavior of the mass flow in conjunction with the influence of the additional fields, before in the following sections, special cases and events on a larger scale are tackled.

In the following, a combination of Cartesian coordinates (X, Y, Z) and terrain-following coordinates (ξ, η, ζ) are applied, with respect to the general coordinate ansatz, see Fig. 5.1 and, for more information, Tai et al. (2018). The computational domain is defined as $(X, Y) \in ([0, 80], [0, 36])$, or $(\xi, \eta) \in ([0, 88.34], [0, 39.43])$, respectively. For the parameter studies concerning the role of the extra pore-fluid pressure and the intergranular stress, the case of a curved, inclined chute was considered, running out into the horizontal plane, see Fig. 5.1. The transition between the ramp and the horizontal plane is smooth and is described by the inclination angle ϑ_s, as

$$\vartheta_s = \begin{cases} \vartheta_0, & 0 \leq X \leq 24, \\ \vartheta_0 \left(1 - (X - 24)/10\right), & 24 < X < 34, \\ 0^\circ, & X \geq 34. \end{cases}$$

The chute has an inclined part in the range $X \leq 24$, a horizontal part in the range for $X \geq 34$, and a transitional part in between. The curved character is achieved with an additional elevation z_b, such that

$$z_b = \begin{cases} Y_d^2 / \cos\vartheta_s, & 0 \leq X \leq 24, \\ Y_d^2 / \cos\vartheta_s \Big[1 - (X - 24)/10\Big], & 24 < X < 34, \\ 0, & X \geq 34, \end{cases}$$

where $Y_d = |\eta - \eta_0|/36$ and $\eta_0 = 18$ (center line). A pile, consisting of a saturated granular-fluid mixture, is released out of rest at the initial time $t = 0$. This initial mass has a parabolic profile, defined with respect to the terrain-following coordinates as

$$h(t = 0, \xi, \eta) = h_0 \left(1 - (\xi - \xi_0)^2/16 - (\eta - \eta_0)^2/16\right),$$

with $h_0 = 2/\cos\vartheta_0$ and $\xi_0 = 8$. Besides the density ratio $\alpha_\rho = \rho^f/\rho^s$, there is a set of four basic parameters

$$\left(\delta_b, \mathrm{N}_R, \alpha_b^f, c_D^s\right),$$

that govern the flow dynamics of a simple, granular-fluid mixture as in Meng & Wang (2016). Their values are given in Table 5.1, together with additional parameters for these simulations. The first one of these basic parameters is the angle of basal solid friction δ_b, determining the resistance of the granular material at the base. This parameter has a precise physical meaning and can be measured by the inclination angle, at which granular material begins to slide on an inclined plane. The basal friction governs the main drag on the granular material, so with an increasing angle of basal friction, steeper gradients of height arise, the mixture mass is moving less far and zones of solid concentration develop more distinctly. For determination of values in experimental investigations, we refer to Savage & Hutter (1991) and Hutter, Koch, Plüss & Savage (1995), where δ_b-values between 19.5° and 25° have been detected.

For the fluid, the viscous behavior is adjusted with N_R. Neglecting the complexity of the viscous fluid behavior in debris flows, in which the viscosity parameter may depend on the shear-rate, on the presence of clay and silk particles in the pore-water, or on other influences, an idealized case is assumed with a constant and dimensionless viscous number $\mathrm{N}_R = 200$. This refers to rather low viscosity of $0.5247\,\mathrm{Pa}\cdot\mathrm{s}$, a value fairly close to the range presented in O'Brien & Julien (1988). The corresponding value of μ^f can be determined with $\mathrm{N}_R = (\rho^f \mathcal{H}\sqrt{g\mathcal{L}})/\mu^f$, where $\mathcal{L} = \mathcal{H} = 0.1$ and the fluid density is $\rho^f = 1060\,\mathrm{kg/m^3}$. In conjunction with viscosity, the fluid friction coefficient α_b^f determines the basal resistance of the fluid. Here, as well as with the drag coefficient c_D^s for the drag between the two phases, we rely on values given and tested in Meng & Wang (2016) and also Tai et al. (2018), not backed by experimental values. For further discussion of these basic parameters, please see both aforementioned works, as well as Pudasaini (2012).

5.2.1 Pore-fluid pressure

As for the effects of the extra pore-fluid pressure, three different parameter settings have been compared in Fig. 5.2: A flow without extra pore-fluid pressure and two configurations, in which the extra pore-fluid pressure takes influence with different intensity, via variations of the Euler number Eu and Eu_b. The respective terms act upon the developing velocities, both in the solid basal friction and in the pressure terms as

Num. Parameter	Value	Description
(n_X, n_Y)	$(161, 73)$	Points in X- and Y-direction
X	$\in [0, 80]$	Domain in X-direction
Y	$\in [0, 36]$	Domain in Y-direction
C_{max}	0.1	CFL number
ϑ_0	40°	Maximum chute inclination angle
$\nu^{s,f}\|^0$	0.5	Initial volume fractions
$v_X^{s,f}\|^0, v_Y^{s,f}\|^0$	0	Initial velocities
Phys. Parameter	**Value**	**Description**
$\alpha_\rho = \rho^f / \rho^s$	1.06/2.65	Density ratio
δ_b	23°	Angle of basal friction
α_b^f	20	Navier fluid friction coefficient
c_D^s	6	Drag coefficient
N_R	200	Viscous number

Table 5.1: Numerical and physical parameters for the studies in Section 5.2.

a driving force. As a main result here, it is apparent that the dynamic extra pressure drives the bulk mass further. When the material is pushed together and compressed during deceleration, the extra pressure is increased, counters settling and reduces the intergranular friction, so the runout length is increased. This matches expectations, since the effects of the dynamic pore-fluid pressure are particularly present during the last, decelerating phase of the flow, when the material reaches the horizontal runout.

As shown in Heß & Wang (2019), an increased initial value of the pore pressure brings this effect to the initial phase, representing a flow onset due to liquefaction, e.g. after intense rainfall. Here, with $\varpi_e^f|^0 = 0.001$, a rather small value is chosen, implying little dynamic pressure at the initiation. The parameters for the pore pressure evolution are chosen with reference to Iverson & George (2014), with a permeability constant of $k_D^0 = 1.0 \cdot 10^{-13}$ and the constant of compressibility $\alpha_D^0 = 1.0$, as well as a critical solid volume fraction $\nu_C^s = 0.62$. The average particle size is chosen as $\delta_P = 0.0001$ and the solid density is $\rho^s = 2650\,\mathrm{kg/m^3}$. Further model parameters in conjunction with dilatancy are $\kappa_{\varpi 1} = 1.1$ and $\kappa_{\varpi 2} = 15$.

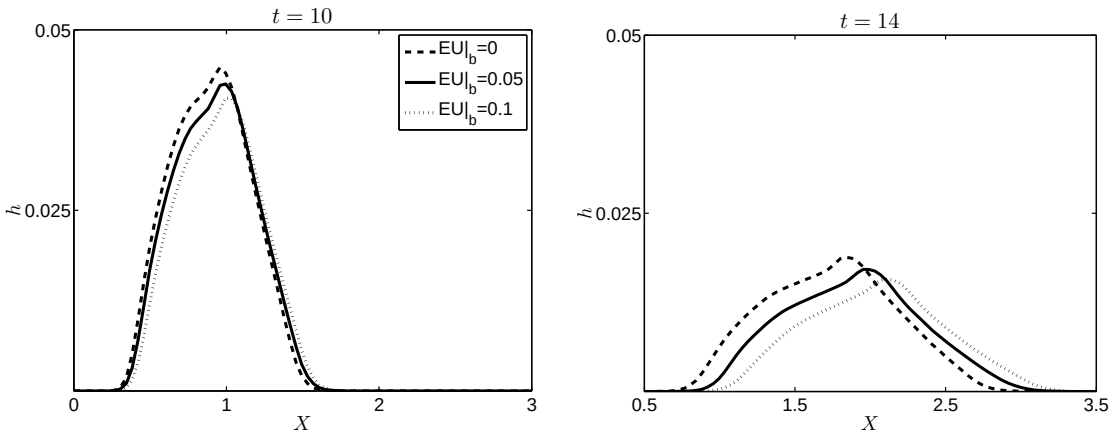

a) Mixture height along the center line for three different values of Eu_b

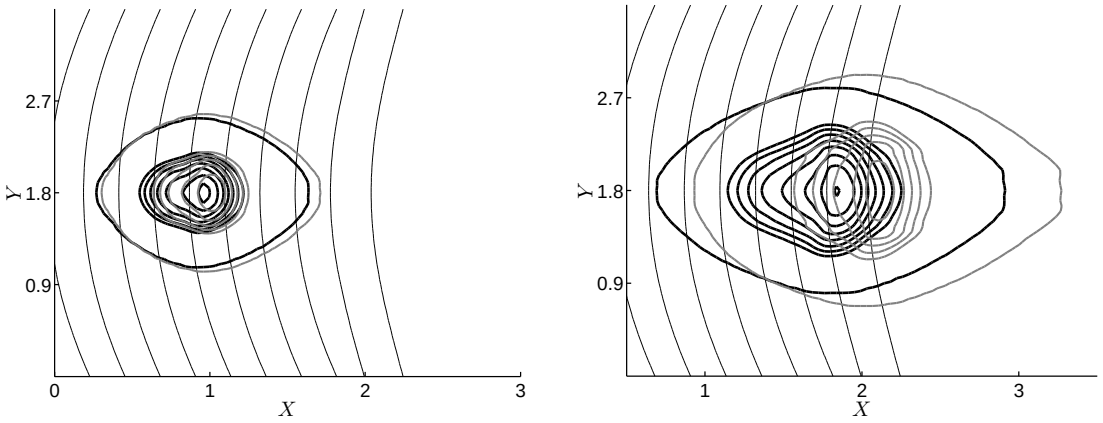

b) Contour of the mixture height for $\mathrm{Eu}_b = 0.0$ (black line) and $\mathrm{Eu}_b = 0.1$ (gray line)

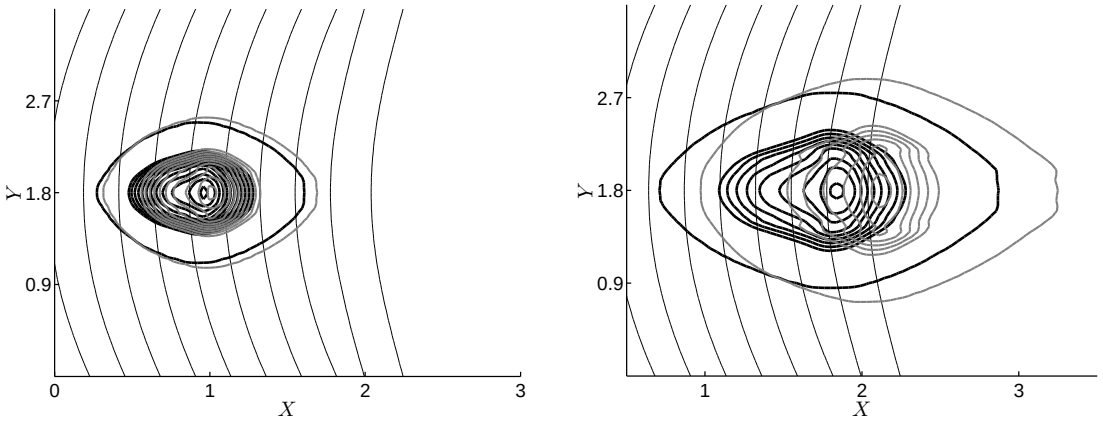

c) Contour of solid volume height for $\mathrm{Eu}_b = 0.0$ (black line) and $\mathrm{Eu}_b = 0.1$ (gray line)

Figure 5.2: Study on the extra pore-fluid pressure: The height profile is compared at $t = 10$ and $t = 14$, together with the volume fraction, for a varying influence of the extra pore-fluid pressure, denoted by changes in Eu_b. In panel **a)**, the dashed line denotes no pore pressure, the solid line gives the results for $\mathrm{Eu}_b = 0.05$ and the dotted line plots the results for $\mathrm{Eu}_b = 0.1$. Note that, while in panel **a)**, a cutline at $Y = 1.8$ (center line) shows the height development, panel **b)** shows a height contour plot, and panel **c)** gives the contour of the solid volume fraction. For the contour plots, only two configurations are presented, the results for $\mathrm{Eu}_b = 0.0$ (black line) and $\mathrm{Eu}_b = 0.1$ (gray line).

A possible range for these values is given in Iverson & George (2014) via the bounds $10^{-10} \leq (k_m\sqrt{\mathcal{L}/g})/(\alpha_D \cdot \mu^f \cdot \mathcal{H}^2) \leq 10^4$, depending on the scale of the event, while we have $(k_D^0\sqrt{\mathcal{L}/g})/(\alpha_D^0 \cdot \mu^f \cdot \mathcal{H}^2) \approx 10^{-10}$. For further explanation of these parameters and their range, see Iverson & George (2014), and for the application to the current model, Heß & Wang (2019).

5.2.2 Intergranluar friction

Further, the influence of hypoplasticity was evaluated in Fig. 5.3. It provides an inner stabilization, preventing the bulk mass from dissolving and enhances the concentration of solid material. So due to the introduction of the intergranular stress, the material piles up with a steeper front. This is in particular apparent if the solid volume fraction is observed, see Fig. 5.3**c)**.

Since the solid material stays in an assembled form, with a rather peaked than copped top, the fluid tends to leak out at the front during settling at later time steps, here of course also depending on the other material parameters such as α_b^f and c_D^s. This depicts a situation in which the granular skeleton is stable after the bulk mass has decelerated, while the fluid runs out of the pores. The influence of the hypoplastic stress can be varied together with the dimensionless number N_Z, giving the relation of the intergranular stress to inertial forces.

The value of the initial intergranular stress is chosen as $Z_{ii}^s|^0 = 0.1$, and, as further parameters, an internal friction angle $\phi_{int} = 23^\circ$ is applied, see Savage & Hutter (1991) and Hutter et al. (1995) for experimental determination, together with the coefficients $f_D^0 = 1.0$ and $f_s^0 = 0.01$, as well as $a_Z^{s,0} = 0.01$. More discussion of the values can be found in Bauer (1996) and Gudehus (1996) and there are numerous works on the calibration of the model parameters. Note that as a simplification, we set $Z_{xz}^s = Z_{yz}^s = 0$.

A draw-back possibly present here is the appearance of unrealistically high values of the solid volume fraction (Heß & Wang 2019), since the maximum packing of the granular particles may be exceeded. As pointed out there and in Pudasaini (2012), this calls for a multi-layer approach as in Meng et al. (2017), in which real phase separation can be depicted. Nonetheless, the introduction of an actual field that is able to depict the contact forces of the granular skeleton provides a further approximation to realistic debris flow behavior.

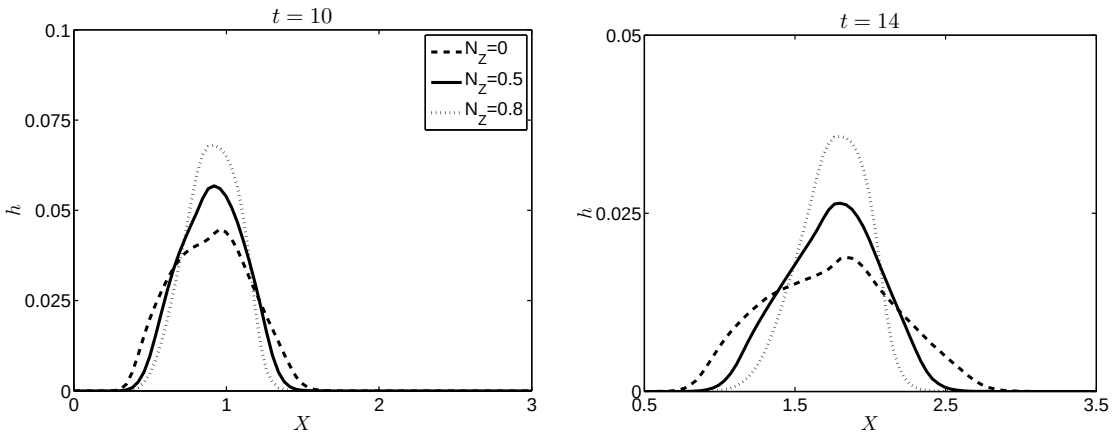

a) Mixture height along the center line for three different values of N_Z

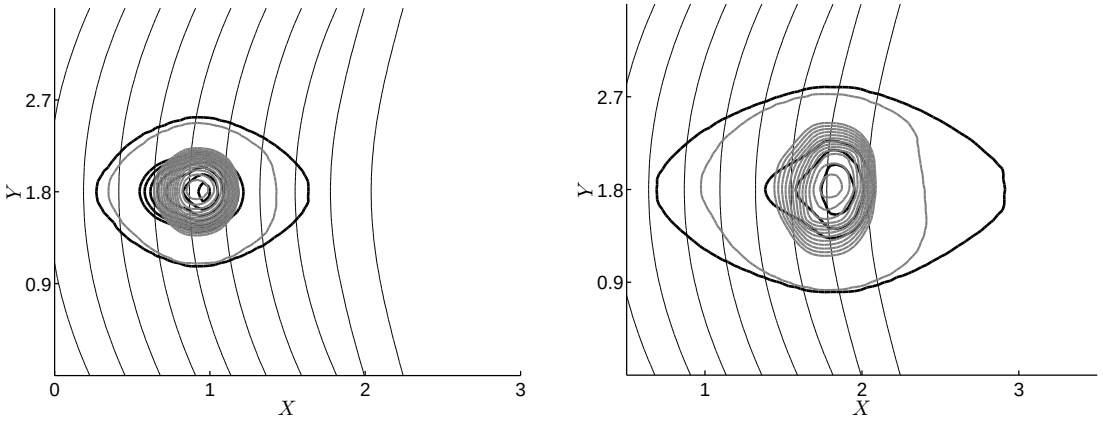

b) Contour of the mixture height for $N_Z = 0.0$ (black line) and $N_Z = 0.8$ (gray line)

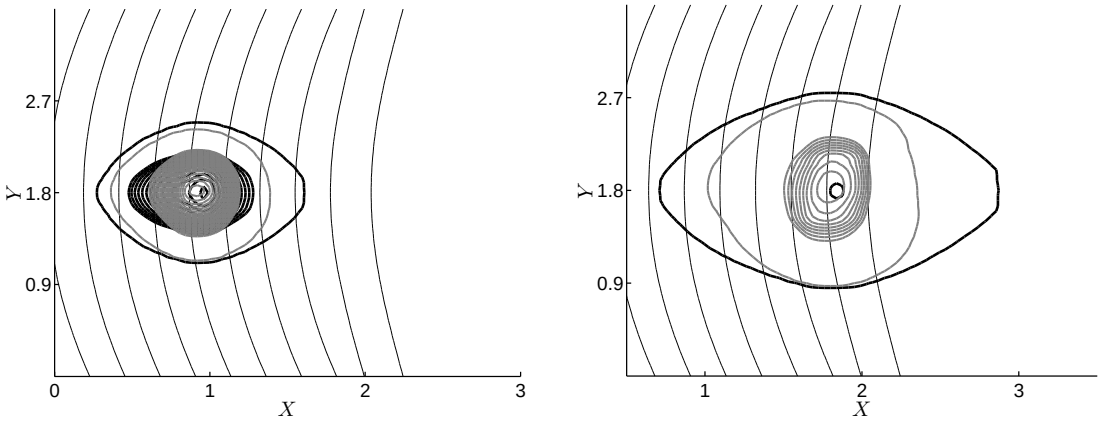

c) Contour of solid volume height for $N_Z = 0.0$ (black line) and $N_Z = 0.8$ (gray line)

Figure 5.3: Height development and volume fraction distribution for a study on the influence of hypoplasticity, given at two different times, $t = 10$ and $t = 14$ in the two rows, respectively. The influence is investigated by varying N_Z, giving three different configurations in panel **a)**, denoted by a dashed line for $N_Z = 0.0$, a solid line for $N_Z = 0.5$ and a dotted line for $N_Z = 0.8$. While panel **a)** presents a plot at $Y = 18$ (center line), panel **b)** gives the height contour and panel **c)** the volume fraction contour plot. For the contour plots, only two configurations are presented, the results for $N_Z = 0.0$ (black line) and $N_Z = 0.8$ (gray line).

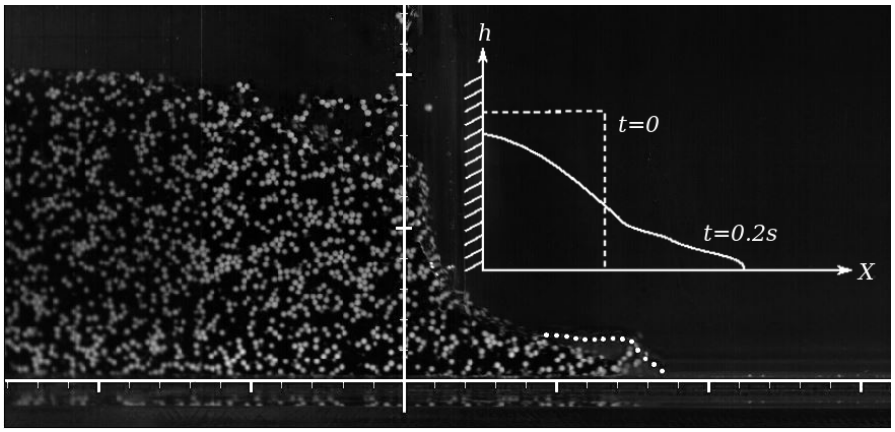

Figure 5.4: Background and setup of the dam break experiment. The photo depicts the height development of the mass (at $t = 0.2\,\mathrm{s}$) as it was evaluated during the experiment. On the right-hand side, in the top corner, a sketch shows the abstract setup, including the initial block of glass beads and water (dashed line) that is supported on the left side by a wall and released at $t = 0$, as well as the developing flow height (solid line) at a later time.

5.3 Comparison with experimental results

Now to check the model against empirical data, a comparison with an experiment was performed. The setup is a classic dam break scenario, conducted by Y.-C. Tai at National Cheng Kung University (NCKU), Taiwan. The results have not been published so far. In this experiment, a block of glass beads, saturated with water, is released from rest and dissolves to one side while on the other side there is a wall supporting the material. There are two transparent smooth sidewalls, so the configuration is approximating a quasi-2D case, with the (X, Z)-plane being observed. Figure 5.4 shows the course of the experiment, captured in a photo, together with a sketch of the experimental setup on the right-hand side. The flow front is investigated by taking pictures from the side at two time steps after the initiation, $t = 0.2\,\mathrm{s}$ and $t = 0.4\,\mathrm{s}$. The main aim of this comparison is to capture the influence of hypoplasticity on the flow front. For further dam break experiments and numerical investigations, we refer to Balmforth & Kerswell (2005), Ionescu, Mangeney, Bouchut & Roche (2015) and Wang, Wang, Peng & Meng (2017).

In Fig. 5.5, the experimental results are compared to numerical results with and without the additional effects at two time steps, i.e. with the parameter configurations $\mathrm{Eu} = 0.0$, $\mathrm{Eu}_b = 0.0$, $\mathrm{N}_Z = 0.0$ and $\mathrm{Eu} = 0.00125$, $\mathrm{Eu}_b = 0.125$, $\mathrm{N}_Z = 1.5$. For further parameter values, please see Table E.1 in Appendix E; values not appearing there are set as before. Panel **a)** shows the developing flow front at $t = 0.2\,\mathrm{s}$, together with the initial profile (dashed gray line). It is apparent that the results for the numerical simulation with the additional effects are roughly compatible to the experimental results, maintaining a rear part with the initial height and, followed by a rather steep decrease near the front while, without the additional effects, the whole bulk mass dissolves and sinks down more like a fluid than a granular structure. The same differing behavior is

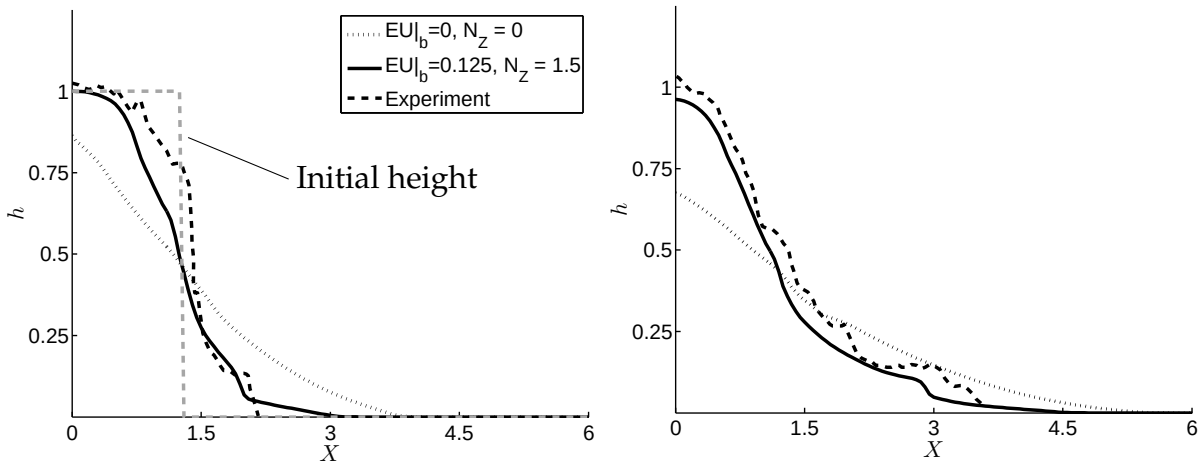

a) $t = 0.2\,\mathrm{s}$ **b)** $t = 0.4\,\mathrm{s}$

Figure 5.5: Dam break Experiment: Comparison of the observable height development at two different time steps with numerical simulations. For the numerical results, two different configurations are applied to investigate on the impact of the additional fields with respect to the description of the height development. The black dashed line depicts the experimental results for the height, the gray dashed line gives the initial height profile, the dotted black line gives the configuration without additional fields, $\mathrm{Eu}_b = 0.0$ and $\mathrm{N}_Z = 0.0$, and the black solid line depicts the results for $\mathrm{Eu}_b = 0.125$ and $\mathrm{N}_Z = 1.5$. Note that, while the results shown in the photograph in Fig. 5.4 display an equal axis scaling, the aspect ratio in the plot is roughly $1 : 3$.

visible at the next time step, $t = 0.4\,\mathrm{s}$, in panel **b)** where a cliff-like socket near the front can be depicted only with the additional fields. This means, the intergranular friction provides a mechanism that hinders the material from dissolving like a fluid, preserving its structure. In contrast, the simulation results without hypolasticity show a rather smoothed front without remnants of the originally sharp edge of the initial block.

To provide further qualitative insights, the flow front at $t = 0.4\,\mathrm{s}$ is depicted more closely in Fig. 5.6, together with the height of the solid part of the mass, hv^s. This zoom-in compares the distribution of the solid material with and without influence of intergranular stress, showing that the latter enables to reproduce a state in which there is a more distinct, sharp solid cliff together with a water flowout. It can be seen that the steep flow front apparent in the experimental results can be reproduced well by the numerical results by taking hypoplasticity into consideration. All of this highlights the possibility of describing the granular material also as a solid-like structure that maintains its form and refrains from dissolving like a fluid.

The apparent limitation of this comparison is due to the application of a system of depth-integrated equations for an actual 2D problem. Nonetheless, the results are usable and satisfying, showing that distinct features in height development are roughly captured by incorporating additional effects.

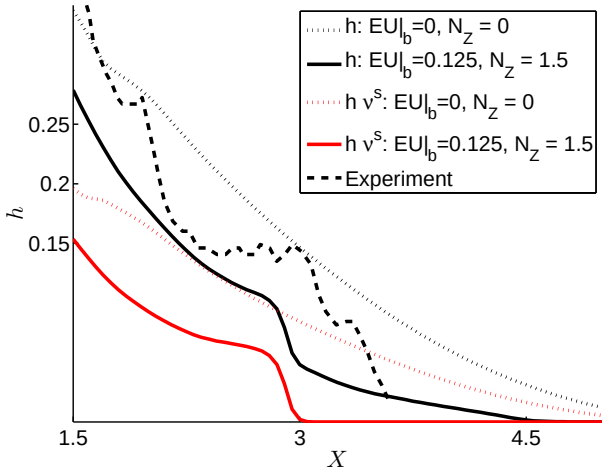

Figure 5.6: Dam break experiment: Zoom-in at the flow front, for $t = 0.4\,\mathrm{s}$. Besides the height of the mixture for the experiment (black dashed line), the height from the numerical studies are given (black solid and dotted lines) and the height of the solid part is depicted (red solid and dotted lines). The dotted lines account for $\mathrm{Eu}_b = 0.0, \mathrm{N}_Z = 0.0$ and the solid lines for $\mathrm{Eu}_b = 0.125, \mathrm{N}_Z = 1.5$.

5.4 A large-scale application: the Hsiaolin event

As a final test of the model and its implementation in the framework of a numerical scheme, the Hsiaolin event is considered. Rather than an investigation on the distinct parameters and the influence of the additional fields, this is thought to be an exemplary study, demonstrating the applicability of the solver to large scale events.

5.4.1 Background of the event

In August 2009, typhoon Morakot hit Taiwan, causing severe flooding and setting new records with respect to precipitation. Accompanied by heavy rainfall, it triggered a series of catastrophic landslides and mudflows. In the mountains of southern Taiwan, the village of Hsiaolin was destroyed by a debris avalanche, resulting in 474 casualties (Kuo, Tai, Chen, Chang, Siau, Dong, Han, Shimamoto & Lee 2011). The events were particularly devastating since the transported debris reached the Qishanxi river and formed a temporary dam there that, when it broke within an hour, flooded the previously spared parts of the village, see Dong et al. (2011) and Lo, Lin, Tang & Hu (2011). Afterwards, a digital elevation model (DEM) was created in order to retrace the course of events and with this, it was estimated that the major body of the landslide had an extent of $57 \cdot 10^4 \mathrm{m}^2$ and a volume of roughly $24 \cdot 10^6 \mathrm{m}^3$ (Kuo et al. 2011). For the geomorphological features and a more detailed description of the terrain, also see Lo et al. (2011).

In the following, we seek to retrace the disastrous event, only briefly providing a comparison of the results with respect to the additionally incorporated fields. Here, the applicability to such large-scale events presents a further aspect of the practical use of

the new model. It is especially interesting to investigate the final extents of the height, since here, a comparison to gathered DEM (or DTM) data and aerial photograph is possible, see Fig. 5.8, panels **c)-d)**. Besides, a discussion of the volume fraction distribution may provide insights that go beyond the findings from the DEM data. Nonetheless, it is not our aim here to present an extensive reassessment of the events, since this would demand a separate work of its own. A broader investigation together with discussion of parameters and results has been conducted in Tai et al. (2018).

The physical parameters are set to $\left(\delta_b, \alpha_b^f, c_D^s, \mathrm{N}_R, \alpha_\rho\right) = (16^\circ, 8, 6, 268, 1.06/2.65)$. These chosen basic parameters are discussed in more detail in Tai et al. (2018). It should be noted that they are not the result of a process of optimized fitting but resemble reasonable values and are rather picked to show the applicability of the model to a large scale event. As for the numerical setting, the grid is given with $(n_X, n_Y) = (371, 222)$ on a domain of $X \in [\,0, 3700\,\mathrm{m}\,], Y \in [\,0, 2210\,\mathrm{m}\,]$, and $CFL = 0.1$. The non-dimensional numbers for the extra pore-fluid pressure and the hypoplastic stress are set to $\mathrm{Eu}_b = 0.075, \mathrm{N}_Z = 0.035$. With respect to the scale of the event, a larger particle diameter value is chosen, $\delta_P = 0.01$, together with a slightly changed critical volume fraction $v_C^s = 0.65$. Furthermore, for the hypoplastic equations, the initial condition is changed to $Z_{ii}^s|^0 = 0.0$, accounting for a fully liquefied state in which the intergranular contact forces are ignored. Besides, the values are left as before.

5.4.2 Numerical studies

The height development is shown in panels **a)-d)** of Fig. 5.7, together with the distribution of the solid volume fraction at two different times in panels **e)-f)**. With this, it can be retraced how the flow advances, splits in different branches, and settles in the valley of the river, forming three deposits.

To allow for an evaluation of the results, Fig. 5.8 depicts a comparison of the deposition at the last time step, $t = 181.83\,\mathrm{s}$, both for a configuration with the additional fields ($\mathrm{Eu}_b = 0.075, \mathrm{N}_Z = 0.035$, panel **a)**) in Fig. 5.8 and without ($\mathrm{Eu}_b = 0.0, \mathrm{N}_Z = 0.0$, in panel **b)**). Furthermore, the results are confronted with an aerial photograph (panel **c)**), and some features are added in the figure with the final deposition height (panel **a)**): the village Hsiaolin is marked by a thick red line, together with the briefly formated dam and the flow direction of the river. The formation of the temporary dam can be retraced, while the subsequent failure and the flooding of the remaining parts is not part of the simulation, since here, the river acting upon the dam is not considered. For more details on the extents of this dam, see Dong et al. (2011) and Wu et al. (2014). While the overall results for the height distribution are not differing massively for both studies (with and without additional fields), it is still apparent that due to the influence of the dynamic pore pressure, more material is driven into the deposition area. With this, the results of the DEM study are met, see panel **d)** in Fig. 5.8, without artificially reducing parameters of solid or fluid friction. Please note that in our simulations, no erosion is depicted, so only the green and blue colors in panel **d)** that resemble deposition are also visible in our results. Even more, it can be reasoned that with the

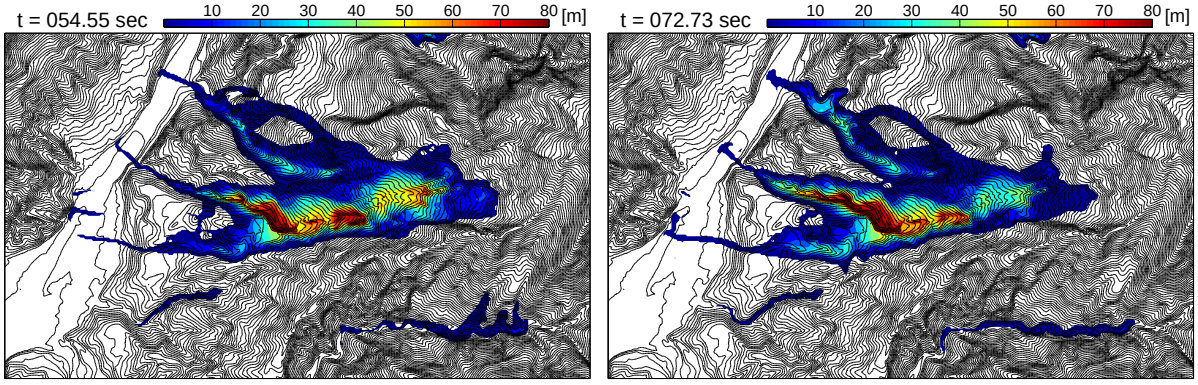

a) Height distribution at early stage **b)** Progressed height distribution

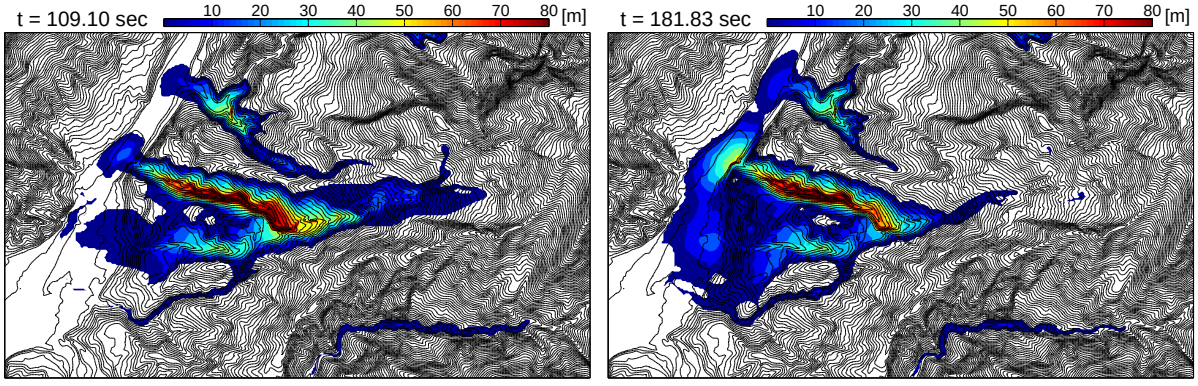

c) Height distribution advanced stage **d)** Final height distribution

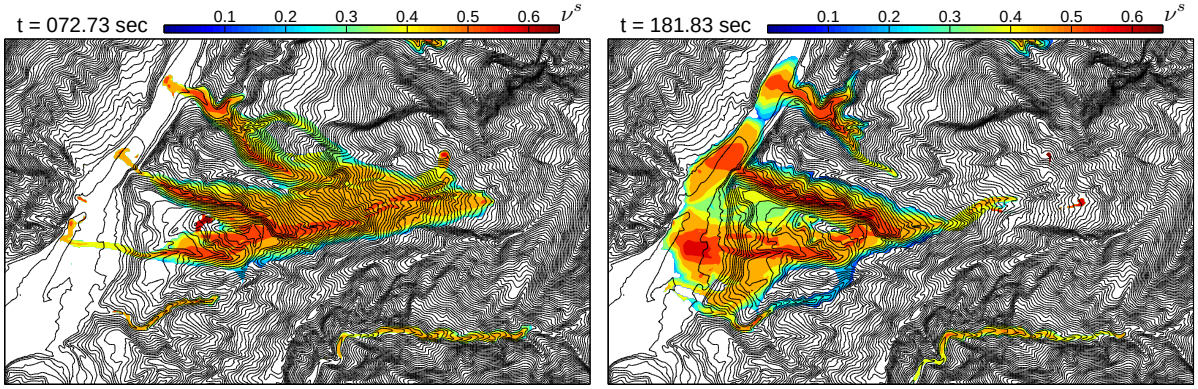

e) Solid Volume Fraction at early stage **f)** Final solid volume fraction distribution

Figure 5.7: Numerical simulation of the Hsiaolin landslide: Height development and deposition depth at 4 different times (panels **a)-d)**), as well as volume fraction development for two time steps (panels **e)-f)**). The basal friction angle is set to $\delta_b = 16^\circ$, the fluid friction coefficient $\alpha_b^f = 5$, the drag coefficient $c_D^s = 6$ and the viscous number $N_R = 268$.

incorporation of an intergranular stress, the apparent formation of the (temporary) dam can be expected in a favorable way, since a solid body formates more distinctly,

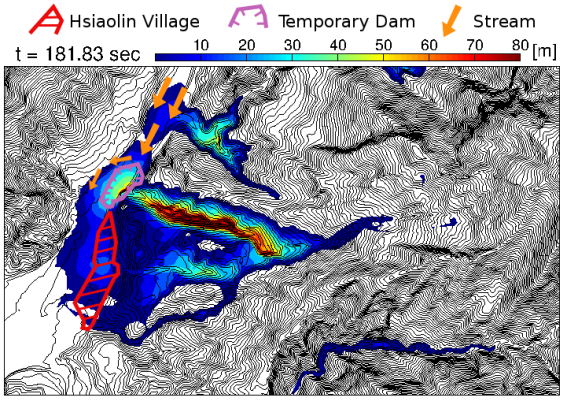

a) Height distribution, $t = 181.83\,\mathrm{s}$, for $\mathrm{Eu}_b = 0.075, \mathrm{N}_Z = 0.035$ with temporary dam and redirected stream

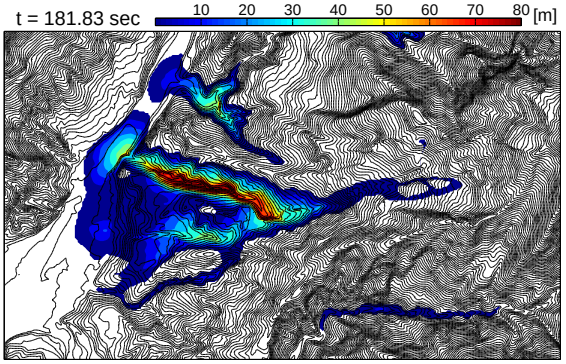

b) Final height distribution at $t = 181.83\,\mathrm{s}$, for the flow configuration without additional fields, i.e. $\mathrm{Eu}_b = 0.0, \mathrm{N}_Z = 0.0$

c) Aerial photograph taken after the event, see Wu et al. (2014) and Tai et al. (2018), showing the overall extents of the event

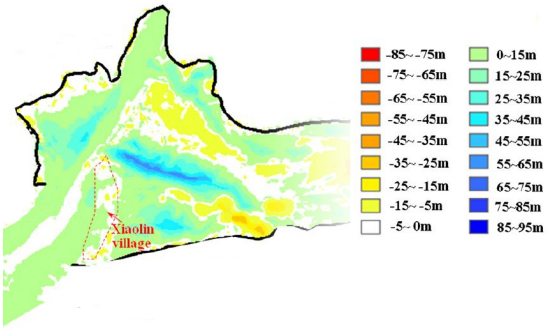

d) DEM study of the event (5 m resolution), displaying the erosion and deposition, taken from Lo et al. (2011) and edited to simplify visual comparison.

Figure 5.8: Comparison of the results for the Hsiaolin landslide: In panel **a)**, the final deposition height and the extents of the Hsiaolin village are displayed, the flow direction of the river and the briefly formated dam have been included, together with the results without the impact of additional fields in panel **b)**. An aerial photograph in panel **c)** shows the extents of the event, followed by the results of a DEM study in panel **d)**.

visible in the increased share of the solid volume fraction at deposition areas at the flow front, see Fig. 5.9.

In this section, the applicability to large scale events, with GIS/DEM data or alike, has been demonstrated, making it possible not only to investigate on a laboratory scale but to look into events on real terrain. It is apparent that the results match qualitatively the investigations that have been conducted after the events (Lo et al. 2011). It also should be noted that with a large scale study like this, small parameter alterations may have a greater effect. Due to the incorporation of the extra pore fluid pressure,

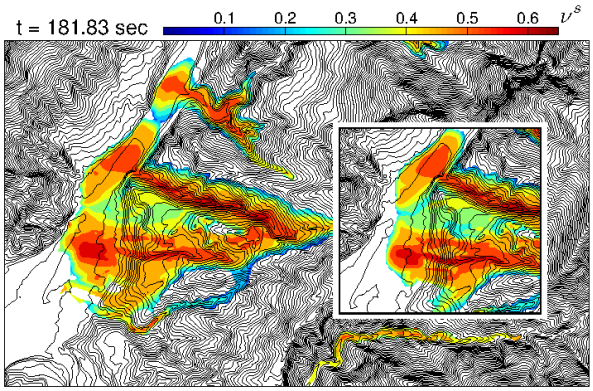

Figure 5.9: Comparison of the solid volume fraction distribution for $t = 181.83\,\mathrm{s}$, highlighting the influence of both the dynamic pore-fluid pressure and the intergranular stress. A flow configuration with the additional effects is compared to the distribution without the influence of extra pore-fluid pressure and without hypoplasticity (small cutout), showing that more solid material is transported further.

a realistic bed friction angle $\delta_b = 16^\circ$ can be applied, so instead of mimicking effects with parameter adjustment (as it is sometimes suggested in the literature), the actual physical mechanisms provide for accurate results. Even more, the hypoplastic stress supports the building of a temporary dam. As for the differences to a study without these additional effects, we refer to Tai et al. (2018), where the respective results have been presented in greater detail.

6 Conclusion and outlook

The present work describes the thermodynamically consistent development of a depth-integrated model for granular-fluid flows on a general topography and numerical simulations for debris flows in different applications. Hereby, it is the aim of the work to investigate on the physical mechanisms, underlying the dynamics of debris flows, by including and combining two additional fields, an extra pore-fluid pressure and hypoplastic, intergranular friction. Different fields of modeling are combined in the process of development, starting from general laws of thermodynamics and ending with the application to real debris flow events. The extra pore-fluid pressure arises from the interaction of the granular skeleton and the pore-fluid and, interfering with the hydrostatic pressure, is able to push the granular particles apart, reduces their apparent friction and thus prolongates the movement of the bulk mass. In contrast, the intergranular stress itself accounts for the non-linear, anelastic behavior of granular material.

Within the framework of mixture theory and the entropy principle in its formulation by Müller and Liu, a continuum model for a general granular-fluid mixture has been derived. Besides the basic fields of mass, momentum and energy, as well as a simple balance equation for the volume fraction, it considers two additional fields in the thermodynamically consistent derivation, one accounting for an intergranular stress, and, as a novelty in this context, a partial pressure, described by a diffusion equation. Exploiting the entropy principle, i.e. in particular the given Liu identities, the integrability conditions and the relations of the thermodynamic equilibrium, a set of restrictions on the constitutive function for such a modeling class was derived and closed with further considerations regarding the pressure configuration. It should be noted that, while the considered material class is not discussed in more detail in this work, with the proposed implementations of the entropy principle in the framework of a symbolic `Maple` scheme, both in its formulation after ML and with a new, solution set-based algorithm, further investigation on the constitutive class would be possible. Taking up this continuum model in a new context, a set of non-dimensionalized, depth-integrated equations is deduced, following an approach for shallow, granular flows. The assumption of a thin-layered and saturated two-phase mixture of granulate and a fluid yields a two-dimensional model. Further closure is achieved with the assumption of a stress free surface, not interacting with the surrounding air, and both Coulomb friction for the solid and a Navier friction relation for the fluid. In order to increase the applicability of the model within the scope of numerical simulations and to overcome some disadvantages of depth-integration, the derived model was further subjected to a coordinate transformation. The concluding equations can be found with reference to so-called general coordinates and allow for the representation of debris flows on real mountainous topography.

The model has been implemented in a shock-capturing non-oscillatory central (NOC)-scheme in order to perform a range of numerical simulations, from parameter studies on a laboratory scale to a large-scale event. The parameter studies emphasize the influence of the introduced fields: While the extra pore-fluid pressure accelerates the whole mixture and prevents the mass from settling, the intergranular friction helps the granular structure to maintain its form, hindering the mass from dissolving like a fluid. Both fields thus meet the expectations arising from physical observations and considerations. They are, for the first time, employed in this combination for a depth-integrated model in the framework of general coordinates.

The modeling work done here establishes a connection between the investigations on granular materials done with the rigorous exploitation of the ML entropy principle, which are often not applied further to numerical studies that go beyond, e.g., simple shear flows, and the more practically orientated class of shallow-flow models. Even more, these additional fields can be seen as the incorporation of information on the particle surfaces and the granular skeleton in its interdependency with the fluid, not depicted in the framework of mixture theory – quite analogously to the modeling of the Reynolds stress tensor, which seeks to reintegrate information on the small-scale turbulent structure into the flow model, lost during the averaging process. It is a central aim of this work to provide a consistent debris flow model, developed with regard of these additional fields and applicable for numerical studies. But rather than already providing a perfectly tuned instrument, this model and its numerical implementation can be regarded as a development environment, indeed as a kind of tool for further research, dealing for example with the refinement of the respective material parameters.

Although the model created in this way provides the framework for the physically consistent description of debris flows, some necessary and possible improvements should be mentioned at this point, together with ideas for further development. They comprise both ideas resulting from observable physical mechanisms as well as extensions rather coming from modeling.

- The inclusion of the hypoplastic stress in the evaluation of the temporal development of the extra stress, $\mathrm{d}_t\sigma_e$, i.e. in the source term of the extra pressure, would offer a connection between hypoplastic material behavior and the modeling of the pore-pressure.
- In return, for the stiffness factor or density factor, the extra pressure could be regarded.
- With regard to the different flow regimes, see Savage (1984), one could introduce the non-dimensional numbers together with parameter functions that assure that for instance, hypoplastic behavior is only relevant for phases of slow motion.

Besides, the model could be extended in a lot of meaningful ways, for instance with regard to processes of erosion, that themselves could be coupled to the pore-fluid pressure, and furthermore, as suggested in Meng (2017), rate-dependency could be employed for the bed friction term. Another interesting field are effects of segregation,

for which multiple granular phases of different size must be considered; for cases like this, the general modeling with the entropy principle offers numerous ways for a incorporation of such effects with regard to the now neglected terms of phase interaction.

7 Bibliography

AHMADI, G. (1982): A generalized continuum theory for granular materials. *International Journal of Non-Linear Mechanics 17*, 1, 21–33.

ANDERSON, T. B., JACKSON, R. (1967): Fluid mechanical description of fluidized beds. Equations of motion. *Industrial & Engineering Chemistry Fundamentals 6*, 4, 527–539.

ARNOLD, M., HERLE, I. (2006): Hypoplastic description of the frictional behaviour of contacts. In: *Numerical Methods in Geotechnical Engineering*, 101–106.

BAGNOLD, R. A. (1954): Experiments on a gravity-free dispersion of large solid spheres in a Newtonian fluid under shear. In: *Proceedings of the Royal Society of London A: Mathematical, Physical and Engineering Sciences*, The Royal Society, vol. 225, 49–63.

BALMFORTH, N., KERSWELL, R. (2005): Granular collapse in two dimensions. *Journal of Fluid Mechanics 538*, 399–428.

BAUER, E. (1996): Calibration of a comprehensive hypoplastic model for granular materials. *Solids and Foundations 36*, 1, 13–26.

BAUER, G. (1997): *Thermodynamische Betrachtung einer gesättigten Mischung*. Ph.D. thesis, Technische Universität Darmstadt.

BLUHM, J., DE BOER, R., WILMAŃSKI, K. (1995): The thermodynamic structure of the two-component model of porous incompressible materials with true mass densities. *Mechanics Research Communications 22*, 2, 171–180.

DE BOER, R. (2005): *The engineer and the scandal*. Springer.

DE BOER, R., EHLERS, W. (1990): The development of the concept of effective stresses. *Acta Mechanica 83*, 1, 77–92.

BOUCHUT, F., FERNÁNDEZ-NIETO, E. D., MANGENEY, A., NARBONA-REINA, G. (2016): A two-phase two-layer model for fluidized granular flows with dilatancy effects. *Journal of Fluid Mechanics 801*, 166–221.

BOUCHUT, F., WESTDICKENBERG, M. (2004): Gravity driven shallow water models for arbitrary topography. *Communications in Mathematical Sciences 2*, 3, 359–389.

CHEVIAKOV, A. F. (2007): GeM software package for computation of symmetries and conservation laws of differential equations. *Computer Physics Communications 176*, 1, 48–61.

CHEVIAKOV, A. F. (2010a): Computation of fluxes of conservation laws. *Journal of Engineering Mathematics 66*, 1-3, 153–173.

CHEVIAKOV, A. F. (2010b): Symbolic computation of local symmetries of nonlinear and linear partial and ordinary differential equations. *Mathematics in Computer Science 4*, 2-3, 203–222.

CHEVIAKOV, A. F., HESS, J. (2018): A symbolic computation framework for constitutive modelling based on entropy principles. *Applied Mathematics and Computation 324*, 105–118.

CHIOU, M.-C., WANG, Y., HUTTER, K. (2005): Influence of obstacles on rapid granular flows. *Acta Mechanica 175*, 1, 105–122.

CLAUSIUS, R. (1865): Über verschiedene für die Anwendung bequeme Formen der Hauptgleichungen der mechanischen Wärmetheorie. *Annalen der Physik 201*, 7, 353–400.

COLEMAN, B. D., GURTIN, M. E. (1967): Thermodynamics with internal state variables. *The Journal of Chemical Physics 47*, 2, 597–613.

COLEMAN, B. D., NOLL, W. (1963): The thermodynamics of elastic materials with heat conduction and viscosity. *Archive for Rational Mechanics and Analysis 13*, 1, 167–178.

DONG, J.-J., LI, Y.-S., KUO, C.-Y., SUNG, R.-T., LI, M.-H., LEE, C.-T., CHEN, C.-C., LEE, W.-R. (2011): The formation and breach of a short-lived landslide dam at Hsiaolin village, Taiwan – part I: Post-event reconstruction of dam geometry. *Engineering Geology 123*, 1-2, 40–59.

ECKART, C. (1940a): The thermodynamics of irreversible processes. I. The simple fluid. *Physical Review 58*, 3, 267.

ECKART, C. (1940b): The thermodynamics of irreversible processes. II. Fluid mixtures. *Physical Review 58*, 3, 269.

ECKART, C. (1940c): The thermodynamics of irreversible processes. III. Relativistic theory of the simple fluid. *Physical Review 58*, 10, 919.

ECKART, C. (1948): The thermodynamics of irreversible processes. IV. The theory of elasticity and anelasticity. *Physical Review 73*, 4, 373.

FANG, C. (2004): On the Correspondence Between Stored Energy Function and Helmholtz Free Energy Function of Granular Materials. *International Journal of Applied Science and Engineering 2*, 2, 117–126.

FANG, C. (2008): Modeling dry granular mass flows as elasto-visco-hypoplastic continua with microstructural effects. I. Thermodynamically consistent constitutive model. *Acta Mechanica 197*, 3, 173–189.

FANG, C. (2016a): A k-ϵ turbulence closure model of an isothermal dry granular dense matter. *Continuum Mechanics and Thermodynamics 28*, 4, 1049–1069.

FANG, C. (2016b): Rapid dry granular flows down an incline: A constitutive theory with an independent kinematic internal length. *Meccanica 51*, 6, 1387–1403.

FANG, C., WANG, Y., HUTTER, K. (2006): Shearing flows of a dry granular material-hypoplastic constitutive theory and numerical simulations. *International Journal for Numerical and Analytical Methods in Geomechanics 30*, 14, 1409–1437.

FILLUNGER, P. (1936): *Erdbaumechanik?* self-published by the author.

GEORGE, D. L., IVERSON, R. M. (2011): A two-phase debris-flow model that includes coupled evolution of volume fractions, granular dilatancy, and pore-fluid pressure. *Italian Journal of Engineering Geology and Environment 10*, 2011–03.

GEORGE, D. L., IVERSON, R. M. (2014): A depth-averaged debris-flow model that includes the effects of evolving dilatancy. II. Numerical predictions and experimental tests. In: *Proceedings of the Royal Society of London A: Mathematical, Physical and Engineering Sciences*, The Royal Society, vol. 470, 20130820.

GOODMAN, M., COWIN, S. (1972): A continuum theory for granular materials. *Archive for Rational Mechanics and Analysis 44*, 4, 249–266.

GOREN, L., AHARONOV, E., SPARKS, D., TOUSSAINT, R. (2010): Pore pressure evolution in deforming granular material: A general formulation and the infinitely stiff approximation. *Journal of Geophysical Research: Solid Earth 115*, B9.

GRAY, J., CHUGUNOV, V. (2006): Particle-size segregation and diffusive remixing in shallow granular avalanches. *Journal of Fluid Mechanics 569*, 365–398.

GRAY, J., EDWARDS, A. (2014): A depth-averaged μ(I)-rheology for shallow granular free-surface flows. *Journal of Fluid Mechanics 755*, 503.

GRAY, J., THORNTON, A. (2005): A theory for particle size segregation in shallow granular free-surface flows. In: *Proceedings of the Royal Society of London A: Mathematical, Physical and Engineering Sciences*, The Royal Society, vol. 461, 1447–1473.

GRAY, J., WIELAND, M., HUTTER, K. (1999): Gravity-driven free surface flow of granular avalanches over complex basal topography. In: *Proceedings of the Royal Society of London A: Mathematical, Physical and Engineering Sciences*, The Royal Society, vol. 455, 1841–1874.

GRAY, J. M. N. T., TAI, Y.-C. (1998): Particle size segregation, granular shocks and stratification patterns. In: *Physics of Dry Granular Media*, H. J. Herrmann, J.-P. Hovi, S. Luding, eds., Springer Netherlands, 697–702.

GREEN, A. E., NAGHDI, P. M. (1965): A general theory of an elastic-plastic continuum. *Archive for rational mechanics and analysis 18*, 4, 251–281.

GUDEHUS, G. (1996): A comprehensive constitutive equation for granular materials. *Soils and Foundations 36*, 1, 1–12.

GUO, X., PENG, C., WU, W., WANG, Y. (2016): A hypoplastic constitutive model for debris materials. *Acta Geotechnica 11*, 6, 1217–1229.

GURTIN, M. E., WILLIAMS, W. O. (1966): On the Clausius-Duhem inequality. *Zeitschrift für Angewandte Mathematik und Physik 17*, 5, 626–633.

HAUSER, R., KIRCHNER, N. (2002): A historical note on the entropy principle of Müller and Liu. *Continuum Mechanics and Thermodynamics 14*, 2, 223–226.

HERLE, I., GUDEHUS, G. (1999): Determination of parameters of a hypoplastic constitutive model from properties of grain assemblies. *Mechanics of Cohesive-frictional Materials: An International Journal on Experiments, Modelling and Computation of Materials and Structures 4*, 5, 461–486.

HESS, J. (2014): *Konstitutive Modellierung von Granulat-Fluid-Mischungen durch Auswertung des Entropieprinzips*. Master's thesis, Technische Universität Darmstadt.

HESS, J., CHEVIAKOV, A. F. (2019): A solution set-based entropy principle for constitutive modeling in mechanics. *Continuum Mechanics and Thermodynamics 31*, 3, 775–806.

HESS, J., WANG, Y. (2019): On the role of pore-fluid pressure evolution and hypoplasticity in debris flows. *European Journal of Mechanics-B/Fluids 74*, 363–379.

HESS, J., WANG, Y., HUTTER, K. (2017): Thermodynamically consistent modeling of granular-fluid mixtures incorporating pore pressure evolution and hypoplastic behavior. *Continuum Mechanics and Thermodynamics 29*, 1, 311–343.

HESS, J., WANG, Y., TAI, Y.-C. (2019): Debris Flows with Pore Pressure and Intergranular Friction on Rugged Topography. *Computers and Fluids 190*, 139–155.

HUANG, W., NÜBEL, K., BAUER, E. (2002): Polar extension of a hypoplastic model for granular materials with shear localization. *Mechanics of materials 34*, 9, 563–576.

HUI, W., LI, P., LI, Z. (1999): A unified coordinate system for solving the two-dimensional Euler equations. *Journal of Computational Physics 153*, 2, 596–637.

HUI, W. H. (2004): A unified coordinates approach to computational fluid dynamics. *Journal of Computational and Applied Mathematics 163*, 1, 15–28.

HUTTER, K. (1977): The foundations of thermodynamics, its basic postulates and implications. A review of modern thermodynamics. *Acta Mechanica 27*, 1-4, 1–54.

HUTTER, K., JÖHNK, K. (2004): *Continuum Methods of Physical Modeling*. Springer.

HUTTER, K., JÖHNK, K., SVENDSEN, B. (1994): On interfacial transition conditions in two phase gravity flow. *Zeitschrift für angewandte Mathematik und Physik 45*, 5, 746–762.

HUTTER, K., KOCH, T., PLÜSS, C., SAVAGE, S. (1995): The dynamics of avalanches of granular materials from initiation to runout. Part II. Experiments. *Acta Mechanica 109*, 1-4, 127–165.

HUTTER, K., LUCA, I. (2012): Two-layer debris mixture flows on arbitrary terrain with mass exchange at the base and the interface. *Continuum Mechanics and Thermodynamics 24*, 4-6, 525–558.

HUTTER, K., SCHNEIDER, L. (2010a): Important aspects in the formulation of solid-fluid debris-flow models. Part I. Thermodynamic implications. *Continuum Mechanics and Thermodynamics 22*, 5, 363–390.

HUTTER, K., SCHNEIDER, L. (2010b): Important aspects in the formulation of solid-fluid debris-flow models. Part II. Constitutive modelling. *Continuum Mechanics and Thermodynamics 22*, 5, 391–411.

HUTTER, K., WANG, Y. (2003): Phenomenological thermodynamics and entropy principles. In: *Entropy*, A. Greven, G. Keller, G. Warnecke, eds., Princeton University Press, 57–77.

HUTTER, K., WANG, Y. (2016): *Fluid and Thermodynamics. Volume 2: Advanced Fluid Mechanics and Thermodynamic Fundamentals*. Springer.

IONESCU, I. R., MANGENEY, A., BOUCHUT, F., ROCHE, O. (2015): Viscoplastic modeling of granular column collapse with pressure-dependent rheology. *Journal of Non-Newtonian Fluid Mechanics 219*, 1–18.

IVERSON, R. M. (1997): The physics of debris flow. *Reviews of Geophysics 35*, 3, 245–296.

IVERSON, R. M., DENLINGER, R. P. (2001): Flow of variably fluidized granular masses across three-dimensional terrain 1. Coulomb mixture theory. *Journal of Geophysical Research 106*, 537–552.

IVERSON, R. M., GEORGE, D. L. (2014): A depth-averaged debris-flow model that includes the effects of evolving dilatancy. I. Physical basis. In: *Proceedings of the Royal Society A: Mathematical, Physical and Engineering Sciences*, The Royal Society, vol. 470.

JACKSON, R. (2000): *The dynamics of fluidized particles*. Cambridge University Press.

JOP, P., FORTERRE, Y., POULIQUEN, O. (2005): Crucial role of sidewalls in granular surface flows: Consequences for the rheology. *Journal of Fluid Mechanics 541*, 167–192.

JOP, P., FORTERRE, Y., POULIQUEN, O. (2006): A constitutive law for dense granular flows. *Nature 441*, 7094, 727.

KIRCHNER, N. P. (2002): Thermodynamically consistent modelling of abrasive granular materials. I. Non–equilibrium theory. In: *Proceedings of the Royal Society of London A: Mathematical, Physical and Engineering Sciences*, The Royal Society, vol. 458, 2153–2176.

KIRCHNER, N. P., TEUFEL, A. (2002): Thermodynamically consistent modelling of abrasive granular materials. II. Thermodynamic equilibrium and applications to steady shear flows. In: *Proceedings of the Royal Society of London A: Mathematical, Physical and Engineering Sciences*, The Royal Society, vol. 458, 3053–3077.

KOLYMBAS, D. (1977): A rate-dependent constitutive equation for soils. *Mechanics Research Communications 4*, 6, 367 – 372.

KOLYMBAS, D. (1985): A generalized hypoelastic constitutive law. In: *Proc. XI Int. Conf. Soil Mechanics and Foundation Engineering, San Francisco*, vol. 5.

KOLYMBAS, D. (1991): An outline of hypoplasticity. *Archive of Applied Mechanics 61*, 3, 143–151.

KOLYMBAS, D., HERLE, I. (2003): Shear and objective stress rates in hypoplasticity. *International Journal for Numerical and Analytical Methods in Geomechanics 27*, 9, 733–744.

KOWALSKI, J., MCELWAINE, J. N. (2013): Shallow two-component gravity-driven flows with vertical variation. *Journal of Fluid Mechanics 714*, 434–462.

KUO, C., TAI, Y.-C., CHEN, C., CHANG, K., SIAU, A., DONG, J., HAN, R., SHIMAMOTO, T., LEE, C. (2011): The landslide stage of the Hsiaolin catastrophe: Simulation and validation. *Journal of Geophysical Research: Earth Surface 116*, F4.

KURGANOV, A., MILLER, J. (2014): Central-upwind scheme for Savage–Hutter type model of submarine landslides and generated tsunami waves. *Computational Methods in Applied Mathematics 14*, 2, 177–201.

KURGANOV, A., TADMOR, E. (2000): New high-resolution central schemes for nonlinear conservation laws and convection–diffusion equations. *Journal of Computational Physics 160*, 1, 241–282.

LIU, I.-S. (1972a): Method of Lagrange multipliers for exploitation of the entropy principle. *Archive for Rational Mechanics and Analysis 46*, 2, 131–148.

LIU, I.-S. (1972b): *On Irreversible Thermodynamics*. Ph.D. thesis, Johns Hopkins University, Baltimore.

LIU, I.-S. (1980): On chemical potencial and imcompressible porous media. *Journal de Mécanique 19*, 2, 327–342.

LIU, I.-S. (2002): *Continuum Mechanics*. Springer.

LIU, I.-S. (2010): On Pore Fluid Pressure and Effective Solid Stress in the Mixture Theory of Porous Media. In: *Continuous Media with Microstructure*, B. Albers, ed., Springer, 19–28.

LIU, I.-S. (2014): A solid-fluid mixture theory of porous media. *International Journal of Engineering Science 84*, 133–146.

LO, C.-M., LIN, M.-L., TANG, C.-L., HU, J.-C. (2011): A kinematic model of the Hsiaolin landslide calibrated to the morphology of the landslide deposit. *Engineering Geology 123*, 1-2, 22–39.

LUCA, I., KUO, C.-Y., HUTTER, K., TAI, Y.-C. (2012): Modeling shallow over-saturated mixtures on arbitrary rigid topography. *Journal of Mechanics 28*, 3, 523–541.

LUCA, I., TAI, Y.-C., KUO, C.-Y. (2016): *Shallow geophysical mass flows down arbitrary topography*. Springer.

MAŠÍN, D. (2005): A hypoplastic constitutive model for clays. *International Journal for Numerical and Analytical Methods in Geomechanics 29*, 4, 311–336.

MEIXNER, J. (1943): Zur Thermodynamik der irreversiblen Prozesse in Gasen mit chemisch reagierenden, dissoziierenden und anregbaren Komponenten. *Annalen der Physik 435*, 4, 244–270.

MENG, X. (2017): *Dynamical modelling and numerical simulation of grain-fluid mixture flows*. Ph.D. thesis, Technische Universität Darmstadt.

MENG, X., WANG, Y. (2016): Modelling and numerical simulation of two-phase debris flows. *Acta Geotechnica 11*, 5, 1027–1045.

MENG, X., WANG, Y., WANG, C., FISCHER, J.-T. (2017): Modeling of unsaturated granular flows by a two-layer approach. *Acta Geotechnica 12*, 3, 677–701.

MÜLLER, I. (1967): On the entropy inequality. *Archive for Rational Mechanics and Analysis 26*, 2, 118–141.

MÜLLER, I. (1968): A thermodynamic theory of mixtures of fluids. *Archive for Rational Mechanics and Analysis 28*, 1, 1–39.

MÜLLER, I. (1970): A new systematic approach to non-equilibrium thermodynamics. *Pure and Applied Chemistry 22*, 3-4, 335–342.

MÜLLER, I. (1971a): The coldness, a universal function in thermoelastic bodies. *Archive for Rational Mechanics and Analysis 41*, 5, 319–332.

MÜLLER, I. (1971b): Die Kältefunktion, eine universelle Funktion in der Thermodynamik viskoser wärmeleitender Flüssigkeiten. *Archive for Rational Mechanics and Analysis 40*, 1, 1–36.

MÜLLER, I. (2007): *A history of thermodynamics: The doctrine of energy and entropy*. Springer Science & Business Media.

MÜLLER, I., LIU, I.-S. (1984): Thermodynamics of mixtures of fluids. In: *Rational Thermodynamics*, C. Truesdell, ed., Springer.

MÜLLER, I., RUGGERI, T. (1998): *Rational Extended Thermodynamics*. Springer.

NESSYAHU, H., TADMOR, E. (1990): Non-oscillatory central differencing for hyperbolic conservation laws. *Journal of Computational Physics 87*, 2, 408–463.

NIEMUNIS, A. (1993): Hypoplasticity vs. Elastoplasticity, selected topics. In: *Modern Approaches to Plasticity*, D. Kolymbas, ed., 277–307.

NOLL, W. (1958): A mathematical theory of the mechanical behavior of continuous media. *Archive for Rational Mechanics and Analysis 2*, 1, 197–226.

NUNZIATO, J. W., WALSH, E. K. (1980): On ideal multiphase mixtures with chemical reactions and diffusion. *Archive for Rational Mechanics and Analysis 73*, 4, 285–311.

O'BRIEN, J. S., JULIEN, P. Y. (1988): Laboratory analysis of mudflow properties. *Journal of Hydraulic Engineering 114*, 8, 877–887.

PAILHA, M., POULIQUEN, O. (2009): A two-phase flow description of the initiation of underwater granular avalanches. *Journal of Fluid Mechanics 633*, 115–135.

PAPENFUSS, C., FOREST, S. (2006): Thermodynamical Frameworks for Higher Grade Material Theories with Internal Variables or Additional Degrees of Freedom. *Journal of Non-Equilibrium Thermodynamics 31*, 4, 319–353.

PASSMAN, S. (1977): Mixtures of granular materials. *International Journal of Engineering Science 15*, 2, 117–129.

PASSMAN, S. L., NUNZIATO, J. W., BAILEY, P. B., REED, K. W. (1986): Shearing motion of a fluid saturated granular material. *Journal of Rheology 30*, 1, 167–192.

PASSMAN, S. L., NUNZIATO, J. W., WALSH, E. K. (1984): A theory of multiphase mixtures. In: *Rational Thermodynamics*, C. Truesdell, ed., Springer.

PENG, C., GUO, X., WU, W., WANG, Y. (2016): Unified modelling of granular media with Smoothed Particle Hydrodynamics. *Acta Geotechnica 11*, 6, 1231–1247.

PITMAN, E. B., LE, L. (2005): A two-fluid model for avalanche and debris flows. *Philosophical Transactions of the Royal Society A: Mathematical, Physical and Engineering Sciences 363*, 1832, 1573–1601.

PUDASAINI, S. P. (2012): A general two-phase debris flow model. *Journal of Geophysical Research 117*.

PUDASAINI, S. P., HUTTER, K. (2003): Rapid shear flows of dry granular masses down curved and twisted channels. *Journal of Fluid Mechanics 495*, 193–208.

RABINBACH, A. (1992): *The human motor: Energy, fatigue, and the origins of modernity*. University of California Press.

REIS, M. C., WANG, Y. (2016): A two-fluid model for reactive dilute solid–liquid mixtures with phase changes. *Continuum Mechanics and Thermodynamics* , 1–26.

RICHARDSON, J., ZAKI, W. (1954): The sedimentation of a suspension of uniform spheres under conditions of viscous flow. *Chemical Engineering Science 3*, 2, 65–73.

SAVAGE, S., IVERSON, R. M. (2003): Surge dynamics coupled to pore-pressure evolution in debris flows. Millpress, vol. 1, 503–514.

SAVAGE, S. B. (1979): Gravity flow of cohesionless granular materials in chutes and channels. *Journal of Fluid Mechanics 92*, 1, 53–96.

SAVAGE, S. B. (1984): The Mechanics of Rapid Granular Flows. *Advances in Applied Mechanics 24*, 289–366.

SAVAGE, S. B., HUTTER, K. (1989): The motion of a finite mass of granular material down a rough incline. *Journal of Fluid Mechanics 199*, 177–215.

SAVAGE, S. B., HUTTER, K. (1991): The dynamics of avalanches of granular materials from initiation to runout. Part I: Analysis. *Acta Mechanica 86*, 201–223.

SCHNEIDER, L., HUTTER, K. (2009): *Solid-Fluid Mixtures of Frictional Materials in Geophysical and Geotechnical Context*. Advances in Geophysical and Environmental Mechanics and Mathematics, Springer.

SHU, C.-W., OSHER, S. (1988): Efficient implementation of essentially non-oscillatory shock-capturing schemes. *Journal of Computational Physics 77*, 2, 439–471.

SVENDSEN, B. (1999): On the thermodynamics of thermoelastic materials with additional scalar degrees of freedom. *Continuum Mechanics and Thermodynamics 11*, 4, 247–262.

SVENDSEN, B., HUTTER, K. (1995): On the thermodynamics of a mixture of isotropic materials with constraints. *International Journal of Engineering Science 33*, 14, 2021–2054.

SVENDSEN, B., HUTTER, K., LALOUI, L. (1999): Constitutive models for granular materials including quasi-static frictional behaviour: Toward a thermodynamic theory of plasticity. *Continuum Mechanics and Thermodynamics 11*, 4, 263–275.

TAI, Y.-C., GRAY, J., HUTTER, K., NOELLE, S. (2001): Flow of dense avalanches past obstructions. *Annals of Glaciology 32*, 281–284.

TAI, Y.-C., HESS, J., WANG, Y. (2018): Modeling Two-Phase Debris Flows with grain-fluid separation over Rugged Topography: Application to the 2009 Hsiaolin event, Taiwan. *Journal of Geophysical Research: Earth Surface 124*, 2, 305–333.

TAI, Y.-C., KUO, C.-Y. (2008): A new model of granular flows over general topography with erosion and deposition. *Acta Mechanica 199*, 1-4, 71–96.

TAI, Y.-C., KUO, C.-Y. (2012): Modelling shallow debris flows of the Coulomb-mixture type over temporally varying topography. *Natural Hazards and Earth System Sciences 12*, 2, 269–280.

TAI, Y.-C., KUO, C.-Y., HUI, W.-H. (2012): An alternative depth-integrated formulation for granular avalanches over temporally varying topography with small curvature. *Geophysical & Astrophysical Fluid Dynamics 106*, 6, 596–629.

TAI, Y.-C., LIN, Y.-C. (2008): A focused view of the behavior of granular flows down a confined inclined chute into the horizontal run-out zone. *Physics of Fluids 20*, 12, 123302.

TERZAGHI, K. V. (1923): Die Berechnung der Durchlassigkeitsziffer des Tones aus dem Verlauf der hydrodynamischen Spannungserscheinungen. *Sitzungsberichte der Akademie der Wissenschaften in Wien, Mathematisch-Naturwissenschaftliche Klasse, Abteilung IIa 123*, 125–138.

TERZAGHI, K. V. (1936): The shearing resistance of saturated soils and the angle between the planes of shear. In: *Proceedings of the 1st International Conference on Soil Mechanics and Foundation Engineering*, vol. 1, 54–56.

TEUFEL, A. (2001): *Simple Flow Configurations in Hypoplastic Abrasive Materials*. Master's thesis, Technische Universität Darmstadt.

TRIANI, V., PAPENFUSS, C., CIMMELLI, V. A., MUSCHIK, W. (2008): Exploitation of the second law: Coleman–Noll and Liu procedure in comparison. *Journal of Nonequilibrium Thermodynamics 33*, 1, 47–60.

TRUESDELL, C. (1957): Sulle basi della termomeccanica. *Rend. Lincei 22*, 8, 33–38.

TRUESDELL, C. (1962): Mechanical basis of diffusion. *The Journal of Chemical Physics 37*, 10, 2336–2344.

TRUESDELL, C. (1984): Thermodynamics of Diffusion. In: *Rational Thermodynamics*, C. Truesdell, ed., Springer.

VOELLMY, A. (1955): Über die Zerstörungskraft von Lawinen. *Schweizerische Bauzeitung 73*, 159–165, 212–217, 246–249, 280–285.

WANG, C., WANG, Y., PENG, C., MENG, X. (2017): Dilatancy and compaction effects on the submerged granular column collapse. *Physics of Fluids 29*, 10, 103307.

WANG, Y., HUTTER, K. (1999a): Comparison of two entropy principles and their applications in granular flows with/without fluid. *Archives of Mechanics 51*, 5, 605–632.

WANG, Y., HUTTER, K. (1999b): A constitutive model of multiphase mixtures and its application in shearing flows of saturated solid-fluid mixtures. *Granular matter 1*, 4, 163–181.

WANG, Y., HUTTER, K. (1999c): A constitutive theory of fluid-saturated granular materials and its application in gravitational flows. *Rheologica Acta 38*, 3, 214–223.

WANG, Y., HUTTER, K. (1999d): Shearing flows in a Goodman-Cowin type granular material-theory and numerical results. *Particulate Science and Technology 17*, 1-2, 97–124.

WANG, Y., HUTTER, K. (2001a): Comparisons of numerical methods with respect to convectively dominated problems. *International Journal for Numerical Methods in Fluids 37*, 6, 721–745.

WANG, Y., HUTTER, K. (2001b): Granular material theories revisited. In: *Geomorphological Fluid Mechanics*, Springer, 79–107.

WANG, Y., HUTTER, K. (2018): Phenomenological thermodynamics of irreversible processes. *Entropy 20*, 6.

WANG, Y., HUTTER, K., PUDASAINI, S. P. (2004): The Savage-Hutter theory: A system of partial differential equations for avalanche flows of snow, debris, and mud. *Zeitschrift für Angewandte Mathematik und Mechanik 84*, 8, 507–527.

WIELAND, M., GRAY, J., HUTTER, K. (1999): Channelized free-surface flow of cohesionless granular avalanches in a chute with shallow lateral curvature. *Journal of Fluid Mechanics 392*, 73–100.

WILMAŃSKI, K. (1996): Porous media at finite strains. The new model with the balance equation for porosity. *Archives of Mechanics 48*, 4, 591–628.

WILMAŃSKI, K. (2005): Continuum Theories of Mixtures – Lecture Notes. La Sapienza, Universita degli Studi di Roma.

WU, C.-H., CHEN, S.-C., FENG, Z.-Y. (2014): Formation, failure, and consequences of the Xiaolin landslide dam, triggered by extreme rainfall from Typhoon Morakot, Taiwan. *Landslides 11*, 3, 357–367.

WU, W., BAUER, E., KOLYMBAS, D. (1996): Hypoplastic constitutive model with critical state for granular materials. *Mechanics of Materials 23*, 1, 45–69.

A Steady shear flow: parameter values and boundary conditions

Quantity	Unit	Value
Solid Viscosity $\mu^{s,0}$	$g/cm \cdot s$	7230
Fluid Viscosity $\mu^{f,0}$	$g/cm \cdot s$	0.01
Solid density ρ^s	g/cm^3	2.2
Fluid density ρ^f	g/cm^3	1
Maximum volume fraction ν^s_∞	-	0.74
Critical volume fraction ν^s_C	-	0.52
Solid shear parameter $a_4^{s,0}$	$cm \cdot g/s^2$	4
Fluid shear parameter $a_4^{f,0}$	$cm \cdot g/s^2$	3
Permeability constant k_D^0	cm^2	$1.5 \cdot 10^{-8}$
Particle diameter δ_P	cm	0.04
Internal friction angle ϕ_{int}	-	30°
Inner Stress Z_{XX}	$g/cm \cdot s^2$	10
Hypoplasticity parameter δ^Z	cm^3/g	10^{-3}

Table A.1: Values applied in the simulations

Quantity	Unit	Horizontal case	Inclined case
Height $\mathcal{L}$	cm	1	0.5
Bottom volume fraction $\nu^s(0)$		0.7	0.6
Top volume fraction $\nu^s(\mathcal{L})$		0.3	-
Bottom solid velocity $v^s_X(0)$	cm/s	0	0
Top solid velocity $v^s_X(\mathcal{L})$	cm/s	1	-
Bottom fluid velocity $v^f_X(0)$	cm/s	0	0
Top fluid velocity $v^f_X(\mathcal{L})$	cm/s	1	-
Bottom extra pressure $\varpi^f_e(0)$	$g/cm \cdot s^2$	0	0
Top extra pressure $\varpi^f_e(\mathcal{L})$	$g/cm \cdot s^2$	0	-

Table A.2: Values applied in the simulations

B Derivation of the depth-integrated model

The depth-integrated solid momentum balances in downslope and cross-slope direction, following from Eqs. (4.12)-(4.13), are

$$\begin{aligned}\frac{\partial}{\partial t}\left(h\overline{\nu^s}\,\overline{v_x^s}\right)+\frac{\partial}{\partial x}\left(h\overline{\nu^s}\,\overline{v_x^s}\,\overline{v_x^s}\right)+\frac{\partial}{\partial y}\left(h\overline{\nu^s}\,\overline{v_y^s}\,\overline{v_x^s}\right)=\epsilon\frac{\partial}{\partial x}\left(h\overline{T_{xx}^s}\right)+[T_{xz}^s]_b\\ +h\overline{\nu^s}g_x+\frac{c_D^s h\overline{\nu^s}\overline{\nu^f}\rho^f}{\rho^s}\left(\overline{v_x^f}-\overline{v_x^s}\right)+\epsilon\frac{\partial\overline{\nu^s}}{\partial x}\left(\frac{\rho^f}{\rho^s}h\overline{\omega_h^s}-\frac{\overline{\nu^s}\rho^s}{\rho}h\overline{\omega_\nu^s}\right)+\mathcal{O}(\epsilon^{1+\chi}).\end{aligned}\tag{B.1}$$

$$\begin{aligned}\frac{\partial}{\partial t}\left(h\overline{\nu^s}\,\overline{v_y^s}\right)+\frac{\partial}{\partial x}\left(h\overline{\nu^s}\,\overline{v_x^s}\,\overline{v_y^s}\right)+\frac{\partial}{\partial y}\left(h\overline{\nu^s}\,\overline{v_y^s}\,\overline{v_y^s}\right)=\epsilon\frac{\partial}{\partial y}\left(h\overline{T_{yy}^s}\right)+\left[T_{yz}^s\right]_b\\ +h\overline{\nu^s}g_y+\frac{c_D^s h\overline{\nu^s}\overline{\nu^f}\rho^f}{\rho^s}\left(\overline{v_y^f}-\overline{v_y^s}\right)+\epsilon\frac{\partial\overline{\nu^s}}{\partial y}\left(\frac{\rho^f}{\rho^s}h\overline{\omega_h^s}-\frac{\overline{\nu^s}\rho^s}{\rho}h\overline{\omega_\nu^s}\right)+\mathcal{O}(\epsilon^{1+\chi}).\end{aligned}\tag{B.2}$$

For the fluid in the downslope x and the cross-slope y direction, it follows that

$$\begin{aligned}\frac{\partial}{\partial t}\left(h\overline{\nu^f}\,\overline{v_x^f}\right)+\frac{\partial}{\partial x}\left(h\overline{\nu^f}\,\overline{v_x^f}\,\overline{v_x^f}\right)+\frac{\partial}{\partial y}\left(h\overline{\nu^f}\,\overline{v_y^f}\,\overline{v_x^f}\right)=\epsilon\frac{\partial}{\partial x}\left(h\overline{T_{xx}^f}\right)+\left[T_{xz}^f\right]_b\\ +h\overline{\nu^f}g_x-c_D^s h\overline{\nu^s}\overline{\nu^f}\left(\overline{v_x^f}-\overline{v_x^s}\right)-\epsilon\frac{\partial\overline{\nu^s}}{\partial x}\left(h\overline{\omega_h^s}-\frac{\rho^s}{\rho^f}\frac{\overline{\nu^s}\rho^s}{\rho}h\overline{\omega_\nu^s}\right)+\mathcal{O}(\epsilon^{1+\chi}).\end{aligned}\tag{B.3}$$

$$\begin{aligned}\frac{\partial}{\partial t}\left(h\overline{\nu^f}\,\overline{v_y^f}\right)+\frac{\partial}{\partial x}\left(h\overline{\nu^f}\,\overline{v_x^f}\,\overline{v_y^f}\right)+\frac{\partial}{\partial y}\left(h\overline{\nu^f}\,\overline{v_y^f}\,\overline{v_y^f}\right)=\epsilon\frac{\partial}{\partial y}\left(h\overline{T_{yy}^f}\right)+\left[T_{yz}^f\right]_b\\ +h\overline{\nu^f}g_y-c_D^s h\overline{\nu^s}\overline{\nu^f}\left(\overline{v_y^f}-\overline{v_y^s}\right)-\epsilon\frac{\partial\overline{\nu^s}}{\partial y}\left(h\overline{\omega_h^s}-\frac{\rho^s}{\rho^f}\frac{\overline{\nu^s}\rho^s}{\rho}h\overline{\omega_\nu^s}\right)+\mathcal{O}(\epsilon^{1+\chi}).\end{aligned}\tag{B.4}$$

Note that in Eqs. (B.1)-(B.4), the stress terms of higher order (of ϵ), like $\partial_y\partial T_{xy}^\alpha$ or $\partial_x\partial T_{xy}^\alpha$ for instance, do not appear anymore, since they are incorporated in $\mathcal{O}(\epsilon^{1+\chi})$, and $g_y=0$.

For the normal direction and without scaling, from Eq. (4.14), we derive

$$\begin{aligned}
&\epsilon\frac{\partial}{\partial t}\left(h\overline{\nu^\alpha}\,\overline{v_z^\alpha}\right)+\epsilon\frac{\partial}{\partial x}\left(h\Psi\overline{\nu^\alpha}\,\overline{v_x^\alpha}\,\overline{v_z^\alpha}\right)+\epsilon\frac{\partial}{\partial y}\left(h\overline{\nu^\alpha}\,\overline{v_y^\alpha}\,\overline{v_z^\alpha}\right)\\
&-\lambda\epsilon^2\kappa_x h\overline{z\nu^\alpha v_x^\alpha v_z^\alpha\Psi^2}-\lambda\kappa h\overline{\nu^\alpha\left(\epsilon^2\left(v_z^\alpha\right)^2-\left(v_x^\alpha\right)^2\right)\Psi}\\
=&\epsilon^{1+\mu}\frac{\partial}{\partial x}\left(h\Psi\overline{T_{xz}^\alpha}\right)+\epsilon^{1+\mu}\frac{\partial}{\partial y}\left(h\overline{T_{yz}^\alpha}\right)-\epsilon^{1+\mu}\Psi T_{xz}^\alpha|_b\frac{\partial b}{\partial x}-\epsilon^{1+\mu}T_{yz}^\alpha|_b\frac{\partial b}{\partial y}+[T_{zz}^\alpha]_b\\
&+h\overline{\nu^\alpha}g_z\pm\frac{\rho^f}{\rho^\alpha}\left[\overline{\nu^s}\right]_b^{\mathfrak{s}}\overline{\omega_{by}}\pm\sqrt{\epsilon}\frac{c_D^s h\overline{\nu^s}\overline{\nu^f}\rho^f}{\rho^\alpha}\left(\overline{v_z^f}-\overline{v_z^s}\right)\\
&-\lambda\epsilon^{2+\mu}\kappa_x h\overline{zT_{xz}^\alpha\Psi^2}-\lambda\epsilon\kappa h\overline{\left(T_{zz}^\alpha-T_{xx}^\alpha\right)\Psi},
\end{aligned}\tag{B.5}$$

where $\overline{\omega_{by}}$ is the buoyancy pressure. Now with some order-reduction, the depth-integrated vertical solid and fluid momentum balance yield

$$\begin{aligned}
\epsilon\frac{\partial}{\partial t}\left(h\overline{\nu^s}\,\overline{v_z^s}\right)+\epsilon\frac{\partial}{\partial x}\left(h\overline{\nu^s}\,\overline{v_x^s}\,\overline{v_z^s}\right)+\epsilon\frac{\partial}{\partial y}\left(h\overline{\nu^s}\,\overline{v_y^s}\,\overline{v_z^s}\right)+\lambda\kappa h\overline{\nu^s}\,\overline{v_x^s}^2=\\
[T_{zz}^s]_b+h\overline{\nu^s}g_z+\sqrt{\epsilon}\frac{c_D^s h\overline{\nu^s}\overline{\nu^f}\rho^f}{\rho^s}\left(\overline{v_z^f}-\overline{v_z^s}\right)+\mathcal{O}(\epsilon^{1+\chi}),
\end{aligned}\tag{B.6}$$

$$\begin{aligned}
\epsilon\frac{\partial}{\partial t}\left(h\overline{\nu^f}\,\overline{v_z^f}\right)+\epsilon\frac{\partial}{\partial x}\left(h\overline{\nu^f}\,\overline{v_x^f}\,\overline{v_z^f}\right)+\epsilon\frac{\partial}{\partial y}\left(h\overline{\nu^f}\,\overline{v_y^f}\,\overline{v_z^f}\right)+\lambda\kappa h\overline{\nu^f}\,\overline{v_x^f}^2=\\
\left[T_{zz}^f\right]_b+h\overline{\nu^f}g_z-\sqrt{\epsilon}c_D^s h\overline{\nu^s}\overline{\nu^f}\left(\overline{v_z^f}-\overline{v_z^s}\right)+\mathcal{O}(\epsilon^{1+\chi}).
\end{aligned}\tag{B.7}$$

For the zz-component of the fluid and the solid stress at the bed, we assume that

$$\left[T_{zz}^f\right]_b=\overline{\nu^f}\,\overline{\omega^f}|_b,\quad [T_{zz}^s]_b=\overline{\nu^s}\frac{\rho^f}{\rho^s}\overline{\omega_h^f}|_b+\overline{\nu^s}\,\tau_R^s,$$

with a solid bed friction τ_R^s. The reduction of Eqs. (B.6)-(B.7) to the order $\mathcal{O}(\epsilon)$ yields

$$\begin{aligned}
\lambda\kappa h\overline{\nu^s}\,\overline{v_x^s}^2&=[T_{zz}^s]_b+h\overline{\nu^s}g_z+\mathcal{O}(\epsilon),\\
\lambda\kappa h\overline{\nu^f}\,\overline{v_x^f}^2&=\left[T_{zz}^f\right]_b+h\overline{\nu^f}g_z+\mathcal{O}(\epsilon).
\end{aligned}\tag{B.8}$$

If we now balance $(B.8)_1$ and $(B.8)_2$, multiplied by the respective densities,

$$\lambda\kappa h\overline{v_x^s}^2-\lambda\kappa h\frac{\rho^f}{\rho^s}\overline{v_x^f}^2=\frac{\rho^f}{\rho^s}\overline{\omega_h^f}|_b-\frac{\rho^f}{\rho^s}\overline{\omega^f}|_b+\tau_R^s+hg_z\left(1-\frac{\rho^f}{\rho^s}\right)+\mathcal{O}(\epsilon),\tag{B.9}$$

it follows for the solid bed friction that

$$\tau_R^s=\lambda\kappa h\left(\overline{v_x^s}^2-\frac{\rho^f}{\rho^s}\overline{v_x^f}^2\right)-\frac{\rho^f}{\rho^s}\overline{\omega_h^f}|_b+\frac{\rho^f}{\rho^s}\overline{\omega^f}|_b-hg_z\left(1-\frac{\rho^f}{\rho^s}\right)+\mathcal{O}(\epsilon),\tag{B.10}$$

which we simplify to

$$\tau_R^s = -\frac{\rho^f}{\rho^s}\overline{\omega_\nu^s} + \mathrm{Eu}_b\,\overline{\omega_e^f}|_b + \lambda\kappa h\left(\overline{v_x^s}^2 - \frac{\rho^f}{\rho^s}\overline{v_x^f}^2\right). \tag{B.11}$$

If Eq. (B.7) is further reduced to order $\mathcal{O}(\epsilon^\chi)$, the fluid pressure equalizes gravity, which yields the hydrostatic pressure balance if no extra pore-fluid pressure is regarded, so

$$0 = \left[T_{zz}^f\right]_b + h\overline{\nu^f} g_z + \mathcal{O}(\epsilon^\chi) \rightarrow \overline{\omega^f}|_b = h g_z. \tag{B.12}$$

Now, we define the depth-integrated hydrostatic fluid-pressure part $\overline{\omega_h^f} = \frac{h}{2} g_z$, i.e. half of the basal pressure, which is consistent with Eq. (B.12), and a configurational pressure $\overline{\omega_\nu^s} = (\frac{\rho^s}{\rho^f} - 1)\frac{h}{2} g_z$, see Eqs. (4.4), so $\frac{\rho^f}{\rho^s}\overline{\omega_\nu^s} = \left(1 - \frac{\rho^f}{\rho^s}\right)\frac{h}{2}$, with gravity shares $g_x = \sin(\vartheta_s)$ and $g_z = \cos(\vartheta_s)$.

C Scaled and depth-integrated hypoplastic equations and source terms

In this chapter, some remarks are given on the equations describing the hypoplastic stress, as well as on their transfer into the depth-integrated form, employing general coordinates.

C.1 The equations of hypoplasticity in vector form

The internal, frictional stress is described in its development by an objective, corrotational rate (Jaumann rate) and its source term Φ_{ij}^s, depending on the stress itself and the strain tensor D_{ij}^s. The (objective) Jaumann rate consists of the material derivative and the product of stress and spin tensor W_{ij}^s, so the equations state, both in index notation and vector notation, respectively,

$$\begin{aligned} \overset{\triangle}{Z}_{ij}^s &= \frac{\mathrm{d}Z_{ij}^s}{\mathrm{d}t} + Z_{ik}^s W_{kj}^s - W_{ik}^s Z_{kj}^s = \Phi_{ij}^s \left(D_{ij}^s, Z_{ij}^s \right), \\ \overset{\triangle}{\boldsymbol{Z}}^s &= \frac{\mathrm{d}\boldsymbol{Z}^s}{\mathrm{d}t} + \boldsymbol{Z}^s \cdot \boldsymbol{W}^s - \boldsymbol{W}^s \cdot \boldsymbol{Z}^s = \boldsymbol{\Phi}^s \left(\boldsymbol{D}^s, \boldsymbol{Z}^s \right). \end{aligned} \tag{C.1}$$

The source term is described with a linear term and a non-linear term (with respect to strain):

$$\begin{aligned} \Phi_{ij}^s &= \mathcal{L}\left(Z_{ij}^s \right) D_{ij}^s + \mathcal{R}\left(Z_{ij}^s \right) \left\| D_{ij}^s \right\|, \\ \boldsymbol{\Phi}^s &= \mathcal{L}\left(\boldsymbol{Z}^s \right) \boldsymbol{D}^s + \mathcal{R}\left(\boldsymbol{Z}^s \right) \left\| \boldsymbol{D}^s \right\|. \end{aligned} \tag{C.2}$$

Due to some considerations, see Teufel (2001) and Section 3.4.2, an additional term $\nu^s \frac{\left(\rho^s - \rho^f\right)}{\rho} \frac{\partial v_k^s}{\partial x_k} Z_{ij}^s$ was amended

$$\begin{aligned} &\frac{\partial Z_{ij}^s}{\partial t} + v_k^s \frac{\partial Z_{ij}^s}{\partial x_k} + Z_{ik}^s W_{kj}^s - W_{ik}^s Z_{kj}^s - \nu^s \frac{\left(\rho^s - \rho^f\right)}{\rho} \frac{\partial v_k^s}{\partial x_k} Z_{ij}^s = \Phi_{ij}^s, \\ &\frac{\partial \boldsymbol{Z}^s}{\partial t} + \boldsymbol{v}^s \cdot \nabla \boldsymbol{Z}^s + \boldsymbol{Z}^s \cdot \boldsymbol{W}^s - \boldsymbol{W}^s \cdot \boldsymbol{Z}^s - \nu^s \frac{\left(\rho^s - \rho^f\right)}{\rho} \left(\nabla \cdot \boldsymbol{v}^s \right) \boldsymbol{Z}^s = \boldsymbol{\Phi}^s \left(\boldsymbol{D}^s, \boldsymbol{Z}^s \right). \end{aligned} \tag{C.3}$$

With this, the depth-integrated equation in vectorial form yields, after some transformation:

$$\begin{aligned}\epsilon\frac{\partial h\boldsymbol{Z}^s}{\partial t}+\epsilon\,\nabla\cdot\left(h\boldsymbol{v}^s\boldsymbol{Z}^s\right)+\epsilon\boldsymbol{Z}^s\cdot\nabla\left(h\boldsymbol{v}^s\right)-\epsilon\nabla\left(h\boldsymbol{v}^s\right)\cdot\boldsymbol{Z}^s-h\boldsymbol{v}^s\boldsymbol{z}^s|_n\\ -\epsilon\left(1+\nu^s\frac{\rho^s-\rho^f}{\rho}\right)\nabla\cdot\left(h\nu^s(\boldsymbol{v}^s-\boldsymbol{v}^f)\right)\boldsymbol{Z}^s=\epsilon\boldsymbol{\Phi}^s h,\end{aligned}\tag{C.4}$$

with $\boldsymbol{z}^s|_n=\left(Z^s_{xz}\left(1-\lambda\kappa\right),Z^s_{xy}\right)^T$ as the parts of the inner stress in the normal direction, regarding curvature. The respective source term states

$$\begin{aligned}\boldsymbol{\Phi}^s h=f_s\Bigg(\epsilon a^s_z h\nabla\boldsymbol{v}^s+\frac{h\boldsymbol{Z}^s}{\|\boldsymbol{Z}^s\|^2}\Bigg(\epsilon h\boldsymbol{Z}^s:\nabla\boldsymbol{v}^s+\epsilon h\boldsymbol{z}^s|_n\cdot\underbrace{\nabla v^s_z}_{(*)}\Bigg)\\ +\epsilon f_D a^s_Z\,\|h\nabla\boldsymbol{v}^s\|\left(\frac{\boldsymbol{Z}^s h}{\|\boldsymbol{Z}^s\|}+\frac{h\left(\boldsymbol{Z}^s-\frac{1}{3}\mathrm{tr}(\boldsymbol{Z}^s)\delta\right)}{\|\boldsymbol{Z}^s\|}\right)\Bigg).\end{aligned}\tag{C.5}$$

C.2 The depth-integrated source terms

These depth-integrated, non-dimensional source terms appearing in Eqs. (4.33)-(4.35) are given as

$$\begin{aligned}\overline{\Phi^s_{xx}}h=f_s\Bigg[\epsilon a^s_z\left(\frac{\partial\overline{v^s_x}h}{\partial x}-\left[v^s_x\frac{\partial h}{\partial x}\right]^{\mathfrak{s}}_b\right)\\ +\frac{h\overline{Z^s_{xx}}}{\left(\overline{Z^s_{xx}}+\overline{Z^s_{yy}}+\overline{Z^s_{zz}}\right)^2}\Bigg(\overline{Z^s_{xx}}\epsilon\left(\frac{\partial\overline{v^s_x}h}{\partial x}-\left[v^s_x\frac{\partial h}{\partial x}\right]^{\mathfrak{s}}_b\right)\\ +\overline{Z^s_{xy}}\epsilon\left(\frac{\partial\overline{v^s_y}h}{\partial x}-\left[v^s_y\frac{\partial h}{\partial x}\right]^{\mathfrak{s}}_b+\frac{\partial\overline{v^s_x}h}{\partial y}-\left[v^s_x\frac{\partial h}{\partial y}\right]^{\mathfrak{s}}_b\right)\\ +\overline{Z^s_{xz}}\epsilon\left(\frac{\partial\overline{v^s_z}h}{\partial x}-\left[v^s_z\frac{\partial h}{\partial x}\right]^{\mathfrak{s}}_b\right)+\overline{Z^s_{yz}}\epsilon\left(\frac{\partial\overline{v^s_z}h}{\partial y}-\left[v^s_z\frac{\partial h}{\partial y}\right]^{\mathfrak{s}}_b\right)\\ +\overline{Z^s_{yy}}\epsilon\left(\frac{\partial\overline{v^s_y}h}{\partial y}-\left[v^s_y\frac{\partial h}{\partial y}\right]^{\mathfrak{s}}_b\right)\Bigg)+\epsilon f_D a^s_Z\left|\frac{\partial\overline{v^s_x}h}{\partial x}-\left[v^s_x\frac{\partial h}{\partial x}\right]^{\mathfrak{s}}_b\right|\Bigg(\frac{\overline{Z^s_{xx}}h}{\overline{Z^s_{xx}}+\overline{Z^s_{yy}}+\overline{Z^s_{zz}}}\\ +\frac{h\left(\frac{2}{3}\overline{Z^s_{xx}}-\frac{1}{3}\overline{Z^s_{yy}}-\frac{1}{3}\overline{Z^s_{zz}}\right)}{\overline{Z^s_{xx}}+\overline{Z^s_{yy}}+\overline{Z^s_{zz}}}\Bigg)\Bigg]+\mathcal{O}(\epsilon^2),\end{aligned}\tag{C.6}$$

$$
\begin{aligned}
\overline{\Phi^s_{yy}}h = f_s \Bigg[& \epsilon a^s_z \left(\frac{\partial \overline{v^s_y} h}{\partial y} - \left[v^s_y \frac{\partial h}{\partial y} \right]^{\mathfrak{s}}_b \right) \\
& + \frac{h \overline{Z^s_{yy}}}{\left(\overline{Z^s_{xx}} + \overline{Z^s_{yy}} + \overline{Z^s_{zz}} \right)^2} \Bigg(\overline{Z^s_{xx}} \epsilon \left(\frac{\partial \overline{v^s_x} h}{\partial x} - \left[v^s_x \frac{\partial h}{\partial x} \right]^{\mathfrak{s}}_b \right) \\
& + \overline{Z^s_{xy}} \epsilon \left(\frac{\partial \overline{v^s_y} h}{\partial x} - \left[v^s_y \frac{\partial h}{\partial x} \right]^{\mathfrak{s}}_b + \frac{\partial \overline{v^s_x} h}{\partial y} - \left[v^s_x \frac{\partial h}{\partial y} \right]^{\mathfrak{s}}_b \right) \\
& + \overline{Z^s_{xz}} \epsilon \left(\frac{\partial \overline{v^s_z} h}{\partial x} - \left[v^s_z \frac{\partial h}{\partial x} \right]^{\mathfrak{s}}_b \right) + \overline{Z^s_{yz}} \epsilon \left(\frac{\partial \overline{v^s_z} h}{\partial y} - \left[v^s_z \frac{\partial h}{\partial y} \right]^{\mathfrak{s}}_b \right) \\
& + \overline{Z^s_{yy}} \epsilon \left(\frac{\partial \overline{v^s_y} h}{\partial y} - \left[v^s_y \frac{\partial h}{\partial y} \right]^{\mathfrak{s}}_b \right) \Bigg) + \epsilon f_D a^s_Z \left| \frac{\partial \overline{v^s_y} h}{\partial y} - \left[v^s_y \frac{\partial h}{\partial y} \right]^{\mathfrak{s}}_b \right| \Bigg(\frac{\overline{Z^s_{yy}} h}{\overline{Z^s_{xx}} + \overline{Z^s_{yy}} + \overline{Z^s_{zz}}} \\
& + \frac{h \left(\frac{2}{3} \overline{Z^s_{yy}} - \frac{1}{3} \overline{Z^s_{xx}} - \frac{1}{3} \overline{Z^s_{zz}} \right)}{\overline{Z^s_{xx}} + \overline{Z^s_{yy}} + \overline{Z^s_{zz}}} \Bigg) \Bigg] + \mathcal{O}(\epsilon^2),
\end{aligned}
\tag{C.7}
$$

$$
\begin{aligned}
\overline{\Phi^s_{xy}}h = f_s \Bigg[& \frac{\epsilon}{2} a^s_z \left(\frac{\partial \overline{v^s_x} h}{\partial y} - \left[v^s_x \frac{\partial h}{\partial y} \right]^{\mathfrak{s}}_b + \frac{\partial \overline{v^s_y} h}{\partial x} - \left[v^s_y \frac{\partial h}{\partial x} \right]^{\mathfrak{s}}_b \right) \\
& + \frac{h \overline{Z^s_{xy}}}{\left(\overline{Z^s_{xx}} + \overline{Z^s_{yy}} + \overline{Z^s_{zz}} \right)^2} \Bigg(\overline{Z^s_{xx}} \epsilon \left(\frac{\partial \overline{v^s_x} h}{\partial x} - \left[v^s_x \frac{\partial h}{\partial x} \right]^{\mathfrak{s}}_b \right) \\
& + \overline{Z^s_{xy}} \epsilon \left(\frac{\partial \overline{v^s_y} h}{\partial x} - \left[v^s_y \frac{\partial h}{\partial x} \right]^{\mathfrak{s}}_b + \frac{\partial \overline{v^s_x} h}{\partial y} - \left[v^s_x \frac{\partial h}{\partial y} \right]^{\mathfrak{s}}_b \right) \\
& + \overline{Z^s_{xz}} \epsilon \left(\frac{\partial \overline{v^s_z} h}{\partial x} - \left[v^s_z \frac{\partial h}{\partial x} \right]^{\mathfrak{s}}_b \right) + \overline{Z^s_{yz}} \epsilon \left(\frac{\partial \overline{v^s_z} h}{\partial y} - \left[v^s_z \frac{\partial h}{\partial y} \right]^{\mathfrak{s}}_b \right) \\
& + \overline{Z^s_{yy}} \epsilon \left(\frac{\partial \overline{v^s_y} h}{\partial y} - \left[v^s_y \frac{\partial h}{\partial y} \right]^{\mathfrak{s}}_b \right) \Bigg) \\
& + \epsilon f_D a^s_Z \left| \frac{\partial \overline{v^s_x} h}{\partial y} - \left[v^s_x \frac{\partial h}{\partial y} \right]^{\mathfrak{s}}_b + \frac{\partial \overline{v^s_y} h}{\partial x} - \left[v^s_y \frac{\partial h}{\partial x} \right]^{\mathfrak{s}}_b \right| \left(\frac{2 \overline{Z^s_{xy}} h}{\overline{Z^s_{xx}} + \overline{Z^s_{yy}} + \overline{Z^s_{zz}}} \right) \Bigg] \\
& + \mathcal{O}(\epsilon^2).
\end{aligned}
\tag{C.8}
$$

C.3 The source terms for general coordinates

The depth-integrated source terms, transferred to the framework of general coordinates, state

$$\Phi^s_{x\xi} J_b h = f_s \Bigg(\epsilon a^s_z h \left(A_{11} \frac{\partial J_b v^s_\xi}{\partial \xi} + A_{21} \frac{\partial J_b v^s_\xi}{\partial \eta} \right) + \frac{h Z^s_{x\xi}}{\left(Z^s_{x\xi} + Z^s_{y\eta} + Z^s_{z\zeta} \right)^2} \left(Z^s_{x\xi} \epsilon h \left(A_{11} \frac{\partial J_b v^s_\xi}{\partial \xi} + A_{21} \frac{\partial J_b v^s_\xi}{\partial \eta} \right) + Z^s_{x\eta} \epsilon h \left(A_{11} \frac{\partial J_b v^s_\eta}{\partial \xi} + A_{21} \frac{\partial J_b v^s_\eta}{\partial \eta} + A_{12} \frac{\partial J_b v^s_\xi}{\partial \xi} + A_{22} \frac{\partial J_b v^s_\xi}{\partial \eta} \right) + Z^s_{y\eta} \epsilon h \left(A_{12} \frac{\partial J_b v^s_\eta}{\partial \xi} + A_{22} \frac{\partial J_b v^s_\eta}{\partial \eta} \right) \underbrace{+ \Pi_Z}_{(*)} \right) + \epsilon f_D a^s_Z \left| h \left(A_{11} \frac{\partial J_b v^s_\xi}{\partial \xi} + A_{21} \frac{\partial J_b v^s_\xi}{\partial \eta} \right) \right| \left(\frac{Z^s_{x\xi} h}{Z^s_{x\xi} + Z^s_{y\eta} + Z^s_{z\zeta}} + \frac{h \left(\frac{2}{3} Z^s_{x\xi} - \frac{1}{3} Z^s_{y\eta} - \frac{1}{3} Z^s_{z\zeta} \right)}{Z^s_{x\xi} + Z^s_{y\eta} + Z^s_{z\zeta}} \right) \Bigg), \tag{C.9}$$

$$\Phi^s_{y\eta} J_b h = f_s \Bigg(\epsilon a^s_z h \left(A_{12} \frac{\partial J_b v^s_\eta}{\partial \xi} + A_{22} \frac{\partial J_b v^s_\eta}{\partial \eta} \right) + \frac{h Z^s_{y\eta}}{\left(Z^s_{x\xi} + Z^s_{y\eta} + Z^s_{z\zeta} \right)^2} \left(Z^s_{x\xi} \epsilon h \left(A_{11} \frac{\partial J_b v^s_\xi}{\partial \xi} + A_{21} \frac{\partial J_b v^s_\xi}{\partial \eta} \right) + Z^s_{x\eta} \epsilon h \left(A_{11} \frac{\partial J_b v^s_\eta}{\partial \xi} + A_{21} \frac{\partial J_b v^s_\eta}{\partial \eta} + A_{12} \frac{\partial J_b v^s_\xi}{\partial \xi} + A_{22} \frac{\partial J_b v^s_\xi}{\partial \eta} \right) + Z^s_{y\eta} \epsilon h \left(A_{12} \frac{\partial J_b v^s_\eta}{\partial \xi} + A_{22} \frac{\partial J_b v^s_\eta}{\partial \eta} \right) \underbrace{+ \Pi_Z}_{(*)} \right) + \epsilon f_D a^s_Z \left| h \left(A_{12} \frac{\partial J_b v^s_\eta}{\partial \xi} + A_{22} \frac{\partial J_b v^s_\eta}{\partial \eta} \right) \right| \left(\frac{Z^s_{y\eta} h}{Z^s_{x\xi} + Z^s_{y\eta} + Z^s_{z\zeta}} + \frac{h \left(\frac{2}{3} Z^s_{y\eta} - \frac{1}{3} Z^s_{x\xi} - \frac{1}{3} Z^s_{z\zeta} \right)}{Z^s_{x\xi} + Z^s_{y\eta} + Z^s_{z\zeta}} \right) \Bigg), \tag{C.10}$$

$$\Phi^s_{x\eta} J_b h = f_s \Bigg(\frac{\epsilon}{2} a^s_z h \left(A_{11} \frac{\partial J_b v^s_\eta}{\partial \xi} + A_{21} \frac{\partial J_b v^s_\eta}{\partial \eta} + A_{12} \frac{\partial J_b v^s_\xi}{\partial \xi} + A_{22} \frac{\partial J_b v^s_\xi}{\partial \eta} \right) + \frac{h Z^s_{x\eta}}{\left(Z^s_{x\xi} + Z^s_{y\eta} + Z^s_{z\zeta} \right)^2} \left(Z^s_{x\xi} \epsilon h \left(A_{11} \frac{\partial J_b v^s_\xi}{\partial \xi} + A_{21} \frac{\partial J_b v^s_\xi}{\partial \eta} \right) + Z^s_{x\eta} \epsilon h \left(A_{11} \frac{\partial J_b v^s_\eta}{\partial \xi} + A_{21} \frac{\partial J_b v^s_\eta}{\partial \eta} + A_{12} \frac{\partial J_b v^s_\xi}{\partial \xi} + A_{22} \frac{\partial J_b v^s_\xi}{\partial \eta} \right) + Z^s_{y\eta} \epsilon h \left(A_{12} \frac{\partial J_b v^s_\eta}{\partial \xi} + A_{22} \frac{\partial J_b v^s_\eta}{\partial \eta} \right) \underbrace{+ \Pi_Z}_{(*)} \right) + \epsilon f_D a^s_Z h \left| \left(A_{11} \frac{\partial J_b v^s_\eta}{\partial \xi} + A_{21} \frac{\partial J_b v^s_\eta}{\partial \eta} + A_{12} \frac{\partial J_b v^s_\xi}{\partial \xi} + A_{22} \frac{\partial J_b v^s_\xi}{\partial \eta} \right) \right| \left(\frac{2 Z^s_{x\eta} h}{Z^s_{x\xi} + Z^s_{y\eta} + Z^s_{z\zeta}} \right) \Bigg), \tag{C.11}$$

where a term Π_Z, related to the velocity in the vertical direction, is left open and set to zero in the following. We give consideration to the fact that is a further possible

starting point for modeling, since here, the velocity in the vertical direction could be coupled to dilatancy, such that

$$\Pi_Z = Z^s_{x\zeta}\epsilon h\left(A_{11}\frac{\partial J_b v^s_\zeta}{\partial \xi} + A_{21}\frac{\partial J_b v^s_\zeta}{\partial \eta}\right) + Z^s_{y\zeta}\epsilon h\left(A_{12}\frac{\partial J_b v^s_\zeta}{\partial \xi} + A_{22}\frac{\partial J_b v^s_\zeta}{\partial \eta}\right),$$

$$v^s_\zeta = -\kappa_d\left(\nu^s_\infty - \nu^s\right)$$

$$\rightarrow \frac{\partial J_b v^s_\zeta}{\partial \xi} = -\kappa_d\frac{\partial J_b\left(\nu^s_\infty - \nu^s\right)}{\partial \xi}, \quad \frac{\partial J_b v^s_\zeta}{\partial \eta} = -\kappa_d\frac{\partial J_b\left(\nu^s_\infty - \nu^s\right)}{\partial \eta}.$$

D Model comparison and limiting cases

In this section, we seek to analytically compare the developed set of depth-integrated momentum balances with some known formulations in the field of debris flow modeling and discuss possible limiting cases. For the sake of clarity, this is done for the formulation of the model for curvilinear coordinates (x, z), since the respective models are also formulated in curvilinear coordinates, and disregarding the cross-slope, y-direction. Originating from the pioneering work of Savage & Hutter (1989), which proposed a set of depth-integrated equations for dry granular flow with a Mohr-Coulomb criterion, Pitman & Le (2005) generalized the approach to a two-phase flow that allows for the consideration of an additional fluid phase. The normal stress component of the solid is linked to the down- and cross-slope stress via the introduction of an earth pressure coefficient to close the model. Also based on the work of Iverson (1997), Pitman & Le (2005) similarly emphasized the role of the pore-fluid, while retaining two full momentum equations instead of merging them to a mixture one. Pudasaini (2012) developed an improved drag coefficient and an enhanced model for the fluid phase by including viscous terms. A further prosecution of the modeling efforts for debris flow has been presented by Meng & Wang (2016), discussing the aforementioned works, extending them to simulate debris flows on a curvilinear surface and proposing corrections on the buoyant term in Pudasaini (2012).
Next we want to show that our model can be reduced to these previous ones by appropriate simplifications. This demonstrates that the present model includes their features in a more general way. An underlying assumption is that, although this does not represent the actual development of the model, the results of our modeling efforts can be seen as an improvement of a basic model by taking more effects into account. This implies in turn that the model can be reduced to the MW-model and with this, the focal point of the research has to be the proof of the meaningfulness of the additionally introduced terms. For this, the gravity shares g_x and g_z are inserted as functions of the inclination angle ϑ_s. Note that we compare the non-dimensional, depth-integrated equations, omitting the respective notation with over-bar and asterisk.
Hence, we will reveal this basic structure of the equations of Pitman & Le (2005), before discussing the equations of the most recent model of Meng & Wang (2016). Also, we will discuss several limiting cases, since these cases disclose possible limitations of the model due to unphysical properties.

D.1 Pitman-Le model

The fundamental two-phase model of Pitman & Le (2005) includes an ideal fluid phase to account for the role of the interstitial fluid in debris flows. The solid is modeled as

an incompressible Coulomb granular material. The interaction of the distinct mixture phases are modeled with the help of averaging models, following Anderson & Jackson (1967), which allows for buoyancy due to different densities and drag between the phases. We give an account of the momentum balances in the downslope direction. In Pitman & Le (2005), for the solid x-momentum balance – neglecting terms of higher ϵ order, i.e. $\mathcal{O}(\epsilon^{1+\chi})$ – it follows that

$$\begin{aligned}
&\frac{\partial}{\partial t}\left(h\nu^s v_x^s\right) + \frac{\partial}{\partial x}\left(h\nu^s v_x^s v_x^s\right) \\
=&h\nu^s \sin(\vartheta_s) - \epsilon\frac{\partial}{\partial x}\left(K_{act/pas}\left(1-\frac{\rho^f}{\rho^s}\right)\cos(\vartheta_s)\nu^s\frac{h^2}{2}\right) - \epsilon\frac{\rho^f}{\rho^s}\nu^s\cos(\vartheta_s)h\frac{\partial h}{\partial x} \\
&- \operatorname{sgn}\left(v_x^s\right)h\nu^s\tan(\delta_b)\left(1-\frac{\rho^f}{\rho^s}\right)\cos(\vartheta_s) + \frac{c_D^{sf}h\rho^f}{\rho^s}\left(v_x^f - v_x^s\right),
\end{aligned} \tag{D.1}$$

while the fluid x-momentum balance yields

$$\begin{aligned}
&\frac{\partial}{\partial t}\left(h\nu^f v_x^f\right) + \frac{\partial}{\partial x}\left(h\nu^f v_x^f v_x^f\right) \\
=&h\nu^f \sin(\vartheta_s) - \epsilon\nu^f\cos(\vartheta_s)\frac{\partial}{\partial x}\left(\frac{h^2}{2}\right) - c_D^{sf}h\left(v_x^f - v_x^s\right).
\end{aligned} \tag{D.2}$$

The solid momentum Eq. (D.1) yields, after a few transformations, the momentum balance of the SH-model, see Savage & Hutter (1989) and also Section 4.1, by assuming that $\rho^f \to 0$, no phase interaction $c_D^{sf} = 0$ and $\nu^s = const.$

D.2 Meng-Wang model

The model of Meng & Wang (2016), similar to Pudasaini (2012), considers in particular the fluid rheology by adding a viscous term as well as a basal fluid friction term that is linearly dependent on the velocity. While in comparison to the Pitman-Le model, the solid momentum balance in the downslope direction is enhanced only in the basal friction term by accounting for the bed curvature, $\lambda\kappa h((v_x^s)^2 - \frac{\rho^f}{\rho^s}(v_x^f)^2)$, yielding

$$\begin{aligned}
&\frac{\partial}{\partial t}\left(h\nu^s v_x^s\right) + \frac{\partial}{\partial x}\left(h\nu^s v_x^s v_x^s\right) \\
=&h\nu^s \sin(\vartheta_s) - \epsilon\frac{\partial}{\partial x}\left(K_{act/pas}\left(1-\frac{\rho^f}{\rho^s}\right)\cos(\vartheta_s)\nu^s\frac{h^2}{2}\right) - \epsilon\frac{\rho^f}{\rho^s}\nu^s\cos(\vartheta_s)h\frac{\partial h}{\partial x} \\
&- \operatorname{sgn}\left(v_x^s\right)h\nu^s\tan(\delta_b)\left[\left(1-\frac{\rho^f}{\rho^s}\right)\cos(\vartheta_s) + \lambda\kappa\left((v_x^s)^2 - \frac{\rho^f}{\rho^s}(v_x^f)^2\right)\right] \\
&+ \frac{c_D^{sf}h\rho^f}{\rho^s}\left(v_x^f - v_x^s\right),
\end{aligned} \tag{D.3}$$

the new fluid momentum balance in downslope direction follows as

$$\begin{aligned}
&\frac{\partial}{\partial t}\left(h\nu^f v_x^f\right) + \frac{\partial}{\partial x}\left(h\nu^f v_x^f v_x^f\right) \\
=&h\nu^f \sin(\vartheta_s) - \epsilon\nu^f \cos(\vartheta_s)\frac{\partial}{\partial x}\left(\frac{h^2}{2}\right) \\
&- c_D^{sf} h\left(v_x^f - v_x^s\right) + \frac{\epsilon}{\mathrm{N}_R^{MW}}\left(2h\frac{\partial^2 v_x^f}{\partial x^2} - \frac{\alpha_b^f v_x^f}{\epsilon^2}\right).
\end{aligned} \tag{D.4}$$

The last term in (D.4) contains a viscous part in conjunction with the second derivative of the fluid x-velocity and the fluid basal friction. Due to the scaling of these terms, the dimensionless variable N_R^{MW} is introduced with $\mathrm{N}_R^{MW} = (\rho^f \mathcal{H}\sqrt{g\mathcal{L}})/(\nu^f \mu^f)$ and the relation to the viscous number introduced in this work is $\mathrm{N}_R = \nu^f \mathrm{N}_R^{MW}$, also see Tai et al. (2018).

D.3 Comparison

If Eqs. (4.26) and (4.28) are rearranged and the solid viscous terms are omitted with $a_1^s = a_2^s = 0$, it follows for the granular phase that

$$\begin{aligned}
&\frac{\partial}{\partial t}\left(h\nu^s v_x^s\right) + \frac{\partial}{\partial x}\left(h\nu^s v_x^s v_x^s\right) \\
=&h\nu^s \sin(\vartheta_s) - \epsilon\frac{\partial}{\partial x}\left(\left(1 - \frac{\rho^f}{\rho^s}\right)\nu^s \cos(\vartheta_s)\frac{h^2}{2} - \mathrm{Eu}h\nu^s\frac{\rho^f}{\rho^s}\varpi_e^f - \mathrm{N}_Z\left(1 - \frac{\rho^f}{\rho^s}\right)h2Z_{xx}^s\right) \\
&- \operatorname{sgn}\left(v_x^s\right)h\nu^s \tan(\delta_b)\left[\left(1 - \frac{\rho^f}{\rho^s}\right)\cos(\vartheta_s) - \mathrm{Eu}_b\varpi_e^f + \lambda\kappa\left((v_x^s)^2 - \frac{\rho^f}{\rho^s}(v_x^f)^2\right)\right] \\
&+ \frac{\epsilon}{\rho^s}\mathrm{N}_Z\frac{\partial \rho h Z_{xx}^s}{\partial x} + \frac{c_D^{sf} h\rho^f}{\rho^s}\left(v_x^f - v_x^s\right) \\
&- \epsilon\frac{\rho^f}{\rho^s}\nu^s \cos(\vartheta_s)h\frac{\partial h}{\partial x} + \epsilon\frac{\rho^f}{\rho^s}\frac{\nu^f\left(\rho^s - \rho^f\right)}{\rho}\frac{h^2}{2}\cos(\vartheta_s)\frac{\partial \nu^s}{\partial x},
\end{aligned} \tag{D.5}$$

so that the movement of the granular phase is governed by gravity, frictional and hypoplastic forces as well as the partial pressure and the momentum interaction forces.

For the fluid phase, the downslope x-momentum balance is given as

$$\begin{aligned}
&\frac{\partial}{\partial t}\left(h\nu^f v_x^f\right)+\frac{\partial}{\partial x}\left(h\nu^f v_x^f v_x^f\right)\\
=&h\nu^f\sin(\vartheta_s)-\epsilon\frac{\partial}{\partial x}\left(\nu^f\cos(\vartheta_s)\frac{h^2}{2}+\mathrm{Eu}h\nu^f\varpi_e^f\right)-c_D^{sf}h\left(v_x^f-v_x^s\right)\\
&+\epsilon\mathrm{Ga}_f^{-\frac{1}{2}}\left(a_1^f+a_2^f\right)\frac{\partial}{\partial x}\left(h\frac{\partial v_x^f}{\partial x}\right)-\frac{\alpha_b^f h\nu^f}{\epsilon\mathrm{N}_R}v_x^f-\epsilon\cos(\vartheta_s)\frac{h^2}{2}\frac{\partial\nu^s}{\partial x}\\
&-\epsilon\frac{\nu^f\left(\rho^s-\rho^f\right)}{\rho}\frac{h^2}{2}\cos(\vartheta_s)\frac{\partial\nu^s}{\partial x}.
\end{aligned}\tag{D.6}$$

If the additional influence of the extra pore-fluid pressure, ϖ_e^f, and the hypoplastic stress part, Z_{xx}^s, in the momentum equations are neglected, the remaining differences between our model and Eqs. (D.5)-(D.6) of Meng & Wang (2016) can be found in the buoyant term. An additional term τ_{by}^a appears here, accounting for the configurational pressure. It should be stated that this term is a direct result of the thermodynamically consistent modeling in conjunction with the entropy principle of Müller and Liu, as derived in Heß et al. (2017). This term

$$\epsilon\rho^f\frac{\nu^f\left(\rho^s-\rho^f\right)}{\rho}\frac{h^2}{2}\cos(\vartheta_s)\frac{\partial\nu^s}{\partial x}:=\tau_{by}^a,$$

represents an additional driving force due to buoyancy rate, coupled to changes in the microstructure, i.e. differences in density times the gradient of the solid volume fraction. Apart from this, the system of equations developed into Eqs. (D.5)-(D.6) can be converted into Eqs.(D.1)-(D.4) as long as an appropriate assumptions for the fluid basal friction and the fluid viscous terms are considered. Also note that, for the simple investigations here, it can be assumed that $\partial_x\left(h\partial_x\left(v_x^f\right)\right)\approx\partial_x^2\left(hv_x^f\right)$, implying that the respective terms in Eqs. (D.4) and (D.6) are equal. The formula for N_R is introduced without the dependence on ν^f, such that

$$\frac{1}{\mathrm{N}_R}=\frac{\mu^f}{\rho^f\mathcal{H}\sqrt{g\mathcal{L}}}=\mathrm{Ga}_f^{-\frac{1}{2}}\left(a_1^f+a_2^f\right).$$

With that, the fluid viscosity can be determined as $\mu^f=\rho^f\mathcal{H}\sqrt{\mathcal{L}g}$, depending on the chosen scaling $\mathcal{H}$ and $\mathcal{L}$ and the values of the fluid density and the gravitational acceleration.

D.4 Limiting cases

We now seek to investigate the compatibility of our model with well-known models and basic principles of fluid and soil mechanics.

Dry granular flow: The governing equations for a dry granular flow can be obtained from the two-phase granular-fluid model by choosing $\nu^s = const$, $\nu^f = 0$, ρ^f, and $\varpi_e^f = 0$. With this, the drag- and momentum interaction forces vanish. If we also leave out the centrifugal forces due to the curvature of the flow chute, it follows for Eq. (D.5) that

$$\begin{aligned}\frac{\partial}{\partial t}\left(hv_x^s\right) + \frac{\partial}{\partial x}\left(hv_x^s v_x^s\right) = h\sin(\vartheta_s) - \epsilon\frac{\partial}{\partial x}\left(\frac{h^2}{2}\cos(\vartheta_s) - 2\mathrm{N}_Z h Z_{xx}^s\right) \\ - \epsilon\mathrm{N}_Z\frac{\partial h Z_{xx}^s}{\partial x} - \operatorname{sgn}\left(v_x^s\right) h\cos(\vartheta_s)\tan(\delta_b).\end{aligned} \tag{D.7}$$

By further omitting the hypoplastic part of the internal friction, i.e. $\mathrm{N}_Z \to 0$, we obtain the classical Savage-Hutter model, as presented in Section 4.1.
Furthermore, the ability of the model to depict the internal friction of static granular materials at a horizontal plane is evaluated. For this case, the gravity in the x-direction and velocities are set to zero, $v_x^s = 0$ and $\sin(\vartheta_s) = 0, \cos(\vartheta_s) = 1$, while $\mathrm{N}_Z \neq 0$ and $\mathrm{N}_Z = const$, so $\partial_x \mathrm{N}_Z = 0$. With this, the remaining momentum balance (D.7) is reduced to

$$\frac{\partial}{\partial x}\left(\frac{h^2}{2}\right) = \mathrm{N}_Z\frac{\partial h Z_{xx}^s}{\partial x}, \tag{D.8}$$

showing that the gradient of height $\partial_x h$ is balanced with the apparent internal friction in conjunction with Z_{xx}^s. Giving a linear correlation between h and Z_{xx}^s in conjunction with the bed friction angle, this shows the importance of hypoplasticity for the settling of granular material on a pile under a corresponding angle of repose.

Hypoplasticity and Mohr-Coulomb friction: Staying with the influence of hypoplasticity – if we identify the shear stress as $\tau = Z_{xz}^s$ and the normal stress as $\sigma = Z_{xx}^s$, with the applied assumption of $Z_{xz}^s = -(3/\sqrt{2})a_Z^s Z_{xx}^s$, we obtain a Coulomb-like friction law $\tau \sim C\sigma\sin(\phi)$. While this comes here as a presumption, it can be derived from hypoplastic equations for the state of simple shearing. If we reduce the depth-integrated evolution equation for the internal granular friction in the xz-plane to the order ϵ^0 and also presume isotropic stress distribution, i.e. $Z_{xx}^s = Z_{zz}^s$, the evolution of the intergranular stress yields

$$\begin{aligned}\underbrace{\left(Z_{zz}^s - Z_{xx}^s\right)}_{=0} h\left[v_x^s\right]_b^{\mathfrak{s}} = f_s a_Z^s\left[v_x^s\right]_b^{\mathfrak{s}} + f_s\frac{\left(Z_{xz}^s\right)^2 h\left[v_x^s\right]_b^{\mathfrak{s}}}{\left(Z_{xx}^s + Z_{zz}^s\right)^2} \\ \to \underbrace{Z_{xz}^s}_{\tau} = -\sqrt{\frac{a_Z^s}{h}}\left(Z_{xx}^s + Z_{zz}^s\right) = -2\sqrt{\frac{a_Z^s}{h}}\underbrace{\left(Z_{xx}^s\right)}_{\sigma}.\end{aligned} \tag{D.9}$$

Therefore, the depth-integrated equations within a hypoplastic rheology can be interpreted as a higher-ϵ-order enhancement of a Coulomb-friction-like material, containing the basic relations between shear stress and normal load. This higher-order hypoplasticity becomes important when the granular flow decelerates and tends to accumulate.

Equal densities: Equal densities $\rho_s = \rho_f$ imply the extinction of the configurational pressure ϖ_ν^s, as well as the vanishing of the buoyancy, i.e. solid particles suspended in the fluid. If we transfer the model equations to the static case again, i.e. with vanishing velocities, bed friction and extra pressure, the momentum balance equation reduces to hydrostatic balance between pressure gradient and gravity. As it is pointed out by Meng & Wang (2016), physically reasonable systems of equations should always reproduce this limiting case of hydrostatic and lithostatic pressure.

The influence of the extra pressure: As described before, a dynamic extra pressure enhances the mobility of the debris flow. Therefore, in this work, it is introduced into the solid bed friction term by $\frac{\rho^f}{\rho^s}\varpi_\nu^s - \mathrm{Eu}_b\varpi_e^f$, decreasing the resistance due to friction. If the bed curvature is omitted, the bed friction term is

$$[T_{xz}^s]_b = -\mathrm{sgn}(v_x^s)\nu^s\mu_b^s\left(\frac{\rho^f}{\rho^s}\varpi_\nu^s - \mathrm{Eu}_b\varpi_e^f\right), \tag{D.10}$$

where, if the extra pressure equalizes the configurational pressure, $\mathrm{Eu}_b\rho^s\varpi_e^f = \rho^f\varpi_\nu^s$, the bed-friction vanishes, $[T_{xz}^s]_b \to 0$. Furthermore, it reduces the spherical solid stress and enhances the fluid pressure.

D.5 Model overview

The following is an overview of a selection of different models for granular and granular-fluid flows. For the sake of clarity, this comparison is given in tabular form, see Tables D.1 and D.2.

Work	Case	Dimension and Depth-Averaging	Layer	Modeling
Pitman & Le (2005)	Granulate-Fluid, start till runout	2D, yes	1	Two phases with momentum interaction, non-viscous fluid
Pailha & Pouliquen (2009)	Granulate-Fluid	1D, yes	1	Quasi-two-fluid-model with dynamic pore-pressure, basal shear stress depending on dilatancy, viscosity and shear rate
Hutter & Schneider (2010a)	Granulate-Fluid	3D, no	1	Visco-Hypoplastic behavior, derivation with ML entropy principle, no simulation
Pudasaini (2012)	Granulate-Fluid, inclined plane	2D, yes	1	Internal and basal Coulomb-friction, continues Pitman & Le (2005)
Hutter & Luca (2012)	Granulate-Fluid	2D, yes	2	Erosion and deposition, jump conditions between layers, particle mass concentration, upper fluid layer
Tai & Kuo (2012)	Granulate-Fluid	2D, yes	1	Erosion and deposition, Coulomb material, quasi one-phase/ mixture Eqs, general coordinates

Table D.1: Overview of granular and granular-fluid models, part I

Work	Case	Dimension and Depth-Averaging	Layer	Modeling
Kowalski & McElwaine (2013)	Granulate-Fluid	1D, yes	1	Coulomb-friction depending on the solid concentration, dynamic pressure at the base
Iverson & George (2014), George & Iverson (2014)	Granulate-Fluid, start till runout	2D, yes	1	Coulomb-friction with dilatancy, dynamic pore-pressure Eq., quasi one-phase/ mixture Eqs.
Gray & Edwards (2014)	Granulate, inclined plane	1D, yes	1	Empirical $\mu(I)$-law, hydrostatic pressure
Bouchut et al. (2016)	Granulate-Fluid	2D, yes	1	Coulomb solid friction and Navier fluid friction, dilatancy effects, no simulation,
Meng & Wang (2016)	Granulate-Fluid	2D, yes	1	Coulomb solid friction and Navier fluid friction, enhanced momentum interaction terms
Guo et al. (2016)	Granulate-Fluid	3D, no	1	Hypoplastic mofrl in combination with Bagnold's model
Meng et al. (2017)	Granulate-Fluid	2D, yes	2	Upper granular layer

Table D.2: Overview of granular and granular-fluid models, part II

E Numerical simulation: applied values

Parameter	Value	Description
(n_X, n_Y)	$(161, 41)$	Points in X- and Y-direction
X	$\in [0, 8]$	Domain in X-direction
Y	$\in [0, 2]$	Domain in Y-direction
C_{max}	0.1	CFL number
$\alpha_\rho = \rho^f / \rho^s$	1.0/2.4	Density ratio
$\nu^s\|^0$	0.6	Initial solid volume fraction
$v_X^{s,f}\|^0, v_Y^{s,f}\|^0$	0	Initial velocities
$\omega_e^f\|^0$	0.001	Initial pore-fluid pressure
$Z_{ii}^s\|^0$	0.1	Initial hypoplastic stress
ν_C^s	0.62	Critical volume fraction
ν_∞^s	0.75	Maximum packing fraction
k_D^0	10^{-13}	Hydraulic permeability coefficient
α_D^0	1.0	Compressibility factor
μ^f	0.01	Fluid viscosity factor
δ_b	36°	Angle of basal friction
α_b^f	40	Navier fluid friction coefficient
c_D^s	12	Drag coefficient
N_R	300	Viscous number
ϕ_{int}	23°	Angle of internal friction
f_D^0	1.0	Density coefficient
f_s^0	0.01	Stiffness coefficient

Table E.1: Parameters for dam break simulations in Section 5.3